Ph.D. Thesis

Numerical analysis of conjugate heat and mass transfer phenomena in food freezing using hydrofluidisation impingement method

---

Author:
Michal STEBEL

Supervisors:
Jacek SMOLKA
Trygve M. EIKEVIK
Michal PALACZ

Silesian
University
of Technology

Scientific discipline: Environmental Engineering, Mining and Energy

Gliwice, Poland, 2022

Author:
Michał Stebel, M.Sc.
Silesian University of Technology
Faculty of Energy and Environmental Engineering
Department of Thermal Technology
Konarskiego 22, 44-100 Gliwice, Poland
e-mail: michal.stebel@polsl.pl

Supervisor:
Prof. Jacek Smołka
Professor at Silesian University of Technology
Faculty of Energy and Environmental Engineering
Depratment of Thermal Technology
Konarskiego 22, 44-100 Gliwice, Poland
e-mail: jacek.smolka@polsl.pl

Co-Supervisor:
Prof. Trygve Magne Eikevik
Professor at Norwegian University of Science and Technology
Department of Energy and Process Engineering
Kolbjørn Hejes vei 1d, 7491 Trondheim, Norway
e-mail: trygve.m.eikevik@ntnu.no

Co-Supervisor:
Michał Palacz, Ph.D.
Assistant Professor at the Silesian University of Technology
Faculty of Energy and Environmental Engineering
Department of Thermal Technology
Konarskiego 22, 44-100 Gliwice, Poland
e-mail: michal.palacz@polsl.pl

Polish title:
Analiza sprzężonego procesu transportu ciepła i masy podczas zamrażania żywności metodą hydrofluidyzacji uderzeniowej

Mojej Gabrysi

Acknowledgements

I would like to express my sincere gratitude to my supervisor Prof. Jacek Smolka for his invaluable support, guidance, and fruitful discussions. I am grateful for all the scientific help along with creating such a friendly and supportive atmosphere in our workgroup which pushed me forward at each step of my work.

I gratefully acknowledge the contribution of Prof. Trygve M. Eikevik, my co-supervisor. I appreciate all the shared knowledge and experience which was invaluable for the preparation of this thesis.

My sincere thanks also go to Dr Michal Palacz, my co-supervisor, and the finest project partner. I am grateful for all the support, suggestions and cooperation during the realisation of the research project. I wish to continue such a positive and friendly partnership.

In addition, I would like to acknowledge the people that I had a chance and pleasure to collaborate with during the last years. I am grateful for the partnership, all worries and triumphs shared with Jakub Bodys. Sincere thanks go to Michal Haida for his positive approach and invaluable advice. I am glad that I had the opportunity to work with Edyta Piechnik, Bartlomiej Melka, and Rafal Fingas. Thank you all for sharing all the successes and all the difficulties we experienced during the implementation of a number of projects.

My particular gratefulness and respect go to Prof. Andrzej J. Nowak not only for the knowledge he shared and the scientific support but most of all, for being an example to follow.

I would like to acknowledge the contribution of Prof. Suzana E. Zorrilla and Prof. Juan Manuel Peralta from INTEC (Santa Fe, Argentina) and Dr Ignat Tolstorebrov from NTNU (Trondheim, Norway). I am glad for the support and all the advice I have received from them.

Finally, my deep and sincere gratitude goes to my loved family and friends. I am thankful for all the care, opportunities and support I was given by my parents during all my youth. Last, but not least, I want to thank my beloved fiancee, Gabriela. I would not be at this place without her support, encourage, and patience, which I truly appreciate.

Contents

List of monothematic publications

The thesis consists of 4 monothematic papers listed below. The contribution of the author is given below the research papers list. The contribution of all co-authors was declared in their statements that are kept by the thesis author and each paper co-author. The full texts of these papers can be found in the Appendices chapter. The papers are referred by the Roman numerals through the thesis.

I. **Michal Stebel**, J. Smolka, M. Palacz, W. Adamczyk, E. Piechnik, *Numerical investigation of the fluid flow distribution for the hydrofluidisation food freezing method*, International Journal of Thermal Sciences, Volume 151, 2020
DOI: 10.1016/j.ijthermalsci.2020.106284
(IF$_{2019}$=3.476)

II. **Michal Stebel**, J. Smolka, M. Palacz, E. Piechnik, M. Halski, M. Knap, E. Felis, T.M. Eikevik, I. Tolstorebrov, J.M. Peralta, S.E. Zorrilla, *Numerical modelling of the food freezing process in a quasi-hydrofluidisation system*, Innovative Food Science and Emerging Technologies, Volume 74, 2021
DOI: 10.1016/j.ifset.2021.102834
(IF$_{2020}$=5.916)

III. **Michal Stebel**, J. Smolka, M. Palacz, M. Halski, A. Widuch, T.M. Eikevik, I. Tolstorebrov, *Numerical analysis of hydrofluidisation food freezing with moving products in different aqueous solutions by using CFD and MPM approaches*, International Journal of Refrigeration, Volume 134, 2022
DOI: 10.1016/j.ijrefrig.2021.12.008
(IF$_{2020}$=3.629)

IV. **Michal Stebel**, J. Smolka, M. Palacz, T.M. Eikevik, I. Tolstorebrov, *Numerical modelling of conjugate heat and mass transfer during hydrofluidisation food freezing in different water solutions*, Innovative Food Science and Emerging Technologies, Volume 75, 2022
DOI: 10.1016/j.ifset.2021.102898
(IF$_{2020}$=5.916)

The author's contribution for each paper was following:

I. **Michal Stebel's contribution** was to develop the numerical model, conduct the numerical campaign, analyse the results and prepare the manuscript. According to the authors' statement, Michal Stebel's contribution was equal to **51 %**.

II. **Michal Stebel's contribution** was to develop and calibrate the numerical model, conduct the numerical campaign, analyse the results and prepare the manuscript. According to the authors' statement, Michal Stebel's contribution was equal to **51 %**.

III. **Michal Stebel's contribution** was to formulate and develop the numerical model of moving samples, establish the methodology to evaluate heat transfer coefficients based on the available results, conduct the simulations, analyse the results and prepare the manuscript. According to the authors' statement, Michal Stebel's contribution was equal to **55 %**.

IV. **Michal Stebel's contribution** was to develop the numerical model of heat and mass transfer, formulate and conduct the numerical campaign, prepare the manuscript. According to the authors' statement, Michal Stebel's contribution was equal to **61 %**.

Supplementary publications

The author of this thesis is the co-author of two research papers related to the hydrofluidisation method of food freezing. These papers are listed below. The contribution of the author is given below the research papers list.

1. M. Palacz, W. Adamczyk, E. Piechnik, **Michal Stebel**, J. Smolka *Experimental investigation of the fluid flow inside a hydrofluidisation freezing chamber*, International Journal of Refrigeration, Volume 107, 2019
   DOI: 10.1016/j.ijrefrig.2019.08.009
   (IF$_{2018}$=3.233)

2. M. Palacz, E. Piechnik, M. Halski, **Michal Stebel**, W. Adamczyk, T.M. Eikevik, J. Smolka *Experimental analysis of freezing process of stationary food samples inside a hydrofluidisation freezing chamber*, International Journal of Refrigeration, Volume 131, 2021
   DOI: 10.1016/j.ijrefrig.2021.06.034
   (IF$_{2020}$=3.629)

The author's contribution for each paper was following:

1. **Michal Stebel's contribution** was to discuss the results and support the manuscript reviewing. According to the authors' statement, Michal Stebel's contribution was equal to **10 %**.

2. **Michal Stebel's contribution** was to support the preparation of measurements at the laboratory test stand. According to the authors' statement, Michal Stebel's contribution was equal to **10 %**.

XII

Nomenclature

Abbreviations

CFD	Computational Fluid Dynamics	
DEM	Discrete Element Method	
DPM	Discrete Phase Model	
EXP	Experimental	
FDM	Finite Difference Method	
FEM	Finite Element Method	
HF	Hydrofluidisation Freezing	
HTC	Heat Transfer Coefficient,	$W \cdot m^{-2} \cdot K^{-1}$
IF	Immersion Freezing	
IQF	Individual Quick Freezing	
MFR	Mass Flow Rate,	$kg \cdot s^{-1}$
MPM	Macroscopic Particle Model	
PCM	Phase Change Material	
PIV	Particle Imaging Velocimetry	
RSM	Particle Imaging Reynolds Stress Model	
SST	Shear Stress Transport	
UDF	User-Defined Function	
UDS	User-Defined Scalar	

Subscripts

ℓ	liquid phase
a	ash
b	bounded water
c	carbohydrate
eff	effective quantity
f	fat
fb	fiber
FP	fluid-particle
i	i-th component
ice	ice
if	initial freezing
n	n-th component
P	particle
p	protein

ref	reference point	
s	solids	
w	liquid water	
wo	total water	

Roman Symbols

$\mathscr{D}$	Mass diffusion coefficient	$m^2 \cdot s^{-1}$
A	Area	m^2
C_D	Drag coefficient	-
c_p	Specific heat capacity	$J \cdot kg^{-1} \cdot K^{-1}$
D	Diameter of spherical sample	m
d	Diameter of orifice	m
F_D	Drag force	$kg \cdot m \cdot s^{-2}$
H	Orifice-stagnation point distance	m
K	Turbulence kinetic energy	$m^2 \cdot s^{-2}$
k	Thermal conductivity	$W \cdot m^{-1} \cdot K^{-1}$
L_0	Latent heat of fusion of ice	$(333\,600 \; J \cdot kg^{-1})$
S	Orifice-orifice distance measured from their centres	m
T	Temperature	K
t	Time	s
u	Velocity component	$m \cdot s^{-1}$
V	Volume	m^3
v	Volumetric fraction	$m^3 \cdot m^{-3}$
x	Mass fraction	$kg \cdot kg^{-1}$
z	Sphere-sphere distance measured from their surfaces	m
Nu	Dimensionless Nusselt number	-
Pr	Dimensionless Prandtl number	-
Re	Dimensionless Reynolds number	-

Greek Symbols

μ	Dynamic viscosity	$kg \cdot m^{-1} \cdot s^{-1}$
ω	Specific dissipation rate	s^{-1}
ρ	Density	$kg \cdot m^{-3}$
τ	Tortuosity	$m^1 \cdot m^{-1}$
ε	Porosity	$m^3 \cdot m^{-3}$

Chapter 1

Introduction

1.1   Background

The food and cold-chain sector in European and worldwide economy is a still grow-
ing branch of industry and an important factor to satisfy the basic needs of modern
society. According to the latest report published in 2020 by the International Institute
of Refrigeration [1], approximately 46% of the total world food production should be
refrigerated, but less than half is. That report also states that approximately 13% of
world food production is wasted. Such numbers prove that food processing is the field
where many improvements have to be applied not only in terms of management, but
also in methods and technology.

   Cooling and freezing are the most popular methods used to guarantee the long
shelf life of food products. Lowering the temperature below the freezing point prevents
or reduces the growth of microorganisms and chemical reactions as well as delays
the metabolic processes in food tissues [2]. In fact, freezing is a process that aims to
maintain food quality. However, that depends on the freezing conditions. The rate of
freezing and time of the process strongly affect the final quality of products [3]. If the
freezing rate is high and the process is rapid, fine and uniformly distributed ice crystals
are formed within the food tissues, which is particularly significant in the case of water-
dominant products. As a consequence, mechanical damage may be minimised and
water spoilage after thawing can be reduced [4].

   Numerous innovative methods were developed to increase the freezing rate and
control the crystallisation process. James et al. [5] reviewed the methods considered as
novel and pointed out some of them, which are essentially improvements of existing
methods. These are designed to ensure high values of heat transfer coefficient (HTC).
The authors also introduced more sophisticated methods based on, e.g., employing
magnetic fields or microwaves, using high-pressure or ultrasound. However, the in-
vestment and operation costs in case of them are significant. The survey conducted by
Khouryieh [6] concludes that investment costs are the main limitation for their global
use on an industrial scale.

   As seen, maintaining the high quality of food products requires a method that
ensures a high freezing rate to prevent the growth of large ice crystals. On the other

hand, the investment and operational costs, as well as the power consumption, must be at the acceptable level for any novel method to be used in the food processing industry.

1.2   Literature survey

1.2.1   Food freezing phenomenon

During the freezing process of food products, sensible and latent heat is removed. Sensible heat removal is associated with temperature lowering, whereas latent heat is related to the phase change process, i.e., the liquid water transition into ice. In fresh food products, the mass fraction of water is often dominant. For fruits and vegetables, the water content is in the range of approximately 75%, e.g., bananas, up to over 90%, e.g., strawberries, radishes, tomatoes [7]. It emphasises how important the issue of ice crystal growth is.

In analyses related to the food freezing process, it is fundamental to characterise the equilibrium between the liquid state and solid state water within the analysed range of temperatures. It is well known that in the case of pure water, crystallisation occurs isothermally, that is, the water solidifies at a constant temperature, which is 0°C under atmospheric pressure. However, in the case of food products, the freezing proceeds in another way. First of all, the *initial freezing temperature* (T_{if}) is lower than 0°C, due to the presence of other components such as carbohydrates, fats, proteins, etc. For fruits and vegetables, the initial freezing temperature is close to 0°C. In case of potatoes it is approximately -1.65°C, depending mainly on the water content, while for other types of food products it can be lower. For example, for various fish, it remains below -2°C and, according to the literature data [7], for some types of cheese, it is estimated that it is even below -10°C. After reaching the initial freezing temperature, the liquid water crystallisation process starts. It is worth underlining that the phase change in food products does not occur at a constant temperature. It is a result of a change in the concentration of liquid water as the freezing progresses. The higher the amount of water that is crystallised, the more concentrated the mixture of liquid water with dissolved solutes is and consequently, the equilibrium temperature of the phase change is depressed. The literature offers different formulas to determine the temperature-dependent functions that describe the ice content in food products. Some of them are based on theoretical analyses, e.g., on Raoult's law [7]. However, the most commonly used for fruits and vegetables is the formula proposed by Tchiegov [8], which is an empirical relationship based on experimental data.

As mentioned, the freezing of food products occurs gradually and the balance between the liquid and solid phases depends on the temperature. It results in a characteristic temperature curve, shown in Fig. 1.1. In this curve, typical for the thermal centre of food products, several characteristic points and stages may be distinguished. The first phase of food freezing is the cooling period when the temperature is reduced and the sensible heat is removed. After reaching the initial freezing temperature, the

liquid water starts to crystallise and the second phase starts. The beginning of the freezing process is nearly isothermal. In this stage, most of the liquid water crystallises and, therefore, most of the removed heat is related to the latent heat. This characteristic part of the freezing curve is called *the freezing plateau.* Along with the process, the intensity of the liquid water crystallisation decreases and the temperature is getting lower. Finally, the thermal equilibrium between the food product and the environment is reached or nearly reached and the process is considered as completed. It is worth noting that the shape of the curve depends on the food product type and size, water content, the exact location of the temperature observation (surface temperature, mean temperature, thermal centre temperature), temperature difference, and the intensity of the freezing process. In addition, between the cooling and crystallisation phases, a characteristic phenomenon can sometimes be observed, which is supercooling. This phenomenon is based on the delay in the growth of ice crystals. The temperature is reduced below the freezing temperature without phase change until, at some moment, the crystallisation is initiated, and the temperature rapidly increases.
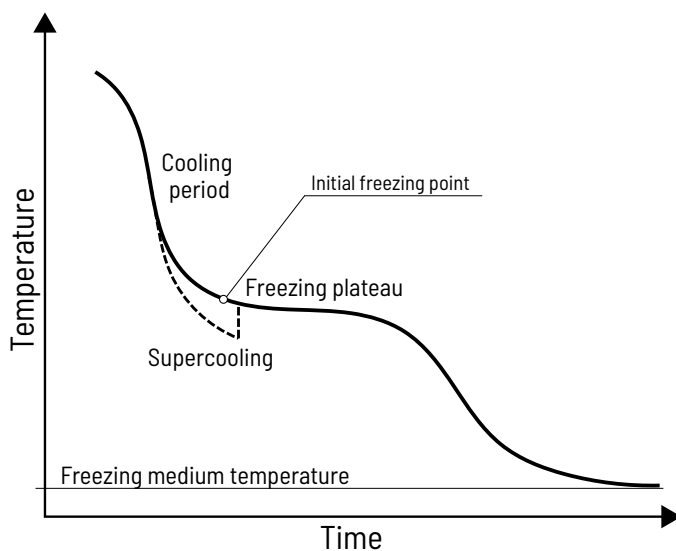
FIGURE 1.1: Temperature at the thermal centre of a water-rich food product during the freezing process.

1.2.2   Food freezing time determination

In industrial practice, food freezing time is one of the most important parameters regardless of the method used for the process. As discussed above, it affects the quality of food products, but is also related to operational costs and energy consumption. Simple analytical or semi-empirical methods to estimate food freezing time are available in

the literature and are used in industrial practice. The first and the most common was proposed in 1913 by Plank [9] for basic shapes. This method has numerous assumptions, e.g. one-dimensional heat transfer, constant properties of the food, or latent heat removal at the constant temperature. Most of the methods developed further are modifications of Plank's equation, e.g., proposed by Cleland and Earle [10] which uses a different concept of equivalent heat transfer dimensions or by Mascheroni and Calvelo [11] which identifies the precooling, phase change, and tempering periods. A more recent method by Pham [12] based on Plank's equation deals with the precooling and freezing heat separately. It is known to be one of the simplest in implementation and the most accurate among other analytical or empirical approaches.

In the review by Pham [13], more advanced approaches were compared, namely the numerical methods for dealing with food freezing analyses and were assessed in terms of their numerical accuracy, time-stepping schemes and other aspects. Pham's quasi-enthalpy method [14] applied for finite-difference method (FDM) and finite-element method (FEM) was identified as very useful due to its accuracy and computational efficiency. In numerical simulations, the phase change may be resolved using different techniques [15]. Latent heat can be defined as a separate source term in the energy balance equation or can be included in the formulation of the food heat capacity as an apparent heat capacity. The latter describes the temperature change of the food product during both sensible and latent heat release. As a result, no additional terms are needed to determine the phase change phenomenon. The drawback of this method is the possibility of latent heat underestimation [2]. Nevertheless, this method was used to take into account the phase change phenomenon that occurs within the food product due to its robustness and widespread usage in studies regarding food freezing and in different applications, e.g., heat transfer with phase-change materials (PCM).

1.2.3 Well-established methods for food freezing

Traditional cold-air based methods

The freezing in a cold air environment is a well-known and common way used for freezing of different types of foods. Several methods can be distinguished, for example, chest freezing or air blast freezing working in batch or continuous mode with some variations related to the freezing unit design like belt or spiral freezers [16]. In all these techniques, different food products (meat carcasses, fish, vegetables, packaged products) are stored in a chamber or transported through the tunnel under significantly reduced air temperature (even at -50°C). The air is still, or the flow can be forced by fans (air blast method) to enhance the convective heat transfer.

That group of freezing methods is well known and fits well for numerous types of food products. Freezing in cold air has numerous advantages: versatility, ease of maintenance, low capital costs, and high throughput [16]. However, numerous drawbacks of these methods also exist: substantial energy consumption needed for fans and the air refrigeration, low HTC values that result in low freezing rate and

decreased quality of products, significant dehydration of foods (2%-3% weight loss [17]) and the ice accumulation at cold surfaces of the refrigeration equipment.

Air fluidisation freezing

A further modification of the air-blast freezer where the stream of cold air is used for food freezing is the fluidisation freezing. High-velocity air jets are passed through the mesh conveyor upward the bed of granular foods, and consequently, higher HTCs are achieved, which allows for food products rapid freezing [16]. The characteristic feature of that method is the movement of individual small food products within the bed, which allows for uniform freezing and prevents the products from sticking together. The term *individual quick freezing* (IQF) was used to characterise that aspect, which is favourable in terms of the food product quality and appearance [3].

The method of air fluidisation guarantees a higher quality of food products in comparison to other methods that employ cold air that were previously introduced. In addition, the process time is shorter, which is another advantage. On the other hand, only small and granular food products benefit from this technique. The energy consumption for powering fans and refrigerators is significant and the water loss issues are still present in air fluidisation freezing [17].

Immersion freezing in liquid medium

In addition to freezing in cold air, there are methods that are based on freezing of food products in a liquid environment. Immersion freezing (IF) is a simple technique in which food products are submerged in a proper liquid that has a temperature low enough to guarantee the freezing of foods. The most popular solutions used in that method are aqueous solutions of sodium chloride, calcium chloride, ethanol, or sugar [18]. Such freezing is effective as a result of the liquid state of the refrigerating medium, which enables reaching much higher HTC values than in the case of a forced flow of air. In the case of IF under free convection conditions, HTC exceeds 200 $W \cdot m^{-2} \cdot K^{-1}$ [18]. Furthermore, the entire external surface of a food product is in contact with the freezing medium [19]. Relatively small food products, i.e., vegetables, fruits, seafood, poultry [18], are frozen with IF because in the case of high HTC, internal heat resistance limits the freezing if the size of foods is large. Consequently, only small food products can be frozen rapidly with IF under IQF conditions [3].

The method of IF has a number of advantages: very high HTCs resulting in better food quality and a short process time, no water loss, and energy savings with respect to air-freezing methods [5]. However, there is a major disadvantage of freezing in a liquid solution, which is the uncontrolled absorption of the solution by a food product. Freezing of packed foods prevents mass transfer in IF [19], but for very small food products (e.g., berries), such a method is not practical.

1.2.4   Method of hydrofluidisation

The preceding paragraphs provide a brief description of selected methods of food freezing. Their physical and thermodynamical principles are the same, which is the convective heat transfer based on the cooling and freezing of food products using a cold medium. On the other hand, all these methods are characterised by different conditions, e.g., the freezing medium phase and the convection regime. A method that combines the advantages of air fluidisation and immersion freezing in liquid medium is known as the hydrofluidisation method (HF).

The origin of hydrofluidisation freezing

The highest freezing rate among the methods described previously is achieved by IF, because the free convection in liquid medium is characterised by HTC that is an order of magnitude higher than forced convection in gases and two orders of magnitude higher than the free convection in gases [20]. Therefore, the opportunity to achieve an even higher HTC is to go a step further and conduct the freezing process in a liquid environment under forced convection conditions.

The method of hydrofluidisation was first proposed by A.G. Fikiin as a technique for intensive chilling and freezing of fish [21]. The author proposed a system design and performed an extensive experimental study to assess the performance of the proposed method with respect to well-known techniques. HF allowed to achieve up to triple higher HTC than IF in case of fish cooling and freezing. Consequently, it resulted in a reduction of the freezing time by half.

The author of that very first study focused on the HF method highlighted the following advantages of the method:

- The highest HTC values among other conventional methods for food freezing.

- Shortened freezing process time and short period of residence within the _critical zone of water crystallisation._

- Excellent quality of food confirmed by the group of third-party experts.

- Ease of maintenance and low labour costs.

- Possibility to use more efficient one-stage refrigeration units to cool the liquid medium (to approx. -22°C) with respect to conventional installations where the air has to be deeply cooled (to approx. -45°C) using, e.g., multistage cascade refrigeration systems.

- Lower investment and operational costs due to the use of efficient and inexpensive one-stage refrigeration systems.

Fig. 1.2(a) presents the simplified scheme of the hydrofluidisation unit showing the refrigerating liquid circulation loop. It is worth noting that the first proposition and

subsequent studies describing lab-scale units were in some aspects different, especially in terms of the equipment and system used for the food products and samples transportation. The main part of the HF unit consists of the tank filled with an appropriate liquid, which should be selected to reach the desired temperature of cooled or frozen food products. The tank is equipped with orifices or nozzles at its bottom, as shown in Fig. 1.2(b). The refrigerating medium (cold water for the cooling process or aqueous solution for freezing) is pumped through orifices and creates impinging jets to achieve the turbulent flow within the tank with food products. Consequently, very high HTCs can be reached to effectively freeze small food products.
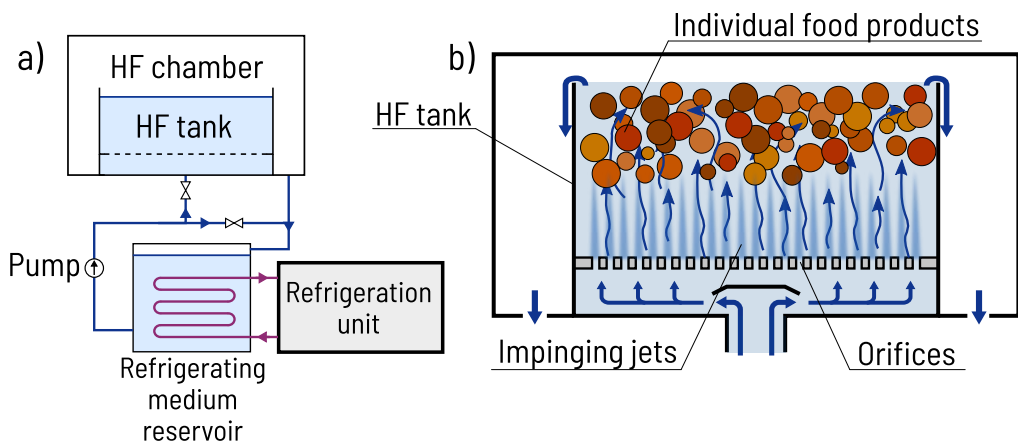
FIGURE 1.2: Scheme of (a) HF freezing unit (simplified) and (b) the process of food products hydrofluidisation freezing in HF chamber.

Determination of HTC in HF method

Numerous studies by several authors were aimed at extending the knowledge on the novel HF method. As mentioned before, the characteristic feature and main advantage of hydrofluidisation freezing is the possibility to achieve enormously high heat transfer coefficients which allow for rapid freezing.

The study of K.A. Fikiin and A.G. Fikiin [22] presents the results of the experimental investigation of HF. In that work, ice slurry was used as a refrigerating medium, which enhances HTC due to the latent heat being a result of the melting of ice, which is the refrigerating medium component. The authors used a medium having a temperature of -25°C and reported HTCs in the range from 1 000 $W \cdot m^{-2} \cdot K^{-1}$ to 2 000 $W \cdot m^{-2} \cdot K^{-1}$. Such values allowed to significantly lower the time required for small foods freezing. For example, strawberries or plums were frozen from the initial temperature of 25°C down to -18°C in 8 min, cherries and raspberries required from 1.5 min to 3 min, while the smallest products, i.e., peas and cranberries needed only 1 min. The authors

emphasised the potential of the method and indicated the interest of industry and academia. They expressed the need for further research of the fundamental processes related to heat transfer, fluid flow, and biochemical phenomena.

To investigate the parameters influencing the HTC in the HF method, Verboven et al. [23] performed an experimental study in a laboratory scale using spherical samples having a different size and made of aluminium in a scenario with a fixed position of samples. The authors used a water-based solution of ethanol and glucose at different temperatures (from -20°C to 0°C) and flow rates from 5 litres per min to 15 litres per min. They indicated the parameters affecting the HTC, i.e., the size of samples (diameter of sphere), refrigerating solution temperature, and flow rate. The HTC values they obtained were in the range of 143 $W \cdot m^{-2} \cdot K^{-1}$ to 1 548 $W \cdot m^{-2} \cdot K^{-1}$. The authors of that paper indicated that numerical tools such as computational fluid dynamics (CFD) would be beneficial for investigating turbulent fluid flow in the HF system.

To determine the effect of geometrical configuration of the HF system on HTC, a similar study was performed by Peralta et al. [24] in the lab scale using spherical copper samples at a fixed position. An aqueous solution of NaCl was used as a refrigerating liquid in this system. The authors proposed a correlation for the Nusselt number to characterise HTC in a simplified HF system based on Reynolds and Prandtl numbers and characteristic geometrical parameters in dimensionless form, i.e. *H/d* and *d/D*, which express ratios between the orifice-sphere stagnation point distance (*H*), orifice diameter (*d*), and the spherical sample diameter (*D*).

Numerical modelling of HF process

The very first attempt to employ numerical tools for the hydrofluidisation method study was made by Peralta et al. [25]. The authors developed a CFD model of the unit presented in their previous experimental work in a basic configuration with only one spherical sample in a fixed position above a single orifice. Their model was validated based on experimental measurements of the metal sample cooling process under turbulent flow of the refrigerating medium. This model allowed to investigate the refrigerating medium flow field distribution and the effect of the turbulence occurring in HF tank.

The same group of authors published several consecutive papers that were the continuation of the firstly published CFD paper describing their HF system. The artificial spherical sample was replaced with a real food product, i.e., potato, of the same shape in the CFD model presented in [26]. The authors investigated the phenomena of heat and mass transfer during the freezing of food products. In that work, the fluid domain was simulated by the CFD model, while the food product was solved using a well-established model formulated previously by Zorrilla and Rubiolo [27], [28] to assess the mass absorption from the solution during IF. According to Peralta et al. [26], the freezing time in HF (assumed as the moment when the centre of the sample reaches -5°C) was approximately 8 min and 5 min during the freezing in a refrigerating

medium with a temperature of -10°C and -15°C, respectively, for a spherical potato sample with a diameter of 20 mm. The results of the authors showed that mass transfer through the food is the most intensive until the phase change process starts and the average concentration of NaCl was in the range from 10 g to 20 g per kg of food product, depending on the conditions.

In the next paper of the same group [29], a more complex scenario was numerically analysed to determine HTC and other physical quantities in the HF unit equipped with numerous orifices. In that paper, an array of 13 spheres was present in the HF unit. The realistic movement of food samples was introduced in the following paper by Orona et al. [30], where food products were simulated with the discrete phase model (DPM). The authors employed the discrete element method (DEM) to include the physics of the mutual collisions of food samples during the HF process. This was the most realistic and advanced numerical model of the HF process developed so far. The authors used it to perform a sensitivity analysis of the main parameters of the HF process [31] and indicated that the geometrical and flow variables affect heat transfer, while mass transfer is dependent mainly on the refrigerating medium temperature.

Challenges for hydrofluidisation freezing method

Apart from the advantages introduced previously, the method of hydrofluidisation has its limitations and disadvantages that need to be addressed. The most important issue, common with the IF method, is the solute uptake. In the case of freezing in a liquid medium, instead of air, components present in the solution are absorbed by the product, which is an unwanted side effect.

A feature of HF that positively reduces the uptake of the solute during freezing is the ability to achieve a very high HTC. During intensive freezing, the surface of the food product freezes rapidly. Frozen structure of food products reduces the effective diffusivity and, consequently, the mass transfer is minimised. Therefore, it is worth the effort to enhance the convective heat transfer coefficients and to minimise the unwanted mass absorption during the process. Simultaneously, more intensive convection reduces the time of the freezing process. Therefore, the enhancement of HTC in any immersive method of food freezing is a key factor in improving the process.

Another aspect worth reviewing is the selection of the refrigerating medium used for the HF process. Several solutions were used in the studies done so far: salt brine [21], NaCl aqueous solution [24], ice slurry with alcohol and sugar [22] and the ternary mixture of alcohol, sugar and water [23]. Similar solutions based on salt, alcohol, sugar, or glycerol were used in studies related to IF [18]. The solution used for the HF process cannot be harmful, should not worsen the flavour and taste of the food product, and has to guarantee an appropriately low temperature for the freezing process. Some types of solution are suitable for some of food products, e.g., according to Fikiin [32], salt brines are used for the freezing of fish, vegetables, and meat, while sugar-based solutions are suitable for the freezing of fruits. Furthermore, some products can benefit

from additives, e.g., additional sugar can improve the taste of desserts. A golden mean has to be found in the formulation of the solution concentration. On the one hand, it has to be sufficiently high to maintain the liquid state of the refrigerating medium at a desired temperature. On the other hand, higher concentration induces the absorption of solutes. Thermophysical properties of the fluid are significant as well; that is, an excessive viscosity requires a higher power for the medium pumping, and the density of the fluid affects the buoyancy of food products submerged in the HF tank.

An aspect that needs to be underlined is the fact that the HF method is beneficial for small food products, e.g., berries, peas, chopped products, or small fish or seafood, characterised by small internal resistance for heat transfer [32]. If the food product is appropriately small, the freezing time can be significantly reduced due to the minimisation of the external resistance for heat transfer. In the case of bigger products like poultry or beef carcasses, HTC enhancement allows for a minimal improvement of the freezing process [5]. On the other hand, if the shape of food products is relatively uniform, small food products are characterised by a high A/V parameter. It characterises the relation of the external area of the sample to its volume. An analysis carried out in this thesis proved that in the case of very small food products, i.e., spheres having a diameter of 5 or 10 mm, the unwanted solute concentration in food products can be significantly high after the freezing, even if the process is rapid. Therefore, it is worth assessing the potential of the HF method for the freezing of food products of different sizes.

1.3   Motivation and objectives

The literature review shows that there is a research gap in the study of HF method. In particular, the complex process of fluid flow during the simultaneous process of the refrigerating medium turbulent flow, and the dynamics of individual food samples were scarcely examined so far. Moreover, no attempt was done to compare various aqueous solutions in terms of the realistic fluidisation effect during HF and simultaneous heat and mass transfer during food freezing. According to Verboven et al. [23], CFD would be a very favourable tool to describe all the processes of fluid flow, heat transfer, and mass transfer occurring during HF process. It is worth noting that such numerical tools are advantageous because they allow to examine the selected parameters of any process effectively without conducting extensive experimental campaigns that are demanding in terms of cost and time.

Therefore, this thesis is aimed to develop tools that are able to simulate different aspects of HF technique and to perform a comprehensive analysis of this novel method dedicated for freezing small food products. The scientific problems discussed in this work are related to the turbulent flow in the HF tank where food products are frozen individually as well as to the rapid freezing process itself where simultaneous heat and mass transfer processes are present. Hence, the following research activities were formulated to reach the objectives of this thesis:

- Development a well-validated CFD model of the impinging jet turbulent flow in a hydrofluidisation tank and its further extension into the full-size HF tank model with multiple orifices and jets.

- Formulation of the numerical model describing the freezing process of fruits and vegetables considering the most accurate formulas describing the properties of a real food product.

- Modelling of the real hydrofluidisation process considering the realistic movement of individual food samples induced by the fluid flow, including the interactions with the entire group of frozen products.

- Development of a conjugated numerical model which describes the freezing process of a food product, including the mass absorption from the liquid medium into the food product interior.

1.4   Scope

The thesis consists of the following chapters:

Chapter 1 is this chapter.

Chapter 2 is dedicated to the simplified flow scenario numerical analysis that was possible to be validated experimentally. For that reason, a test rig was built and an experimental campaign was conducted. A comprehensive study devoted to the experimentally determined flow field present in the test rig was performed by Palacz et al. [33]. Selected results were used for the validation of the CFD model developed during this research activity. At this stage, characteristic velocity profiles were described for a basic case with one orifice and a spherical sample at a fixed position above the orifice. Thus, the fundamental flow character, namely, the liquid jet in orifice-sample configuration, was analysed. It allowed for the selection of an appropriate turbulence model for the HF system and the assessment of the accuracy of the CFD model that describes the flow of refrigerating liquid in the HF process. The PIV validation confirmed that the developed numerical model predicts the fluid flow with high accuracy.

Chapter 3 describes a more complex flow configuration that was simulated by extending the previously developed CFD model into the full-size HF tank present in the test rig. At this stage, 49 or 64 orifices creating the jets were present in the tank and a static configuration of 7 spherical food products in a fixed position was considered. In that chapter, the second research problem was addressed, which is the formulation of the food freezing mathematical model. To guarantee the reliability and stability of the model, an enthalpy-based energy equation was employed. Properties of the potato, assumed as the reference food product, were based on its composition with the emphasis on the water content that was determined experimentally. The most accurate expressions describing the ice content along with the freezing process, effective thermal conductivity, and apparent heat capacity were used. In the analysis conducted at this

stage, various geometrical configurations, as well as different temperatures of the refrigerating liquid were examined. Moreover, the method of hydrofluidisation was compared with immersion freezing, characterised also by freezing in liquids but under conditions of significantly lower HTC.

Chapter 4 is focused on development the state-of-the-art CFD model of hydrofluidisation process. It was based on a novel macroscopic particle model (MPM) approach where the individual food products were treated in Lagrangian frame of reference and the refrigerating medium flow was fully resolved. At this stage, the investigated parameters were the refrigerating liquid mass flow rate, type of liquid, and HF tank load. Three different liquids with different properties were compared, i.e., the water-ethanol solution (mass concentration 30%), the water-glycerol solution (mass concentration 40%), and the ternary solution of water-alcohol-glucose (mass concentration 15%/25%). The hydrodynamics of the HF system and the convective heat transfer were analysed for various conditions. Movement of the food product in a liquid medium was validated based on high-speed camera recordings in the basic scenario, and the HTCs determined using CFD-MPM model were verified using the results obtained during the previous analysis with the disabled movement. During this research activity, HTCs possible to obtain during HF process were determined numerically and characterised.

Chapter 5 deals with the simultaneous heat and mass transfer analysis within the food product during freezing using HF method. The model of mass absorption was based on a porous body approach where the solid skeleton, liquid phase, and ice are distinguished. Mass transfer equations were formulated based on Fick's law for each analysed component separately. This research task was aimed to characterise the freezing time and the total mass absorbed from different aqueous solutions under different temperatures by food products having a different size. Such analysis allowed to characterise the conditions that allow to limit the unwanted mass transfer. Consequently, the results are focused on two aspects, i.e., the freezing time and the total mass absorbed during the HF process. These results may be treated as quantitative indicators related to the frozen food product that may allow the final consumer to assess the quality of HF-treated foods in certain conditions using a specific aqueous solution used as the refrigerating medium.

Chapter 2

Validated model of turbulent flow in hydrofluidisation system - Paper I

The characteristic feature of the HF method is the forced flow of the refrigerating liquid over food products. Significant velocity of the fluid and turbulent flow pattern guarantees enhanced convective heat transfer that results in rapid freezing. For that reason, an accurate prediction of the refrigerating liquid flow was considered as a fundamental aspect of the whole hydrofluidisation process and further modelling of food freezing.

As summarised in the experimental study of the HF method by Verboven et al. [23], CFD analyses are desired for a more detailed investigation of the flow field in the HF method. Although Peralta et al. [25] developed a CFD model of the fluid flow in a simplified HF system followed by numerical analyses of more detailed scenarios, a comprehensively validated model of the fluid flow has not been published yet.

2.1 Test rig for the study of the hydrofluidisation method

Because a comprehensive investigation of flow characteristics in the HF method is missing in the literature, a test rig was designed under the framework of the *CoolFood* research project for both experimental research and numerical investigation of the HF method, which is the subject of this thesis. The test rig is presented in Fig. 2.1. The most significant part of it is the HF chamber with transparent walls that allow the PIV measurements to be carried out. The HF process occurs within the HF tank that is placed inside the chamber. In addition to that, the test rig is equipped with the coolant reservoir, a pump with inverter, and Coriolis-type mass flow metres for precise control of the mass flow rate of the refrigerating medium. During the PIV measurements, which were discussed in detail in the study of Palacz et al. [33], the laser used to highlight the 2-D cross section was placed on the left-hand side of the test rig and the camera used to capture the velocity field was positioned in the front of the HF chamber.

The exact process of the flow field and the further freezing of food samples is carried out in the HF tank installed in the HF chamber, as presented in Fig. 2.2. The refrigerating liquid flows into the chamber through orifices drilled in the steel plate located at the
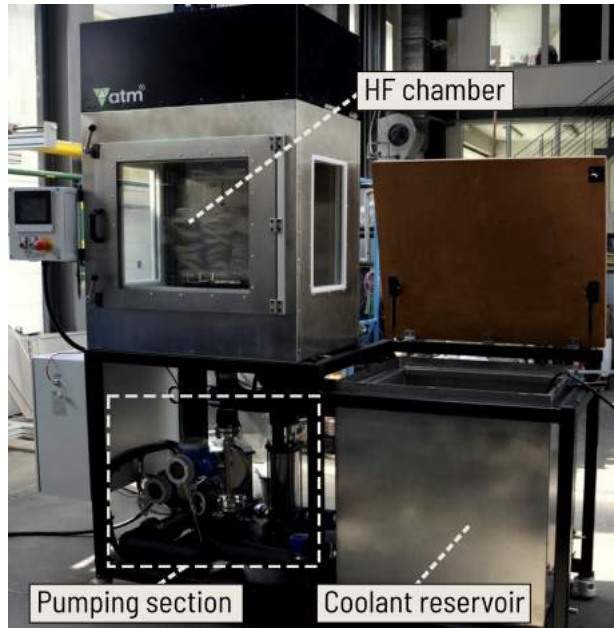
FIGURE 2.1: Laboratory test rig built for experimental activities of *CoolFood* project and for the validation of numerical models.

bottom of the tank. The plate is replaceable to allow for the investigation of different scenarios with a variable number of orifices and jets. In the basic scenario discussed in this chapter, one orifice was present to create a single jet striking the stagnation point of one spherical sample having a diameter D of 20 mm and made of copper. Two values of the orifice diameter d were tested, namely, 3 mm and 5 mm. As seen in Fig. 2.2, the spherical sample is attached to the frame that allows moving up and down to change the H value which is the distance between the orifice and the stagnation point on the sphere bottom. The range of that parameter was from 50 mm to 70 mm in this analysis.

2.2 Formulation and validation of the CFD model

The first numerical model presented in this thesis was developed using the commercial ANSYS Fluent software for CFD simulations. It solves a set of governing equations, which in this case were: continuity, momentum, and energy balance along with additional equations for the turbulence modelling. At the stage of the fluid flow model formulation, verification and validation, two approaches were considered, i.e. K-ω SST model and the Reynolds Stress Model (RSM). The first is a popular approach, widely used for wall-bounded flows or flows over curved surfaces [34]. The second approach for turbulence modelling is characterised by direct solving of the Reynolds stresses as

FIGURE 2.2: Flow of the refrigerating liquid over the artificial sample
inside the HF tank at the test rig.

transport equations [35]. The numerical results obtained using these two turbulence models were compared with the velocity fields obtained experimentally, and finally, K-ω SST model was selected as more appropriate one for modelling of fluid flow in the HF process.

Several aspects were analysed to define the numerical model of the fluid flow in the HF tank:

- Dimensionality of the numerical domain. Due to the symmetrical character of the orifice-sample relationship, the 2-D axisymmetric and 3-D geometrical domains are supposed to predict the same flow field. Consequently, that model can be used in both 2-D axisymmetric and 3-D domains.

- Inlet boundary condition formulation. An attempt was made to simplify the geometrical domain by defining the velocity-based inlet boundary condition at the orifice. The results proved that it affected the velocity profile along the jet axis. Therefore, the inlet was defined far below the orifice and no simplification of the geometrical domain below the orifices was applied in the numerical mesh.

- Selection of the turbulence model. The two approaches for turbulence modelling were tested and compared with the PIV measurements. As mentioned, K-ω SST model provided more accurate results, therefore it was selected as an appropriate approach for further analyses.

One of the most significant results of the analysis introduced in this chapter is the comparison of the velocity field shown in Fig. 2.3 for two different cases (a) and (b), which are characterised by different orifice diameters (3 mm and 5 mm), positions of the sample above the orifice (60 mm and 70 mm) and different mass flow rate (0.051

kg·s^{-1} and 0.113 kg·s^{-1}). As seen, the developed numerical model was able to predict the velocity flow field with high accuracy when K-ω turbulence model is used. The characteristic pattern in the two flow regions was well predicted, i.e., the region of the jet and the area of the stream detachment from the wall. In addition, local velocity values were compared. In case of the jet region, three points (Pt1-Pt3) located in the jet axis 3 mm, 4 mm, and 5 mm below the sphere stagnation point were selected, and as a result, the average error of the velocity prediction by the model at these points related to the measurements was approximately 9% and 3% for the two test cases presented in Figs. 2.3(a) and (b). In case of the second flow region, other points (Pt4-Pt6) were selected. Pt4 was located 1 mm away from the sample surface as seen in Fig. 2.3(a), while Pt5 and Pt6 were located 3 mm and 6 mm above Pt4, respectively. Eventually, for these three points, the average error was approximately 4% and 25% for the same two cases presented in the figure below.
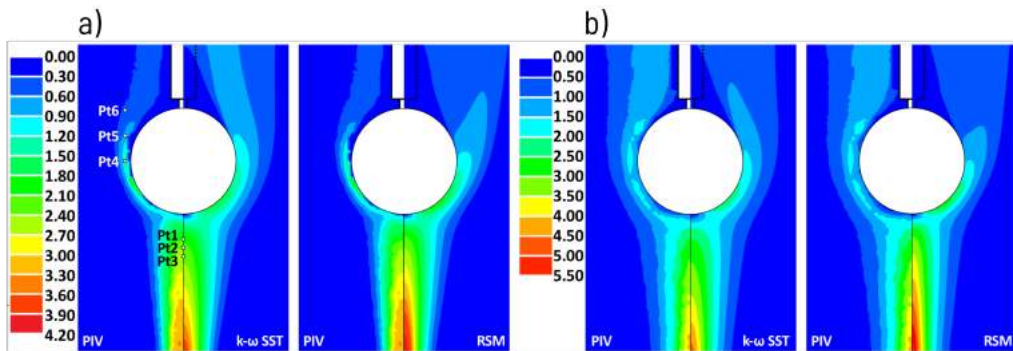
FIGURE 2.3: The velocity contours in m·s^{-1} obtained using two approaches for turbulence modelling compared with the experimental results for two selected cases characterised by different conditions (Source: [36]).

2.3   Conclusions for the next steps

The major outcome of this part of the research is the confirmation that the developed numerical model was able to predict the velocity field well with a high accuracy. Only the local velocity values in one test case were significantly different from the experimental results. However, it is worth pointing out that the Pt4-Pt6 points selected for the comparison were located only 1 mm from the spherical sample surface in a region with very high gradients of velocity.

In addition, the numerical campaign conducted at this stage confirmed that the characteristic velocity profile along the jet axis was consistent if the H/d ratio was

constant, even when the orifice diameter d was changed. It suggests that the orifice diameter can be a variable geometrical parameter in the case of HF tank design.

Chapter 3

Development of the food freezing numerical model - Paper II

The next step of the numerical analysis of the HF method was the formulation of the food freezing model coupled with the extended CFD model of fluid flow in the HF tank. Based on the experimental validation of the basic flow scenario that was investigated previously, it was assumed that a more comprehensive flow of jets in HF tank shall be modelled with appropriate accuracy as well. Additionally, at this stage of the numerical study, local temperatures at two characteristic locations within the food product were compared with the experimentally obtained values for a more careful confirmation that the numerical results are reliable.

3.1 Assumed conditions of the flow in the HF tank

The extension of the fluid flow conditions in the analysed scenario was based mainly on the assumption that the HF tank is equipped with 64 orifices instead of a single orifice. For that reason, the axisymmetric domain was replaced by a 3-D geometrical domain that included a number of orifices in the HF tank, but the numerical domain was reduced to ¼of the real geometry due to the symmetrical geometry of the tank. Such a number of orifices is a reasonable representation of a full-size tank for the HF method.

At the current stage, a group of food products was assumed to be present within the HF tank in a fixed position. Seven spherical samples were placed at a polar angle, and the middle sample was assumed to be a representative sample from the whole group. Because no movement of food samples was assumed at this stage, the fluid flow field could be assumed as quasi-steady, and the distribution of HTC on the food sample surface could be assumed to be stabilised after a few seconds of the process when the boundary layer was stabilised. The first objective of this stage was the sensitivity analysis to determine which geometric parameters can significantly affect the HTC during the process:

- The position of the food product group above the orifices (H) and the H/d ratio.

- Distance S between each row of orifices that determines the design of the HF unit inflow section.

- Distance z between individual food samples in a small group of food products.

- Diameter d of orifices for selected cases.

- Position of food samples with respect to the array of jets.

This analysis proved that the H/d ratio and the S distance affect HTC much more than other parameters. Therefore, in designing the HF system, one must take into account the size (height) of the HF tank to determine the appropriate orifice diameter and the number of orifices at the bottom of the tank.

3.2   Food freezing phenomenon modelling

Physically, the food product freezing model formulated for the HF analysis in this thesis can be characterised by the time-dependent heat transfer equation with the assumption that mass transfer is neglected. The latter phenomenon is described in Chapter 5 and the conjugated heat and mass transfer is the subject of final analyses. Thus, the analysis described in this chapter is limited to heat transfer.

From the thermodynamics and heat transfer point of view, the fundamental in the freezing process of food product analysis is the Fourier-Kirchhoff equation for the unsteady heat conduction within the solid material. An additional aspect in this particular process is the thermal effect of the phase change.

For a better understanding of the development of the food freezing model, the properties of the food product are first characterised. The formulation of the heat balance equation and its numerical implementation are described afterwards.

3.2.1   Properties of the food product

In the formulation of the mathematical model of food freezing, the first step is to define the properties of the selected food product. In this case, the fundamental aspect is the composition. To guarantee a relevant accuracy in freezing analysis, it is sufficient to consider the following components: water (in liquid or solid state), protein, fat, carbohydrates, fiber, and ash. In the food product model developed for this study of the HF method, the composition of potatoes was based on the popular ASHRAE database [7]. However, to minimise the error related to the inaccurate assumption of the water content, which is fundamental in the analysis of the freezing process, the water content of potates that were locally accessible for the experiments was determined experimentally within the framework of the *CoolFood* research project. Eventually, the composition of this food product selected for the modelling of the freezing process was assumed as listed in Table 3.1.

TABLE 3.1: Mass fractions of the food product components for the potato sample.

Water	Protein	Fat	Carbohydrate	Fibre	Ash
x_{wo}	x_p	x_f	x_c	x_{fb}	x_a
80.05%	1.97%	0.09%	15.53%	1.52%	0.84%

As seen, the moisture represents approximately 80% of the potato mass fraction. As outlined in the Chapter 1 of this thesis, during the process of food freezing, the liquid water crystallises gradually as the temperature is lowered. The characteristics of all the properties as a function of temperature are crucial for the accurate modelling of food freezing. Therefore, the mass fraction balance for the liquid water and the ice was required to be defined prior to all the thermophysical properties formulation.

In theoretical analyses related to the ice content in frozen products, two formulas are used most often, i.e., the analytical formula that is based on Raoult's law [7] and the empirical relationship by Tchigeov [8]. The latter was recognised as more accurate for the prediction of the ice content in water-rich foods such as fruits and vegetables [37]. Therefore, it was used to characterise the ice and liquid water content in the numerical model presented in this thesis and is given in Eq. (3.1).

$$x_{ice}(T) = \frac{1.105 x_{wo}}{1 + \frac{0.7138}{ln(T_{if} - T + 1)}} \tag{3.1}$$

where x_{ice} is the mass fraction of ice, x_{wo} is the total mass fraction of moisture, T_{if} is the initial freezing temperature in °C, and T is the temperature of the food product in °C.

The initial freezing temperature that indicates the point where the ice begins to appear was assumed to be -1.65°C based on the analysis of the freezing curves obtained during the measurements of the HF process of potato samples. The ice content as a function of the temperature was presented in Fig. 3.1 based on Eq. (3.1).

As a consequence of the prediction of the ice content in the frozen potato sample, the liquid water content in the frozen product can be evaluated using Eq. (3.2).

$$x_w(T) = x_{wo} - x_{ice}(T) \tag{3.2}$$

where x_w is the liquid water content.

The knowledge of the food product composition in the range of temperatures above and below the initial freezing point allows to characterise all the thermophysical properties required to formulate the mathematical model of food product freezing. The first and most important one in the developed model is the specific heat capacity.

A convenient approach for freezing analysis is to formulate the apparent heat capacity for food products [13]. This quantity characterises the sensible and latent heat gain or release during the change of the temperature of the food product. This approach
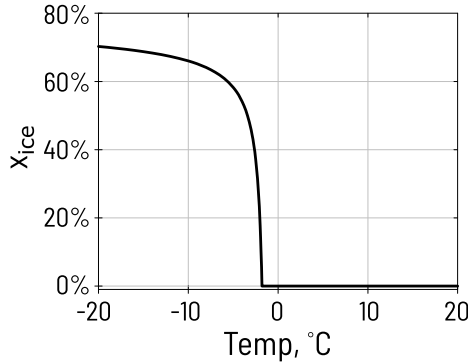
FIGURE 3.1: The ice content in % as a function of temperature in °C
for the potato.

is advantageous for the formulation of the numerical model of freezing because no additional heat source is needed to include the phase change. Thus, only one material needs to be defined in the numerical solver, and the governing energy equation is in the simplest form of Fourier-Kirchhoff's equation for unsteady heat transfer.

In the numerical model, the approach proposed by Chen [38] was used to describe the apparent heat capacity and the specific enthalpy of the food product. Eqs. (3.3) and (3.4) describe the apparent heat capacity of food above and below the initial freezing point, respectively. Consequently, the specific enthalpy is described in that approach by Eqs. (3.5) and (3.6) for the same ranges of temperature.

$$c_p = 4.19 - 2.30x_s - 0.628x_s^3 \tag{3.3}$$

$$c_p = 1.55 + 1.26x_s - \frac{(x_{wo} - x_b)L_0 T_{if}}{T^2} \tag{3.4}$$

$$h = h_{if} + \left(T - T_{if}\right)\left(4.19 - 2.30x_s - 0.628x_s^3\right) \tag{3.5}$$

$$h = \left(T - T_{ref}\right)\left[1.55 + 1.26x_s - \frac{(x_{wo} - x_b)L_0 T_{if}}{T_{ref} T}\right] \tag{3.6}$$

where x_s is the mass fraction of solid components, x_b is the mass fraction of bound water, L_0 is the latent heat of fusion of water (333.6 kJ·kg^{-1}), T is the temperature of the food product in °C, h_{if} is the specific enthalpy of the food product at the initial freezing point evaluated using Eq. (3.6), and T_{ref} is the reference temperature (-40°C).

To have a complete definition of the amount of energy dissipated from the food product during freezing, the density of the food sample has to be determined. In HF analyses, which are the subject of this thesis, the density has been evaluated experimentally. For this reason, cubic samples of potato have been prepared, measured, and weighted. As a result, the average density was evaluated to be 1 062 kg·m^{-3}.

The mechanism that deals with the heat dissipation from the food product during freezing is the heat conduction, which can be expressed by Fourier's law. Therefore, the thermal conductivity of the food product must be determined prior to any freezing analysis. As mentioned, the food product is the composition of substances such as water, carbohydrate, protein, etc. Moreover, the liquid water transforms into ice during the process. For that reason, the effective thermal conductivity has to be formulated using an appropriate approach. Depending on the type of food product (fruit, meat, etc.), structure (porous or solid), and state (unfrozen or frozen), different approaches can be used. For solid vegetables, the formulation of Levy [39] was recognised as appropriate for freezing analysis [40]. In this multistage approach, the first step is the evaluation of the effective thermal conductivity using a more basic parallel formulation considering only the unfrozen components according to Eq. (3.7). At this step, the thermal conductivity of each of the components is based on the formulas proposed by Choi and Okos [41] for all the components of the food product considered in the analysis. Then, Levy's formulation is employed to evaluate the final effective thermal conductivity of the food product with the ice included in its composition as shown in Eq. (3.8). It should be pointed out that in the thermal conductivity formulation, volumetric fractions need to be considered rather than mass fractions because of the spatial character of this property.

$$k_I = \sum k_i v_i \tag{3.7}$$

$$k_{eff} = k_{ice} \frac{2k_{ice} + k_I - 2(k_{ice} - k_I)F}{2k_{ice} + k_I + (k_{ice} - k_I)F} \tag{3.8}$$

with

$$F = \frac{2/G - 1 + 2(1 - v_{ice}) - \sqrt{[2/G - 1 + 2(1 - v_{ice})]^2 - 8(1 - v_{ice})/G}}{2}$$

and

$$G = \frac{(k_{ice} - k_I)^2}{(k_{ice} + k_I)^2 + k_{ice}k_I/2}$$

where k_I is the thermal conductivity of first-stage components, i.e., liquid water, protein, fat, carbohydrate, fibre, and ash, k_i is the thermal conductivity of the i-th single-stage component, v_i is the volumetric fraction of the i-th single-stage component, k_{eff} is the thermal conductivity of food product according to Levy's model, k_{ice} is the thermal conductivity of ice, v_{ice} is the volumetric fraction of ice, and F and G are the functions related to mathematical formulation of Levy's model.

In HF analysis, where small food products are frozen under forced convection, a proper determination of thermal conductivity is of great importance. It is because in such process the convective thermal resistance is minor and practically the heat conduction is the process limiting the heat transfer.

For the potato sample analysed in this thesis, both thermophysical properties discussed above were shown graphically. Fig. 3.2(a) presents the apparent heat capacity

according to Chen's approach and Fig. 3.2(b) presents the effective thermal conductivity based on Levy's equation. As can be seen, the rapid change in these properties occurs at the initial freezing point, where ice starts to form. As a consequence, the numerical solution can be unstable while passing this region. To overcome this, the mathematical model has to be formulated in a certain way.
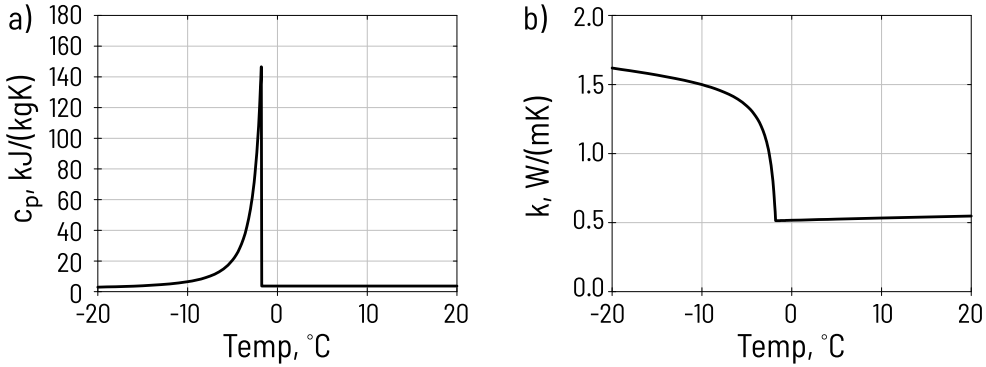
FIGURE 3.2: (a) the apparent heat capacity in kJ·kg^{-1}·K^{-1} and (b) the thermal conductivity in W·m^{-1}·K^{-1} in the function of temperature in °C for the potato.

3.2.2   Energy equation and its implementation

It was already mentioned that the mathematical model of food freezing can be solved using a simple form of time-dependent heat conduction if the latent heat is included in the formulation of the apparent specific heat. However, the consequence of such an approach is a rapid peak in the food product specific heat below the initial freezing point as seen in Fig. 3.2(a). It can lead to significant instability of the numerical model. For that reason, the energy equation was formulated in an alternative way by considering the specific enthalpy as the balanced quantity instead of the temperature [13].

Consequently, the energy balance equation is formulated as in the following Eq. (3.9).

$$\frac{\partial \rho h}{\partial t} - \nabla \left(\frac{k_{eff}}{c_p} h \right) = 0 \tag{3.9}$$

where ρ is the density of the food product, h is the specific enthalpy, t is the time, and c_p is the apparent heat capacity.

That equation had to be implemented in the ANSYS Fluent [42] software used for all the simulations performed during the PhD project. For that reason, the standard heat balance equation was disabled in the software. Instead, the enthalpy-based energy equation was implemented using a used-defined scalar (UDS) along with a set of

user-defined functions (UDF) that were defined to characterise the time-dependent term and the diffusive term of the transport equation for the energy equation in the numerical solver. At the same stage, all the required properties were implemented, namely, density, thermal conductivity, and apparent heat capacity using UDFs.

3.3 Selected results discussion

The results analysed at this stage cover 36 cases used for the CFD model validation that were described in detail in a separate experimental study related to HF freezing [43] and the other 53 cases formulated to investigate the effect of the selected process parameters. First, the accuracy of the numerical model was determined on the basis of experimental measurements of the local temperature in the centre of potato samples and near the surface within the samples. The comparison of the locally measured temperatures is presented in Fig. 3.3 for two selected cases (a) and (b) where a very satisfactory agreement with the experiments was achieved. For both cases in which the potato samples had different diameters (30 mm and 20 mm for cases (a) and (b), respectively), no significant discrepancy can be observed between the predicted freezing curve and the measured temperature. It suggests that the water content in fresh potatoes, the relation between liquid water and ice have been accurately characterised and the models defining thermophysical properties were appropriately selected.
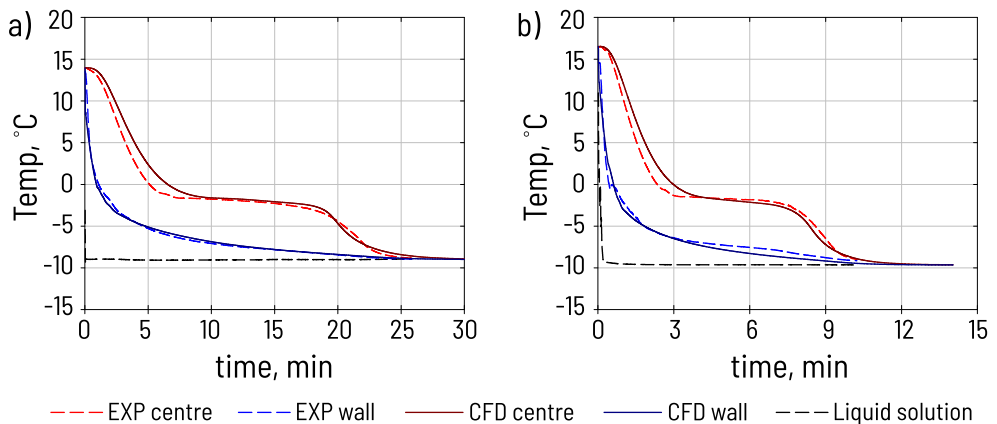
FIGURE 3.3: The comparison of the temperatures within the potato samples at the centre and near the surface during HF obtained experimentally and numerically for two different cases (a) and (b) (Source: [44]).

The further results were related to characterise the effect of different process parameters on the HTC values and the predicted freezing time.

3.4   Conclusions

The general observations from the analysis performed at this stage and presented in the research paper are as follows:

- Geometrical parameters (position of samples, diameter of orifices, etc.) affect the HTC in the HF system. However, within the investigated conditions, i.e., HTC in order of 3 000 $W \cdot m^{-2} \cdot K^{-1}$ to 4 000 $W \cdot m^{-2} \cdot K^{-1}$ and the sample size of 20 mm, the HTC change had a minor effect on the freezing time.

- The temperature of the refrigeration liquid significantly affects the freezing time, e.g., the reduction of the temperature from -10°C to -20°C shortened the freezing time by half.

- In general, for the freezing of spherical food products, the freezing time is correlated with the squared diameter of the sample. This quadratic relationship is very strong in the case of HF due to high HTC.

- Hydrofluidisation was compared to immersion freezing. Freezing time in HF can be reduced by 40%-60% when HF is applied. The smaller the size of the food, the more significant the reduction in freezing time.

Chapter 4

Modelling of hydrofluidisation hydrodynamics - Paper III

The characteristic aspect of the HF process is the free movement of individual food products. It is caused by the balance between gravitational and buoyancy forces, the drag force being a result of the refrigerating liquid flow, and the mutual interactions between individual samples. For that reason, an appropriate method has to be used to model the liquid-solid arrangement in the HF process. Moreover, the selection of the refrigerating medium used for HF is crucial, mostly because of different density or viscosity of various solutions that can be used for the freezing of food products.

The literature related to the HF process modelling is limited. According to the author's best knowledge, until now, only one numerical model has been developed to predict the realistic behaviour of food products during HF [30]. However, the authors analysed only one type of water-based solution used for freezing, i.e., the NaCl solution, which had significantly higher density than the food samples (potatoes). The authors employed the DEM approach, which is very popular in food-related analyses [45]. This approach has a particular limitation that becomes a significant disadvantage in the HF analysis. Namely, the size of the solid particles should be smaller than the numerical grid resolution used in the CFD simulation. Consequently, when dealing with whole food products or samples having a diameter of the order of centimetres, a very coarse mesh is required to achieve the stability of the numerical solution. In the HF method where fluid jets are present, it may result in a far insufficient accuracy of the fluid flow modelling.

At this stage of the numerical analysis of the HF process, an appropriate approach had to be used which allows for an accurate prediction of the hydrodynamics of the liquid-solid system. The aim was to characterise the flow of food samples and to determine HTC achievable in the realistic HF process using different refrigerating liquids. The process parameters that were investigated at this stage were the mass flow rate of the refrigerating liquid and the type of liquid solution. Different values of mass flow rate were assumed for the analysis, i.e., 0.1 kg·s^{-1}, 0.2 kg·s^{-1}, 0.5 kg·s^{-1}, 1.0 kg·s^{-1} and 2.0 kg·s^{-1}. Three different solutions were compared, i.e., water-ethanol solution (mass concentration 30%), water-glycerol solution (40%) and water-ethanol-glucose

solution (15%/25%). Medium size food samples having a diameter of 20 mm were analysed in all the cases.

4.1   Macroscopic Particle Model approach characterisation

In CFD, there are several approaches that can deal with multiphase granular flows. If one wants to recognise individual particles, they need to be tracked in Lagrangian frame of reference. A novel approach which tracks the spherical particles having a considerable size using the Lagrangian principle is the Macroscopic Particle Model [46]. In this approach, an individual particle is observed when moving in the numerical grid, as presented in Fig. 4.1(a). To include the interaction with the Eulerian phase of the liquid, the group of numerical cells that the particle occupies within a certain time step is patched with the fixed velocity vector of that particle, as shown in Fig. 4.1(b). Consequently, the velocity field within the volume of the particle gets the value and direction of the particle velocity vector. The cells that are within the range of the velocity adjustment are called *touched cells* in this approach. In MPM, interactions between individual particles are considered to follow Newtonian laws of momentum conservation in a similar way as in DEM.
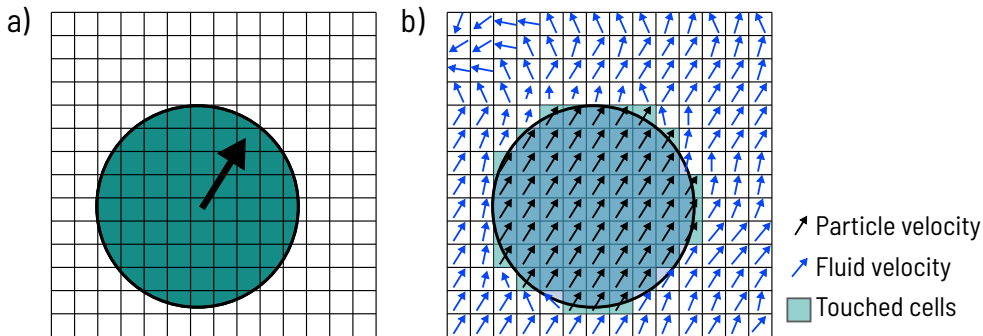
FIGURE 4.1: (a) individual particle moving within the numerical domain along its velocity vector and (b) the velocity vectors within the fluid domain and in the touched cells of the numerical mesh.

In the MPM approach, the drag and torque forces are computed directly using the velocity, pressure, and shear stress distribution in the fluid cells surrounding the particle. To achieve a proper accuracy of the results, the grid must be appropriately refined, i.e., the diameter of the particle should cover approximately 20-30 numerical cells [47].

4.2 Heat transfer coefficient determination in the developed model

The multiphase model developed for the simulation of a realistic HF process was considered adiabatic. A well-established way to determine Reynolds number in typical Euler-Lagrange analyses is to compute the slip velocity, which is the velocity of the particles relative to the velocity of the fluid. In the model developed for the HF analysis based on the MPM approach, the determination of the fluid velocity is not explicit because the macroscopic particle affects the fluid flow field and the resulting velocity field is not uniform around the particle. Therefore, the mathematical relationship between the drag force acting on each particle (computed directly based on MPM features) and the slip velocity was used, as presented in Eq. (4.1). The same equation is commonly used to determine the drag force based on the slip velocity for spherical objects. In the proposed model, this formula allowed to determine the slip velocity based on the drag force. The drag coefficient for the spherical objects was based on the Morsi-Alexander equation, shown in Eq. (4.2), which was recognised as accurate for a wide range of Reynolds numbers. Finally, the Reynolds number can be determined using Eq. (4.3).

$$F_D = \frac{1}{2} A \rho \, u_{FP}^2 C_D \tag{4.1}$$

$$C_D = a_1 + \frac{a_2}{\mathrm{Re}_P} + \frac{a_3}{\mathrm{Re}_P^2} \tag{4.2}$$

$$\mathrm{Re}_P = \frac{\rho \, D \, u_{FP}}{\mu} \tag{4.3}$$

where F_D is the drag force, u_{FP} is the relative (slip) velocity between the fluid phase and the particle, C_D is the drag coefficient, a_1, a_2 and a_3 are the coefficients for the Morsi-Alexander formulation and Re_P is the Reynolds number for the particle.

Finally, another assumption of the proposed HF process model that is common with a DPM or DEM analyses is employing the empirical correlations for the Nusselt number [42]. On the basis of the Reynolds number determined using Eq. (4.3) and the Prandtl number known for the fluids used in this analysis, the Nusselt number can be assessed, which allows for a direct calculation of HTC. In this study, the correlation by Whitaker [48] was employed, which was confirmed in numerous papers to be accurate for similar conditions of the flow over spheres.

The accuracy of HTC determination based on the methodology described above was examined on the basis of the HTC determined with CFD simulations that were conducted during the analysis of the scenario with stationary samples (Chapter 3). Selected conditions that were previously simulated using the validated CFD model were repeated with the new CFD-MPM model. To obtain the same conditions, the movement of samples modelled with the MPM approach was disabled. As a result

of 9 cases comparison, the error of HTC determination was above 10% for only one case. For 5 cases, the error of HTC determination using CFD-MPM was less than 5% with respect to CFD simulations. Summarising, the accuracy of the convective heat transfer prediction using the developed CFD-MPM model can be considered more than sufficient.

4.3   Discussion on selected results

First, it is worth characterising the flow pattern of the food samples within the HF tank. In this study, three different aqueous solutions were compared, that is, the water-ethanol solution (mass concentration 30%), the water-glycerol solution (40%) and the ternary solution of water-ethanol-glucose (15%/25%) at the constant temperature of -15°C. Fig. 4.2 presents the density comparison for all of these solutions and the potato sample. In the case of the water-ethanol solution, its density was 971.4 kg·m^{-3}, which is below the density of potato samples (1 062 kg·m^{-3}). The opposite relationship was for other considered solutions. For the water-glycerol and water-ethanol-glucose solutions, the densities were 1 111.5 kg·m^{-3} and 1 087.3 kg·m^{-3}, respectively.
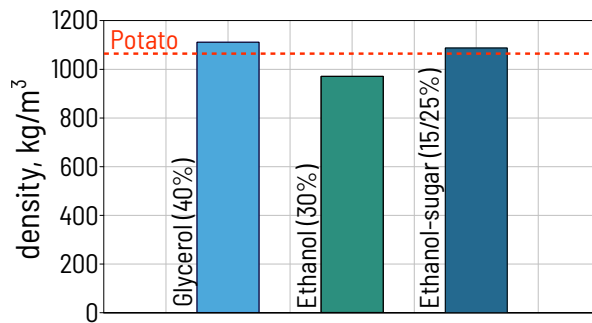
FIGURE 4.2: The density of three solutions used in HF analysis compared with the potato density.

In the case of the water-ethanol solution, at a very low flow rate, the food samples were in the bottom of the HF tank, as seen in Fig. 4.3(a) for the MFR of 0.1 kg·s^{-1}. For the same liquid and a higher MFR of 0.5 kg·s^{-1}, the refrigeration liquid exceeded the minimal fluidisation velocity and the food samples freely floated within the volume of the HF tank. That scenario is presented in Fig. 4.3(b). For higher MFRs of e.g., 1.0 kg·s^{-1} or 2.0 kg·s^{-1}, the intensive flow generated the drag force sufficient to transport the food samples toward the top of the HF tank, as presented in Fig. 4.3(c) for the MFR of 1.0 kg·s^{-1}. The same characteristics of the food samples transportation can be noticed for water-glycerol and water-ethanol-glucose solutions regardless the MFR, which is a consequence of their densities higher than the food samples density.
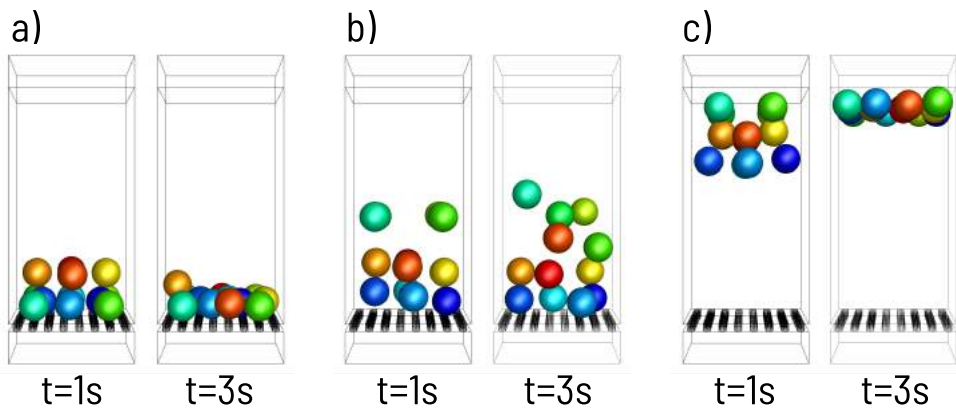
FIGURE 4.3: Arrangement of food samples after 1 s and 3 s of the flow for water-ethanol solution at at the mass flow rate of (a) 0.1 kg·s^{-1}, (b) 0.5 kg·s^{-1}, and (c) 1.0 kg·s^{-1} (Source: [49]).

The results indicated that in the case of dense fluids, the dynamics of movement of the food samples was the same. Namely, the food samples flowed upward and created a static bed near the semi-permeable net, which was used to prevent the samples from leaving the HF tank. In this case, it is worth considering the design modification of the HF unit, that is, placing the inflow section at the top of the HF tank instead of at the bottom. Such organisation of flow is called *inverse fluidisation* and, in case of fluid density higher than foods, would guarantee the dynamic fluidisation process in relatively high velocities of the fluid flowing downwards from the top. In the case of the ethanol-based solution, a favourable feature of such fluid arisen. A low density allowed to achieve a suspension of food products within the HF tank. In this case, individual food samples could be naturally mixed, therefore, a uniform freezing rate would be achieved for a large group of food products under such conditions.

The HTC achieved for the analysed conditions ranged from approximately 800 W·m^{-2}·K^{-1} to 4 500 W·m^{-2}·K^{-1} as seen in Fig. 4.4. The value of HTC was strongly dependent on the mass flow rate of the liquid. However, it is worth highlighting that in case of very high MFR, which would guarantee excessive HTC, a significant power for pumping the liquid medium is required. Moreover, the primary refrigeration unit needs higher capacity to cool down the higher amount of the aqueous solution used in HF. On the other hand, at a certain HTC level of approximately 2 000 W·m^{-2}·K^{-1} in the case of medium size products, i.e., having a diameter of 20 mm, the freezing time cannot be more lowered by the HTC increase due to the internal heat resistance. Therefore, optimisation should be carried out for a certain case taking into account the size of the food product.

Also, after the analysis of the results presented in Fig. 4.4, one can conclude that
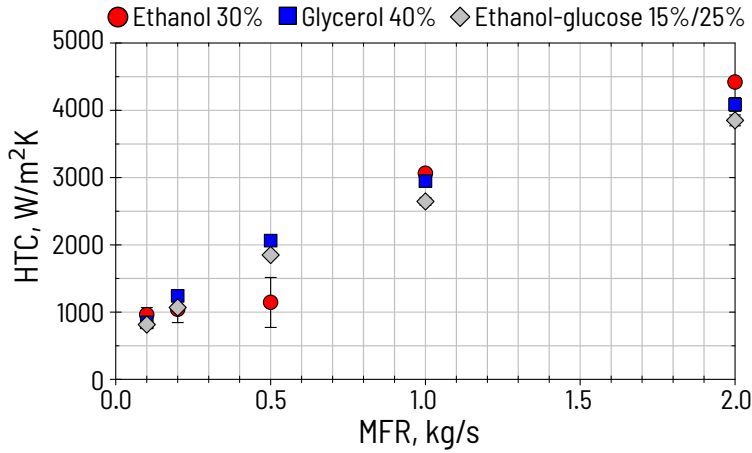
FIGURE 4.4: Average values of HTC for a whole food products group
obtained for various MFR and different types of the refrigerating liquid
(Source: [49]).

the type of refrigerating liquid has a minor effect on the HTC. Therefore, apart from
the general flow characteristics, the selection of the liquid does not affect the thermal
characteristics of the HF process. The most important effect of the type and concentra-
tion of the solution would be the uptake of the solution and the possible change in the
composition of the food product. Therefore, this aspect is the subject of the discussion
presented in the following Chapter 5.

Chapter 5

Numerical modelling of conjugate heat and mass transfer during hydrofluidisation freezing - Paper IV

The method of hydrofluidisation, despite its excellence related to the rapid freezing of individual products, has a possible limitation due to the side effect, which is the solute absorption. It is fundamental to examine HF in terms of solution uptake in different freezing conditions, because that is the main aspect that can hinder HF from having an industrial application. Therefore, a numerical tool enabling the prediction of the mass concentration in food products after the HF process and the knowledge of how all the process parameters affect the mass absorption are crucial.

5.1   Assumption for the mass transfer modelling

The process of mass transport from the liquid solution to the food product is very complex, i.e. numerous components are present within the food product, different parts and types of food have a different structure of the tissues, the freezing process and temperature variability can affect the properties and the process itself. For that reason, several assumptions were necessary to conduct the numerical analysis of the mass transfer during the HF process:

1. Because the dynamics of the mass diffusion in the analysed process is much lower than the heat diffusion, the heat transfer and the freezing were assumed to be independent of the mass transfer. On the other hand, the mechanism of the mass transfer was assumed to be dependent on the heat transfer because the temperature level strongly affects this process. Therefore, the conjugated heat and mass transfer model can be considered as one-way coupled.

2. The mass transfer was assumed to be purely diffusive. Thus, Fick's law was implemented to characterise the transfer of different components within the food product. The substances that were considered in the mass transfer analysis

were the liquid water and each of the solutes present in all the tested solutions, that are the same as in the analysis described in Chapter 4. The idea behind the developed model is based on the Whitaker formulation of porous medium [50], in which solid skeleton and the liquid phase can be distinguished. The mass was assumed to be transported only within the liquid phase. Water as the main component of the food product was included in the mass transfer analysis, and the equation describing the liquid water diffusion is presented in Eq. (5.1). A source term is present at the right-hand side of this equation and describes the liquid water content reduction based on the relationship discussed in Chapter 3. Analogous mass balances for the other components have the form of Eq. (5.2) but without any source terms.

$$\frac{\partial \left(\rho_\ell \, x_w \right)}{\partial t} - \nabla \left(\rho_\ell \, \mathscr{D}_{eff} \, x_w \right) = \frac{\partial x_{ice}(T)}{\partial t} \tag{5.1}$$

$$\frac{\partial \left(\rho_\ell \, x_n \right)}{\partial t} - \nabla \left(\rho_\ell \, \mathscr{D}_{eff} \, x_n \right) = 0 \tag{5.2}$$

where ρ_ℓ is the density of the liquid phase assumed as the water density, x_w is the mass fraction of liquid water, $\mathscr{D}_{eff}$ is the effective mass diffusivity and x_n is the mass fraction of the n-th component of the solution.

3. The intensity of the mass transfer in the Fick's law is described by the mass diffusivity. In the developed model, it was assumed that solutes diffuse through the liquid phase of the food structure. Therefore, the effective diffusivity describing the transport of a given substance through the structure of the potato sample was formulated. It was determined on the basis of the diffusivity of the pure substance, e.g., glycerol, in liquid water, including the porosity of the porous medium and the tortuosity, as shown in Eq. (5.3). These two parameters describe the volume fraction of the liquid in the food product and the effect of the internal structure of the food on mass transfer, respectively.

$$\mathscr{D}_{eff,n} = \varepsilon \frac{\mathscr{D}_n}{\tau} \tag{5.3}$$

where $\mathscr{D}_{eff,n}$ is the effective mass diffusivity of the n-th component in potato, ε is the porosity being the volume fraction of the liquid phase, $\mathscr{D}_n$ is the mass diffusivity of the n-th component at infinite dilution in water and τ is the tortuosity.

4. The process of mass absorption from the liquid medium by the food product in HF is driven by the concentration gradient, but also by the conditions of the flow and the fluid properties, similarly to the convective heat transfer. Due to the heat and mass transfer analogy, the mass transfer coefficient can be evaluated based on the heat transfer coefficient on the basis of the Chilton-Colburn analogy [20].

The values of the heat transfer coefficients were assumed as input data for these analyses based on the results presented in Chapter 4.

5. In the numerical model developed within the framework of this thesis, no additional mass transfer resistance was defined to characterise the effect of food product peel on mass absorption. It is because: (1) the food product assumed as the sample in all the analyses included in this thesis is the spherical potato sample cut out from the whole product; (2) the model that does not include that resistance can be considered as giving the worst case scenario results in terms of the unwanted mass uptake, therefore, that resistance can be omitted; (3) accurate determination of the mass resistance would be very challenging, and the mass transfer could be a sensitive parameter to numerous factors related to the individual food sample conditions.

5.2   Range of analysed parameters

In the food product freezing numerical analysis during the HF process accompanied by the solute uptake modelling, several parameters were investigated to determine the amount of solute absorbed by the food product during the freezing process. The parameters recognised eventually as important to analyse are as follows:

- HTC characteristics for the HF process based on simulations conducted using CFD-MPM model and presented in Chapter 4. The wide HTC range of 1 000 $W{\cdot}m^{-2}{\cdot}K^{-1}$ to 4 000 $W{\cdot}m^{-2}{\cdot}K^{-1}$ was assumed to guarantee the broad perspective of the effect of the fluid flow intensity. To evaluate the HF process compared to the IF method, the HTC of 300 $W{\cdot}m^{-2}{\cdot}K^{-1}$, which is characteristic for the latter method was assumed for selected cases.

- Diameter D of the spherical sample that can represent various food products. In this study, the range of 5 mm to 30 mm was analysed to determine how much solute can be absorbed by different samples.

- Type of refrigerating liquid. Three different solutes that were previously investigated in Chapter 4 were compared, i.e., the water-ethanol solution (mass concentration 30%), the water-glycerol solution (40%) and the water-ethanol-glucose solution (15%/25%).

In addition, two aspects related to the selection of refrigerating medium for the HF process were analysed:

- Effect of the temperature of the solution having the same concentration. Solute uptake by samples that had different sizes (5 mm, 15 mm, and 30 mm) in a solution of water-ethanol (30%) was compared during freezing at -10°C, -15°C, and -20°C.

- Effect of keeping the minimum temperature of the solution having various concentrations. Solute uptake was tested under different conditions characterised by various concentrations of water-glycerol solution (20%, 30%, 40%, 50%) at the lowest possible temperature in the liquid state.

5.3   Effect of the freezing phenomenon on mass transfer

The common feature of all methods for quick freezing that are characterised by high HTCs is the immediate freezing of the outer surface of the product. It is particularly beneficial for freezing in liquid medium because ice formation significantly reduces mass transfer through the frozen layer of the food sample. For that reason, in addition to the reduction in freezing time and the improvement of food quality, the intensification of the freezing rate also results in a smaller uptake of solutes during freezing in a liquid medium.

Fig. 5.1 compares the concentration of ethanol, ice fraction, and temperature within the food product in 3 characteristic moments of the process for the selected case.
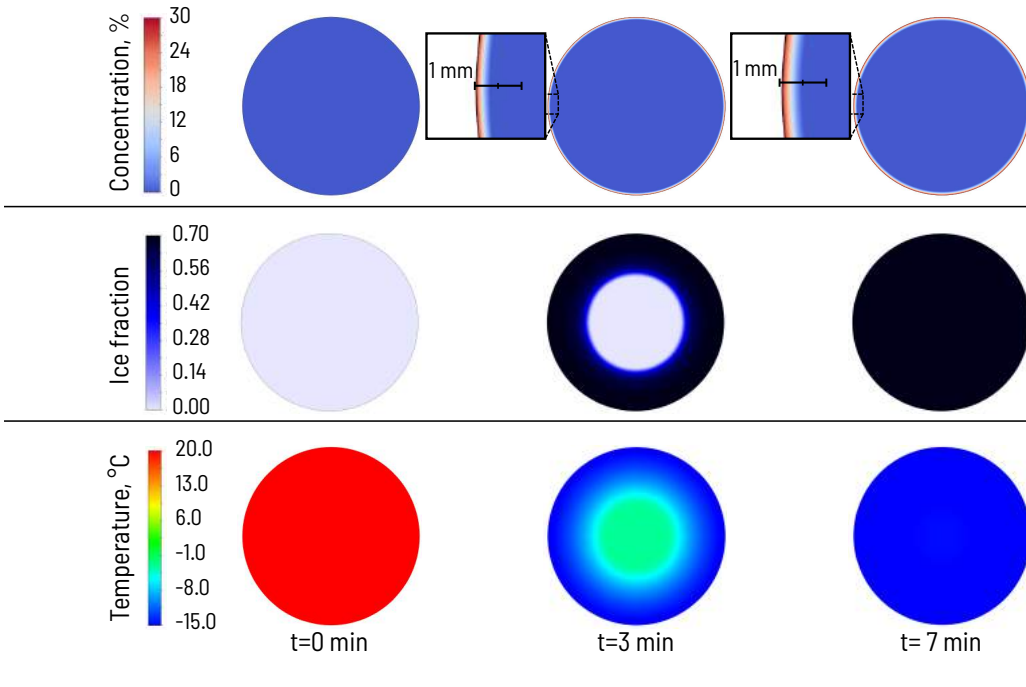
FIGURE 5.1: Spatial distribution of the ethanol concentration, ice fraction and the temperature within the food sample at the beginning of the process, after 3 min and after 7 min (Source: [51]).

As seen in these example fields, the phase change front, which is represented by the ice content, propagated towards the centre of the food sample and covered

approximately half of the radius of the sample after 3 min. In the same case, after 7 min, the product was completely frozen. The solute was absorbed by the outer surface of the food product and penetrated the thickness of less than 0.5 mm. It is worth noticing that there is no significant difference between the field of solute concentration after 3 min of the process and after 7 min. It confirms that the freezing time of the outer layer is the key parameter in terms of mass absorption during freezing.

In terms of the effect of HTC on the uptake of the solution, it was crucial to determine this for food products having different sizes. It was recognised that the size and shape of the food product in this analysis can be better represented by using the external area to volume ratio A/V. Fig. 5.2 presents the concentration of the ethanol solution after freezing spherical samples having a diameter of 5 mm to 30 mm under different conditions of HF (1 000 W·m^{-2}·K^{-1}-4 000 W·m^{-2}·K^{-1}) compared to IF. As seen, a higher A/V ratio (and lower diameter of the spherical sample) results in a higher concentration of solutes in the frozen product. This relationship is stronger for IF, which in general allows for higher absorption of the solute. HTC of approximately 2 000 W·m^{-2}·K^{-1} allows for a sufficient reduction of the mass transfer. Further intensification of the freezing rate does not significantly improve the process.
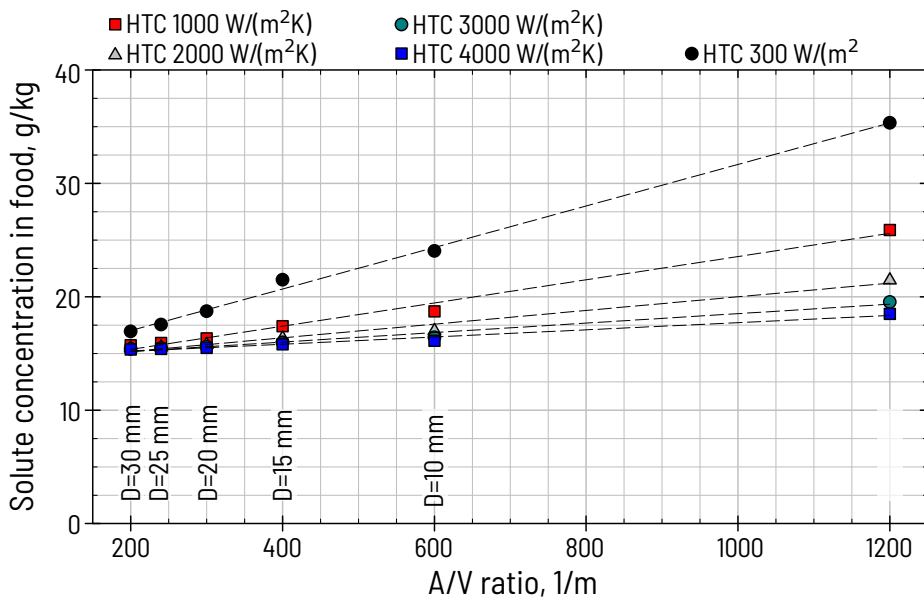
FIGURE 5.2: Volume-average concentration of the solute (ethanol) in g per 1 kg of the potato after HF process at different HTCs and after the IF process for different size food samples (Source: [51]).

The second important parameter was the temperature of the solution. As seen in Fig. 5.3, reduction of the refrigerating medium temperature allows the solute uptake

to be reduced. Reduction of the temperature from -10°C to -20°C in general allows reducing the solute concentration in frozen food by approximately 40%.
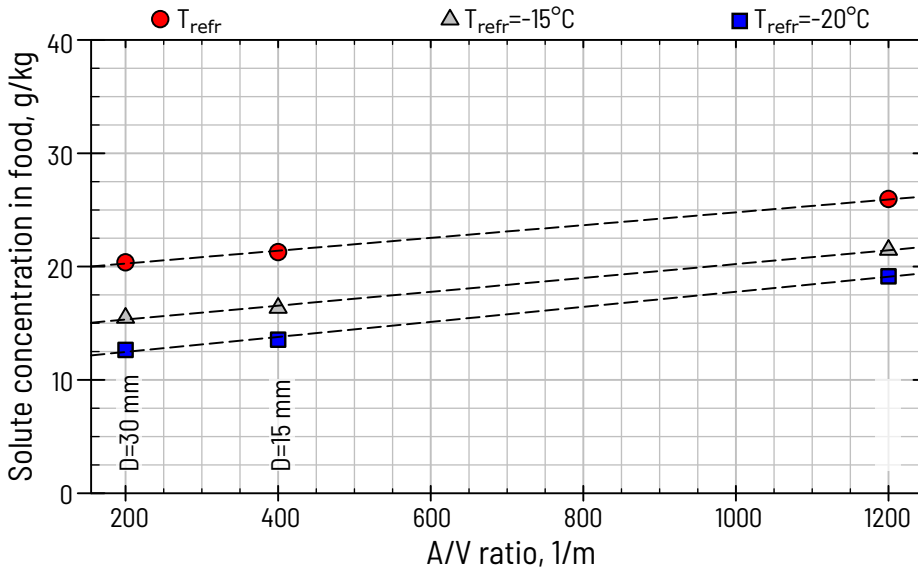
FIGURE 5.3: The average concentration of the solute (ethanol) in g per 1 kg of the potato after HF under different refrigerating liquid temperatures for different size food samples (Source: [51]).

5.4 Remarks for the solution uptake control

On the basis of all the results briefly presented in this chapter and in the research paper [51], several important conclusions can be formulated which are related to the appropriate conduction of HF process having in mind the solute uptake. These are as follows:

- The method of HF guarantees lower solution uptake with reference to a similar IF method. In the case of the first technique for food freezing, higher HTC results in faster freezing of the outer surface of the food product, which significantly reduces the intensity of the mass transfer. In the range of conditions analysed, HTC of 2 000 W·m^{-2}·K^{-1} was recognised as the value for which further intensification of heat transfer does not significantly improve the process.

- For smaller food products, the final concentration of the solute (volume-averaged) in the whole product is higher because of the higher A/V.

- The lower temperature of the solution guarantees a lower concentration of the solute in the frozen food product. It confirms that, in any case, lowering the temperature is beneficial for the food from a product quality point of view. The only limitation may arise from the freezing temperature of the aqueous solution.

- For freezing in ethanol aqueous solution with a mass concentration of 30%, HF guarantees the average concentration of the solute in the food in the range from approximately 15 $g \cdot kg^{-1}$ to 25 $g \cdot kg^{-1}$. It is strongly dependent on the size of the food product and HTC. For other solutions, the solute concentration in frozen food products can be related to the mass concentration of the solution. For a simple assessment, the linear relationship between the solute concentration in a liquid and the solute absorbed by the food product provides a decent estimation.

- Numerous types of food products, e.g., berries or peas, have a peel on their outer surface. Therefore, the mass transfer would be further limited. For this reason, the results related to the uptake of the solution in HF presented in this thesis can be considered the worst case.

Chapter 6

Summary and conclusions

The scope of this thesis was the numerical investigation of the hydrofluidisation method for rapid food freezing and developing numerical tools being able to predict the whole process, and consequently, being useful to design the HF unit for an effective freezing of small food products.

The first stage was to characterise the fluid flow over a spherical food sample in the simplified scenario, i.e., with one sphere positioned in a fixed position. Two promising approaches for turbulence modelling were examined to select the most appropriate one for further analyses. The experimental measurements of the velocity field under such conditions by using the PIV method allowed to validate the fluid flow CFD model. A total number of 9 different operating conditions was used for the model validation. The results confirmed that the K-ω SST model allows to predict the velocity field in the jet and stream detachment regions with a good accuracy. The average error of the velocity prediction for all the 9 cases discussed in detail in the peer-review article was approximately 11.5%. Furthermore, the results confirmed that this turbulence approach can be used for HF modelling in axisymmetric and 3-D geometrical domains. According to the results, the H/d ratio is an important parameter that characterises the velocity profile within the impingement jet. The outcome of this part of the investigation allowed to formulate the remarks about which geometrical parameters affect the fluid flow, and to confirm that the fluid flow model provides a good accuracy in a wide range of conditions.

The numerical model of food freezing was developed. Special attention was paid to determine the composition of a food product (potato) and to formulate thermophysical properties of this food product. The validation of the temperature at two characteristic locations confirmed that the temperature prediction is very accurate. For a food product having a diameter of 20 mm, the variations in freezing time were minor for HTC of more than 2 500 W·m^{-2}·K^{-1}. It was confirmed that the refrigerating medium temperature reduction allows the freezing time to be significantly reduced. Moreover, the HF method was compared with IF and it was proven that the HF allows the freezing time of food products to be reduced by approximately 40%-60% depending on the food product size. Moreover, the time of residence within the critical zone of water crystallisation can be significantly reduced when HF is used instead of IF.

In the next step, the realistic hydrodynamics of the HF process was investigated using a novel MPM approach for the simulation of large particles movement in a liquid environment. Three different water-based solutions were compared. For dense aqueous solutions (glycerol, alcohol-sugar), the high density resulted in creating a static bed of food products near the HF tank top. For the alcohol-based solution having a density lower than that of a food product, the behaviour was dependent on the mass flow rate of the fluid. The results confirmed that the HTC of 2 000 W·m^{-2}·K^{-1} was achievable in the HF tank with a refrigerating liquid mass flow rate of 0.5 kg·s^{-1}.

To assess the possible mass uptake from the solution during HF, which is the main limitation of this method, a conjugated heat and mass transfer model was developed. It allowed to assess the average concentration of the given solutes that were present in the refrigerating medium. The results showed that the mass absorption is lower for HF compared to the IF method because of more intensive freezing of the food product surface, which creates a frozen crust immediately. The solution uptake was strongly dependent on the composition of the refrigerating medium and, more specifically - on the mass concentration of a given solute in the liquid. For example, for a water-ethanol solution with a mass concentration of 30%, the average ethanol content was in the range of 15-25 g per kg of the food product and was dependent on the HTC and the size of the food product. The results also confirmed that reduction of the refrigerating medium temperature allows the mass absorption to be minimised.

The results presented in this thesis allow formulating a number of suggestions for conducting the HF process. First, the HTC of approximately 2 000 W·m^{-2}·K^{-1} to 2 500 W·m^{-2}·K^{-1} is sufficient to maximise the convective heat transfer for food products having a diameter of 20 mm, which is related to a vast of food products, e.g., strawberries, grapes. Due to the internal heat resistance, further increase of HTC would be beneficial only for smaller foods. Second, the selection of the refrigerating liquid is crucial. For aqueous solutions having a density smaller than that of a food product, the fluidisation effect is achievable. This behaviour is desired because it allows individual food products to mix within the HF tank and obtain a more uniform HTC distribution in a large group of food products. It confirms that the water-ethanol solution can be used in that method. In the case of other solutions such as water-glycerol or water-ethanol-glucose, which have a higher density, it is worth reconsidering the HF tank design and installing the orifices on the top of the tank. Such a configuration would allow to achieve the so-called, *reverse fluidisation*, which would result in obtaining the fluidisation in any liquid having a high density. Furthermore, the heat and mass transfer analysis confirmed that the lowering of the temperature has an enormous effect on the freezing time and the solution uptake. It suggests that the refrigerating liquid should be cooled down to a possible low temperature. In this case, the limitation can be a high concentration of the solution. The results presented in this thesis and in the peer-review paper confirmed that in some cases the final concentration of the solution in the food product after freezing can be lower if the freezing is carried out in a more concentrated solution, which allowed for a reduction of the temperature. In any

case, this aspect should be optimised taking into account the type and size of the food product, the desired temperature, and the refrigerating medium used for the process.

To conclude, several numerical models useful for the HF technique development were formulated. The outcome of this PhD thesis is the extension of the current state of knowledge related to the HF method, which is not well known, but has a potential to be applied for small food products rapid freezing. The numerical tools developed in this thesis may be useful for optimisation of the process and designing the HF unit for practical use, especially taking into consideration the excellent food freezing time and the advantages of HF method that were underlined by the previous researchers.

Nevertheless, further work is required to carry on with the issues that were highlighted in this work. First, the selection of the refrigerating medium is fundamental to freeze the food products taking into consideration the food quality aspects with priority. Therefore, a variety of aqueous solutions should be compared and analysed to find the most promising liquids characterised by appropriately low freezing point and a composition that would be approved by the final consumers. Moreover, the organisation of the fluid flow in the HF tank should be reconsidered. As mentioned before, *reverse fluidisation* would be beneficial for such process as a potential option to maintain the effective circulation of individual foods within the tank filled with the liquid. Finally, the geometrical parameters investigated in this thesis, especially the diameter of orifices, their arrangement in the array, and the height of HF tank should be optimised along with the flow parameters like the flow rate of the liquid and the temperature. Such optimisation should be conducted for specific food products having a certain size. The economical aspects like the power required for the pumping of the refrigerating medium and for maintaining the low temperature should be considered as well. The numerical tools would be invaluable to optimise and improve the overall process. That would allow the HF food freezing method to reveal all its advantages and superiority over various food freezing methods that are nowadays used globally.

Bibliography

[1] IIR, "The role of refrigeration in worldwide nutrition - 6th informatory note on refrigeration and food," 2020.

[2] A. E. Delgado and D. Sun, "Heat and mass transfer models for predicting freezing processes – a review," *Journal of Food Engineering*, vol. 47, no. 3, pp. 157–174, 2001.

[3] R. P. Singh and D. R. Heldman, "Introduction to food engineering, Chapter 7 - Food freezing," in San Diego: Academic Press, 2014, pp. 521–563.

[4] K. A. Fikiin, "Emerging and novel freezing processes," in *Frozen Food Science and Technology*. Blackwell Publishing Ltd., Oxford, UK, 2008, ch. 5, pp. 101–123.

[5] C. James, G. Purnell, and S. J. James, "A review of novel and innovative food freezing technologies," *Food and Bioprocess Technology*, vol. 8, no. 8, pp. 1616–1634, 2015.

[6] H. A. Khouryieh, "Novel and emerging technologies used by the U.S. food processing industry," *Innovative Food Science and Emerging Technologies*, vol. 67, p. 102 559, 2021.

[7] ASHRAE, *ASHRAE handbook: Refrigeration : SI Edition*. American Society of Heating, Refrigerating and Air-Conditioning Engineers, 2006.

[8] G. Tchigeov, "Thermophysical processes in food refrigeration technology," *Moscow, Russia: Food Industry*, 1979.

[9] R. Plank, "Die gefrierdauer von eisblocken," *Zeitschrift fur die gesamte Kalte Industrie*, vol. 20, no. 6, pp. 109–114, 1913.

[10] A. C. Cleland and R. L. Earle, "Freezing time prediction for foods — a simplified procedure," *International Journal of Refrigeration*, vol. 5, no. 3, pp. 134–140, 1982.

[11] R. H. Mascheroni and A. Calvelo, "A simplified model for freezing time calculations in foods," *Journal of Food Science*, vol. 47, no. 4, pp. 1201–1207, 1982.

[12] Q. T. Pham, "Simplified equation for predicting the freezing time of foodstuffs," *International Journal of Food Science & Technology*, vol. 21, no. 2, pp. 209–219, 1986.

[13] Q. T. Pham, "Modelling heat and mass transfer in frozen foods: A review," *International Journal of Refrigeration*, vol. 29, no. 6, pp. 876–888, 2006.

[14] Q. T. Pham, "A fast, unconditionally stable finite-difference scheme for heat conduction with phase change," *International Journal of Heat and Mass Transfer*, vol. 28, no. 11, pp. 2079–2084, 1985.

[15] V. Voller, "An overview of numerical methods for solving phase change problems," in *Advances in Numerical Heat Transfer*, W. J. Minkowycz and E. M. Sparrow, Eds., London: CRC Press, 1996, pp. 341–375.

[16] P. J. Fellows, "Freezing," in *Food Processing Technology (Third Edition)*, ser. Woodhead Publishing Series in Food Science, Technology and Nutrition, P. J. Fellows, Ed., Woodhead Publishing, 2009, pp. 650–686.

[17] G. V. Barbosa-Canovas and P. J. Uliano, "Adaptation of classical processes to new technical developments and quality requirements," *Journal of Food Science*, vol. 69, no. 5, E240–E250, 2004.

[18] T. Lucas and A. L. Raoult-Wack, "Immersion chilling and freezing in aqueous refrigerating media: Review and future trends," *International Journal of Refrigeration*, vol. 21, no. 6, pp. 419–429, 1998.

[19] K. Muthukumarappan, C. Marella, and V. Sunkesula, "Food Freezing Technology," in *Handbook of Farm, Dairy and Food Machinery Engineering (Third Edition)*, M. Kutz, Ed., Academic Press, 2019, pp. 389–415.

[20] Y. A. Cengel, *Heat Transfer: A Practical Approach*. McGraw-Hill, 2015.

[21] A. G. Fikiin, "New method and fluidized water system for intensive chilling and freezing of fish," *Food Control*, vol. 3, no. 3, pp. 153–160, 1992.

[22] K. A. Fikiin and A. G. Fikiin, "Individual quick freezing of foods by hydrofluidisation and pumpable ice slurries," vol. 55, pp. 15–18, 2001.

[23] P. Verboven, N. Scheerlinck, and B. M. Nicolai, "Surface heat transfer coefficients to stationary spherical particles in an experimental unit for hydrofluidisation freezing of individual foods," *International Journal of Refrigeration*, vol. 26, no. 3, pp. 328–336, 2003.

[24] J. M. Peralta, A. C. Rubiolo, and S. E. Zorrilla, "Design and construction of a hydrofluidization system. study of the heat transfer on a stationary sphere," *Journal of Food Engineering*, vol. 90, no. 3, pp. 358–364, 2009.

[25] J. M. Peralta, A. C. Rubiolo, and S. E. Zorrilla, "Mathematical modeling of the heat transfer and flow field of liquid refrigerants in a hydrofluidization system with a stationary sphere," *Journal of Food Engineering*, vol. 99, no. 3, pp. 303–313, 2010.

[26] J. M. Peralta, A. C. Rubiolo, and S. E. Zorrilla, "Mathematical modeling of the heat and mass transfer in a stationary potato sphere impinged by a single round liquid jet in a hydrofluidization system," *Journal of Food Engineering*, vol. 109, no. 3, pp. 501–512, 2012.

[27] S. E. Zorrilla and A. C. Rubiolo, "Mathematical modeling for immersion chilling and freezing of foods: Part I: Model development," *Journal of Food Engineering*, vol. 66, no. 3, pp. 329–338, 2005.

[28] S. E. Zorrilla and A. C. Rubiolo, "Mathematical modeling for immersion chilling and freezing of foods: Part II: Model solution," *Journal of Food Engineering*, vol. 66, no. 3, pp. 339–351, 2005.

[29] E. E. Belis, S. E. Zorrilla, and J. M. Peralta, "Effect of the number of orifices and operative variables on the heat and mass transfer in a hydrofluidization system with static spheres," *Journal of Food Engineering*, vol. 153, pp. 96–107, 2015.

[30] J. D. Orona, S. E. Zorrilla, and J. M. Peralta, "Computational fluid dynamics combined with discrete element method and discrete phase model for studying a food hydrofluidization system," *Food and Bioproducts Processing*, vol. 102, pp. 278–288, 2017.

[31] J. D. Orona, S. E. Zorrilla, and J. M. Peralta, "Sensitivity analysis using a model based on computational fluid dynamics, discrete element method and discrete phase model to study a food hydrofluidization system," *Journal of Food Engineering*, vol. 237, pp. 183–193, 2018.

[32] K. Fikiin, O. Tsvetkov, Y. Laptev, A. Fikiin, and V. Kolodyaznaya, "Thermophysical and engineering issues of the immersion freezing of fruits in ice slurries based on sugar-ethanol aqueous solution," *Ecolibrium, Aug*, pp. 10–15, 2003.

[33] M. Palacz, W. Adamczyk, E. Piechnik, M. Stebel, and J. Smolka, "Experimental investigation of the fluid flow inside a hydrofluidisation freezing chamber," *International Journal of Refrigeration*, vol. 107, pp. 52–62, 2019.

[34] T. J. Chung, *Computational Fluid Dynamics*. Cambridge University Press, 2010.

[35] S. B. Pope, *Turbulent flows*. Cambridge University Press, 2000.

[36] M. Stebel, J. Smolka, M. Palacz, W. Adamczyk, and E. Piechnik, "Numerical investigation of the fluid flow distribution for the hydrofluidisation food freezing method," *International Journal of Thermal Sciences*, vol. 151, p. 106 284, 2020.

[37] K. A. Fikiin, "Ice content prediction methods during food freezing: a survey of the Eastern European literature," *Journal of Food Engineering*, vol. 38, no. 3, pp. 331–339, 1998.

[38] C. S. Chen, "Thermodynamic analysis of the freezing and thawing of foods: Enthalpy and apparent specific heat," *Journal of Food Science*, vol. 50, no. 4, pp. 1158–1162, 1985.

[39] F. L. Levy, "A modified Maxwell-Eucken equation for calculating the thermal conductivity of two-component solutions or mixtures," *International Journal of Refrigeration*, vol. 4, no. 4, pp. 223–225, 1981.

[40] J. K. Carson, J. Wang, M. F. North, and D. J. Cleland, "Effective thermal conductivity prediction of foods using composition and temperature data," *Journal of Food Engineering*, vol. 175, pp. 65–73, 2016.

[41] Y. Choi and M. R. Okos, "Effects of temperature and composition on the thermal properties of food," *Food Engineering and Process Applications*, pp. 93–101, 1986.

[42] ANSYS, *ANSYS Fluent user's guide, Release 18.2*. Canonsburg, PA, 2017.

[43] M. Palacz, E. Piechnik, M. Halski, *et al.*, "Experimental analysis of freezing process of stationary food samples inside a hydrofluidisation freezing chamber," *International Journal of Refrigeration*, 2021.

[44] M. Stebel, J. Smolka, M. Palacz, *et al.*, "Numerical modelling of the food freezing process in a quasi-hydrofluidisation system," *Innovative Food Science and Emerging Technologies*, vol. 74, p. 102 834, 2021.

[45] N. Malekjani and S. M. Jafari, "Simulation of food drying processes by Computational Fluid Dynamics (CFD); recent advances and approaches," *Trends in Food Science & Technology*, vol. 78, pp. 206–223, 2018, ISSN: 0924-2244.

[46] M. Agrawal, "Macroscopic Particle Model tracking big particles in CFD," in *AIChE Annual Meeting, Austin, USA, 2004*, 2004.

[47] ANSYS, "Chapter 4. Fluent Macroscopic Particle Module," in *ANSYS Fluent advanced add-on modules*. Canonsburg, PA, 2016, pp. 193–226.

[48] S. Whitaker, "Forced convection heat transfer correlations for flow in pipes, past flat plates, single cylinders, single spheres, and for flow in packed beds and tube bundles," *AIChE Journal*, vol. 18, pp. 361–371, 1972.

[49] M. Stebel, J. Smolka, M. Palacz, *et al.*, "Numerical analysis of hydrofluidisation food freezing with moving products in different aqueous solutions by using CFD and MPM approaches," *International Journal of Refrigeration*, vol. 134, 2022.

[50] S. Whitaker, "Simultaneous heat, mass, and momentum transfer in porous media: A theory of drying," in ser. Advances in Heat Transfer, J. P. Hartnett and T. F. Irvine, Eds., vol. 13, Elsevier, 1977, pp. 119–203.

[51] M. Stebel, J. Smolka, M. Palacz, T. M. Eikevik, and I. Tolstorebrov, "Numerical modelling of conjugate heat and mass transfer during hydrofluidisation food freezing in different water solutions," *Innovative Food Science and Emerging Technologies*, vol. 75, p. 102 898, 2022.

Abstract

Nowadays, freezing and chilling are the most common methods for achieving the long shelf life of food products. It is also the first element of the whole food cold chain. However, according to the latest data, while 46% of global food production should be refrigerated, less than half of that number is subjected to this process. It results in enormous food waste, which is estimated to account for approximately 13% of global production. Novel food freezing methods should be developed to be energy efficient, economically attractive, and to guarantee a high quality of frozen food products. A method that guarantees such conditions is hydrofluidisation (HF), which was proposed for the rapid chilling and freezing of small food products. It is based on freezing in a liquid medium that is additionally agitated by the flow through a group of orifices located at the bottom of the HF tank. As a result, very high heat transfer coefficients (HTC) of over $2\,000$ W·m^{-2}·K^{-1} can be reached. Moreover, food products behave as a fluidised bed which allows them to freeze individually and achieve a uniform freezing process for all the products in the whole group.

This work focuses on different aspects of the numerical investigation of the HF process. First, the jet flow over the food sample having a spherical shape was modelled. In this stage, the fluid flow model was formulated with the appropriate turbulence modelling approach, which is K-ω SST model. Several aspects of the numerical domain formulation were also examined. The numerical model of the fluid flow was validated by comparing the velocity fields obtained numerically with the experimental measurements of the velocity fields. The accuracy of the fluid velocity field prediction was approximately 11.5%, which is very satisfactory considering very high velocity gradients in the region that was analysed. In further steps, the geometrical domain of the HF tank included a full array of orifices and several food products, in a static configuration and with realistic movement. The static configuration allowed for the examination of several geometric parameters such as the ratio of the position of food products above the orifice and the orifice diameter (H/d) or the effect of the spacing between the orifices (S) or between food samples (z) on HTC. The parameters H/d and S were shown to significantly affect HTC, but the freezing time is no longer reduced when HTC is higher than $2\,500$ W·m^{-2}·K^{-1}. In the second scenario, the realistic HF process was investigated for a group of spherical samples having a diameter of 20 mm using the macroscopic particle model (MPM) approach for Lagrangian modelling of individual particle movement. In this case, different refrigerating medium mass flow rates were tested in the range of 0.1 kg·s^{-1} to 2.0 kg·s^{-1}. Furthermore, three different water-based

solutions were compared, i.e., the aqueous solution of ethanol (mass concentration 30%), the aqueous solution of glycerol (40%) and the aqueous solution of ethanol and glucose mixture (15%/25%). In the case of the solution of ethanol, the behaviour of food products in the HF tank was dependent on the flow rate, because of the lower density of this solution compared to the density of the food product (potato). For other fluids that are denser than the food, the samples formed a static bed at the top of the tank. For such conditions, HTC was in the range of $1\,000$ W·m^{-2}·K^{-1} up to $4\,000$ W·m^{-2}·K^{-1} for a very high fluid mass flow rate of 2.0 kg·s^{-1}.

The second aspect that was investigated in this study is the phenomenon of heat and mass transfer within the food product during the freezing process. First, the heat transfer model based on the apparent heat capacity approach was developed to characterise the temperature distribution within the food product during the freezing process. The developed model was validated using the temperature measurements of the potato sample. The agreement with the measurements was very high. The model was used to determine the freezing time for different conditions. In the water-ethanol solution with a temperature of -15°C, the freezing time of the 20 mm potato sphere was 6 min. For smaller products, it was even lower, e.g., 1.5 min for a 10 mm sample. The freezing times were compared with the immersion freezing (IF) method, which is similar, but the fluid flow is not forced. The comparison proved that the freezing process can be significantly faster when HF is used instead of IF. The freezing time was reduced by approximately 40% for spherical food samples having a diameter of 30 mm and by up to 60% for smaller foods having a diameter of 10 mm. In a further step of the investigation, the food product model was complemented by the mass transfer analysis. It allowed quantifying the unwanted side effect of HF, which is the absorption of the solution components by the food product. The model was based on several assumptions and compared with data from the literature for similar conditions to confirm its reliability. It turned out that depending on HTC and the size of the food product (5-30 mm), the uptake of the solution components is in the range of 15-26 g·kg^{-1} of food for the ethanol solution (30%) and 20-35 g·kg^{-1} of food for the glycerol solution (40%). Using the solution of ethanol and sugar mixture (15%/25%) allowed to preserve the ethanol concentration in the food product in the range of 9-15 g·kg^{-1} and the glucose concentration in the range of 16-24 g·kg^{-1} for the same cases. Furthermore, the results confirmed that the reduction in the temperature of the refrigerating medium from -10°C to -20°C allows one to reduce the mass absorption by approximately 40%. It is worth noting that HF allowed for a significant reduction of the mass uptake with respect to the IF method.

Streszczenie

Zamrażanie i schładzanie to obecnie najczęstsze metody osiągania długiego okresu przydatności do spożycia produktów spożywczych. Jest to również pierwszy element całego łańcucha chłodniczego dla żywności. Jednakże, według najnowszych danych, w sytuacji gdy 46% światowej produkcji żywności powinno być schładzane, mniej niż połowa tej liczby jest poddana temu procesowi. W rezultacie, powoduje to marnowanie ogromnych ilości żywności, które według szacunków stanowią około 13% światowej produkcji. Nowatorskie metody zamrażania żywności powinny być rozwijane w taki sposób, aby były energooszczędne, atrakcyjne pod kątem ekonomicznym oraz gwarantowały wysoką jakość zamrożonych produktów spożywczych. Metodą gwarantującą takie warunki jest hydrofluidyzacja (HF), która została zaproponowana do szybkiego schładzania i zamrażania drobnych produktów spożywczych. Polega ona na zamrażaniu w ciekłym medium, które jest dodatkowo wzburzone przepływem przez grupę kryz umieszczonych na dnie zbiornika HF. W efekcie możliwe jest osiągnięcie bardzo wysokich współczynników wnikania ciepła (WWC) przekraczających 2 000 $W \cdot m^{-2} \cdot K^{-1}$. Ponadto produkty spożywcze zachowują się jak złoże fluidalne, co pozwala na indywidualne zamrażanie pojedynczych produktów i uzyskanie jednolitego procesu zamrażania dla wszystkich produktów w całej grupie.

Niniejsza praca skupia się na różnych aspektach badania numerycznego procesu hydrofluidyzacji. W pierwszej kolejności zamodelowano przepływ strugi wokół próbki produktu o kulistym kształcie. Na tym etapie sformułowano model przepływu płynu, stosując odpowiednie podejście do modelowania turbulencji, czyli model K-ω SST. Zbadano również kilka sposobów formułowania domeny numerycznej. Model numeryczny przepływu płynu został zwalidowany poprzez porównanie otrzymanych numerycznie pól prędkości z eksperymentalnymi pomiarami pól prędkości. Dokładność modelowania pola prędkości płynu wyniosła około 11,5%, co jest bardzo zadowalającym wynikiem, biorąc pod uwagę bardzo duże gradienty prędkości w analizowanym obszarze. W dalszych krokach domena geometryczna zbiornika hydrofluidyzacyjnego obejmowała pełny układ kryz i kilka produktów spożywczych w konfiguracji statycznej oraz w realistycznym ruchu. Konfiguracja statyczna pozwoliła na zbadanie kilku parametrów geometrycznych takich jak stosunek odległości produktów spożywczych od otworów do średnicy kryzy (H/d), czy wpływ rozstawu kryz (S) lub odległości pomiędzy próbkami żywności (z) na WWC. Wykazano, że parametry H/d i S znacząco wpływają na WWC, ale czas zamrażania nie podlega skracaniu, gdy WWC przewyższa 2 500 $W \cdot m^{-2} \cdot K^{-1}$. W drugim scenariuszu zbadano realistyczny proces HF dla grupy

sferycznych próbek o średnicy 20 mm przy użyciu makroskopowego modelu cząstek (MPM) do modelowania Lagrange'owskiego ruchu poszczególnych drobin. W tym przypadku przetestowano różne masowe natężenia przepływu czynnika chłodniczego w zakresie od 0,1 kg·s^{-1} do 2,0 kg·s^{-1}. Ponadto porównano trzy różne roztwory wodne, tj. wodny roztwór etanolu (stężenie masowe 30%), wodny roztwór gliceryny (40%) oraz wodny roztwór mieszaniny etanolu i glukozy (15%/25%). W przypadku roztworu etanolu zachowanie produktów spożywczych w zbiorniku HF było zależne od natężenia przepływu, ze względu na mniejszą gęstość tego roztworu w porównaniu z gęstością produktu spożywczego (ziemniaka). W przypadku innych płynów, które są gęstsze niż mrożone produkty, próbki tworzyły statyczną grupę w górnej części zbiornika. WWC dla takich warunków mieściły się w przedziale od 1 000 W·m^{-2}·K^{-1} do 4 000 W·m^{-2}·K^{-1} dla bardzo wysokiego masowego natężenia przepływu płynu 2,0 kg·s^{-1}.

Drugim aspektem, który był badany w niniejszej pracy, jest zjawisko wymiany ciepła i masy w produkcie spożywczym podczas procesu zamrażania. Najpierw opracowano model wymiany ciepła oparty na podejściu pozornej pojemności cieplnej, aby scharakteryzować rozkład temperatury w produkcie spożywczym podczas procesu zamrażania. Opracowany model poddano walidacji za pomocą pomiarów temperatury próbki ziemniaka. Okazało się, że zgodność z pomiarami była bardzo wysoka. W związku z tym, model posłużył do wyznaczenia czasu zamrażania w różnych warunkach. W wodnym roztworze etanolu o temperaturze -15°C czas zamrażania kulki ziemniaczanej o średnicy 20 mm wynosił 6 min. W przypadku mniejszych produktów, czas był jeszcze krótszy, np. 1,5 min dla próbki o średnicy 10 mm. Uzyskane czasy zamrażania porównano z metodą zamrażania zanurzeniowego (IF), która również realizowana jest w cieczy, ale w której przepływ płynu nie jest wymuszony. Wyniki udowodniły, że proces zamrażania może być znacznie szybszy, gdy stosuje się metodę HF zamiast IF. Czas zamrażania został skrócony o około 40% dla sferycznych próbek żywności o średnicy 30 mm i aż o 60% dla mniejszych produktów spożywczych o średnicy 10 mm. W kolejnym etapie badania model produktu spożywczego został uzupełniony o analizę transportu masy. Umożliwiło to ilościowe określenie niepożądanego efektu ubocznego metody HF, jakim jest wchłanianie składników roztworu przez produkt spożywczy. Model oparto na kilku założeniach i porównano z danymi literaturowymi dla podobnych warunków w celu potwierdzenia jego wiarygodności. W zależności od WWC i wielkości produktu spożywczego (5-30 mm) wchłanianie składników roztworu mieści się w zakresie 15-26 g·kg^{-1} produktu dla roztworu etanolu (30%) oraz 20-35 g·kg^{-1} produktu dla roztworu gliceryny (40%). Zastosowanie roztworu mieszanki etanolu z cukrem (15%/25%) pozwoliło na utrzymanie stężenia etanolu w produkcie spożywczym w zakresie 9-15 g·kg^{-1} oraz stężenia glukozy w zakresie 16-24 g·kg^{-1} dla tych samych przypadków. Ponadto wyniki potwierdziły, że obniżenie temperatury czynnika chłodniczego z -10°C do -20°C pozwala na zmniejszenie wchłaniania masy o około 40%. Warto zauważyć, że metoda HF pozwoliła na znaczne zmniejszenie wchłaniania masy w stosunku do metody zanurzeniowej.

Appendices

In this Chapter, the full-text papers that were briefly described in Chapters 2 - 5 are presented. The papers are listed in the following order:

    I. M. Stebel, J. Smolka, M. Palacz, W. Adamczyk, E. Piechnik, *Numerical investigation of the fluid flow distribution for the hydrofluidisation food freezing method*, International Journal of Thermal Sciences, Volume 151, 2020
DOI: 10.1016/j.ijthermalsci.2020.106284

    II. M. Stebel, J. Smolka, M. Palacz, E. Piechnik, M. Halski, M. Knap, E. Felis, T.M. Eikevik, I. Tolstorebrov, J.M. Peralta, S.E. Zorrilla, *Numerical modelling of the food freezing process in a quasi-hydrofluidisation system*, Innovative Food Science and Emerging Technologies, Volume 74, 2021
DOI: 10.1016/j.ifset.2021.102834

    III. M. Stebel, J. Smolka, M. Palacz, M. Halski, A. Widuch, T.M. Eikevik, I. Tolstorebrov, *Numerical analysis of the hydrofluidisation food freezing process of moving products within different liquid water-based solutions using CFD with MPM approaches*, International Journal of Refrigeration, Volume 134, 2022
DOI: 10.1016/j.ijrefrig.2021.12.008

    IV. M. Stebel, J. Smolka, M. Palacz, T.M. Eikevik, I. Tolstorebrov, *Numerical modelling of conjugate heat and mass transfer during hydrofluidisation food freezing in different water solutions*, Innovative Food Science and Emerging Technologies, Volume 75, 2022
DOI: 10.1016/j.ifset.2021.102898

Paper I: Validated model of turbulent flow in hydrofluidisation system

Check for updates

Numerical investigation of the fluid flow distribution for the hydrofluidisation food freezing method

Michal Stebel [*], Jacek Smolka, Michal Palacz, Wojciech Adamczyk, Edyta Piechnik

Institute of Thermal Technology, Silesian University of Technology, Konarskiego 22, 44-100 Gliwice, Poland

ABSTRACT

The food freezing method of hydrofluidisation is based on submerging small food products in an appropriate water-based solution, which is pumped into the tank through orifices in order to increase the heat transfer between the food products and the liquid by creating agitating jets. The highly turbulent refrigerating medium flow, which can be analysed using Computational Fluid Mechanics (CFD), creates significantly higher heat transfer coefficients in comparison to other techniques offering effective freezing, e.g. immersion or impingement jet methods. Therefore, rapid freezing of food products may occur. The aim of this study was to investigate the turbulent refrigerating medium flow within a hydrofluidisation freezing unit. The liquid used for the process was an aqueous solution of ethanol with a mass concentration of 5%. An axisymmetric CFD model has been developed to analyse the configuration with a single orifice and a spherical-shaped artificial food product located at different positions. The parameters being analysed were the orifice diameter (2–5 mm), sphere diameter (5–30 mm), position of the product above the orifice (20–80 mm) and the refrigerating medium mass flow rate (0.00267–0.15 kg·s^{-1}). All cases covered the Reynolds number range of 1700–93,000. The developed model employed two turbulence models: k-ω SST and Reynolds stress model (RSM) which are appropriate for modelling an impinging flow over spherical objects. Validation has been performed using the PIV technique on a hydrofluidisation freezing unit designed for this study. The results being compared were the angle of the boundary layer separation and velocity profiles along the impinging jet and around the spherical object. The results of the CFD simulations confirmed by PIV measurements proved that the refrigerating medium flow is highly agitating around the samples. In addition, the preliminary results of sphere shape potato samples during the cooling process have been presented in this paper.

1. Introduction

The food industry has been transformed significantly over the last several decades due to customer requirements. Food products need to keep their freshness during storage and transport because of both biological stability and customer preferences. The most widespread method used for post-harvest pre-treatment products to achieve a long shelf-life is cooling and freezing, which is a basic part of the food cold chain [1]. Apart from health and hygiene matters, the market demands have become crucial; therefore, huge significant development of this important branch of industry and technology has occurred.

However, during the freezing process, food structures may be affected by the formation of ice crystals within and outside cells [2]. It was proven that rapid freezing has a favourable impact on the biological quality of food products [1]. The small size and uniform distribution of those crystals may be assured by employing emerging

food freezing methods, i.e., impingement jet freezing (IJF) or hydrofluidisation freezing (HF), both of which are characterised by high freezing rates [3].

The issue of damage to food products has been investigated using scanning electron microscopy [4]. The authors compared fresh and frozen strawberries subjected to differing freezing times. The structure of the fruits that were frozen slowly was strongly damaged, while the second sample was almost unaffected at the micro scale. Additionally, slow food freezing results in protein damage [5] and high moisture loss when thawed [3]. Finally, freezing rates adversely affect the taste, which was mentioned in a comparison of different food freezing techniques [6].

The most common technique used currently is air-blast freezing based on convective heat transfer in continuous or batch systems [6]. Its advantages are the ease of maintenance and flexibility; however, the freezing times are long due to the low heat transfer coefficients relative

Nomenclature

Roman Symbols

C_P	Pressure coefficient
c_p	Specific heat capacity, J kg^{-1} K^{-1}
D	Sphere diameter, mm
d	Orifice diameter, mm
g	Gravitational acceleration, m s^{-2}
H	Orifice-stagnation point distance, mm
$H*$	Dimensionless orifice-stagnation point distance, –
k	Turbulence kinetic energy, m^2 s^{-2}
k_t	Thermal conductivity, W m^{-1} K^{-1}
$\dot{m}$	Mass flow rate, kg s^{-1}
p	Static pressure, Pa
R	Radial coordinate measured from axis, mm
r	Radial distance for spherical coordinates, mm
Re	Reynolds number, $(\rho \cdot v_o \cdot D \cdot \mu^{-1})$
T	Temperature, K
t	Time, s
V	Velocity value, m s^{-1}
$V*$	Dimensionless velocity value in reference to maximum value within considered range, –
v_o	Refrigerating medium mean velocity in orifice, m s^{-1}
y+	Dimensionless wall-cell centre distance, –

Greek Symbols

δ_{ij}	Kronecker delta
δ	Relative difference, %
θ	Polar angle, °
μ	Dynamic viscosity, Pa s
μ_T	Turbulent viscosity, Pa s
ρ	Density, kg m^{-3}
ϕ	Azimuthal angle, °
ω	Specific turbulent dissipation rate, s^{-1}

Subscripts

0	Initial conditions
ax	Axial velocity component
rad	Radial velocity component

Abbreviations

CFD	Computational Fluid Dynamics
HF	Hydrofluidisation Freezing
IJF	Impingement Jet Freezing
IF	Immersion Freezing
PIV	Particle Image Velocimetry
$RANS$	Reynolds–averaged Navier–Stokes
RSM	Reynolds Stress Model

to alternative methods [6,7]. Another method being used widely is immersion freezing (IF). In this case, food products are directly submerged in refrigerating medium (water or aqueous solutions) [6]. This method has both pros and cons. The heat transfer is more intensive in comparison with the aforementioned air-blast freezing; however, the food is directly submerged in the liquid. Thus, an uncontrolled solute uptake by the product may occur as an unwanted effect [8].

Two novel methods that have recently been investigated are air fluidisation [9] and IJF, which was investigated for real food products [10] and for objects with simpler shapes like spheres [11]. Another emerging method is HF freezing, which is the subject of this study. In all of these methods, the heat transfer rate is much larger due to the forced fluid flow. Therefore, the freezing process is relatively fast and the quality of the food products can satisfy market needs.

Freezing and cooling with the IJF method is widely used in industry because high heat transfer rates may be reached using the highly turbulent flow. High velocity jets flowing through nozzles strike the surface directly, and therefore, the turbulent flow intensifies the heat transfer within the boundary layer. This method is characterised by the highest heat transfer rate among all single-phase arrangements [12].

Food freezing method of hydrofluidisation, which is a subject of this paper, has been patented by Fikiin [13]. Basically, this technique brings together advantages of immersion and impingement methods. Strongly turbulent refrigerating medium, e.g. ice slurry, [1,14], an aqueous solution of ethanol and sucrose or glucose [15,16] or NaCl water solution [17], is pumped upwards through orifices or nozzles into the refrigerating medium tank. This kind of the flow creates agitating jets inside that tank, where small food products are immersed. During the process, the group of food products behaves as a fluidised bed [6]. The highly turbulent flow over the submerged products increases the convective heat transfer coefficients, which has been confirmed in several studies.

Firstly, the method has been compared with other immersion-type methods for the fish chilling and freezing [18]. It was determined that the freezing times of different kinds of fish using this technique were reduced by half and the heat transfer coefficients were two times or almost three times higher comparing with sprinkling and immersion methods, respectively. The HF system design was proposed in this paper as well. This method has shown its potential; however, there is scarce literature describing it and currently no commercial manufacturers offer HF food freezing systems to the best of the authors' knowledge.

Further laboratory-scale studies were aimed at measuring the cooling process with simpler objects instead of real food products. Verboven et al. performed an experimental study with aluminium spheres instead of food samples [15]. To describe the heat transfer, they proposed Nusselt number correlation based on the sphere diameter, fluid flow rate, the temperature of the fluid during the process and the level of fluid agitation. They suggested that the use of numerical methods could bring a valuable contribution in terms of fluid flow investigations for the freezing technique. Recent studies were performed to examine the HF method using laboratory-scale measurements performed in similar way together with computational fluid dynamics (CFD). Peralta et al. presented the experimental work that resulted in Nusselt number correlation taking into account the main geometrical dependencies in the flow within the HF unit [17]. In the next work of the same group, a mathematical model of the simplified system, which was in good agreement with measurements performed in the previous study, was proposed [19]. That numerical work was complemented with heat and mass transfer phenomena occurring within real food products [20]. Later studies dealt with more complex systems, namely, with numerous products and orifices [21] and an HF numerical model with movement of the food products and mutual collisions [22]. The latter has been complemented with a sensitivity analysis of the variables affecting fluid flow, heat, and mass transfer in an HF unit [23].

The most recent paper describing the HF method is an experimental study of the same system as proposed in the current paper [24]. Palacz et al. used a PIV technique to capture the refrigerating liquid flow field around the stationary spherical sample. They analysed the velocity distribution under different Reynolds numbers and for different values of the orifice-stagnation point distance to the orifice diameter ratio. It

is the only experimental work focused on the velocity distribution in hydrofluidisation units.

In this study, a numerical model of the refrigerating liquid flow around the food products for the idealised case in the hydrofluidisation unit has been presented. Using the CFD modelling supported with PIV measurements allowed for a detailed and reliable assessment of the velocity field in such a system. The motivation of this study was to investigate the refrigerating liquid flow for different geometrical configurations using two turbulence modelling approaches. This is particularly valuable because local quantities have not been measured and validated for HF food freezing systems yet.

Spherical food product sizes and positions above the orifice as well as the orifice diameter are the parameterised variables. Highly turbulent refrigerating medium flow has been described employing k-ω SST turbulence model, which was confirmed to be appropriate for such a flow in a similar study [19] and Reynolds stress modelling, which has not been used for HF system models before. The second approach is more relevant for complex fluid flow analyses [25].

The real process of hydrofluidisation food freezing takes place in the tank with more complex setup of orifices. In addition, the arrangement of real-shape food products is arbitrary and dynamic due to the process of intensive fluid flow. However, this study is focused on the investigation of some parameters identified as important in terms of the fluid flow pattern. The numerical model validation using PIV method could be performed for that kind of the arrangement. The results obtained from the study of the reported simplified system can bring some conclusions and suggestions for further works with more complex setups, e.g. the appropriate selection of the diameter of the orifices for the particular size of food products.

2. Laboratory test rig and measurements

2.1. HF cooling chamber features

For this investigation of the HF method using CFD, it is necessary to validate the obtained results with measurements. A laboratory test rig has been designed and built at the Institute of Thermal Technology in Gliwice, Poland. Apart from the refrigerating medium preparation loop, the HF freezing unit consists of the cooling chamber shown in Fig. 1. The latter was made of ASI 316L stainless steel, thermally insulated and equipped with transparent windows to make the PIV measurements possible. The exact process of HF freezing takes place inside it within a cuboid-shaped tank made of a transparent material, opened from the top. The tank is 150 mm high, 445 mm wide and 280 mm deep. The refrigerating medium flows into it through orifices made in a plate placed at the bottom of the tank. The plate, made of stainless steel, is removable to perform tests with different inflow configurations. Under

the inflow plate with the orifice, a steel deflector was placed to stabilise the pressure level and the liquid flow under the entire plate that occurs due to the impact of the fluid stream from the inflow pipe. Each of two side walls of the tank had two rectangular outflow openings, 20 mm high and 30 mm wide, located in the top corners as presented in Fig. 1 at the left side. They allowed the liquid to flow back to the refrigerating medium reservoir by the gravity. Their location prevents the tank front wall and the middle part of side walls from getting wet during the continuous operation of the HF system. This is significant for the PIV measurements performing, because the liquid film or droplets would perturb the laser beam and result in the light reflections.

2.2. Objects within the field of the refrigerating medium flow

During the investigation of parameters that affect the distribution of the fluid flow within the HF system, processes that occur inside food products may be neglected. Therefore, for the fluid flow study, the food products have been replaced with a single artificial object, namely, a copper sphere with a 20 mm diameter attached to the movable aluminium frame. Only preliminary analyses of the cooling process have been performed using the potato sample having also the spherical shape, which will be discussed further. Samples were hung on a plastic rod, which assures good thermal insulation and stability of the sphere position. Moreover, the rod does not disturb the refrigerating medium turbulent flow in the sensitive areas, which is important for simplifying the numerical model and ensuring that it is possible to perform the PIV measurements. The position of the sphere hanging frame is controlled by two stepper motors. Therefore, the location of samples may be fixed at an exact place and their movements within the tank may be assured in both the vertical and horizontal dimensions.

2.3. Refrigerating medium selection

As mentioned before, different liquids have been used in recent studies of the HF freezing method. For the fluid flow analyses, a diluted solution of ethanol was prepared with a mass concentration of 5%. The potato cooling analyses were performed with a different solution concentration, namely 30%. The main thermal requirement for the refrigerating medium, apart from the density, the viscosity and the heat capacity, is that its freezing temperature be below the initial freezing point of food products. Therefore, using different solutes is a common practice in freezing methods using liquids as a freezing medium. During the process of food product freezing, simultaneous heat and unwanted mass transfer occurs. However, for a rapid freezing method such as HF, the solute intake is expected to be significantly lower when the freezing starts due to a decrease in the effective diffusion coefficient [20]. The effect of mass transfers between the liquid and food products will be investigated during further stages of this research.

Fig. 1. The refrigerating medium tank inside the HF cooling chamber (middle) with a close-up of the side outflow (left) and the copper sphere and orifice arrangement (right). The PIV observation field is shown in red frame.

2.4. Measurement instruments and equipment employed

A test rig has been equipped with appropriate instrumentation. For mass flow rate measurements, two Coriolis type Endress+Hauser Promass E 300 flow meters were installed with a stated accuracy of $\pm 0.1\%$ for mass flow rates higher than 5 kg s^{-1}. A maximum error of approximately $\pm 2\%$ is stated for lower flow rates close to zero. The pressure is measured in the refrigerating medium preparation loop and directly below the plate with orifices by the side of the inflow tank section. Measurement errors from the WIKA S-10 pressure sensors are below $\pm 0.5\%$ of its range. Temperature measurements are performed in five places in the refrigerating medium preparation loop using thermocouples. The location of these sensors along the whole loop is as follows: (1) at the side wall of the compartment being below the refrigerating medium tank, (2) between the refrigerating medium reservoir and the pump, (3) between the pump and the mass flow meter, (4) after the mass flow meter, (5) before the reservoir in the return pipe. Temperature measurements in these places allowed to control if the fluid flow is already stabilised and homogenised. Additionally, temperature measurements may be made at the centre of the cooled sphere and in 36 different spots within the refrigerating medium tank if necessary. T-type thermocouples with a maximum error of ± 1 K were applied for these measurements.

The fluid flow distribution of the refrigerating medium within the tank was visualised using a PIV method using the Dantec Flow Sense 4M MK4 II system equipped with a high-resolution camera and a twin pulse laser. The camera has a CCD sensor with a resolution of 2048×2048 and a pixel size of 7.3 μm. Additionally, a Carl Zeiss APO-Sonnar T* 135 mm f/2 lens with a magnification of 4 was used. The camera was placed facing the front side of the chamber. The field of observation is a rectangle area around the sphere, 63 mm high and wide. The laser illuminates that section from the side. It is a Quantel Twin BSL 200 with a wavelength of 532 nm and an energy output of 200 mJ. For the PIV measurements 5 μm polyamide particles were used as a seed material.

3. Mathematical modelling and computing procedure

3.1. Computational domain

The numerical domain includes the tank with the refrigerating medium, the inflow pipe and the section below the orifice plate with the deflector placed inside, as shown in Fig. 2, which presents the 3-D domain containing one-fourth of the real system and a reduced 2-D axisymmetric domain.

The numerical 3-D domain of the refrigerating medium tank has been reduced to one-quarter with two vertical planes of symmetry. The placement of boundary conditions for that domain is shown in Fig. 2 on the left side. Instead of modelling the free surface of the liquid, the tank has been closed by the wall from its top, since it is not affected by the refrigerating fluid flow within the region of interest. The dimensions exactly reflect the test rig described previously. For the case being considered, the cooled sphere had a 20 mm diameter and was placed 50 mm above the plate. A single orifice with a diameter of 5 mm was placed in the centre of the 5 mm thick plate. The orifice had a chamfered edge with an angle of 45° and a depth of 0.5 mm at the bottom to represent the geometry of the real plate in detail. This case has been selected as a benchmark for the simplified 2-D domain verification.

Due to the tank size, the geometry of the sphere and orifice as well as their mutual placement, an axisymmetric simplified domain could be a proper approach because of the significant decrease in the required computational effort. A comparison of results obtained using the axisymmetric and 3-D domains is presented in further paragraphs.

The axisymmetric 2-D domain has been prepared to have the same configuration as the previously described 3-D domain. It is presented in Fig. 2 on the right side. The radius of the refrigerating medium tank was 200 mm. This value was determined with the assumption of a fixed tank volume. The diameter of the sphere and the distance between the inflow plate and the stagnation point at the bottom of the sphere are parameterised dimensions. Another parameterised dimension for this study was the orifice diameter. The numerical model makes it possible to investigate those values in the range of 20–80 mm for the distance between the inflow plate and the stagnation point of the sphere, 2–5 mm for the single orifice diameter and 5–30 mm for the sphere diameter.

For the fluid flow study, the artificial food product has been excluded from the domain because only the refrigerating medium behaviour has been investigated. However, including of the food product was required for the further preliminary analyses of the cooling process. In addition, the supporting rod that maintains the sphere position has been excluded from the computational domain, like in the numerical model proposed by Peralta et al. [19], because it has no practical effect on the freezing process and the impingement jet flow. Nonetheless, the location of the rod has been marked on the scheme in Fig. 2. Furthermore, the authors of the mentioned paper presented the distribution of the heat transfer coefficient at the sphere surface. It proved, that the heat transfer occurs mainly in the area below the separation point. Therefore, the area of recirculation is less significant in terms

Fig. 2. Numerical domain of the 3-D variant, including one-quarter of the real geometry (left side) and a 2-D axisymmetric variant (right side) with all dimensions indicated in mm.

of the heat transfer. In the unit presented in this study, the rod is situated far above the boundary layer separation point. Hence, the perturbation of the flow occurs only in the area of recirculation, which was not analysed in comparison with the measurements. The results of preliminary analyses proved, that in the area being compared with PIV measurements, flow field distribution was not affected due to supporting rod removing. The velocity has been verified in several points around the sphere. The average differences between the velocity magnitude for the cases with and without the rod were in order of 1%. Maximum difference was 3% and was reported for the point in the region of the flow recirculation.

3.2. Computational procedure

The procedure of numerical processing and data generation has been arranged using the *CoolFoodPL* tool developed for this research. It makes it possible to perform numerous serial simulations by automating the process of geometry and mesh generation, running CFD simulations and generating results. The scheme of the operations sequence is presented in Fig. 3. The commercial software used for the process is ICEM CFD and ANSYS Fluent. The input data describing the operating conditions and geometry are processed, and based on that, a numerical mesh is generated to perform numerical simulations and finally to generate results.

To solve the mathematical model in ANSYS Fluent software, the COUPLED solver has been used for the pressure–velocity coupling for the steady-state computations of the fluid flow field. It turned out to be stable and the most efficient one. All the equations were discretised using second-order upwind schemes. To guarantee the stability of each simulation, the first 100 iterations were performed with lowered values of the under-relaxation factors.

Each solution was considered to be converged when the normalised residuals were less than $1 \cdot 10^{-5}$ for the continuity, both components of the velocity and the turbulence quantities and less than $1 \cdot 10^{7}$ for the energy equation. Moreover, the local values of the velocity were monitored in several points selected arbitrarily located less than 10 mm from the sphere surface.

Apart from the steady-state analyses of the fluid flow, which are the main results of this study, the time-dependent simulations of the cooling process were performed. For these cases, the cooling process was solved after the flow field has been established during steady-state computations.

3.3. Numerical mesh

The numerical 3-D mesh containing one-fourth of the refrigerating medium tank consists of over 8,000,000 hexahedronal elements, which leads to time-consuming calculations. This grid was prepared using a blocking method, which resulted in a structured topology around curved surfaces like the sphere and cylindrical orifice. Within these areas, o-grid mesh structures were applied. Cells sizes do not exceed

1.5 mm in most significant areas, i.e., within the jet flow region, around the sphere or near the orifice. Mesh independence was verified comparing the velocity profiles. Further mesh refinements do not cause significant changes in the refrigerating medium flow distribution.

Numerical meshes for 2-D axisymmetric simulations were generated automatically using the *CoolFoodPL* tool, which makes it possible to generate the geometry and numerical mesh based on input parameters, namely, the orifice diameter, the sphere diameter and the distance between the inflow plate and the sphere stagnation point. Each mesh contains approximately 130,000 quadrilateral elements (depending on the geometry configuration). For that domain, the mesh was arranged to keep the same grid structure, nodes distribution and cell size for the 3-D mesh. Fig. 4 presents an axisymmetric mesh generated for a sample case for the fluid flow field analysis with details in significant areas. A mesh independence study has been performed comparing a few axial and radial velocity profiles, for example along the jet axis. The thickness of the first cell layer around the sphere was set to keep the $y+$ value far below 1.0 for each case being calculated. In this case, the grid complexity was reduced and the quality of cells was improved.

3.4. Governing equations

Fluid flow using the finite volume method was solved by a set of equations. They form so-called governing equations used to describe incompressible flow in terms of mass and momentum conservation in a steady-state or transient flows. The continuum and momentum equations are solved using Reynolds–averaged equations. These equations, given in Eqs. (1) and (2), respectively, include accumulative terms, being neglected during steady-state fluid flow analyses. Moreover, the time-dependent cooling analyses required an additional energy equation, presented in Eq. (3).

- Continuity

$$\frac{\partial \rho}{\partial t} + \frac{\partial}{\partial x_i}\left(\rho u_i\right) = 0 \tag{1}$$

- Momentum

$$\frac{\partial}{\partial t}\left(\rho u_i\right) + \frac{\partial}{\partial x_j}\left(\rho u_i u_j\right) = -\frac{\partial p}{\partial x_i} + \frac{\partial}{\partial x_j}\left[\mu\left(\frac{\partial u_i}{\partial x_j} + \frac{\partial u_j}{\partial x_i} - \frac{2}{3}\delta_{ij}\frac{\partial u_k}{\partial x_k}\right)\right] + \frac{\partial}{\partial x_j}\left(-\overline{\rho u_i' u_j'}\right) + \rho g_j \tag{2}$$

- Energy

$$\rho\frac{\partial T}{\partial t} + \rho u_i\frac{\partial T}{\partial x_i} = \frac{\partial}{\partial x_i}\left[\frac{k_t}{c_p}\frac{\partial T}{\partial x_i} - \rho\overline{T' u_i'}\right] \tag{3}$$

where ρ is the density, t is the time, u_i is the average velocity vector component, u_i' is the fluctuating velocity component, p is the average pressure, μ is the dynamic viscosity, δ_{ij} is the Kronecker delta and g_j is the gravitational acceleration vector component, T is the average temperature, T' is the fluctuating temperature, k_t is the thermal conductivity and c_p is the specific heat capacity.
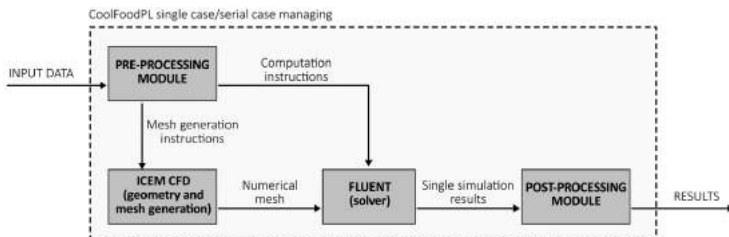
Fig. 3. Scheme of the operations performed for automatic serial computations.
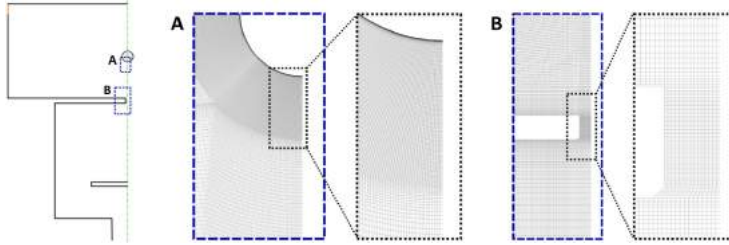
Fig. 4. Details of the 2-D axisymmetric numerical mesh with nearly 130,000 elements presenting quadrilateral elements near the sphere surface (A) and within the orifice area (B) for the case described by the geometrical parameters: $D = 20$ mm, $H = 50$ mm, $d = 5$ mm.

The k-ω SST turbulence model solves two additional equations i.e. for the turbulence kinetic energy and the specific dissipation rate:

• Turbulence kinetic energy

$$\frac{\partial}{\partial x_i}\left(\rho k u_i\right) = \frac{\partial}{\partial x_j}\left[\left(\mu + \frac{\mu_T}{\sigma_k}\right)\frac{\partial k}{\partial x_j}\right] + G_k - Y_k \tag{4}$$

• Specific dissipation rate

$$\frac{\partial}{\partial x_i}\left(\rho \omega u_i\right) = \frac{\partial}{\partial x_j}\left[\left(\mu + \frac{\mu_T}{\sigma_\omega}\right)\frac{\partial \omega}{\partial x_j}\right] + G_\omega - Y_\omega + D_\omega \tag{5}$$

where k is turbulence kinetic energy, μ_T is the turbulent viscosity, σ_k is the turbulent Prandtl number for k, G_k is the generation of k due to mean velocity gradients Y_k is dissipation of k due to turbulence, ω is the specific dissipation rate, σ_ω is the turbulent Prandtl number for ω, G_ω is the generation of ω, Y_ω is the dissipation of ω due to turbulence, and D_ω is the cross-diffusion term.

The effects of turbulence are represented by the term $-\overline{\rho u_i' u_j'}$ in Eq. (2). These are the Reynold stresses. The k-ω SST turbulence model solves Reynolds stresses using the Boussinesq approximation according to Eq. (6). The turbulent viscosity is computed in this approach using a blending function as shown in Eq. (7).

$$-\overline{\rho u_i' u_j'} = \mu_T \left(\frac{\partial U_i}{\partial x_j} + \frac{\partial U_j}{\partial x_i}\right) - \frac{2}{3} k \delta_{ij} \tag{6}$$

$$\mu_T = \frac{\rho k}{max\left(\frac{1}{\alpha^*}; \frac{SF_2}{a_1 \omega}\right)} \tag{7}$$

where α^* is the constant for high-Reynolds formulation, S is the strain rate magnitude, F_2 is the blending function for this model and a_1 is the model constant. Constants $\alpha^* = 1$ and $\alpha_1 = 0.31$

For the Reynolds Stress Model, the Boussinesq approximation is not valid because all the stresses are solved separately. As described in detail in Section 4.2, this model has finally been rejected due to its accuracy comparing with k-ω SST for this particular case. For that reason, a detailed mathematical description of this turbulence modelling approach is not provided in that paper.

3.5. Turbulence modelling

The intensified freezing rate during the HF process is a result of turbulent fluid flow over the food product's surface. Hence, the proper modelling of such a flow is fundamental for the numerical model development of the HF system. Likewise, in impingement flows, Olsson et al. pointed out the jet region, the stagnation zone and the wake zone behind the frozen object [26]. In this study, the k-ω SST and RSM models were used. The first one combines the advantages of Wilcox's original k-ω and the widely used k-ϵ two-equation models, while the second, also called the second-moment-closure model, is the

most complex among all classical turbulence models and solves many simple and complex flows with high accuracy [25].

The first model is widely used for wall-bounded flows. This model solves two additional equations for the turbulence kinetic energy and the specific dissipation rate [27]. It has proven excellent performance with the CFD model of the HF system developed by Peralta et al. [19]. A similar study, namely, a numerical analysis of food cooling using a single jet, was performed, again using the k-ω SST model [11]. In that case, the air jet impinging the cylindrical surface was modelled with good accuracy. Yet, more complex arrangements with multiple spherical samples and inlets were analysed in a work by Olsson et al. using the same turbulence model [26]. In that paper, the heat transfer coefficient distribution was determined with good agreement with experimental data. The further development of HF numerical models described previously proved that the k-ω SST is a good approach for more complex systems involving multiple products and jets [21] and even sphere movement within the refrigerating medium tank [22]. However, it also shows some drawbacks, like an overprediction of the heat transfer rate [26] and a turbulence intensity in some areas mentioned in the paper by Peralta et al. [19].

Another turbulence model employed in this study was the RSM that is known as the most complex among all RANS approaches. It does not assume isotropic eddy viscosity but solves additional transport equations for the Reynolds stresses, with one quantity providing the turbulence length or time scale, e.g., dissipation [28]. The study comparing several turbulence models for impingement flow proved that this model may give more accurate results for the jet region's velocity than other models [29]. Olsson et al. confirmed that RSM predicts heat transfer better than k-ω SST within the recirculation region [30].

The numerous studies mentioned above are based on turbulence modelling in systems close to HF in terms of flow pattern. All those studies, together with the comparison of turbulence numerical modelling and PIV measurements [31], indicate the necessity of investigating this novel food freezing method using different turbulence modelling approaches.

3.6. Fluid physical properties

The refrigerating medium was assumed to be a Newtonian fluid. All properties required for modelling the fluid flow within the HF system were defined using the CoolPack software, wherein the water-ethanol properties are based on the VDI Heat Atlas [32]. Fluid thermo-physical properties, namely, the density, the thermal conductivity, the specific heat and the dynamic viscosity, were computed using polynomial functions of temperature that are presented in Table 1 for constant ethanol concentrations.

Table 1
Polynomial functions of temperature in Kelvin describing the thermo-physical properties for a water-ethanol solution of 5% and 30% concentration.

Property	5% mass concentration	30% mass concentration
Density (kg m^{-3})	$-0.0076019 \cdot T^2 + 4.1835 \cdot T + 415.60$	$-0.0026348 \cdot T^2 + 0.95759 \cdot T + 899.74$
Thermal conductivity (W m^{-1} K^{-1})	$0.0016005 \cdot T + 0.94434$	$0.00063878 \cdot T + 0.22316$
Specific heat (J kg^{-1} K^{-1})	$-0.000014411 \cdot T^2 + 0.012460 \cdot T + 6.6587$	$-0.000044944 \cdot T^2 + 0.028190 \cdot T - 0.18395$
Dynamic viscosity (10^{-3} kg m^{-1} s^{-1})	$0.0042965 \cdot T^2 - 2.4563 \cdot T + 352.83$	$0.016267 \cdot T^2 - 9.4377 \cdot T + 1370.9$

Table 2
Thermo-physical properties of unfrozen potato sample.

Property	Value
Density (kg m^{-3})	1062
Thermal conductivity (W m^{-1} K^{-1})	0.485 [33]
Specific heat (J kg^{-1} K^{-1})	3670 [34]; 3450 [35]

3.7. Physical properties of potato sample

For the preliminary cooling analyses with spherical-shaped potato samples, the properties of this product also had to be evaluated. For a potato with a temperature being above its initial freezing temperature, i.e. about −1.8 °C, the phase change does not occur. Therefore, the properties can be assumed as constant. It is worth to mention that when the phase change is progressing, the sample temperature is decreasing, while the ice content gradually rises. It has a crucial effect on all the properties. For that reason, evaluation of thermal properties of frozen and unfrozen foods is a challenging task. Table 2 presents the properties assumed for this study. The density has been evaluated by measuring the mass and the volume of the group of over 20 potato samples. The thermal conductivity and the specific heat of unfrozen potato have been found in the literature. Because the literature presents different values of the specific heat, this paper covers the results obtained by using two different values of this quantity.

3.8. Boundary conditions

Both the 3-D and 2-D axisymmetric numerical domains are described using several boundary conditions, including the axis of symmetry, as well as the inlet, outlet and wall boundary conditions in order to obtain a complete definition of the mathematical model. The inlet, outlet and spherical wall are indicated in Fig. 2 using captions. The symmetry planes are shown as grey surfaces on the 3-D domain scheme, while the axis is marked using a green line on the 2-D axisymmetric domain scheme. The remaining surfaces are the inflow pipe, the deflector, orifice edges and walls of both chambers, which are described as adiabatic walls.

- The inlet boundary condition is based on the liquid mass flow rate value. Defined quantities are the mass flow rate specified for each case, the temperature of the refrigerating medium as 0 °C and the turbulent intensity, estimated at 5% for this kind of boundary condition arrangement [36].
- The outlet boundary condition is defined by the static pressure value of 10^5 Pa, which corresponds to the ambient pressure.
- In terms of boundary conditions, the top wall was assumed as slip wall, because it is a representation of the liquid free surface. All the other walls are defined as no-slip, adiabatic walls.
- Symmetry within the HF unit was assured by symmetry planes in the case of the 3-D domain and by an axis for the 2-D axisymmetric case.

4. Numerical model verification and validation

4.1. Verification

4.1.1. Domain dimensionality analysis

The laboratory scale HF system designed by Peralta et al. [17], and the numerical model of that unit developed later [19], consists of a cylindrical-shaped tank that can be easily reduced to its parts, e.g., a 60° section due to the axial symmetry of that shape. This type of tank shape also assures more effective freezing since there are no areas such as corners where a decreased agitation level of the liquid flow occurs [15].

However, PIV measurements would be difficult to perform in a refrigerating medium tank of such shape. Therefore, for this study, a rectangle-shaped tank has been designed to make those measurements possible. Furthermore, this configuration of the tank enables a numerical domain reduction into its 90° section.

Further reductions of the rectangle-shaped tank to its axisymmetric simplification may be performed only if the flow pattern is not affected by the shape of the tank. In this study, the orifice and sphere are located at the centre of the tank. Additionally, the field of interest includes only the central area of the tank. For that reason, a simplified axisymmetric domain has been prepared, as described before.

To verify if the flow is dimension-independent, values of the refrigerating medium velocity were compared at several points located 2 mm or 4 mm around the sphere surface. The location of these points and their velocity values are shown in Fig. 5. The origin has been set as the centre point of the sphere. The polar angle ϕ is measured starting from the stagnation point placed at the bottom of the sphere and increases along the flow direction. The comparison was performed for ten groups (P1–P10) of points within the 3-D domain differing only by the azimuthal angle θ together with a corresponding point from the 2-D axisymmetric domain having the same polar angle. Due to the assumption that the refrigerating medium flow is symmetrical around the axis, the azimuthal position around the sphere should not significantly
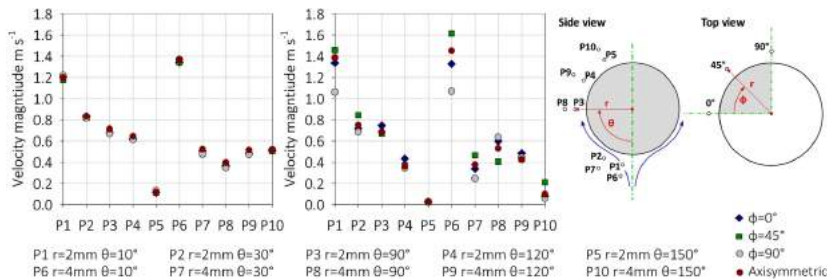
Fig. 5. Velocity values in m s^{-1} for groups of corresponding points for the k-ω SST (left chart) and the RSM (right chart) models with explanations of their placement.

affect the flow, so the velocity values should be approximately the same for all points within each group.

Fig. 5 compares the velocity values within point groups P1–P10 located around the sphere for both the $k\text{-}\omega$ SST and RSM turbulence models. As seen in the figure, the velocity values match with very good agreement for the $k\text{-}\omega$ SST model. The maximum variance of velocity magnitudes equals 0.04 m s^{-1} for group P1 for that model. The velocity values from the 2-D axisymmetric domain are the same as those from the 3-D domain. Therefore, it can be confirmed that the physical behaviour of the flow allows the domain to be reduced into a 2-D axisymmetric view. However, for the RSM turbulence model, variations in the values within several groups of points, especially P1 and P6, are significantly higher and reach up to 0.54 m s^{-1} for the P6 group. This may be a result of anisotropic turbulence formulation, which is a characteristic feature for that particular numerical approach [25]. This suggests that this model might be more adequate for 3-D analyses.

4.1.2. Mesh sensitivity study

As mentioned before, the numerical mesh sensitivity study has been performed comparing some velocity profiles. Fig. 6 presents the velocity profile along the jet axis (the left chart) and the velocity profile in the radial direction from the sphere surface (the right chart). Five different meshes were generated for the case with the sphere diameter of 20 mm, orifice diameter of 5 mm and 50 mm in the distance between the orifice and the stagnation point. They consisted of approximately 38, 57, 83, 125 and 183 thousands of hexagonal cells. The mass flow rate for the grid sensitivity study was set as 0.15 kg s^{-1}, which was a maximum value of a range being studied.

As seen, compared profiles obtained with the mesh having approximately 125,000 elements were roughly the same as the ones obtained with the finest mesh. For that reason, it has been selected as appropriate for this numerical model. The thickness of the first cell layer around the sphere was set to keep the $y+$ value far below 1.0 for every considered case.

4.1.3. Orifice arrangement

The orifice being used to create the fluid jet may be represented in two general ways within the domain. The first way is to define it as an inlet boundary condition using the proper velocity profile, which was done in the numerical model of an HF system developed by Peralta et al. [19]. Another solution is to include the orifice together with the entire inflow section of the domain. This decision is significant, because in such a flow, the orifice design may affect the shear layer behaviour at the jet exit and the jet evolution as a result. That issue was described in the experimental comparison of two jets, where the first one was formed by a smooth contraction nozzle and the second was created by the flow in a long pipe, where the flow profile was fully developed [37]. Fig. 7 contains a description of all arrangements

of the orifice that were compared for model verification. Variants A–C are simplified cases with inlet boundary conditions being used with a uniform velocity value along the boundary. The difference in these cases is its location. For Variants A and B, this boundary condition was defined at the top or bottom of the inflow plate. Variant C includes an additional section for developing the velocity profile. Other options that were compared, namely, Variants D and E, include the fluid domain below the orifice. The orifice in Variant D is a simplified cylindrical opening, while Variant E describes the geometry in detail with all chamfers.

The velocity profiles along the axis from the orifice level to the stagnation point for all described Variants are shown in Fig. 7. For each case, the velocity in the jet core remains stable until reaching a height of 25 mm. Only Variant C results in a smooth drop in the velocity, which may be an effect of the jet profile formation below the orifice. Similar behaviour may be observed in experimental investigations of fully developed impingement jets performed by Lee et al. [38] or in a numerical study by Peralta et al. [19], where the authors assumed the 1/7th power velocity profile. The velocity values for Variant D are significantly higher than those of the others. This is caused by the sharp orifice edge at the bottom. The fluid flowing through the orifice was stagnated near its wall, so the velocity in the jet core increases. For Variant E, this was not observed. The flow had the same behaviour as for Variants A and B in that area. The velocity values are the same for those three variants until it starts to drop after reaching a distance of approximately 30 mm. Variant B tends to show similar behaviour as the one with a developed velocity profile.

This comparison suggested that the proposed Variants A–D give more or less different velocity profiles than the most detailed variant, namely, E. For that reason, the numerical model of the HF system presented in this study includes Variant E.

4.2. Validation

The numerical model validation has been carried out on the laboratory test rig described previously. Measurements of the inflow mass flow rate and the temperature of the refrigerating medium within the loop were used to control the operating conditions. PIV recordings were directly used to compare the velocity within the jet region and around the sphere. At this stage of the experimental study, the PIV fluid flow distribution analysis was conducted at ambient temperature. Therefore, the heat transfer during that investigation was neglected.

The full description of the experimental study in the same HF system is presented in the separate paper [24]. This study describes the velocity distribution using PIV method in detail. Measurements were performed during the continuous process of the fluid flow inside the test rig in a steady-state. Each PIV recording was executed during the period of approximately 30 s when 200 double frames were captured. The recordings were performed at least three times for each case being
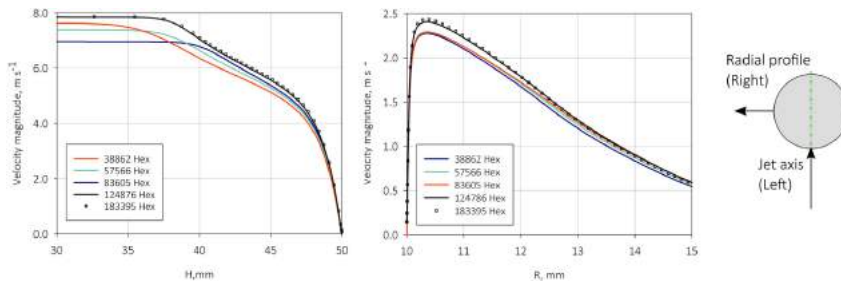
Fig. 6. The velocity profiles compared for the grid sensitivity study along the jet axis (left) and in the radial direction from the sphere surface (right).
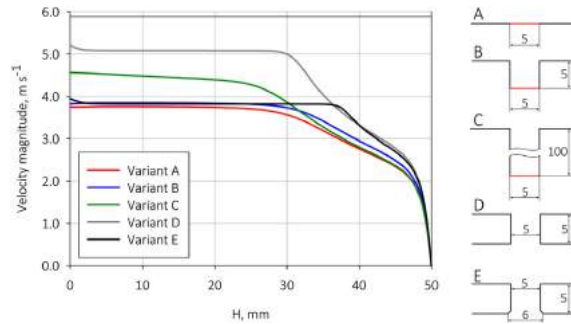
Fig. 7. Comparison of the velocity profiles in m s^{-1} along the axis for different orifice arrangements with their geometrical description and dimensions indicated in mm.

considered. The collected data were analysed using Dantec Dynamic-Studio software. Several procedures were executed in order to improve the quality of the recorded snapshots and the steady-state velocity analyses. Firstly, the Sobel filter was used to increase the contrast, which improved the seeding particles detection. Then, the average correlation was applied to obtain a single scalar map of the refrigerating medium velocity field. The averaging is beneficial for this analysis, because some random defects can be eliminated, e.g. air bubbles flow within the field of observation, laser light reflections, occurrence of the seeding particle with the size significantly different from the median value. For that reason, average correlation method increases the fidelity of the steady-state analysis. In addition, to investigate the fluctuations of the velocity, the recordings were analysed using adaptive correlation method. Values of velocity fluctuations were significant, especially in the area close to the sphere surface. Random defects caused by the air bubbles, seeding particles or the light reflections affected the velocity fluctuations, because they could not be eliminated using that method. Nevertheless, the general trends of the velocity fluctuations were used to analyse the results in terms of this quantity.

The model validation is based on the measurements performed at the different operating conditions presented in Table 3. All the numerical results used for the validation of the model were obtained for the same operational conditions as described measurements. The validation covers a comparison of the refrigerating medium velocities at 6 points, for which the locations are presented in Fig. 8. The same figure presents the measured contours of the fluid velocity distribution that will be described in detail in further paragraphs. Points 1–3 are located along the jet axis, 3 mm, 4 mm and 5 mm below the stagnation point, respectively. Point 4 is located by the left side of the sphere, at the same height as its centre but 1 mm away from its surface. Points 5 and 6 are located 3 mm and 6 mm exactly above the previous point, respectively. Table 4 presents a set of velocity values obtained from all 9 measurement configurations as well as relative differences comparing the CFD results with the PIV measurements, as defined in (8).

$$\delta_{\%} = \left| \frac{v_{PIV} - v_{CFD}}{0.5 \cdot (v_{PIV} + v_{CFD})} \right| \qquad (8)$$

As seen in Table 4, relative differences between measurements and CFD results are generally clearly higher for RSM model than for k-ω SST. For Points 1–3, the mean value of relative difference for all the measurements is equal to 16.3% for RSM model and 11.5% for k-ω SST. It can be noticed that relative difference for Test Cases 3 and 6 at Point 2 exceeds 60%. The mean value of relative difference in that point excluding mentioned measurements is equal to 4.6% for the k-ω SST model. In addition, the Test Case 6 presents high divergence for Point 3 comparing with the results obtained from the k-ω SST model. Points 1–3 were located in the area below the sphere. The measurements of the

Table 3
Operational conditions for the cases used for validation.

Test Case	d (mm)	H (mm)	T (°C)	$\dot{m}$ (kg s^{-1})
1	3	50	17.05	0.04086
2	3	60	17.05	0.04086
3	3	70	17.05	0.04086
4	3	50	17.05	0.05162
5	3	60	17.05	0.05162
6	3	70	17.05	0.05162
7	5	50	16.73	0.1144
8	5	60	16.74	0.1132
9	5	70	16.74	0.1132

refrigerating medium local velocity within regions close to the liquid free surface in the tank were affected by the free surface waving. It was caused by the liquid intensive flow from the orifice. Therefore, measured values at Points 1–3 are most reliable.

The comparison of results from both turbulence models with the PIV results for Point 4 again shows the tendency that values obtained using the k-ω SST model were in better agreement with measured velocity values than the RSM model. The mean relative difference for all test cases was equal to 11.6% and 26.7% for those turbulence models, respectively. It is worth mentioning that this point could be mostly affected by the sphere and the laser beam position, since its distance from the sphere surface was the smallest among all considered points and the velocity gradients are very high near the wall.

Two points located above the area of fluid detachment from the sphere surface are Points 5 and 6. It is seen that the values obtained using the k-ω SST model are in good agreement with the PIV results for Point 5, except for Test Cases 1 and 9. The mean value of the relative difference excluding them is equal to 4.1%. The RSM results do not show such a tendency; the relative differences for that model are equal to 23.0% and 22.9%, including and excluding the mentioned test cases, respectively. However, the comparison for Point 6 shows that the results for both turbulence models differ from the PIV measurements.

In addition, the fluid velocity contours from both turbulence models were compared with two test cases, namely, 5 and 9. That comparison is presented in Fig. 8. The field of observation for these velocity contours is approximately 62 mm high and 42 mm wide. It includes the closest area of the sphere, partially with the fluid jet created by the orifice (nearly 30 mm of the area below the stagnation point is presented in the contours). It is seen that the values of velocity and the thickness of the jet core are closer to the measurements for the k-ω SST model. In addition, the refrigerating medium flow within the region above the sphere is simulated much better using that model, which confirms that the k-ω SST model performs well for flows with the stream detachment from the wall [25]. The RSM model predicts a more

Table 4
Comparison of the velocity magnitude values in m s^{-1} with the values of the relative difference for both turbulence models at 6 points indicated in Fig. 8 for the operating conditions described in Table 3.

Point	Test Case 1			Test Case 2			Test Case 3		
	v_{PIV} (m s^{-1})	$\delta_{\%k-\omega}$	$\delta_{\%RSM}$	v_{PIV} (m s^{-1})	$\delta_{\%k-\omega}$	$\delta_{\%RSM}$	v_{PIV} (m s^{-1})	$\delta_{\%k-\omega}$	$\delta_{\%RSM}$
1	1.57 ± 0.26	12.4%	28.2%	1.56 ± 0.06	15.0%	0.4%	1.08 ± 0.05	1.2%	2.6%
2	1.91 ± 0.05	3.0%	18.8%	1.64 ± 0.06	8.0%	6.7%	1.16 ± 0.03	60.6%	8.5%
3	1.98 ± 0.07	6.2%	21.8%	1.72 ± 0.04	6.1%	8.7%	1.21 ± 0.04	7.5%	11.9%
4	0.59 ± 0.06	12.6%	35.5%	0.70 ± 0.07	1.6%	35.3%	0.57 ± 0.04	0.0%	2.1%
5	0.73 ± 0.13	12.6%	35.1%	0.81 ± 0.10	1.6%	27.1%	0.75 ± 0.10	0.0%	8.9%
6	0.80 ± 0.15	18.0%	12.4%	0.85 ± 0.14	6.9%	5.8%	0.92 ± 0.11	5.1%	6.1%

Point	Test Case 4			Test Case 5			Test Case 6		
	v_{PIV} (m s^{-1})	$\delta_{\%k-\omega}$	$\delta_{\%RSM}$	v_{PIV} (m s^{-1})	$\delta_{\%k-\omega}$	$\delta_{\%RSM}$	v_{PIV} (m s^{-1})	$\delta_{\%k-\omega}$	$\delta_{\%RSM}$
1	2.07 ± 0.31	7.8%	21.8%	1.89 ± 0.13	11.2%	2.6%	1.20 ± 0.07	10.8%	14.2%
2	2.43 ± 0.17	2.2%	16.3%	2.08 ± 0.09	9.6%	0.7%	1.25 ± 0.04	74.1%	22.6%
3	2.46 ± 0.13	7.5%	21.4%	2.16 ± 0.08	6.4%	2.8%	1.31 ± 0.10	21.6%	25.5%
4	1.08 ± 0.10	0.7%	64.8%	0.81 ± 0.06	5.9%	24.1%	0.72 ± 0.10	4.2%	1.9%
5	1.04 ± 0.49	0.7%	41.4%	1.05 ± 0.13	5.9%	26.8%	0.91 ± 0.14	4.2%	2.9%
6	1.00 ± 0.65	18.2%	7.2%	1.15 ± 0.18	0.6%	9.9%	1.13 ± 0.18	3.4%	3.0%

Point	Test Case 7			Test Case 8			Test Case 9		
	v_{PIV} (m s^{-1})	$\delta_{\%k-\omega}$	$\delta_{\%RSM}$	v_{PIV} (m s^{-1})	$\delta_{\%k-\omega}$	$\delta_{\%RSM}$	v_{PIV} (m s^{-1})	$\delta_{\%k-\omega}$	$\delta_{\%RSM}$
1	4.33 ± 0.20	11.9%	18.8%	2.58 ± 0.20	5.9%	28.4%	1.96 ± 0.20	7.7%	30.1%
2	4.48 ± 0.23	6.2%	21.8%	2.96 ± 0.18	2.6%	24.0%	2.36 ± 0.04	0.5%	22.1%
3	4.52 ± 0.27	1.0%	25.0%	3.32 ± 0.14	2.3%	18.3%	2.55 ± 0.17	0.2%	21.1%
4	1.39 ± 0.42	7.8%	50.9%	1.06 ± 0.12	8.3%	18.2%	1.04 ± 0.18	24.0%	7.5%
5	1.43 ± 0.66	7.8%	34.4%	1.34 ± 0.21	8.3%	19.7%	1.09 ± 0.15	24.0%	9.7%
6	1.47 ± 0.56	19.0%	8.8%	1.56 ± 0.33	7.2%	8.2%	1.23 ± 0.21	26.1%	21.7%
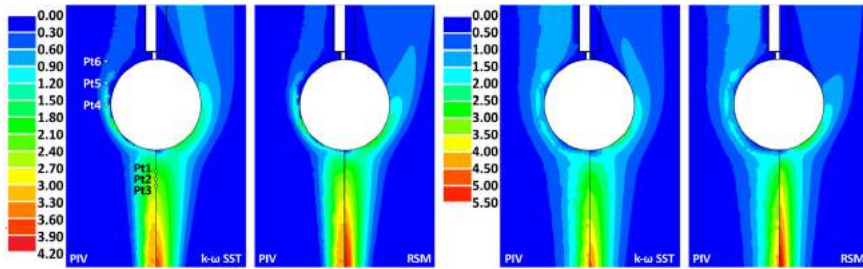
Fig. 8. The velocity contours of the jet and of the area around the sphere in m s^{-1} obtained using the k-ω SST or the RSM turbulence models compared with the PIV results for Test Case 5 (left pair of contours) and Test Case 9 (right pair of contours). The location of the PIV observation region is presented in Fig. 1.

dispersed flow in that area. In Fig. 9, the velocity values were compared along the three characteristic Profiles A, B and C for the previously discussed Test Cases 5 and 9. Those values along Profile A in the jet axis confirm that the k-ω model predicts the refrigerating medium flow within that region with high accuracy. Depending on the case, the simulated profiles start to diverge from the measured values around 12–20 mm below the stagnation point. However, those differences are not significant from the point of view of the HF freezing method. The velocity profiles obtained using the RSM model show that this model overpredicts the velocity within the area of the jet core. Similar situation was described by Shademan et al. [29]. They compared the jet centreline velocity values simulated using k-ω SST and RSM turbulence models with the measurements performed by Rajaratnam et al. [39]. In that comparison, k-ω SST predicted the velocity profile more accurately. Also in their study, the measured velocity values were lower than the numerical results in some distance below the stagnation point. The authors indicated, that the nozzle geometry could be a reason of this discrepancy.

Velocity comparisons along Profile B, located in the radial direction starting from the stagnation point, show that both turbulence models accurately predict the tendency of the velocity to decline along this profile. Fig. 9 also presents velocity values along Profile C located

exactly 5 mm above Profile B. In that case, the PIV and the CFD results are different, especially close to the sphere surface. Within that area, the measurements were most sensitive for all the factors mentioned before. However, the shape of the velocity profile starts to be comparable 2 mm from the sphere surface.

To summarise, the numerical model predicts the refrigerating medium velocity with satisfactory accuracy for both turbulence models within the points and profiles being examined. However, the velocity values obtained using the k-ω SST model are more accurate than the RSM in comparison with the PIV measurements, especially within the jet region, which affects the liquid flow over a spherical object. Moreover, the shape of the jet obtained using the k-ω SST and presented in Fig. 8 suggests that this model performs better for the flow within such a system. For this reason, this turbulence model has been selected for the presentation of results in further paragraphs.

5. Results

5.1. Investigated configurations

The range of conditions being studied using numerical models employing the k-ω SST turbulence model covers different configurations of

Fig. 9. Validation of the velocity in m s^{-1} along profiles A (top), B (centre), and C (bottom).

Table 5
Parameters of the considered cases.

Case number	d (mm)	D (mm)	H (mm)	$\dot{m}$ (kg s^{-1})	v_o (m s^{-1})	Re
Case 0	5	20	50	0.08333	4.28	34,365
Case 1	5	20	50	0.05000	2.57	20,619
Case 2	5	20	50	0.11673	5.99	48,112
Case 3	5	20	50	0.1500	7.71	61,858
Case 4	5	5	50	0.083330	7.71	15,464
Case 5	5	10	50	0.08333	4.28	17,183
Case 6	5	15	50	0.08333	4.28	25,774
Case 7	5	25	50	0.08333	4.28	42,957
Case 8	5	30	50	0.08333	4.28	51,548
Case 9	5	20	20	0.08333	4.28	34,365
Case 10	5	20	40	0.08333	4.28	34,365
Case 11	5	20	60	0.08333	4.28	34,365
Case 12	5	20	80	0.08333	4.28	34,365
Case 13	2	20	50	0.01333	4.28	34,365
Case 14	3	20	50	0.03000	4.28	34,365
Case 15	4	20	50	0.05333	4.28	34,365
Case 16	3	20	30	0.03000	4.28	34,365
Case 17	3	20	45	0.03000	4.28	34,365
Case 18	3	20	60	0.03000	4.28	34,365
Case 19	3	20	40	0.05000	7.14	57,276
Case 20	4	20	60	0.05000	4.01	32,218
Case 21	4	20	80	0.05000	4.01	32,218
Case 22	5	20	75	0.08333	4.28	34,365

Due to the vast amount of data, the results for only the representative variants given in Table 5 are presented in this study. Case 0 can be considered as a reference case, as it is compared with the other cases commonly.

5.2. Boundary layer separation

The enhancement of convective heat transfer in the IJF method is a result of the boundary layer breaking up [40]. Heat transfer coefficient profiles along a spherical surface are dependent on the location of the boundary layer separation point. Values of this coefficient suddenly drop at the point of separation; however, behind that spot, they increase due to the occurrence of fluid wakes [11].

Boundary layer separation points have been found using coordinates where the velocity vector changes its direction dramatically within cells near the sphere surface. Coordinates are given using the polar angle of a spherical coordinate system, where 0° corresponds to the stagnation point position. The mean value with its standard deviation of the separation angle from all 5304 cases is $146.2 \pm 1.1°$. Fig. 10 presents the effects of sphere position, sphere diameter, orifice diameter and refrigerating medium mass flow rate on the separation angle. It can be seen that these parameters have a minor impact on its value; however, when the sphere has a diameter less than 15 mm, a decrease in the separation angle is clear.

For the range of Reynolds number being investigated in this study, the separation angle value is close to values reported in the literature. According to Cengel, the boundary layer separation angle of 140° for the flow over a sphere was noticed for the Reynolds number range that corresponds with this study [35]. In the paper of a similar system by Peralta et al. the value of the angle was approximately 138° [19]. Those authors pointed out that the delay of the boundary layer separation for such a flow can be a result of Coanda effect [41].

5.3. Pressure coefficient

In many papers describing the flow over some objects, the distribution of the pressure coefficient on the surface is presented. This quantity, defined according to Eq. (9), is dimensionless. Therefore it is convenient for comparison, even for cases with different geometry. In the numerical study of similar system, the pressure coefficient was compared for different values of the H/d ratio, Reynolds number and

geometrical parameters like the orifice diameter, the sphere diameter and the sphere position above the inflow plate given as the distance between the orifice and stagnation point. The refrigerating medium mass flow rate was also investigated in this study. The orifice diameter varied from 2 mm to 5 mm with steps of 1 mm. The diameter of the sphere was 5 mm to 30 mm with steps of 5 mm. The last investigated geometrical parameter was the distance between the orifice and the sphere stagnation point, which varied from 20 mm to 80 mm with steps of 5 mm. It has to be mentioned that the mass flow rate range was dependent on the orifice diameter in order to keep the same level of mean jet velocity. Therefore, for the orifice diameter of 2 mm, the range was from 0.002667 kg s^{-1} to 0.024 kg s^{-1}, while for the diameter of 3 mm, it varied from 0.006 kg s^{-1} to 0.054 kg s^{-1}. For an orifice diameter of 4 mm, the range varied from 0.01067 kg s^{-1} to 0.096 kg s^{-1}. Finally, for a diameter of 5 mm, it ranged from 0.01667 kg s^{-1} to 0.15 kg s^{-1}. For each orifice diameter, 17 values of the mass flow rate were investigated, and the values of the step change were 0.00133 kg s^{-1}, 0.003 kg s^{-1}, 0.00533 kg s^{-1} and 0.00833 kg s^{-1} for the mentioned orifices diameters in ascending order. The refrigerating medium temperature was set as 0 °C for all cases. Reynolds number, defined taking into consideration the mean fluid velocity in the orifice and the sphere diameter, covered a range of 1700–93,000. There were 5304 single cases simulated in total.

Fig. 10. Values of the boundary layer separation angle for different values of the parameters being investigated: *H*, *D*, *d* and *ṁ*.

the liquid temperature [19]. It was proven, that the distance between the orifice and the stagnation point has a significant effect on the pressure coefficient if the orifice diameter is fixed. The authors also confirmed that similar profiles are observed for cases with the jets impinging curved or flat surfaces.

$$C_P = \frac{p - p_\infty}{\frac{1}{2}\rho v_0} \quad (9)$$

where C_P is the pressure coefficient, p is the static pressure at the point of the pressure coefficient evaluation, p_∞ is the static pressure in the free-stream and v_0 is the average velocity in the orifice.

Fig. 11 presents the distribution of the pressure coefficient on the sphere surface in the function of the angular position. In the region of stagnation point, the pressure coefficient reaches the values in the range of 0.42 and 0.52. At the position of 30–50°, it reaches the value being slightly below 0 and then remains stable. The cases being compared with the literature [19] are characterised by the same H/d ratio of 10 and similar Reynolds numbers. As seen, Case 16 is in a good agreement with the literature, while the pressure coefficient for Case 0 is significantly higher. Both cases have the same Reynolds number and the H/d ratio, however, the orifice diameter for both cases is different. In the papers describing the jet impinging curved [38] or flat surfaces [29], Reynolds number is defined using the orifice diameter as a characteristic length. However, in the HF method, the frozen product dimension, e.g. the sphere diameter, is considered as the representative length [19]. Hence, when different orifice diameters are compared, this matter has to be taken into account.
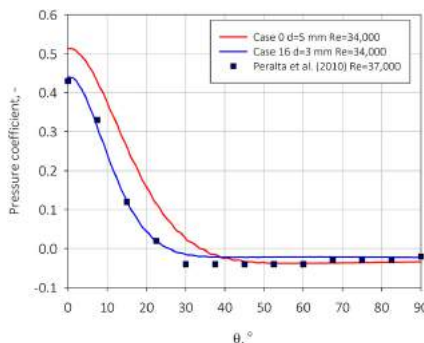
5.4. Velocity profile along the jet axis

The velocity distribution within the jet has characteristic features. Within the region of the jet potential core, the refrigerating medium velocity remains constant along the axis after flowing through the orifice. The velocity starts to decrease until reaching the stagnation point, where the jet impinges the sphere surface.

The parameters being investigated in this case, namely, the orifice diameter, the sphere diameter, the sphere position above the orifice and the refrigerating medium mass flow rate, may have an impact on the jet profile, which finally affects the fluid flow over a spherical artificial food product.

To compare the effects of all the mentioned parameters on the velocity profile, the velocity values as well as the profile length were shown using dimensionless quantities. The dimensionless velocity was defined as the ratio of the local refrigerant velocity to the mean velocity at the orifice. The dimensionless orifice-stagnation point profile length was defined as the ratio of the local position measured from the orifice to the total length of this profile.

As seen in Fig. 12, the refrigerating medium mass flow rate has a negligible impact on the jet profile shape. Within a Reynolds number range from 21,000 to 62,000 the flow pattern is the same. The velocity profile tends to decline closer to the stagnation point for cases with a higher mass flow rate. However, the increasing mass flow rate magnifies the fluid velocity; therefore, this tendency is insignificant. Fig. 13 presents the same comparison of profiles for cases with various sphere diameters. It can be seen that this parameter does not affect the flow within the jet potential core. Reynolds number change from 15,000 to

Fig. 11. Pressure coefficient on the sphere surface for two cases with different orifice diameter compared with the case from the literature.
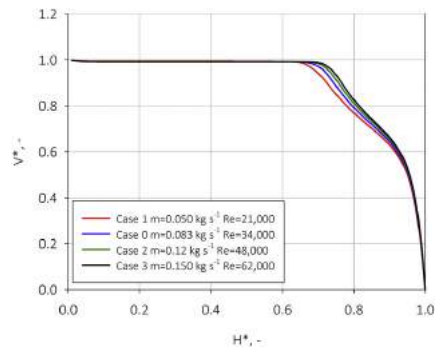
Fig. 12. Velocity profiles along the jet axis for different mass flow rates.
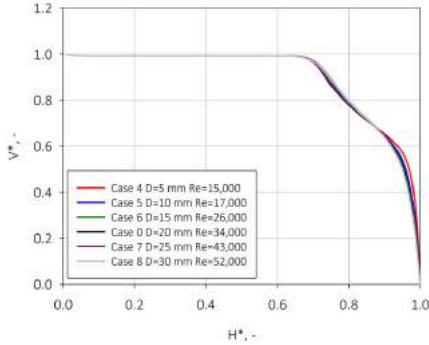
Fig. 13. Velocity profiles along the jet axis for different sphere diameters.
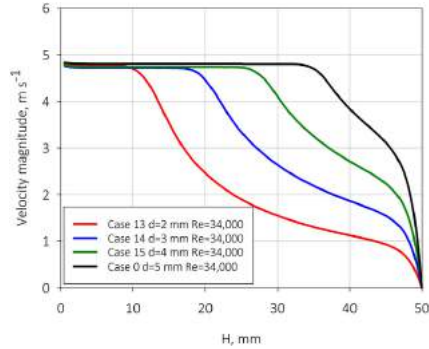
Fig. 15. Velocity profiles along the jet axis for different orifice diameters.

52,000 has not affected the flow along the axis. The only difference can be observed directly below the stagnation point. In addition, the case for which of the velocity profile differs from the others is Case 4, with the smallest sphere diameter of 5 mm and the lowest Reynolds number of approximately 15,000.

Different parameters that have an influence on the jet potential core diameter and length are the orifice diameter and the sphere position. As seen in Fig. 14, a change in the orifice-stagnation point distance significantly affects the velocity profile. A comparison of the presented profiles suggests that the velocity along the jet axis is not affected by the sphere until it approaches the region of stagnation. Refrigerating medium velocity decreased approximately 5–20 mm below the stagnation point, depending on the specific case. For variants where the sphere is placed higher, the jet stagnation tends to be smoother. In Case 9 and Case 10 this region has been reached before the velocity started to decrease due to the jet potential core decay. Similar situation was observed in the numerical and experimental study of similar case, where the maximum H/d ratio was 4 [42]. As was mentioned, the orifice diameter also plays a major role. For variants with a smaller orifice, the jet potential core is significantly shortened, as shown in Fig. 15.

The paper describing similar configurations of jets impinging spherical surfaces [38] and the HF system analysis [17] suggest that the ratio

of the orifice-stagnation point distance to the orifice diameter seems to be essential for this analysis. Fig. 16 compares configurations with different orifice diameters and sphere positions using a dimensionless velocity and distance between the orifice and the stagnation point. The combination of these variants brings three different values of the orifice-stagnation point distance to the orifice diameter ratio. It is noticed that keeping the same value of this ratio results in having comparable velocity profiles along the jet axis, although changes in individual parameters affect the profile shape, as was shown previously. It is worthy to refer to the study of Shademan et al. where the authors extensively described the velocity profiles along the axis for cases with different H/d ratios [29]. According to this study, the H/d value of 18.5 is sufficient for the full development of all the jet sub-regions.

5.5. Velocity distribution around the sphere surface

Refrigerating medium flow was also investigated along an orbital profile located 0.5 mm away from the sphere surface. Both the axial and radial components of velocity were compared. All given parameters were tested in terms of characterising the flow. However it was observed that the only parameter that did not affect the fluid flow profile along the profile was the orifice diameter. For that reason, profiles of the velocity components were compared for cases with different orifice
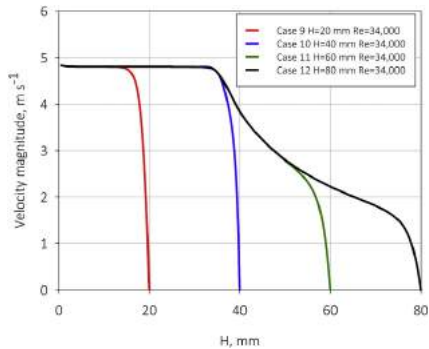
Fig. 14. Velocity profiles along the jet axis for different orifice-stagnation point distances.
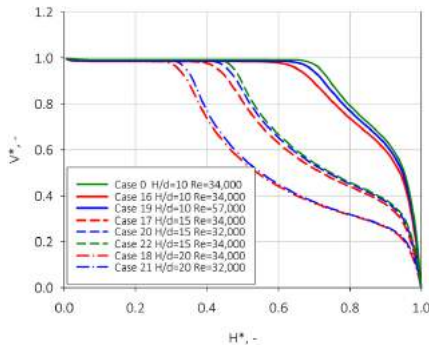
Fig. 16. Velocity profiles along the jet axis for H/d ratio values of 10, 15, and 20.

diameters. The comparison was performed again using a dimensionless velocity, defined as the ratio of the local radial or axial velocity to its value reached at the profile's maximum value.

It can be seen in Fig. 17 that the orifice diameter affects the axial velocity near the stagnation point region. This is in good agreement with the comparison of the velocity profiles along the jet axis for cases with different orifice diameters, where a similar tendency was noticed. The highest axial velocity value is reached at the same point located 60° from the stagnation point for all the considered cases. All the profiles again diverge above that point. This suggests that both the orifice diameter and the refrigerating medium jet affect the fluid flow above the sphere. Negative values of the axial velocity are reached at angles of 130–140°, depending on the case. Wakes start to occur there, and the refrigerating medium starts to recirculate, which results in the convective heat transfer being enhanced.

Fig. 18 presents the radial velocity component along the same profile. For all cases, the velocity rises from zero near the stagnation point and reaches a maximum value at approximately 30°. The profiles start to diverge after reaching an angle of 100°. Again, the wakes are noticeable above the sphere where the values of the radial velocity are positive.
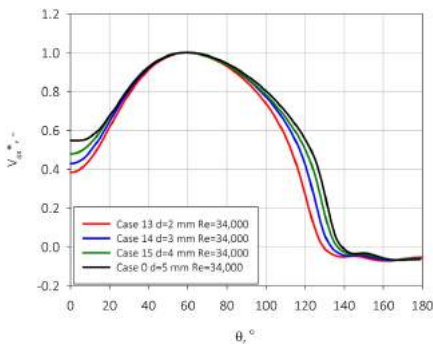
Fig. 17. Axial velocity profiles along the profile around the sphere for variants with different sphere diameters.
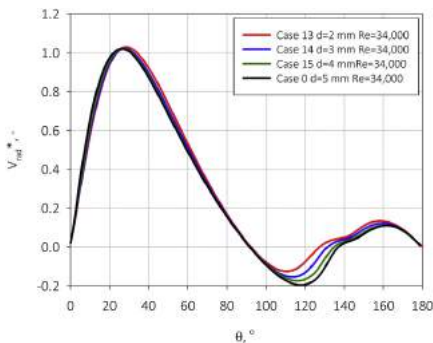
Fig. 18. Radial velocity profiles along the profile around the sphere for variants with different sphere diameters.

Table 6
Operational conditions for the cases used for cooling analyse.

Case number	d (mm)	H (mm)	T (°C)	$\dot{m}$ (kg s^{-1})	D (mm)	T_0 (°C)
Case HT.1	5	50	−0.4	0.05000	30	14.9
Case HT.2	5	50	−1.1	0.08333	30	13.8

5.6. Preliminary cooling analysis of food sample

In order to assess the heat transfer in the presented system, a preliminary cooling analysis has been performed. Due to high thermal conductivity, a copper sphere used for a fluid flow analysis would be cooled down in seconds and, as a consequence, results would be not accurate. Therefore, at this stage, an artificial object has been replaced by a real food product. The product selected for this analysis was a potato because it is a common product with a uniform internal structure. To achieve repeatable results, spherical samples having a diameter of 30 mm were cut out from a whole potato piece.

In this study, only the cooling of these samples is presented, therefore the temperatures were held above the freezing point of potatoes. The exact process of the phase change within the foods is more complex and was not implemented in the model presented in this paper. The characteristic feature for a freezing of foods is that it does not occur at a fixed temperature or a specific range of temperatures, but it is a process progressing gradually below an initial freezing temperature of a food product. It takes place in such a manner due to the concentration change of the solids being dissolved in a liquid water within the food tissues during the freezing [43].

As mentioned before, the samples were cooled in temperature above the initial freezing point of samples. The cases being compared cover experimental results with the numerical results obtained with the k-ω SST and RSM turbulence approaches. The operating conditions used for this comparison are described in Table 6.

The results of numerical simulations and experimental measurements of the spherical potato sample cooling in the HF unit are presented in Fig. 19. For both cases, 500 s of the cooling process was enough to cool the samples down to the temperature being close to the refrigerating medium. The potato samples centre temperatures after this time were 1.8 °C and 1.6 °C higher than the refrigerating medium temperatures for cases HT.1 and HT.2, respectively. It should be mentioned that the solution temperature was relatively high for both cases, there was only one orifice installed in the system and the sample had relatively high diameter in comparison with the food products being more appropriate for the HF method. At the industrial scale, food products cooling would be much quicker.

The differences between the results obtained numerically using different turbulence approaches are not significant. In the process, where the heat transfer realised by the forced convection is very intensive, the heat transfer by conduction within the food product causes the major thermal resistance. This relation may be different and depend on the refrigerating medium flow conditions and on the food product itself, i.e. its properties, the shape and the size.

For the case HT.1, differences between the simulated and measured temperatures reach up to 2 K, which is higher value than the thermocouple measurement error. The difference depends on the turbulence model as well as on the value of the specific heat of the food product. The time required to cool down the potato sample centre point to the temperature of 2 K is about 70 s higher for the measurements than for the numerical results with the k-ω SST turbulence approach employed with the specific heat value of 3670 J kg^{-1} K^{-1}. The highest difference in time required to reach that temperature with respect to the experimental results is for the case with k-ω SST model and the specific heat of 3450 J kg^{-1} K^{-1}, while the lowest is for the case with RSM model and the specific heat assumed as 3670 J kg^{-1} K^{-1}. These differences are 90 s and 40 s, respectively.
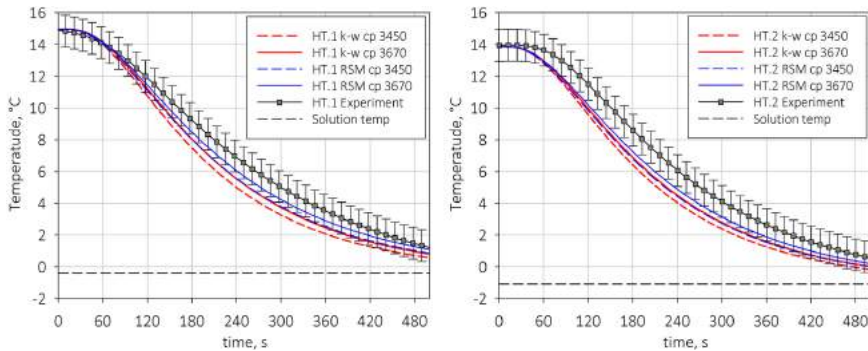
Fig. 19. The temperatures of the spherical potato samples HT.1 and HT.2 during the HF cooling.

For the Case HT.2, differences in the temperatures are slightly higher and reach up to 3 K. Comparing the time required to cool down the centre point of the potato to the temperature of 2 °C, the higher difference concerning the measurements is about 80 s and the lowest is 40 s for the same simulation settings as for the first case. As seen, for the cases HT.1 and HT.2, the assumed value of the specific heat is at least as much important as the turbulence model used for the numerical simulation.

Taking into consideration the fact of handling with real food product in such a flow, the presented results are satisfactory. Apart from the physical properties evaluation, the measurements were very sensitive to the sample shape, its positioning and the positioning of the thermocouple measuring the temperature at the centre point of the sample. The reason for selecting quite high diameter of the sample was to minimise the error based on the thermocouple positioning in the centre point of the spherical sample.

6. Conclusions

In this study, a CFD model of refrigerating medium flow within a laboratory-scale HF system has been proposed. A numerical domain has been defined based on the HF unit designed for this work. Real food products have been replaced by a copper sphere in order to study the fluid flow around an artificial object having a regular shape. One arrangement of the single orifice and single sphere was used to study the refrigerating medium flow within a wide range of the geometrical variations in such a system. For this type of HF system, two turbulence models were examined: k-ω SST and RSM. The results of the validation performed using the PIV technique suggested that the k-ω SST model predicts the fluid flow with higher accuracy, especially within the area of the highly turbulent refrigerating medium jet.

The performance of numerous simulations with various geometrical configurations and operating conditions was conducted by employing the *CoolFoodPL* application designed for automatically preparing and solving multiple cases.

The main purpose of this study was to develop, verify and validate a numerical model for simulating the turbulent flow of refrigerating medium within an HF system. The obtained results proved that the velocity profiles along the axis of the fluid jet core are mostly affected by the orifice-stagnation point distance and the orifice diameter. In addition, the profiles are similar if the ratio of those geometric parameters is maintained. The shapes of the axial and radial velocity profiles also show similar trends along the profiles close to the sphere surface, with exceptions in some characteristic areas. The angle of separation point of the boundary layer near the sphere surface was not significantly affected by the parameters that were investigated and was equal to approximately 147° for all cases.

Moreover, the preliminary study of a real food product cooling has been presented. The process has been conducted above the initial freezing temperature of a potato. The results give an overview of the time required to start freezing in the presented simplified HF system. The measurements of the potato centre point temperatures have been compared with the numerical results obtained with different values of specific heat and with both approaches of the turbulence modelling used in the proposed HF system model. The accuracy of the CFD results is satisfactory in comparison with the measurements, taking into consideration the difficulties in performing such an experiment and in the evaluation of the real food product physical properties.

The refrigerating medium flow in the HF unit being studied was properly modelled with appropriate assumptions and a turbulent model. This has been confirmed by comparing the numerical results with the performed PIV measurements for 9 cases varied by the refrigerating medium mass flow rate, the orifice diameter and the sphere placement.

Declaration of competing interest

The authors declare that they have no known competing financial interests or personal relationships that could have appeared to influence the work reported in this paper.

Acknowledgements

References

[1] K.A. Fikiin, Emerging and novel freezing processes, in: Frozen Food Science and Technology, Blackwell Publishing Ltd., Oxford, UK, 2008, pp. 101–123, chapter 5.

[2] C. James, G. Purnell, S.J. James, A review of novel and innovative food freezing technologies, Food Bioprocess Technol. 8 (8) (2015) 1616–1634.

[3] T. Marazani, D.M. Madyira, E.T. Akinlabi, Investigation of the parameters governing the performance of jet impingement quick food freezing and cooling systems - A review, Procedia Manuf. 8 (2017) 754–760.

[4] A.E. Delgado, A.C. Rubiolo, Microstructural changes in strawberry after freezing and thawing processes, LWT - Food Sci. Technol. 38 (2) (2005) 135–142.

[5] D. Góral, F. Kluza, Physical changes of vegetables during freezing by conventional and impingement methods, Acta Agrophys. 7 (1) (2006) 59–71.

[6] R.H. Mascheroni, Operations in Food Refrigeration, CRC Press, 2012.

[7] P. Dempsey, P. Bansal, The art of air blast freezing: Design and efficiency considerations, Appl. Therm. Eng. 41 (2012) 71–83.

[8] S.E. Zorrilla, A.C. Rubiolo, Mathematical modeling for immersion chilling and freezing of foods: Part II: Model solution, J. Food Eng. 66 (3) (2005) 339–351.

[9] D. Góral, F. Kluza, Heat transfer coefficient in impingement fluidization freezing of vegetables and its prediction, Int. J. Refrig. 35 (4) (2012) 871–879.

[10] F. Erdogdu, M. Ferrua, S.K. Singh, R.P. Singh, Air-impingement cooling of boiled eggs: analysis of flow visualization and heat transfer, J. Food Eng. 79 (3) (2007) 920–928.

[11] C. Dirita, M.V.D. Bonis, G. Ruocco, Analysis of food cooling by jet impingement, including inherent conduction, J. Food Eng. 81 (1) (2007) 12–20.

[12] A. Dewan, R. Dutta, B.V. Srinivasan, Recent trends in computation of turbulent jet impingement heat transfer, Heat Transfer Eng. 33 (4–5) (2012) 447–460.

[13] A.G. Fikiin, Method and System for Hydrocooling of Fish, Invention Certificate No. 40164, Bulgarian Patent Agency INRA, 1985.

[14] K.A. Fikiin, W. Ming-Jian, M. Kauffeld, T.M. Hansen, Direct contact chilling and freezing of foods in ice slurries, 2005, pp. 251–271.

[15] P. Verboven, N. Scheerlinck, B.M. Nicolai, Surface heat transfer coefficients to stationary spherical particles in an experimental unit for hydrofluidisation freezing of individual foods, Int. J. Refrig. 26 (3) (2003) 328–336.

[16] K.A. Fikiin, O.B. Tsvetkov, Y.A. Laptev, A.G. Fikiin, V.S. Kolodyaznaya, Thermophysical and engineering issues of the immersion freezing of fruits in ice slurries based on sugar-ethanol aqueous solutions, 2001, pp. 10–15.

[17] J.M. Peralta, A.C. Rubiolo, S.E. Zorrilla, Design and construction of a hydrofluidization system. Study of the heat transfer on a stationary sphere, J. Food Eng. 90 (3) (2009) 358–364.

[18] A.G. Fikiin, New method and fluidized water system for intensive chilling and freezing of fish, Food Control 3 (3) (1992) 153–160.

[19] J.M. Peralta, A.C. Rubiolo, S.E. Zorrilla, Mathematical modeling of the heat transfer and flow field of liquid refrigerants in a hydrofluidization system with a stationary sphere, J. Food Eng. 99 (3) (2010) 303–313.

[20] J.M. Peralta, A.C. Rubiolo, S.E. Zorrilla, Mathematical modeling of the heat and mass transfer in a stationary potato sphere impinged by a single round liquid jet in a hydrofluidization system, J. Food Eng. 109 (3) (2012) 501–512.

[21] E.E. Belis, S.E. Zorrilla, J.M. Peralta, Effect of the number of orifices and operative variables on the heat and mass transfer in a hydrofluidization system with static spheres, J. Food Eng. 153 (2015) 96–107.

[22] J.D. Oroná, S.E. Zorrilla, J.M. Peralta, Computational fluid dynamics combined with discrete element method and discrete phase model for studying a food hydrofluidization system, Food Bioprod. Process. 102 (2017) 278–288.

[23] J.D. Oroná, S.E. Zorrilla, J.M. Peralta, Sensitivity analysis using a model based on computational fluid dynamics, discrete element method and discrete phase model to study a food hydrofluidization system, J. Food Eng. 237 (2018) 183–193.

[24] M. Palacz, W. Adamczyk, E. Piechnik, M. Stebel, J. Smolka, Experimental investigation of the fluid flow inside a hydrofluidisation freezing chamber, Int. J. Refrig. 107 (2019) 52–62.

[25] H.K. Versteeg, W. Malalasekera, An Introduction to Computational Fluid Dynamics: The Finite Volume Method, Pearson Education, 2007.

[26] E.E.M. Olsson, L.M. Ahrne, A.C. Trägårdh, Flow and heat transfer from multiple slot air jets impinging on circular cylinders, J. Food Eng. 67 (3) (2005) 273–280.

[27] T.J. Chung, Computational Fluid Dynamics, Cambridge University Press, 2010.

[28] S.B. Pope, Turbulent Flows, Cambridge University Press, 2000.

[29] M. Shademan, R. Balachandar, R. Barron, CFD analysis of the effect of nozzle stand-off distance on turbulent impinging jets, Can. J. Civil Eng. 40 (7) (2013) 603–612.

[30] E.E.M. Olsson, H. Janestad, L.M. Ahrné, A.C. Trägårdh, R.P. Singh, Determination of local heat-transfer coefficients around a circular cylinder under an impinging air jet, Int. J. Food Prop. 11 (3) (2008) 600–612.

[31] F. Bode, K. Sodjavi, A. Meslem, I. Nastase, Comparison of turbulence models in simulating a cruciform impinging jet on a flat wall, in: Proceedings of the 15th International Heat Transfer Conference, 2014.

[32] V. Gesellschaft, VDI Heat Atlas, Springer Berlin Heidelberg, 2010.

[33] M.S. Rahman, Food Properties Handbook, CRC press, 2009.

[34] ASHRAE, ASHRAE handbook: Refrigeration : SI Edition, American Society of Heating, Refrigerating and Air-Conditioning Engineers, 2006.

[35] Y.A. Cengel, Fluid Mechanics, McGraw-Hill Education, 2010.

[36] F. Russo, N.T. Basse, Scaling of turbulence intensity for low-speed flow in smooth pipes, Flow Meas. Instrum. 52 (2016) 101–114.

[37] G. Xu, R. Antonia, Effect of different initial conditions on a turbulent round free jet, Exp. Fluids 33 (5) (2002) 677–683.

[38] D.H. Lee, Y.S. Chung, D.S. Kim, Turbulent flow and heat transfer measurements on a curved surface with a fully developed round impinging jet, Int. J. Heat Fluid Flow 18 (1) (1997) 160–169.

[39] N. Rajaratnam, D.Z. Zhu, S.P. Rai, Turbulence measurements in the impinging region of a circular jet, Can. J. Civil Eng. 37 (5) (2010) 782–786.

[40] L.D. Kaale, T.M. Eikevik, T. Rustad, K. Kolsaker, Superchilling of food: A review, J. Food Eng. 107 (2) (2011) 141–146.

[41] T.E. Faber, Fluid Dynamics for Physicists, Cambridge University Press, 1995.

[42] E. Baydar, Y. Ozmen, An experimental and numerical investigation on a confined impinging air jet at high Reynolds numbers, Appl. Therm. Eng. 25 (2–3) (2005) 409–421.

[43] R.P. Singh, D.R. Heldman, Introduction to Food Engineering, Chapter 7 - Food Freezing, Academic Press, San Diego, 2014, pp. 521–563.

Paper II: Development of the food freezing numerical model

Contents lists available at ScienceDirect

Innovative Food Science and Emerging Technologies

journal homepage: www.elsevier.com/locate/ifset

Numerical modelling of the food freezing process in a quasi-hydrofluidisation system

Michal Stebel [a,*], Jacek Smolka [a], Michal Palacz [a], Edyta Piechnik [a], Michal Halski [a], Magdalena Knap [b], Ewa Felis [b], Trygve Magne Eikevik [c], Ignat Tolstorebrov [c], Juan Manuel Peralta [d], Susana E. Zorrilla [d]

[a] *Department of Thermal Technology, Silesian University of Technology, Konarskiego 22, 44-100 Gliwice, Poland*
[b] *Environmental Biotechnology Department, Silesian University of Technology, Krzywoustego 8, 44-100 Gliwice, Poland*
[c] *Department of Energy and Process Engineering, NTNU, Kolbjørn Hejes Vei 1D, Trondheim 7491, Norway*
[d] *Instituto de Desarrollo Tecnológico para la Industria Química (INTEC) (CONICET-UNL), Güemes 3450, S3000GLN Santa Fe, Argentina*

A B S T R A C T

The paper presents a study of food freezing using hydrofluidisation method, characterised by very high heat transfer coefficients exceeding $2500\,W \cdot m^{-2}\,K^{-1}$, which constitutes a novel and promising technology. A numerical analysis of a system with a stationary group of food products was performed. This study aimed to investigate the geometrical parameters governing the freezing process, i.e., the position of food products above the orifices (from 50 mm to 70 mm), their mutual position, the diameter of orifices (3 mm or 5 mm), and the spacing of the orifices in an array (from 8 mm to 12 mm). In this method, the freezing time was from 3 min for 10 mm spherical food sample in moderate refrigerating medium temperatures up to 12 min for 30 mm spherical sample. Moreover, the freezing times at different liquid temperatures were compared in the range of $-20\,°C$ to $-5\,°C$. Reducing the temperature by 5 K may lead to shortening the process by up to 50%. The hydrofluidisation method was assessed versus the immersion freezing for spherical products of different sizes showing the reduction of the process time from about 35% to over 60%.

1. Introduction

Cooling and freezing are the most common methods used for post-harvest preservation of food products. Considering the growth in the global population, the more demanding preferences of the market, and the need for sustainable development, this branch of industry is becoming increasingly significant. Extending the food shelf life by a freezing process is based on reductions in the growth rate of microorganisms, enzymatic reactions or oxidation due to the reduced temperature (Singh & Heldman, 2014). However, during the freezing process on a microscale, liquid water migrates through the cell membranes, causing shrinkage of cells. In addition, the growth of ice crystals causes physical changes in the structure of tissues, which results in unfavourable final quality of foods after thawing (Fikiin, 2008). According to that author, when the so-called *critical zone of water crystallisation*, described as the temperature range from $-1\,°C$ to $-8\,°C$, is passed through quickly, the final quality of the food product is improved.

Within this temperature range, most of the water freezes, and the ice crystals are finer if the process is quick enough. Rapid food freezing minimises the unwanted effect of ice crystals growth, which was confirmed by Delgado and Rubiolo (2005) in a comparison of fresh strawberry tissues with those frozen at different freezing rates. The survey conducted by Khouryieh (2021) confirmed that the food nutrient and sensory quality are major factors that drive the companies to seek novel methods for food preservation. It is worth to mention that other processes like the food storage or thawing also affect the food final quality. The freezing, which is an important process, is one of the first steps of the whole cold-chain (Fikiin, 2008) but it is essential to control this stage properly.

Numerous techniques are investigated to increase the quality of food during the freezing or controlling the ice crystals growth, i.e., conducting the freezing process in high-pressure (Luscher, Schlüter, & Knorr, 2005) or employing the microwaves (Xanthakis, Le-Bail, & Ramaswamy, 2014) or ultrasounds (Xu, Zhang, Bhandari, Sun, & Gao, 2016). These methods are attractive but may be challenging. The easiest

Nomenclature

Bi	Biot number, ($HTC \cdot D \cdot k^{-1}$)
c_p	specific heat capacity, $kJ \cdot kg^{-1} \cdot K^{-1}$
D	sample diameter, mm
d	orifice diameter, mm
H	orifice-stagnation point distance, mm
HTC	heat transfer coefficient, $W \cdot m^{-2} \cdot K^{-1}$
h	specific enthalpy, $kJ \cdot kg^{-1}$
k	thermal conductivity, $W \cdot m^{-1} \cdot K^{-1}$
L_0	latent heat of fusion of ice, ($333.6 \, kJ \cdot kg^{-1}$)
Re	Reynolds number, ($\rho \cdot v_0 \cdot D \cdot \mu^{-1}$)
S	orifice–orifice distance measured from their centres, mm
T	temperature, °C
t	time, s
v	volume fraction, –
v_0	refrigerating medium mean velocity in orifice, $m \cdot s^{-1}$
x	mass fraction, –
z	sphere–sphere distance measured from their surfaces, mm

Greek symbols

Γ_h	diffusion coefficient for the enthalpy equation, $kg \cdot m^1 \cdot s^{-1}$
δ	error, difference
θ	polar angle, °
ρ	density, $kg \cdot m^{-3}$
μ	dynamic viscosity, $Pa \cdot s$

Abbreviations

CFD	computational fluid dynamics
DNS	direct numerical simulations
FDM	finite difference method
FEM	finite element method
FVM	finite volume method
HF	hydrofluidisation freezing
IF	immersion freezing
LES	large eddy simulations
PIV	particle image velocimetry
UDS	user-defined scalar

Subscripts

b	bounded water as a food component
end	end of the process
exp	experimental value
i	ith food component
ice	ice as a food component
if	initial freezing point
in	initial moment
liq	liquid medium
num	numerical value
ref	reference point
s	solid food components
w	liquid water as a food component
wo	total humidity as a food component

solution for enhancement of freezing may be achieved by the intensification of convective heat transfer during the process. This may be realised by employing high-velocity jets impinging on the food product surface during cold air-blast freezing or by selecting a liquid medium for the process as in the immersion freezing (IF) method, where the food products are submerged in various solutions with a lowered temperature.

An alternative method that brings together the advantages of freezing within a liquid medium and the effect of impinging jets is hydrofluidisation freezing (HF). It is based on submerging a group of small food products in a tank filled with an appropriate liquid, pumped in through an array of orifices or nozzles located at the bottom. Due to the intensive flow of the liquid medium, food products behave as a fluidised bed inside the tank, which is characteristic of this particular method and unique among the well-known methods of food freezing (Fikiin & Fikiin, 2001). This method was proposed and patented by Fikiin (1992). That author presented the hydrofluidisation system for cooling and freezing of fish and described advantages of the new method: reduced process time compared with immersion freezing, lower operational costs, ease of maintenance, and better final quality of food products due to the initial freezing stage, wherein most ice crystals are formed, being rapidly passed through. Moreover, Fikiin (1992) also noted that HF systems can be operated with refrigeration units having a higher evaporation temperature than two-stage systems powering air-blast freezing units, which results in a higher coefficient of performance for this kind of systems. A more recent study by Fikiin and Fikiin (2001) presented the results of HF with ice slurry as a cooling medium for several food products achieving remarkably high surface heat transfer coefficient of the order of $1000-2000 \, W \cdot m^{-2} \cdot K^{-1}$. The freezing time from the initial temperature of 25 °C to −18 °C was 8–9 min for plums, apricots or strawberries, less than 3 min for raspberries or cherries, and 1 min for green peas or cranberries in a liquid medium at a temperature of −25 °C. This confirms that this method is beneficial, especially for freezing of small food products. For products of bigger size, the enhancement of the convective heat transfer is not as beneficial, because the internal heat resistance plays a major role during

the cooling and freezing. The assessment of the heat transfer in a sample of a given size in terms of the internal and external heat resistance may be described using the Biot number.

Verboven, Scheerlinck, and Nicolai (2003) performed an experimental study with aluminium spheres instead of food products to assess the heat transfer coefficient (HTC) values in the HF system with an aqueous solution of ethanol and glucose as a medium. They reported HTC values in the range of $154-1548 \, W \cdot m^{-2} \cdot K^{-1}$ depending on the sample diameter, flow rate of the solution and temperature. The authors stated that HTC values were strongly affected by the agitating jets within the HF system. A complementary study was performed by Peralta, Rubiolo, and Zorrilla (2009) using a copper sphere in a system with NaCl solution as a medium. These authors analysed various scenarios with different sphere diameters (D) and positions of the sphere stagnation point above a single orifice (H) with a fixed diameter (d). They proposed a correlation for the Nusselt number also taking into consideration the effect of these geometrical variables in dimensionless form.

Peralta, Rubiolo, and Zorrilla (2010) expanded the work of Peralta et al. (2009) by performing a numerical study of the same HF system employing computational fluid dynamics (CFD) to present the turbulent flow of the liquid medium in such a system. The numerical results were in good agreement with the thermal measurements performed on their test rig. After that, the model was complemented with heat and mass transfer phenomenon analyses within a real food product, i.e., a potato (Peralta, Rubiolo, & Zorrilla, 2012). In their study, the food product domain was considered a porous body with the conservation equations solved for each of three phases: the solid matrix, the liquid, and the ice. A more complex system with numerous orifices and a group of food products was studied by Belis, Zorrilla, and Peralta (2015). The authors analysed cases with different arrangements of orifices and numbers of spheres in a group. Oroná, Zorrilla, and Peralta (2017) proposed a more advanced model to describe the free movement of food products during the HF process with mutual collision of food samples. Therefore, the analysed case was closer to the real scenario. The last paper regarding that particular HF unit presented a sensitivity analysis of the parameters in the system (Oroná, Zorrilla, & Peralta, 2018). The authors identified

the important parameters of the heat and the mass transfer in the proposed system.

The most recent experimental study regarding the HF system describes the refrigerating medium flow field followed by thermal measurements. On the test rig equipped with a transparent HF tank, Palacz, Adamczyk, Piechnik, Stebel, and Smolka (2019) captured the velocity field of the refrigerating medium around a single spherical sample at ambient temperature using the particle image velocimetry (PIV) method. The liquid used in this system was an aqueous solution of ethanol. The authors presented the velocity field distribution for different Reynolds numbers and orifice-sphere stagnation point distance to orifice diameter ratios. This was the first experimental study of the HF system regarding fluid flow analysis. Then, thermal measurements were performed to assess HTCs and the time required to freeze food samples of several sizes and types (Palacz et al., 2021). The same HF system was investigated numerically by the same research group. Stebel, Smolka, Palacz, Adamczyk, and Piechnik (2020) performed CFD analysis of the fluid flow for various geometrical arrangements of this simplified system. Available experimental flow field measurements allowed model validation and selection of an appropriate turbulence model describing the fluid flow in the considered system.

The aim of this study is to investigate the freezing process of real food samples (potatoes) in the proposed HF system with a water-ethanol solution used as a freezing medium. All the geometrical parameters and operating conditions cover the ranges that can be achieved in the dedicated laboratory test rig, i.e., the refrigerating medium temperature and mass flow rate as well as the geometrical dimensions such as the orifice diameter (3 mm or 5 mm), orifice spacing (8–12 mm) and position of products above the orifices (50–70 mm). The size of food products was selected to be within the range that might be especially beneficial for this particular food freezing method, which was assumed to be 10–30 mm. This range can be related to a vast range of small fruits and vegetables. The freezing model presented in this study was based on the apparent heat capacity method and the enthalpy-based energy equation implemented via User-Defined Scalar (UDS) in ANSYS Fluent commercial software. A variety of the cases being studied in a transient scenario allowed examining the HTC distribution for different cases and the times required for the freezing process dependent on the process parameters. In addition, the HF method was assessed by comparing the freezing times against the IF results.

2. Laboratory test rig and experiments

2.1. HF chamber

The laboratory test rig used in this study was designed and built at the Institute of Thermal Technology, Silesian University of Technology in Gliwice, Poland. An experimental study by Palacz et al. (2019) includes a more detailed description of this HF unit along with all its components. Briefly, the main part of this HF unit is a cuboid-shaped HF tank, presented in Fig. 1(a), made of transparent material and open at the top. The tank is 150 mm high, 445 mm wide and 280 mm deep. The process of food freezing occurs within the HF tank. The sample for the freezing tests is mounted at a fixed position using a plastic rod attached to a moveable frame. Two step motors are used to precisely position the samples during freezing or to perform experiments with controlled movement in two horizontal directions. The refrigerating medium flows into the tank through the plate with orifices located at the tank bottom. In this plate, orifices were drilled to create fluid jets during fluid flow. The plate is replaceable in order to perform experiments with different arrangements of the orifices, i.e., a single orifice located at the central position, one row of orifices or a full array with several rows of orifices, as presented in Fig. 1(b). Plates with 3 mm or 5 mm orifices were used in this work.
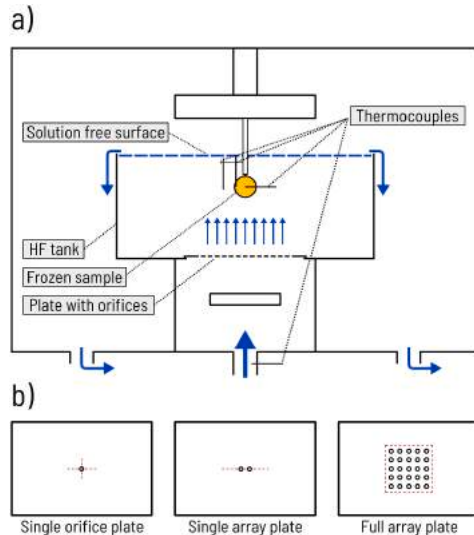
Fig. 1. (a) Simplified scheme of the HF unit, and (b) arrangements of the orifices considered in this study.

2.2. Food sample preparation and freezing experiments

As mentioned before, potato (*Solanum tuberosum L.*) was used as a food product due to its availability in local markets during all seasons and its internal structure uniformity showing no visible pores or seeds. Moreover, the relatively high moisture content of potato would make it a good food model representing most of the fruits and vegetables. In this study, spherical food samples were used. Fresh potatoes were stored at room temperature prior experiments. The samples were cut out using melon ballers just before the freezing process. This kind of treatment allowed the authors to obtain spherical samples with diameters of approximately 20 mm and 30 mm. The surface of the potato spheres was smooth. However, due to the sample preparation method and the tool used for that, the curvature of the spherical sample was slightly flattened on one side. For that reason, each sample was weighted to verify its mass on a laboratory scale (model *PD 600.R2*, Radwag, Poland). The 20 mm and 30 mm diameter potato samples weighted 4.62 ± 0.24 g and 16.48 ± 0.41 g, respectively. To ensure more reliable conditions for the model validation, samples were mounted on the hanging rod by facing the imperfect side upwards away from the main flow where the sample curvature affects the refrigerating medium flow and the boundary layer separation.

Sample temperatures were measured by two T-type thermocouples having the sheath diameter of 1 mm and placed at their spherical centres and close to their surfaces as shown in Fig. 1(a). These measurements were done by a data acquisition device *cDAQ-9581* (National Instruments, Austin, USA) and a temperature module *NI-9212* (National Instruments, Austin, USA). The CFD model was validated with the temperature values obtained from the experiments in these two characteristic locations. An additional T-type thermocouple was installed on the moveable frame to measure the liquid temperature during the freezing process. Thermocouples were calibrated in a glycol cryostat bath *DD-100FF* (Julabo, Seelbach, Germany) with a temperature stability declared to be ± 0.01 K. Therefore, the accuracy of thermal measurements was estimated as ± 0.1 K.

The thermal properties of foods are strongly dependent on their composition. The dominant component for fruits and vegetables is water. To determine the water content in potatoes processed using the HF method, groups of 5 frozen samples were dried in an oven at 102 °C for 24 h. The mass of each sample was measured between the freezing and drying processes, 2 h after the drying started and after 24 h of drying to evaluate the total moisture loss due to drying. The sample drying experiment was repeated three times to determine the average value of the total water content and the standard deviation. According to that test, the water content of potatoes used in this study was determined to be $80.05 \pm 2.18\%$.

3. Mathematical modelling

3.1. Computational domain

The numerical domain includes the HF tank and a part of the section below the plate with orifices. One-quarter of the 3-D numerical domain representation was used for the simulations due to the symmetrical arrangement of orifices and spheres, as shown in Fig. 2(a), using an isometric view of the whole domain. Instead of modelling the free surface of the liquid, this surface was closed and treated as a wall boundary condition. The top view of the group of food products positioned above the orifices is shown in Fig. 2(b) for one of the considered cases. The reduced domain includes one full sphere, one hemisphere and one-quarter of the sphere placed in the central position of the HF tank. Depending on the case, the jets can strike the surface of food products from different positions.

In this paper, several possible arrangements of the orifice plate configuration were studied: (1) the single orifice case, (2) the single array case with 2 orifices in a row to create twin jets striking the food product surface from two sides, and (3) the full array case with a group of 4, 49 or 64 orifices configured in a rectangular array. Depending on the case, the orifice diameter (d) was set as 3 mm or 5 mm. The distance between the orifice centres (S) was assumed to be 8 mm, 12 mm or 16 mm.

Food products were positioned at the same height, measured from the top surface of the inflow plate with orifices to the stagnation point of each sphere. This distance (H) was 50 mm, 60 mm or 70 mm depending on the case. The group of food products consisted of one spherical sample located in the centre, which is a representative sample for the analysis of the results, and the remaining six spheres located around it. The diameter of each sphere (D) was the same and equal to 20 mm in almost all cases. The distance between the surfaces of the neighbouring

samples (z) was assumed to be 5 mm, 10 mm or 15 mm.

In addition, HF was compared with IF for products of different sizes. Therefore, for this particular analysis, the range of the spherical sample diameters was extended to the range of 10 through 30 mm, which will be discussed in subsequent paragraphs. For the purpose of the model validation, scenarios with a single sphere having a diameter of 20 mm or 30 mm were considered. For these cases, the polyamide hanging rod was also included in the numerical domain for the best representation of the test rig configuration presented in Fig. 1(a).

All the cases with different geometrical and flow parameters that are analysed in this study are listed in subsequent sections.

3.2. Numerical mesh

For the study presented in this paper, overset meshes also called Chimera meshes, were used. This approach employs two or more numerical grids, generated independently, to be used within one numerical domain. In this method, one grid is used to discretise the entire volume of the domain (background mesh) and separate grids are used for discretisation of selected elements (component meshes). The entire numerical grid discretised using the background mesh and three component meshes around the sample spheres is presented in Fig. 3(a). In the region where the background mesh is replaced by the component mesh, some cells are excluded from the computations, which is shown in Fig. 3(b) and (c), after the procedure of the grids connection. The cells being excluded are called *dead cells*, while the active cells are called *solve cells*. In the region where the background mesh overlaps the outer cells of the component mesh, the temperature field, the flow field, etc. are interpolated by *donor* and *receptor* cells (ANSYS Inc., 2017). For the cases being used for the validation, i.e., with one spherical sample and the hanging rod, the numerical mesh was prepared in the manner shown in Fig. 3(d).

Overset meshing allows for effective discretisation of areas with complex geometry even with high-quality structured elements. In the current study, overset grids are beneficial due to the various geometrical configurations being analysed and the possibility of creating high-quality meshes in the fluid region near the surface of spheres located at a close distance. In addition, the number of elements could be reduced with this method.

The background mesh included the HF tank with the entire orifice plate and the region below it, but excluded the food products being meshed separately with component meshes. The background mesh was created with over 2 000 000 hexahedral elements using a blocking technique. Within each orifice, the O-grid structure was applied. To
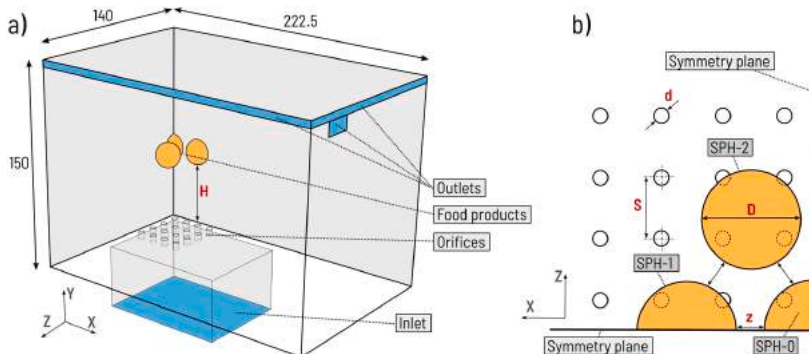
Fig. 2. Numerical domain including one-quarter of the simulated system: (a) isometric view with the tank main dimensions given in mm, and (b) top view presenting the mutual position of the orifices and food products. (For interpretation of the references to color in the text, the reader is referred to the web version of this article.)
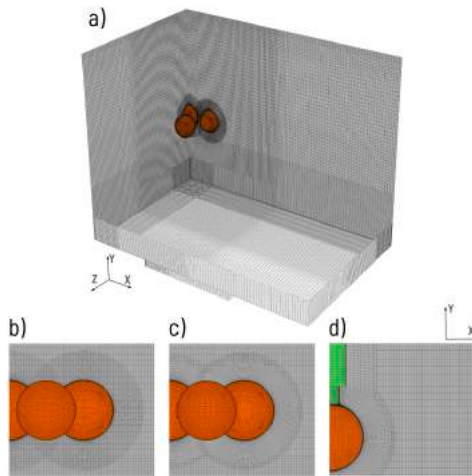
Fig. 3. (a) Isometric view of the whole numerical mesh without the side and top HF tank walls, (b) front view close-up of the region with food products included in separate component meshes, (c) same view after the mesh connection procedure, and (d) front view close-up of a single food product with the hanging rod in a single component mesh after connection with the background mesh.

achieve uniform distribution of high-quality hexahedral elements within the area of the overlapping regions with the component meshes, a non-conformal interface was set 20 mm above the orifices.

Each component mesh included the food product interior and a fluid layer surrounding the sphere having a thickness equal to the sphere radius. The component meshes with the food products were placed in close proximity and were overlapping as presented in Fig. 3(b). They were built with structured grids using the O-grid topology with approximately 1 000 000 hexahedral elements in total. The thickness of the first cell layers around the spheres was set to keep the y+ value below 2.0 for all the simulations being conducted. It is worth mentioning that the thickness of the first cell layer guaranteed y+ equal to 1 for most of the considered cases. This quantity that describes the thickness of the cell in a dimensionless form regarding the fluid velocity and viscosity is required to be low enough to properly simulate the turbulent flow near the wall by using a particular turbulence model.

The grid independence was tested on a selected case using calculated HTC values for different meshes. The comparison was performed after 15 s of the process, i.e., with a fully developed flow field and after thermal stabilisation of the boundary layer. The heat transfer coefficient is a quantity that characterises the convective heat transfer. Therefore, it was selected as a proper indicator for the mesh examination in this

study. Table 1 presents the average and maximum values of the HTC at the surface of each sphere and the relative difference in these values for each mesh with respect to the most refined mesh. *SPH-0* refers to the centre sample in the group, while *SPH-1* and *SPH-2* refer to the remaining samples present in the numerical domain shown in Fig. 2(b), which are a semi-sphere cut by the symmetry plane and a full sphere. As seen, further refinement of the background or component meshes of Grid #4 did not affect the HTC significantly. The values of the HTC differ from the most refined case by less than 2% for the average and local maximum values, which is considered an acceptable difference. The difference is even smaller considering only *SPH-0*. For this reason, Grid #4 was selected for the model.

In this study, the entire freezing process was modelled separately from the fluid flow within the HF unit, which was described previously in Section 1. For the simulations of freezing, the numerical model was solved only within the food product domain. Thus, only the food product interior from the component mesh was used in this second step of the whole process analysis. In that case, the *SPH-0* food product interior was discretised with approximately 8300 hexahedral elements in O-grid topology. The food product interior mesh independence test was performed as well. Further refinement of the mesh did not result in the change of the local temperatures within the food product. Therefore, this mesh size was selected as an appropriate for further simulations.

3.3. Governing equations

The fluid flow in the proposed CFD model was solved with the set of governing equations. They describe the incompressible flow in the transient scenario. The equations include the continuum, momentum and energy conservation equations, which were already presented and described in the previous study of the authors regarding the fluid flow in the HF system (Stebel et al., 2020). In the present study, highly turbulent flow was again modelled using the well-known k-ω shear stress transport model as in the previous study. It has been confirmed (and validated against PIV experiments) that this model provides a higher accuracy than others, which were used because it showed optimal results in predicting the flow characteristics of HF systems (Palacz et al., 2019; Stebel et al., 2020). This is partly due to its accuracy in predicting the onset and the amount of flow separation under adverse pressure gradients (Belis et al., 2015).

Heat transfer was solved within the food product domain by using the enthalpy-based energy equation. The ANSYS Fluent commercial software allows customisation of the numerical model by defining user defined scalars in the form of the so-called transport equation (Smolka, 2018). For the case of time-dependent heat conduction, the transport equation consists of the accumulative term and the diffusive term. The equation formulated to solve the food freezing problem using the enthalpy method has the form given in Eq. (1) with the diffusion coefficient defined in Eq. (2). Values of HTC discussed in this paper were evaluated based on the heat balance between the sample surface and the fluid domain, i.e., the heat flux, the temperature of the food sample surface and the fluid bulk temperature allowed to determine HTC for each case.

Table 1
Average and maximum values of the HTC in W · m^{-2}· K^{-1} and relative differences with respect to the most refined case for several grids for the selected case with Re = 15 000, D = 20 mm, H = 50 mm, d = 3 mm, z = 10 mm and S = 12 mm.

	Number of cells		SPH-0 (avg)		SPH-1 (avg)		SPH-2 (avg)		SPH-0 (max)		SPH-1 (max)		SPH-2 (max)	
	Background	Components	HTC	δ%	HTC	δ%	HTC	δ%	HTC	δ%	HTC	δ%	HTC	δ%
Grid #1	920 700	282 881	8044	3.0%	8426	5.3%	7394	5.2%	12 736	3.8%	13 615	6.8%	13 320	5.2%
Grid #2	1 065 513	419 960	8166	1.5%	8457	4.9%	7571	2.9%	12 969	2.0%	13 880	5.0%	13 770	2.0%
Grid #3	1 425 060	1 066 853	8094	2.4%	8565	3.7%	7547	3.2%	12 617	4.7%	13 786	5.6%	13 734	2.3%
Grid #4	2 080 163	1 066 853	8301	−0.1%	8760	1.5%	7665	1.7%	13 012	1.7%	14 483	0.8%	13 818	1.7%
Grid #5	2 316 863	1 066 853	8347	−0.7%	8827	0.8%	7753	0.6%	13 208	0.2%	14 491	0.8%	13 858	1.4%
Grid #6	2 316 863	1 461 841	8290	–	8897	–	7797	–	13 239	–	14 606	–	14 054	–

$$\frac{\partial \rho h}{\partial t} - \nabla(\Gamma_h h) = 0 \qquad (1)$$

$$\Gamma_h = \frac{k}{c_p} \qquad (2)$$

where ρ is the density, h is the specific enthalpy, t is the time, Γ_h is the diffusion coefficient defined for the enthalpy-based transport equation, k is the thermal conductivity and c_p is the apparent heat capacity.

Second order upwind scheme was used for convective terms in the equations describing the momentum and energy conservation, pressure discretisation and the two equations used for turbulence modelling. Diffusion terms were solved with central differencing scheme. Also, the time discretisation required for transient simulations was done with second order scheme.

3.4. Thermophysical properties

An ethanol aqueous solution was used as the freezing medium in this study. The concentration of ethanol in the applied solution was equal to 30% (mass), which corresponds to the concentration of ethanol in the experimental rig described earlier. All the properties of the aqueous solution of ethanol required for fluid flow modelling, were defined using polynomial functions of temperature, as presented in Table 2.

The thermophysical properties of the potato samples were estimated through their composition. The water content was evaluated experimentally as described in Section 2.2. The other components of the considered potato were assessed based on the data available in ASHRAE (2006), which describes the composition of fresh food products after harvesting. Table 3 presents the assumed mass fraction values of different components based on the performed experiments and the aforementioned literature.

Water is a dominant component in most fresh foods, especially fruits and vegetables, affecting significantly the overall properties of the products. For the freezing process, the mass fractions of liquid water and ice start to change below the freezing point. The initial freezing temperature (T_{if}) for the potato samples was assumed to be $-1.65\,°C$ and it was determined using a tangential method based on the extrapolation of the curves during the pre-cooling period and the plateau of the freezing stage from the measured temperature profiles. This was the stage at which the water started to crystallise; hence, the temperature level was assumed to be the initial freezing temperature. The ice fraction in the frozen food product can be described by several theoretical or empirical relationships. One of them, proposed by Tchigeov (1979), is presented in Eq. (3). It is a function of the temperature, initial freezing temperature and total moisture content. The assumed formula applies for a variety of food products with satisfactory accuracy, which has been confirmed experimentally by Fikiin (1998). The same author stated that Tchiegov's formula provides a satisfactory accuracy for food products having the initial freezing temperature from $-2\,°C$ to $-0.4\,°C$ and within the temperature range from $-45\,°C$ up to initial freezing temperature. It confirms the validity of using this relationship in this study.

Table 2
Polynomial functions of temperature in K describing the thermophysical properties for a water-ethanol solution of 30% concentration in the temperature range between 253.15 K and 293.15 K (VDI Gesellschaft, 2010).

Property	Polynomial function
Density, $kg \cdot m^{-3}$	$-0.0055474 \cdot T^2 + 2.9813 \cdot T + 564.97$
Thermal conductivity, $W \cdot m^{-1} \cdot K^{-1}$	$0.0006559 \cdot T + 0.21911$
Specific heat, $J \cdot kg^{-1} \cdot K^{-1}$	$1.9602 \cdot T + 3634.8$
Dynamic viscosity, $10^{-3} kg \cdot m^{-1} \cdot s^{-1}$	$-0.000001161 \cdot T^3 +$ $0.0009517 \cdot T^2 - 0.2605 \cdot T + 23.81$

Table 3
Mass fractions of the food product components for the potato sample.

Moisture	Protein	Fat	Carbohydrate	Fibre	Ash
80.05%	1.97%	0.09%	15.53%	1.52%	0.84%

$$x_{ice} = \frac{1.105 x_{wo}}{1 + \frac{0.7138}{\ln(T_{if} - T + 1)}} \qquad (3)$$

where x_{ice} is the mass fraction of ice, x_{wo} is the total mass fraction of moisture, T_{if} is the initial freezing temperature in $°C$ and T is the food product temperature in $°C$.

The potato bulk density has been evaluated based on mass and volume measurements of over 20 cubic samples. This shape allowed for simple measurements of the size and the volume of each sample. Based on that, the density value with the standard deviation was determined to be $1062 \pm 31\,kg \cdot m^{-3}$. A similar value was found and used in a preliminary study of potato cooling using the HF system (Stebel et al., 2020). For this study, the same constant density value was assumed for potato freezing.

The correct evaluation of the food product thermal conductivity is a major issue because the freezing process is highly sensitive to this property. The literature offers a variety of models that depend on the food composition, e.g., parallel and serial models analogous to electrical resistance, which provide the upper and lower bounds of the thermal conductivity for most foods (ASHRAE, 2006). The Levy's model was used in this study (Levy, 1981). The model is a multistage approach recommended for frozen, non-porous foods (Carson, Wang, North, & Cleland, 2016). Here, the thermal conductivity of the unfrozen components of the foods is firstly evaluated by means of another single-stage model excluding the ice in the volume fractions. According to Wang, Carson, Willix, North, and Cleland (2009), the parallel model given in Eq. (4) is recommended at this point. The second stage is the evaluation of the frozen food thermal conductivity using Eq. (5) as a mixture of unfrozen components and ice.

$$k_I = \sum k_i v_i \qquad (4)$$

$$k_{Levy} = k_{ice} \frac{2k_{ice} + k_I - 2(k_{ice} - k_I)F}{2k_{ice} + k_I + (k_{ice} - k_I)F} \qquad (5)$$

with

$$F = \frac{2 \big/ G - 1 + 2(1 - v_{ice}) - \sqrt{[2/G - 1 + 2(1 - v_{ice})]^2 - 8(1 - v_{ice})\big/ G}}{2}$$

and

$$G = \frac{(k_{ice} - k_I)^2}{(k_{ice} + k_I)^2 + k_{ice} k_I / 2}$$

where k_I is the thermal conductivity of single-stage components, i.e., liquid water, protein, fat, carbohydrate, fibre, and ash, k_i is the thermal conductivity of the i-th single-stage component, v_i is the volumetric fraction of the ith single-stage component, k_{Levy} is the thermal conductivity of food product according to Levy's model, k_{ice} is the thermal conductivity of ice, v_{ice} is the volumetric fraction of ice, and F and G are the functions related to mathematical formulation of Levy's model.

As mentioned before, the effect of the latent heat release was included in the apparent heat capacity formulation. The literature provides several models describing the apparent heat capacity of food products and the specific enthalpy. In this study, the model proposed by Chen (1985) was selected. According to that author, this formulation is applicable to various types of food products with a water content greater than 40%. Eqs. (6) and (7) present the apparent heat capacity functions for the temperature ranges above and below the initial freezing

temperature, respectively. The functions describing the specific enthalpy are presented in Eqs. (8) and (9) for the temperature ranges above and below the initial freezing temperature, respectively.

$$c_p = 4.19 - 2.30x_s - 0.628x_s^3 \tag{6}$$

$$c_p = 1.55 + 1.26x_s - \frac{(x_{\text{wo}} - x_b)L_0 T_{\text{if}}}{T^2} \tag{7}$$

$$h = h_{\text{if}} + (T - T_{\text{if}})\left(4.19 - 2.30x_s - 0.628x_s^3\right) \tag{8}$$

$$h = (T - T_{\text{ref}})\left[1.55 + 1.26x_s - \frac{(x_{\text{wo}} - x_b)L_0 T_{\text{if}}}{T_{\text{ref}} T}\right] \tag{9}$$

where x_s is the mass fraction of solid components, x_b is the mass fraction of bound water, L_0 is the latent heat of fusion of water (333.6 kJ · kg^{-1}), T is the food product temperature in °C, h_{if} is the food product specific enthalpy at the initial freezing point evaluated using Eq. (9) and T_{ref} is the reference temperature (−40 °C).

Additionally, for the cases used for model validation, the hanging rod made of polyamide was included in the domain. The properties of this material were set as constant values based on data from the literature (VDI Gesellschaft, 2010). The density was set as 1150 kg · m^{-3}, specific heat capacity was 1600 J · kg^{-1} · K^{-1}, and the thermal conductivity was 0.25 W · m^{-1} · K^{-1}.

3.5. Boundary and initial conditions

The numerical model was completed with boundary and initial conditions. The model proposed in this study has several types of boundary conditions, i.e., symmetry and wall boundary conditions as well as inlet and outlet boundary conditions, to simulate the proper flow of the ethanol solution in the HF system. The inlet and outlet boundary conditions are indicated in Fig. 2(a) using blue colour and labels. The symmetry planes are marked with grey colour in the same scheme. A detailed description of the applied boundary conditions is given in the following:

- The inlet boundary condition was defined by the liquid mass flow rate value estimated based on the Reynolds number required for each case. The temperature of the fluid at the inlet depends on each case, which will be listed in Sections 4.1 and 4.2.
- The outlet boundary condition located near the top edge of the tank was defined as a static pressure value of 10^5 Pa according to the ambient pressure.
- Two planes of symmetry were used to simplify the computational domain to one-quarter. Therefore, the HF tank, section below the orifices and number of food products and orifices were reduced, as presented in Fig. 2(b).
- The top surface of the domain was defined as an adiabatic slip wall because it represented the free surface of the liquid.
- Surfaces of food products were defined as no-slip walls. During the first stage of simulation with the fluid flow and the heat transfer being solved, these surfaces allowed for coupling of the temperature and the specific enthalpy equations. After 15 s of the fluid flow simulation, when the heat transfer coefficient at these surfaces was stabilised, the surface spacial-average value of that quantity and the refrigerating medium bulk temperature were treated as input data for the subsequent stage of simulation. Then, the food product surfaces were treated as a boundary condition of the third kind.
- All other walls were defined as no-slip adiabatic walls.

During the experiments, the food samples were placed at their position above the jets by lowering the whole assembly holding the sample using step motors. The food products were immersed in the liquid when the fluid was already flowing through the orifices. To simulate a similar

scenario in the CFD analysis, the transient freezing process was initialised with an already developed fluid velocity field in the entire domain. The time-step size of each simulation was set as 0.01 s. The sensitivity test confirmed that the finer time discretisation does not affect the results. At the initial moment of the process, the food enthalpy had a uniform distribution within the entire volume of food products with a value that corresponded to the initial food product temperature taken from a test or assumed depending on the particular analysis.

4. Results and discussion

4.1. Model validation

The experiments conducted on the dedicated laboratory test rig allowed the authors to validate the numerical model of the HF process. The measurements of the product temperature within two locations described in Section 2.2 were compared to numerical results. The cases used for validation were focused on freezing of a single food sample hung using the rod above a plate with a single orifice directly below the food sample, two orifices in a row or four orifices in an array as depicted previously in Fig. 1(b). The list of the validation scenarios covers 36 cases, as presented in Table 4, with different geometrical parameters, such as the number and diameter of orifices (d), the spherical sample diameter (D), and the position of the sample above the plate (H). For the cases with two or four orifices, the distance between them (S) had a fixed value of 10 mm. The dimensionless ratio H/d, which is a characteristic parameter for such a system, was discussed by Peralta et al. (2009) and Palacz et al. (2019). In this study, this parameter ranged between 10.0 and 23.3. Depending on the case, the initial food sample temperature was between 12.4 and 20.2 °C due to the different ambient conditions during the tests. The refrigerating medium temperature was maintained at an average temperature of approximately −10 °C, as listed in the table. However, due to variations in the refrigerating medium temperature during the process, time-dependent temperatures were implemented in the simulations according to the experimental recordings. For each case, the Reynolds number (Re) that characterises the turbulent flow in the process was maintained at approximately 9000 or higher. According to Peralta et al. (2009), this quantity is defined for HF systems based on the spherical food sample diameter and the jet velocity (v_o) averaged at the orifice cross-section as given in Eq. (10).

$$\text{Re} = \frac{\rho v_o D}{\mu} \tag{10}$$

where μ is the fluid dynamic viscosity.

The temperatures in the food product for all 36 cases were compared with the experimental results using the mean temperature differences for the sample centre and the near-surface point. It was determined as the absolute difference between the measured and calculated temperatures averaged over the entire freezing process period as given in Eq. (11).

$$\delta T = \frac{\int_{t_{\text{in}}}^{t_{\text{end}}} \left|T_{\text{exp}}(t) - T_{\text{num}}(t)\right| \mathrm{d}t}{t} \tag{11}$$

where δT is the averaged difference between the experimental and numerical temperatures, t_{in} and t_{end} describe the beginning and end of the HF process, $T_{exp}(t)$ is the time-dependent local temperature obtained from the tests and $T_{num}(t)$ is the time-dependent local temperature obtained from the simulations.

The results are presented in third section of Table 4 for all cases. As seen, depending on the case, the difference between the numerical and experimental results was in the range of 0.2 K to 4.2 K. However, most of these values were under 1.5 K, which can be interpreted as very good agreement, considering the numerous difficulties: the quality of the particular food product, preparation of each food sample, evaluation of thermophysical properties and accuracy of the positioning of

Table 4

Description of cases used for model validation, HTC, time-averaged differences of the local sample temperatures between experimental and numerical results and the HF process time. The bolded cases are presented in detail in Fig. 4.

Test case	d	D	H	H/d	T_{in}	T_{liq}	v_o	Re	HTC	δT_C	δT_W	t_{exp}	t_{num}	δt	$\delta t_\%$
	(mm)	(mm)	(mm)		(°C)	(°C)	(m s⁻¹)		(W·m⁻²K⁻¹)	(K)	(K)	(min)	(min)	(min)	(%)
Case 1	1 × 5	20	50	10.0	13.59	−9.81	5.41	9061	4760	1.7	2.2	10.0	9.3	0.70	7.1%
Case 2	1 × 5	20	60	12.0	12.44	−10.04	5.41	8927	4190	1.4	1.2	9.0	8.9	0.15	1.7%
Case 3	1 × 5	20	70	14.0	13.24	−9.66	5.41	9149	3825	1.1	2.2	9.4	8.9	0.53	5.7%
Case 4	1 × 3	20	50	16.7	18.24	−9.36	5.69	9811	3156	1.2	0.9	10.9	11.0	−0.15	−1.3%
Case 5	**1 × 3**	**20**	**60**	**20.0**	**13.87**	**−9.15**	**5.69**	**9943**	**2814**	**2.2**	**1.4**	**12.5**	**11.6**	**0.94**	**7.5%**
Case 6	1 × 3	20	70	23.3	18.48	−9.56	5.69	9685	2588	2.7	0.9	9.0	9.9	−0.97	−10.8%
Case 7	1 × 5	30	50	10.0	13.96	−10.65	4.31	1024	2864	1.2	1.4	21.5	21.4	0.12	0.6%
Case 8	1 × 5	30	60	12.0	15.07	−10.51	4.20	10 084	2635	1.2	1.8	20.4	21.7	−1.27	−6.2%
Case 9	1 × 5	30	70	14.0	18.37	−9.50	4.31	11 039	2559	2.0	1.5	32.4	22.4	10.06	31.0%
Case 10	**1 × 3**	**30**	**50**	**16.6**	**14.42**	**−8.98**	**3.65**	**9664**	**1870**	**1.3**	**0.7**	**27.5**	**23.4**	**4.06**	**14.8%**
Case 11	1 × 3	30	60	20.0	18.87	−8.79	3.65	9781	1809	1.5	3.3	27.8	25.1	2.69	9.7%
Case 12	1 × 3	30	70	23.3	16.70	−9.67	3.65	9247	1721	1.4	2.0	24.5	22.6	1.94	7.9%
Case 13	2 × 5	20	50	10.0	15.20	−10.88	8.27	12 914	8944	4.2	2.9	7.4	9.6	−2.12	−28.5%
Case 14	2 × 5	20	60	12.0	12.77	−10.92	8.03	12 511	7534	3.8	1.1	8.0	8.7	−0.86	−10.7%
Case 15	2 × 5	20	70	14.0	14.83	−10.75	8.03	12 654	6926	4.1	1.6	7.4	8.3	−0.94	−12.8%
Case 16	2 × 3	20	50	16.7	16.76	−8.60	8.17	14 782	5472	1.0	1.5	11.0	11.4	−0.39	−3.5%
Case 17	2 × 3	20	60	20.0	15.17	−8.96	8.17	14 450	4787	0.9	1.1	11.0	11.4	−0.38	−3.4%
Case 18	2 × 3	20	70	23.3	14.06	−9.00	8.17	14 414	4789	0.8	1.4	10.9	11.2	−0.28	−2.6%
Case 19	2 × 5	30	50	10.0	14.36	−9.38	8.27	21 367	7033	0.8	0.3	23.1	24.5	−1.36	−5.9%
Case 20	2 × 5	30	60	12.0	14.24	−9.22	8.04	20 970	6245	0.6	0.3	24.4	24.7	−0.30	−1.2%
Case 21	**2 × 3**	**30**	**70**	**14.0**	**13.96**	**−9.01**	**8.04**	**21 252**	**5921**	**0.7**	**0.2**	**25.8**	**25.2**	**−1.36**	**−5.7%**
Case 22	2 × 3	30	50	16.7	18.87	−8.89	3.58	9525	2075	1.7	2.1	30.3	23.5	6.85	22.6%
Case 23	2 × 3	30	60	20.0	13.60	−8.30	3.58	9884	2025	1.9	2.5	29.4	25.4	3.98	13.5%
Case 24	2 × 3	30	70	23.3	17.74	−9.05	3.65	9622	1958	1.5	1.8	29.4	23.2	6.15	20.9%
Case 25	4 × 5	20	50	10.0	16.61	−9.81	5.36	8973	6113	2.3	0.3	9.8	10.1	−0.32	−3.3%
Case 26	4 × 5	20	60	12.0	17.00	−9.70	5.36	9037	5696	1.7	0.7	10.8	10.5	0.26	2.4%
Case 27	**4 × 5**	**20**	**70**	**14.0**	**16.52**	**−9.16**	**5.36**	**9090**	**5394**	**0.7**	**0.5**	**10.4**	**10.4**	**0.01**	**0.1%**
Case 28	4 × 3	20	50	16.7	15.14	−8.86	4.96	8829	3472	1.4	0.7	15.0	11.3	3.71	24.7%
Case 29	4 × 3	20	60	20.0	16.60	−9.96	4.96	8228	3104	1.5	2.6	12.2	10.0	2.23	18.3%
Case 30	4 × 3	20	70	23.3	12.48	−9.81	4.96	8308	2986	0.9	1.3	14.5	10.1	4.36	30.1%
Case 31	4 × 5	30	50	10.0	20.20	−9.18	3.60	9413	3598	1.1	0.3	25.3	25.0	0.33	1.3%
Case 32	4 × 5	30	60	12.0	15.48	−9.51	3.60	9216	3261	2.4	0.6	23.4	23.8	−0.40	−1.7%
Case 33	4 × 5	30	70	14.0	18.30	−9.44	3.60	9257	3056	1.5	1.1	28.2	23.8	4.37	15.5%
Case 34	4 × 3	30	50	16.7	15.50	−9.70	3.32	8399	2205	1.4	1.5	30.5	22.3	8.13	26.7%
Case 35	4 × 3	30	60	20.0	16.25	−9.24	3.39	8840	2182	1.0	0.5	27.0	22.9	4.19	15.5%
Case 36	4 × 3	30	70	23.3	16.71	−9.15	3.39	8891	2118	1.4	1.8	30.2	23.1	7.17	23.7%

thermocouples.

To assess the numerical model accuracy for all 36 experimental cases, the HF process time duration was also compared as a global indicator. Because the food product final temperature was relatively high, i.e., the liquid water was not entirely frozen, and due to slightly various conditions for all the cases, the freezing temperature for this comparison was assumed for the food sample centre as 0.5 K above the refrigerating medium temperature. Table 4 presents the freezing time in minutes according to the experimental results, numerical results and the differences expressed as the actual differences and the relative differences with respect to the experimental results. Negative values indicate the under prediction of the freezing time by the numerical model. These numbers are presented at the right-hand side of the table. As seen, the freezing time predicted by the numerical model is different by less than 1 min for 18 cases, which accounts for half of the number of conditions compared. For two-third of the cases, the freezing time accuracy prediction is less than 2 min, which may be considered fairly acceptable. For 6 of the cases, the difference between the measured and simulated freezing time is higher than 5 min. However, these cases were related to freezing of 30 mm samples, which in general require more time for the process. The differences were shown also as relative quantities to assess if the sample size affects the accuracy of the process time determination. As seen, although the values of relative error are relatively high for some of cases, no effect of the sample size or other parameter on the relative was noticed. The lack of any tendency suggests that the disagreement between predicted and measured freezing times may be caused by the difficulties related to the precise measurements of temperatures in food samples rather than by the incorrect definition of thermal properties of food sample (Cleland & Earle, 1984). In case of inaccurate

determination of thermal properties, the temperature curve obtained from numerical simulation would be always under or above the experimentally determined temperature. Also, according to Cleland and Earle (1984), wrong evaluation of the food temperature during the freezing caused by incorrect HTC evaluation is typical only for processes characterised by low Bi numbers, which is not the case discussed in this paper. Consequently, the deviation between the experimental and numerical results is likely to be caused by the difficulties related to performing the experiments, i.e., obtaining the perfect spherical shape of samples and thermocouples positioning in food samples centre and near the surface.

The local temperatures at the characteristic points, i.e., sample centre and near surface, for the whole freezing process are presented in Fig. 4 for some selected cases. As seen in all these cases, the simulated centre temperatures were slightly higher than the values obtained experimentally in the first stage of the process before the initial freezing point was reached. During the subsequent stages of the process, minor differences occurred randomly, which can be a result of the difficulties related to the sample shape and thermocouples positioning accuracy. The latter issue was important during the experiments because in small food product the temperature gradients were relatively high. As a result, the local temperatures, which were compared, were sensitive to thermocouples positioning. In some of the experiments, supercooling occurred, which can be noted in Fig. 4(b) for the near-surface temperature but especially in Fig. 4(a) for both locations. During this phenomenon, the temperature of the food product drops below the initial freezing point without a phase change. At some moment, ice nucleation and a phase change occur instantly, which is manifested by rapid temperature growth (Singh & Heldman, 2014). Supercooling was not
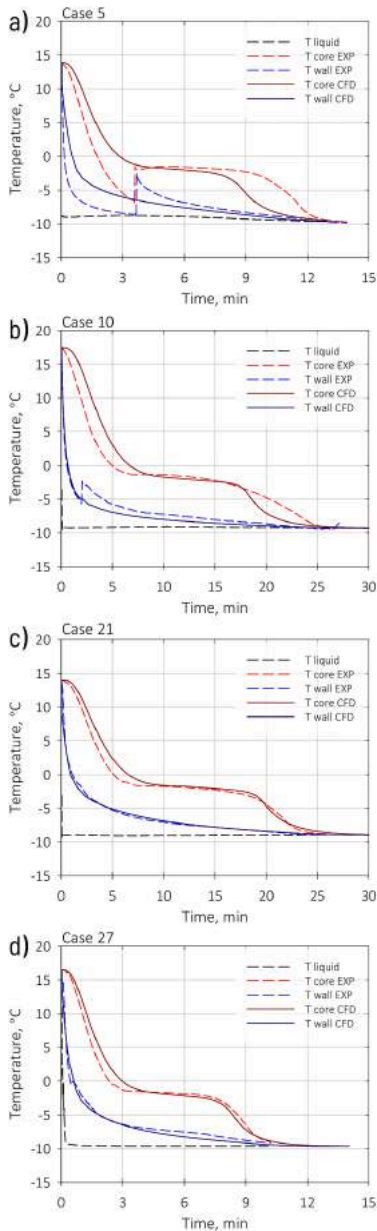
Fig. 4. Temperatures in °C at the potato centre and near the surface during the HF process obtained with the model and compared to experiments for (a) Case 5 where supercooling occurs, (b) Case 10, (c) Case 21 and (d) Case 27.

included in the mathematical model due to the difficulty in predicting its onset.

Based on the results, the mathematical model showed good prediction levels. Taking into consideration all the difficulties related to the experimental work and the assumptions used for the model development, the differences between the experiments and the simulated temperatures are not significant, especially from the practical point of view for industrial HF method application.

4.2. Parametric study

Food hydrofluidisation freezing systems can be described by characteristic geometrical parameters related to the orifices (diameter, arrangement, spacing, size, and mutual position), and the location of food products above the orifices plate, which in practice can represent the size of the HF tank when foods are floating near the free surface. These quantities affect the HTC, as discussed by Peralta et al. (2009) for the basic configurations and by Belis et al. (2015) for more complex HF scenario. In addition, flow conditions such as the fluid temperature, flow rate or refrigerating medium type itself affect the freezing process, whereas the Reynolds and the Prandtl numbers that describe the convective heat transfer are functions of these physical quantities. In this paper, the geometrical parameters have been investigated in the range of conditions that are practically possible to obtain on the dedicated test rig. Table 5 presents all the cases, specifying the values of the main operative variables, used for the parametric study of the mathematical model and also some characteristic results discussed in further sections. Several analyses were performed based on these variants:

- Cases 37–63 describe different scenarios where the spacing between orifices (S), mutual positions of the same food products (z) and position of the whole group of food products (H) were various.
- Cases 64–69 cover the scenarios where the diameter of orifices (d) was extended from 3 mm through 5 mm.
- Cases 70–75 are aimed at comparing situations where the food products are at different locations with reference to the array of impinging jets. This comparison and the previous one for Cases 64–69 regarding the orifice diameter (d) were tested for different distances between the orifices and the sphere stagnation point because the development of the jet is strongly dependent on the H/d ratio.
- Cases 76–79 are characterised by a different range of sub-zero temperatures that still guarantee the liquid state of the solution having a mass concentration of 30%. The effect of the ethanol aqueous solution temperature on the freezing rate and the process time is tested in these cases.
- Cases 80–89 are devoted to assessing the HF method in comparison with typical IF for food products of different sizes.

4.2.1. Effect of the geometrical arrangement

As mentioned previously, the convective heat transfer in the HF method was compared for different geometrical configurations with a different spacing between orifices (8–16 mm), the distances between sphere surfaces (5–15 mm) and the heights measured from the inflow plate to the sphere stagnation point (50–70 mm). Fig. 5 presents the spatially-averaged HTC for the sample placed at the group centre presented previously in Fig. 2. For the selected cases, this value was in the range of 2685 W· m^{-2} K^{-1} through 4727 W· m^{-2} K^{-1}. In the CFD model, the local values of the heat flux obtained directly from the FVM heat balance along with the difference between the food product surface local temperature and the refrigerating medium mean temperature allowed for the determination of the HTC values.

The distance between the spheres (z) had a minor effect on the convective heat transfer for all cases. Within the studied parameter range, the HTC varied by approximately 200 W · m^{-2} K^{-1}. The situation

Table 5

Cases used to investigate the effect of geometrical or flow parameters on the heat transfer and freezing process, HTC, and the time required to complete HF process obtained for these cases.

Case	d	D	H	z	S	H/d	T_{in}	T_{liq}	v_a	Re	HTC	t
	(mm)	(mm)	(mm)	(mm)	(mm)		(°C)	(°C)	(m s⁻¹)		(W · m⁻² K⁻¹)	(min)
Case 37	64 × 3	20	50	5	8	16.7	15	−15	7.67	9000	4624	5.9
Case 38	64 × 3	20	60	5	8	20.0	15	−15	7.67	9000	4404	5.9
Case 39	64 × 3	20	70	5	8	23.3	15	−15	7.67	9000	3525	6.0
Case 40	64 × 3	20	50	10	8	16.7	15	−15	7.67	9000	4727	5.9
Case 41	64 × 3	20	60	10	8	20.0	15	−15	7.67	9000	4509	5.9
Case 42	64 × 3	20	70	10	8	23.3	15	−15	7.67	9000	3509	6.0
Case 43	64 × 3	20	50	15	8	16.7	15	−15	7.67	9000	4620	5.9
Case 44	64 × 3	20	60	15	8	20.0	15	−15	7.67	9000	4474	5.9
Case 45	64 × 3	20	70	15	8	23.3	15	−15	7.67	9000	3414	6.0
Case 46	64 × 3	20	50	5	12	16.7	15	−15	7.67	9000	3485	6.0
Case 47	64 × 3	20	60	5	12	20.0	15	−15	7.67	9000	3251	6.0
Case 48	64 × 3	20	70	5	12	23.3	15	−15	7.67	9000	3099	6.0
Case 49	64 × 3	20	50	10	12	16.7	15	−15	7.67	9000	3580	6.0
Case 50	64 × 3	20	60	10	12	20.0	15	−15	7.67	9000	3242	6.0
Case 51	64 × 3	20	70	10	12	23.3	15	−15	7.67	9000	3178	6.0
Case 52	64 × 3	20	50	15	12	16.7	15	−15	7.67	9000	3506	6.0
Case 53	64 × 3	20	60	15	12	20.0	15	−15	7.67	9000	3261	6.0
Case 54	64 × 3	20	70	15	12	23.3	15	−15	7.67	9000	3011	6.0
Case 55	64 × 3	20	50	5	16	16.7	15	−15	7.67	9000	3043	6.0
Case 56	64 × 3	20	60	5	16	20.0	15	−15	7.67	9000	2865	6.0
Case 57	64 × 3	20	70	5	16	23.3	15	−15	7.67	9000	2686	6.1
Case 58	64 × 3	20	50	10	16	16.7	15	−15	7.67	9000	3111	6.0
Case 59	64 × 3	20	60	10	16	20.0	15	−15	7.67	9000	2930	6.0
Case 60	64 × 3	20	70	10	16	23.3	15	−15	7.67	9000	2737	6.1
Case 61	64 × 3	20	50	15	16	16.7	15	−15	7.67	9000	3209	6.0
Case 62	64 × 3	20	60	15	16	20.0	15	−15	7.67	9000	2903	6.0
Case 63	64 × 3	20	70	15	16	23.3	15	−15	7.67	9000	2685	6.1
Case 64	64 × 3	20	50	5	12	16.7	15	−15	7.67	9000	3485	6.0
Case 65	64 × 3	20	60	5	12	20.0	15	−15	7.67	9000	3251	6.0
Case 66	64 × 3	20	70	5	12	23.3	15	−15	7.67	9000	3099	6.0
Case 67	64 × 5	20	50	5	12	10.0	15	−15	7.67	9000	4531	5.9
Case 68	64 × 5	20	60	5	12	12.0	15	−15	7.67	9000	4309	5.9
Case 69	64 × 5	20	70	5	12	14.0	15	−15	7.67	9000	4376	5.9
Case 70	64 × 3	20	50	5	12	16.7	15	−15	7.67	9000	3485	6.0
Case 71	64 × 3	20	60	5	12	20.0	15	−15	7.67	9000	3251	6.0
Case 72	64 × 3	20	70	5	12	23.3	15	−15	7.67	9000	3099	6.0
Case 73	49 × 3	20	50	5	12	16.7	15	−15	7.67	9000	3470	6.0
Case 74	49 × 3	20	60	5	12	20.0	15	−15	7.67	9000	3236	6.0
Case 75	49 × 3	20	70	5	12	23.3	15	−15	7.67	9000	3077	6.0
Case 76	64 × 3	20	60	5	12	20.0	15	−5	4.02	9000	2754	19.3
Case 77	64 × 3	20	60	5	12	20.0	15	−10	5.44	9000	2930	9.1
Case 78	64 × 3	20	60	5	12	20.0	15	−15	7.67	9000	3251	6.0
Case 79	64 × 3	20	60	5	12	20.0	15	−20	11.12	9000	3500	4.6
Case 80	64 × 3	10	60	5	12	20.0	15	−15	15.35	9000	9051	1.5
Case 81	64 × 3	15	60	5	12	20.0	15	−15	10.23	9000	4574	3.4
Case 82	64 × 3	20	60	5	12	20.0	15	−15	7.67	9000	3251	6.0
Case 83	64 × 3	25	60	5	12	20.0	15	−15	6.14	9000	2606	9.4
Case 84	64 × 3	30	60	5	12	20.0	15	−15	5.12	9000	2302	13.5
Case 85	64 × 3	10	60	5	12	20.0	15	−15	0.085	50	475	3.5
Case 86	64 × 3	15	60	5	12	20.0	15	−15	0.057	50	381	6.8
Case 87	64 × 3	20	60	5	12	20.0	15	−15	0.043	50	343	11.1
Case 88	64 × 3	25	60	5	12	20.0	15	−15	0.034	50	322	15.9
Case 89	64 × 3	30	60	5	12	20.0	15	−15	0.028	50	297	21.6

could be different in another arrangement of the unit in which one food product partially protects a second one from being impinged by the jets.

The highest values of the HTC were noted for the cases with a smaller spacing between the orifices in the array (*S*) for Cases 37–45. This result suggests that a setup with a higher density of orifices can result in maximisation of the convection in the HF system. In such a situation, more volume in the tank is occupied by the agitating jets, which causes more intensive heat transfer. However, for the cases with the foods placed at the highest position, i.e., 70 mm above the orifices, the difference in HTC was not significant when the orifice spacing was changed. Doubling the orifices density resulted in an increase in the average HTC value by approximately 30% (Cases 57 and 39, 60 and 42, 63 and 45), while for the cases with food samples at the lowest position,

this quantity increased by approximately 50–60% (Cases 55 and 37, 58 and 40, 61 and 43). The conclusion is that at certain heights characterised by H/d ratios over 23.3, jets were sufficiently developed, and an increase in the orifice amount did not provide any increase in heat transfer.

Within the investigated range, an increase in the HTC is guaranteed when the sample position above the orifices is lower. For all cases, lowering the H/d ratio resulted in an increase in the HTC.

The effect of the H/d ratio on the heat transfer can also be seen, when comparing Cases 64–66 with Cases 67–69. For these variants, the diameter of the orifices was changed from 3 mm to 5 mm. This change resulted in an increase in the average HTC, as presented in Fig. 6. It is worth emphasising that the mass flow rate of the fluid was adjusted to
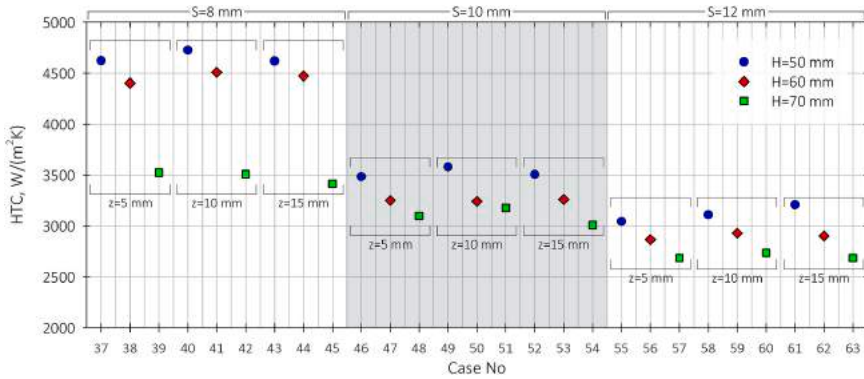
Fig. 5. Average values of the HTC given in $W \cdot m^{-2} K^{-1}$ at the spherical food sample surface for Cases 37–63 showing the effect of H, S and z.
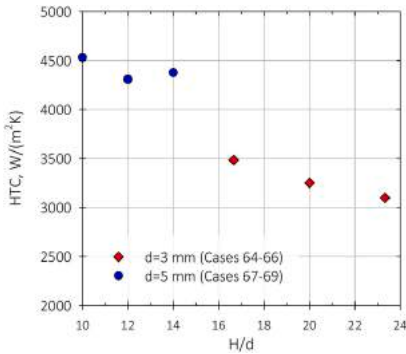
Fig. 6. Values of HTC given in $W \cdot m^{-2} K^{-1}$ for Cases 64–69 showing the effect of H/d and d.

the orifice diameter so that average velocity of the fluid flowing through orifices remained the same. More intensive convection was observed in cases with H/d ratio in the range of 10.0 to 14.0 and orifices with diameters of 5 mm. Significantly lower HTC values were observed in cases with H/d ratio ranging 16.7–23.3 and smaller orifices of 3 mm.

For all the cases already presented, the middle sphere in the group was positioned in the centre between the array of jets. Cases 70–75 present the comparison of such a scenario with the arrangement where the food sample was placed directly above one of the orifices in the array. Fig. 7 presents the average HTC for these cases. No significant differences were observed between the cases with H ranging from 50 mm to 70 mm when the position above the orifices was changed. For the reference position, the average values of the HTC were $3485\ W \cdot m^{-2} K^{-1}$, $3251\ W \cdot m^{-2} K^{-1}$ and $3099\ W \cdot m^{-2} K^{-1}$ for Cases 70, 71 and 72, respectively. Changing the position of the food sample resulted in the HTC changing to $3470\ W \cdot m^{-2} K^{-1}$, $3236\ W \cdot m^{-2} K^{-1}$ and $3077\ W \cdot m^{-2} K^{-1}$. Thus, it can be concluded that the situation with four jets striking the food product surface is more favourable than the case with one jet impinging on the stagnation point of the spherical sample supported by the other jets agitating the region close to the food. However, the difference is insignificant.

As discussed before, changing the different geometrical parameters
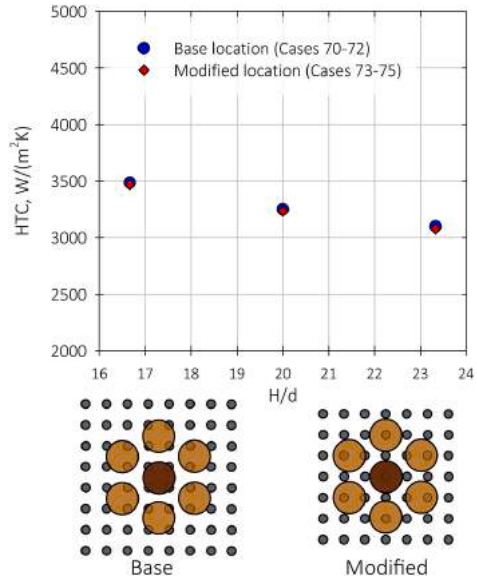
Fig. 7. Average values of the HTC given in $W \cdot m^{-2} K^{-1}$ at the spherical food sample surface for Cases 70–75 showing the effect of the sample position with respect to the array of jets.

during small food sample freezing in the HF unit using a liquid medium can lead to a change in the HTC distribution at the food surface, which characterises the convective heat transfer during food freezing. The geometrical parameters in Cases 37–75 provided average HTC in the range from $2685\ W \cdot m^{-2} K^{-1}$ to $4727\ W \cdot m^{-2} K^{-1}$.

Apart from convection, the second mechanism that affects food freezing is the heat conduction within the food interior, where the exact phase change occurs. The combination of both mechanisms determines the temperature change near the centre of the spherical food sample, where the temperature drop is the slowest. Fig. 8 presents the
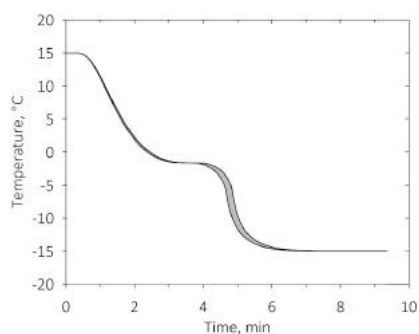
Fig. 8. Temperature range in °C within the potato centre during the HF process presented jointly for Cases 37–75 showing the overall effect of the geometrical parameters change.

Fig. 9. Temperature in °C of the potato centre during the HF process for Cases 76–79 showing the effect of liquid temperatures.

temperature change during the freezing process jointly for Cases 37–75. The grey area represents the range of the temperature variation during the freezing process. The upper and lower edges of the field marked on the graph refer to the most and less intensive freezing process for Cases 37–75. As seen, despite the high discrepancy in the HTC listed in Table 5 and discussed in previous paragraphs, the temperature variation within the food product centre is minor between the investigated cases. The overall process temperature defined as the moment when the food centre temperature becomes less than 0.5 K higher than the refrigerating medium temperature does not change significantly within these cases. As presented in Table 5, for Cases 37–75 it is approximately 6 min and varies by just several seconds. It can be justified that under these conditions, i.e., the fluid temperature and food product properties and size, the values of the HTC are sufficiently high, and further intensification of the convection does not significantly reduce the freezing time.

4.2.2. Effect of the refrigerating medium temperature

The effect of lowering the refrigerating medium temperature is twofold. First, when the freezing process is completed, the food product temperature is lower, what is favourable in terms of the foodstuff quality. Second, a higher temperature gradient accelerates the freezing process which is beneficial for many reasons. Cases 76–79 present the analysis of the food freezing process with different liquid medium temperatures in the range from −5 °C, which is a temperature slightly lower than the initial freezing temperature for the potato, down to −20 °C, which is close to the solidification temperature for aqueous ethanol solution having a mass concentration of 30%. It is worth mentioning that within this temperature range, the properties of the considered liquid change significantly. Therefore, the mass flow rate had to be adjusted in these cases to maintain a constant Reynolds number. Moreover, the higher viscosity of a cold medium results in higher friction losses in the entire HF refrigerating medium loop and a higher power required for the pumping.

Fig. 9 presents the temperature of the potato sphere centre during HF in ethanol solutions with different temperatures. At lower refrigerating medium temperatures, the freezing process was faster, especially during the phase change stage. To quantify the freezing process time for different conditions in this study, freezing was considered to be finished when the centre temperature reached 0.5 K higher than the liquid temperature for each case. These times are listed in Table 5 for all the cases. For most of them, that value is at similar level, but it differs significantly in Cases 76–79, therefore it is additionally marked in Fig. 9. As seen, reducing the refrigerating medium temperature from −5 °C through −10 °C allowed for a reduction of the process time by half.
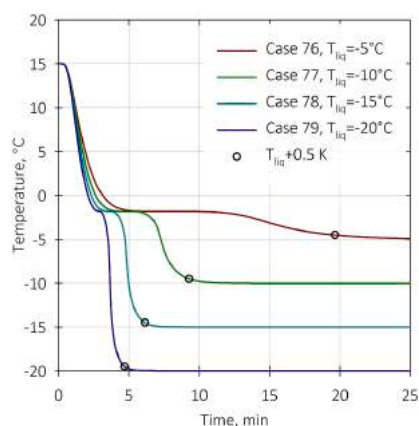
When the liquid temperature was assumed to be −20 °C, the time required to complete the process less than 5 min. These results suggest that the freezing medium temperature has a significant effect on the overall time required for the freezing process. Despite the fact that more energy is required for refrigerating medium temperature lowering, it can considerably reduce the process time. As a result, in industrial HF freezers, more food can be processed in the same time using the same HF unit.

As mentioned before, the temperature level during the freezing process is also important when considering the quality of food tissues. Fikiin (2008) identified the *critical zone of water crystallisation* to be within the temperature range from −1 °C to −8 °C. If the food temperature is maintained within this range in a shorter period of time, then the quality of the food product can be higher. Fig. 10 compares the process duration when the centre temperature is kept within this range of temperatures for Cases 77–79. Lowering the refrigerating medium temperature from −10 °C by 5 K enabled reduction of this stage by approximately 55%, while a 10 K temperature reduction resulted in
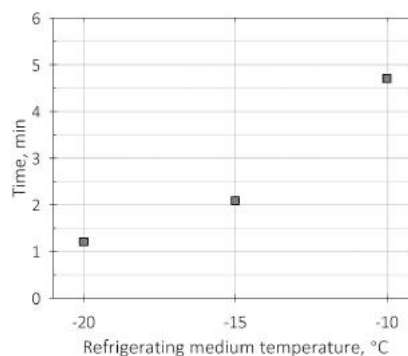
Fig. 10. Total time of the potato central temperature being within the range of the critical zone of water crystallisation for different liquid temperatures in Cases 77–79.

shortening of this stage by almost 75%.

If the HF method is used for pre-freezing of the crust of individual food products, then the matter of the *critical zone of water crystallisation* would rather be an aspect of a secondary stage in which full freezing would be achieved by employing another process. However, if the HF method is used as a standalone process for deep freezing, then the temperature should be maintained at the lowest possible level, considering the freezing temperature of the liquid solution and the economic aspects.

4.2.3. Effect of hydrofluidisation for different food sizes

Apart from the HTC distribution and the temperature of the freezing medium, the size of the individual food product affects the whole process. The HF process is described in the literature as a method especially beneficial for freezing small foods due to the very high values of the HTC. A comparison of Cases 80–89 indicates the difference in freezing food products of different sizes from 10 mm to 30 mm using the HF method and IF. For the latter case, the flow was defined with the Reynolds number of 50 to simulate a calm flow of the liquid within the tank. Table 6 presents the values of the HTC obtained during the freezing of different size foods. The simulations using IF conditions showed HTC values ranging 297 $W \cdot m^{-2} K^{-1}$ to 475 $W \cdot m^{-2} K^{-1}$, which are in agreement with HTC values reported in literature for similar conditions (Zorrilla & Rubiolo, 2005).

The freezing times of spherical potato samples with different diameters were compared in terms of the total process time and the residence time within the critical zone of water crystallisation. Fig. 11(a) presents the values of these time indicators for Cases 80–89, i.e., HF and IF of different size foods.

In general, HF appeared to be significantly faster than IF. For example, for the smallest food products with a diameter of 10 mm, the IF process needed approximately 3.5 min (Case 85), while HF lasted for 1.5 min (Case 80). In the case of the largest products being investigated, which have a diameter of 30 mm, the freezing times were 22 min and nearly 14 min for the IF and HF methods analysed in Cases 89 and 84, respectively.

Theoretically, according to numerous analytical or semi-empirical models for the freezing time prediction (Pham, 1986; Plank, 1913), the freezing time should be proportional to the sample diameter squared, i.e., $t \sim D^2$. Fig. 11(b) compares the time required to the complete HF and IF for the same conditions as in Fig. 11(a) for samples having a diameter from 10 mm to 30 mm but formulated as a function of the diameter squared.

As seen, in case of IF the results, a minor discrepancy from the linear relationship between the freezing time and the food sample diameter squared is seen. It is a result of different HTC value for each food sample diameter. As a consequence, these variations affect the freezing time under the conditions of the IF with relatively low Bi numbers. In the case of the HF method, the freezing times are undoubtedly proportional to the food sample diameter squared and no variations are observed.

Apart from the freezing process times, Fig. 11(a) also presents the time required to pass the critical zone of water crystallisation for different size products, and the differences for the IF and HF methods are also evident. For Cases 85 and 80, which describe the freezing of 10 mm

Table 6

HTC obtained for HF and IF of food samples with different diameters in Cases 80–89.

Cases	D (mm)	HF (Re = 9000)	IF (Re = 50)
		HTC ($W \cdot m^{-2} K^{-1}$)	
Case 80/85	10	9051	475
Case 81/86	15	4574	381
Case 82/87	20	3251	343
Case 83/88	25	2606	322
Case 84/89	30	2302	297
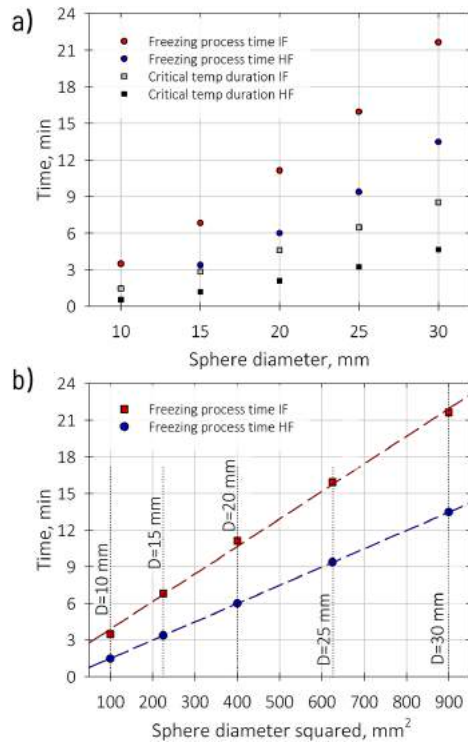
Fig. 11. (a) Total time of the whole HF process, time of the potato centre temperature being within the range of the critical zone of water crystallisation for different size potato spheres in Cases 80–89 and (b) the freezing times for the same cases presented as a relationship related to the sphere diameter squared.

potato samples with the IF and HF methods, the centre temperature was in the critical range for 1.5 min and 0.5 min, respectively. In the case of the 30 mm samples, these times were 9 min for the IF method and 5 min for the HF method, which were analysed in Cases 89 and 84.

A detailed comparison of the freezing process shortening and the reduction of the residence within the critical zone due to HF is presented in Fig. 12. It presents these two time indicators for HF relative to those for the IF method in dimensionless form. This comparison presents how much the food freezing process and the critical zone duration may be reduced if the HF method is used instead of IF for a food product of a specific size. As seen, the use of HF is favourable mostly for the smallest foods. When the sample had a diameter of 10 mm, which may represent, e.g., different berries or brussels sprouts, the total freezing time was reduced by more than 60%, while the duration in the critical zone of crystallisation was reduced by over 50%. Nonetheless, HF is also advantageous for slightly large food products. For the sample with a diameter of 30 mm, the total process time and the period in the critical zone of water crystallisation were reduced by approximately 45% and 40%, respectively.
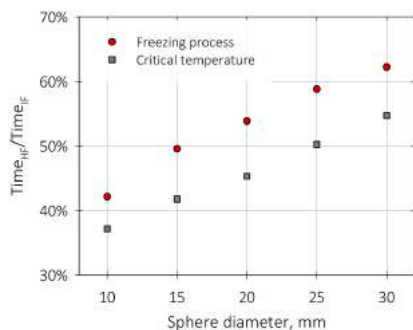
Fig. 12. Total time of the whole freezing process and time of the potato centre temperature being within the range of the critical zone of water crystallisation for the HF method relative to IF for different potato sizes in Cases 80–89.

5. Conclusions

A mathematical model and a CFD study of a HF system using sphere potatoes as food samples and testing different configurations were presented. The operative variables tested were the orifice diameter (3 to 5 mm), the spacing between orifices (8 to 16 mm), the distance orifices-samples (50 to 70 mm), sample diameter (10 to 30 mm), the spacing between samples (5 to 15 mm), the level of alignment of samples and jets, and the refrigerating medium temperature (−5° to −20 °C). HF and IF conditions were simulated and compared.

The numerical model of the freezing process was developed using ANSYS Fluent commercial software by using the enthalpy-based energy equation and the apparent heat capacity approach, which takes into account the latent heat from the phase change phenomenon. The mathematical models describing the transfer phenomena in the fluid and the heat transfer in the solid were coupled using a convective boundary condition at the external surfaces of food products. The complete model captured the key points to consider in an efficient numerical implementation.

The model has been validated using experiments performed on the dedicated test rig designed for this study. Thermal measurements of the food product surface temperature and the centre temperature for 36 different cases were used for the model validation. The mean temperature difference between the simulated and measured temperatures did not exceed 1.5 K, which is considered a satisfactory result.

A parametric study of the HF system showed that geometrical variables significantly affected the HTC, especially when the *H/d* ratio of the sphere position above the orifice to the orifice diameter is changed or when the density of orifices is changed under some operating conditions. In the range of geometrical parameters analysed represented by high Biot numbers over 37, the freezing process was not changed significantly due to the relationship between convective and the conductive thermal resistances. However, the relevance of this systematic analysis is to explore scenarios that can be taken into account in the next steps such as optimisation or control of HF systems.

The temperature of the liquid medium affected the freezing process of the food sample. Reducing the temperature from −5 °C to −10 °C resulted in a two times shorter freezing process. It also reduced the time when the food product temperature was in the range of the critical zone of water crystallisation that may lead to worsening of the food product quality.

Although the hydrodynamics of the presented system is simplified, i. e., the food samples movement was not modelled, the results allowed for the estimation of the potential of HF method. Moreover, it allowed to conduct an experimental validation of the model by measuring the local

food temperatures during the freezing process. Numerous geometrical configurations were studied to assess the range of HTC possible to obtain at a certain range of *H*, *H/d*, *S*, etc. The freezing time of food was evaluated for different positions of food samples in the HF tank, for different temperatures of refrigerating medium and for different size of food samples. The outcome of this study can be useful for future works regarding the HF method. It is clear that the geometrical arrangement of the system does not affect the freezing process as much as the refrigerating medium temperature and the size of food products. In a more realistic scenario study, the other aspects should be investigated as well, e.g., the refrigerating medium selection in terms of the HF process itself, for the freezing times and for the unwanted solution intake.

This study showed that HF can be an attractive method for freezing small products. The overall freezing time can be reduced by 50% in the case of the HF process. This advantage leads to the reduction of the processing time and operational costs and may improve the food product quality depending on the substantial stages of the food product processing and the cold chain.

Declaration of Competing Interest

The authors declare no conflict of interest.

Acknowledgements

References

ANSYS Inc.. (2017). *Chapter 5.5. Overset Meshes* (pp. 175–238). Canonsburg, PA, USA: ANSYS.

ASHRAE. (2006). *ASHRAE Handbook: Refrigeration: SI edition*. American Society of Heating, Refrigerating and Air-Conditioning Engineers.

Belis, E. E., Zorrilla, S. E., & Peralta, J. M. (2015). Effect of the number of orifices and operative variables on the heat and mass transfer in a hydrofluidization system with static spheres. *Journal of Food Engineering, 153*, 96–107.

Carson, J. K., Wang, J., North, M. F., & Cleland, D. J. (2016). Effective thermal conductivity prediction of foods using composition and temperature data. *Journal of Food Engineering, 175*, 65–73.

Chen, C. S. (1985). Thermodynamic analysis of the freezing and thawing of foods: Enthalpy and apparent specific heat. *Journal of Food Science, 50*(4), 1158–1162.

Cleland, A. C., & Earle, R. L. (1984). Assessment of freezing time prediction methods. *Journal of Food Science, 49*(4), 1034–1042.

Delgado, A. E., & Rubiolo, A. C. (2005). Microstructural changes in strawberry after freezing and thawing processes. *LWT – Food Science and Technology, 38*(2), 135–142.

Fikiin, A. G. (1992). New method and fluidized water system for intensive chilling and freezing of fish. *Food Control, 3*(3), 153–160.

Fikiin, K. A. (1998). Ice content prediction methods during food freezing: A survey of the eastern European literature. *Journal of Food Engineering, 38*(3), 331–339.

Fikiin, K. A. (2008). *Emerging and novel freezing processes* (pp. 101–123). Oxford, UK: Blackwell Publishing Ltd. ISBN 978144430232 (Chapter 5).

Fikiin, K. A., & Fikiin, A. G. (2001). Individual quick freezing of foods by hydrofluidisation and pumpable ice slurries. *Materials Science, 55*, 15–18.

VDI Gesellschaft. (2010). *VDI heat atlas*. Springer Berlin Heidelberg.

Khouryieh, H. A. (2021). Novel and emerging technologies used by the US food processing industry. *Innovative Food Science and Emerging Technologies, 67*, 102559.

Levy, F. L. (1981). A modified maxwell-eucken equation for calculating the thermal conductivity of two-component solutions or mixtures. *International Journal of Refrigeration, 4*(4), 223–225.

Luscher, C., Schlüter, O., & Knorr, D. (2005). High pressure-low temperature processing of foods: Impact on cell membranes, texture, color and visual appearance of potato tissue. *Innovative Food Science and Emerging Technologies, 6*(1), 59–71.

Oroná, J. D., Zorrilla, S. E., & Peralta, J. M. (2017). Computational fluid dynamics combined with discrete element method and discrete phase model for studying a food hydrofluidization system. *Food and Bioproducts Processing, 102*, 278–288.

Oroná, J. D., Zorrilla, S. E., & Peralta, J. M. (2018). Sensitivity analysis using a model based on computational fluid dynamics, discrete element method and discrete phase model to study a food hydrofluidization system. *Journal of Food Engineering, 237*, 183–193.

Palacz, M., Adamczyk, W., Piechnik, E., Stebel, M., & Smolka, J. (2019). Experimental investigation of the fluid flow inside a hydrofluidisation freezing chamber. *International Journal of Refrigeration, 107*, 52–62.

Palacz, M., Piechnik, E., Halski, M., Stebel, M., Adamczyk, W., Eikevik, T. M., et al. (2021). Experimental analysis of freezing process of stationary food samples inside a hydrofluidisation freezing chamber. *International Journal of Refrigeration.* https://doi.org/10.1016/j.ijrefrig.2021.06.034

Peralta, J. M., Rubiolo, A. C., & Zorrilla, S. E. (2009). Design and construction of a hydrofluidization system, study of the heat transfer on a stationary sphere. *Journal of Food Engineering, 90*(3), 358–364.

Peralta, J. M., Rubiolo, A. C., & Zorrilla, S. E. (2010). Mathematical modeling of the heat transfer and flow field of liquid refrigerants in a hydrofluidization system with a stationary sphere. *Journal of Food Engineering, 99*(3), 303–313.

Peralta, J. M., Rubiolo, A. C., & Zorrilla, S. E. (2012). Mathematical modeling of the heat and mass transfer in a stationary potato sphere impinged by a single round liquid jet in a hydrofluidization system. *Journal of Food Engineering, 109*(3), 501–512.

Pham, Q. T. (1986). Simplified equation for predicting the freezing time of foodstuffs. *International Journal of Food Science & Technology, 21*(2), 209–219.

Plank, R. (1913). Die gefrierdauer von eisblocken. *Zeitschrift fur die gesamte Kalte Industrie, 20*(6), 109–114.

Singh, R. P., & Heldman, D. R. (2014). chapter 7 – food freezing. *Introduction to food engineering* (pp. 521–563). San Diego: Academic Press.

Smolka, J. (2018). *User-defined functions programming in ansys fluent.* Silesian University of Technology.

Stebel, M., Smolka, J., Palacz, M., Adamczyk, W., & Piechnik, E. (2020). Numerical investigation of the fluid flow distribution for the hydrofluidisation food freezing method. *International Journal of Thermal Sciences, 151*, 106284.

Tchigeov, G. (1979). *Thermophysical processes in food refrigeration technology.* Moscow, Russia: Food Industry.

Verboven, P., Scheerlinck, N., & Nicolai, B. M. (2003). Surface heat transfer coefficients to stationary spherical particles in an experimental unit for hydrofluidisation freezing of individual foods. *International Journal of Refrigeration, 26*(3), 328–336.

Wang, J. F., Carson, J. K., Willix, J., North, M. F., & Cleland, D. J. (2009). Application of a co-continuous composite model of effective thermal conductivity to ice-air systems. *International Journal of Refrigeration, 32*(3), 556–561.

Xanthakis, E., Le-Bail, A., & Ramaswamy, H. (2014). Development of an innovative microwave assisted food freezing process. *Innovative Food Science and Emerging Technologies, 26*, 176–181.

Xu, B. G., Zhang, M., Bhandari, B., Sun, J., & Gao, Z. (2016). Infusion of co2 in a solid food: A novel method to enhance the low-frequency ultrasound effect on immersion freezing process. *Innovative Food Science and Emerging Technologies, 35*, 194–203.

Zorrilla, S. E., & Rubiolo, A. C. (2005). Mathematical modeling for immersion chilling and freezing of foods: Part I: Model development. *Journal of Food Engineering, 66*(3), 329–338.

Paper III: Modelling of hydrofluidisation hydrodynamics

Numerical analysis of hydrofluidisation food freezing with moving products in different aqueous solutions by using CFD and MPM approaches

Michal Stebel [a, *], Jacek Smolka [a], Michal Palacz [a], Michal Halski [a], Agata Widuch [a], Ignat Tolstorebrov [b]

[a] Department of Thermal Technology, Silesian University of Technology, Konarskiego 22, 44-100 Gliwice, Poland
[b] Department of Energy and Process Engineering, Norwegian University of Science and Technology, NO-7491, Trondheim, Norway

ARTICLE INFO

ABSTRACT

Hydrofluidisation (HF) is an original method of food freezing that allows very high heat transfer coefficients to be reached and significantly reduces the freezing time of small foods. This paper presents a numerical study of HF for food products immersed in different liquids: binary solutions of ethanol (30%) and glycerol (40%) and a ternary solution of ethanol and glucose (15% and 25%). The particle movement (0.02 m diameter) was simulated using the Macroscopic Particle Model (MPM) approach to extend the CFD simulation by the particle flow, which affects the liquid phase velocity field. The numerical model developed in that study fully describes the hydrodynamics of HF process and is the most realistic out of all the numerical studies performed so far due to the ability to resolve the fluid flow locally on a smaller scale than in other models where the movement of foods in HF was introduced. Experiments with high-speed camera recordings validated the numerical model. A wide range of liquid mass flow rates in the range from 0.1 kg·s−1 to 2.0 kg·s−1 was investigated. As a result, heat transfer coefficients from 1 000 W·m−2·K−1 to 4 500 W·m−2·K−1 were reached, depending on the fluid mass flow rate. The liquid type had a minor effect on the heat transfer coefficient (HTC) but affected the behaviour of food samples. The effect of the food product suspension within the HF tank was noticed only for the ethanol solution with a moderate mass flow rate.

Nomenclature

A	Area, m^2
C_D	Drag coefficient
D	Sample diameter, m
D_ω	Cross-diffusion term, kg m−1·s−3
d	Orifice diameter, m
e	Coefficient of restitution
F	Force, kg m·s−2
G	Generation term, kg·m−1·s−3
g	Gravitational acceleration, m·s−2
H	Inflow plate-sphere stagnation point distance, m
HTC	Heat transfer coefficient, W·m−2·K−1
J	Impulse force, kg·m·s−1
K	Turbulence kinetic energy, m^2·s−2·K−1
k	Thermal conductivity, W·m−1·K−1
$\dot{m}$	Mass flow rate, kg·s−1

m	Mass, kg
n	Unit vector in normal direction
p	Pressure, kg m−1·s−2
r	Radius, m
S	Orifice-orifice distance measured from their centres, m
S_{MPM}	Source term from MPM model, kg m−2·s−2
t	Time, s
t	Unit vector in tangential direction
Y	Dissipation term, kg·m−1·s−3
u	Velocity, m·s−1
Re	Dimensionless Reynolds number
Nu	Dimensionless Nusselt number
Pr	Dimensionless Prandtl number

Abbreviations

CFD	Computational Fluid Dynamics

* Corresponding author.
   E-mail address: michal.stebel@polsl.pl (M. Stebel).

Note: Low-resolution images were used to create this PDF. The original images will be used in the final composition.
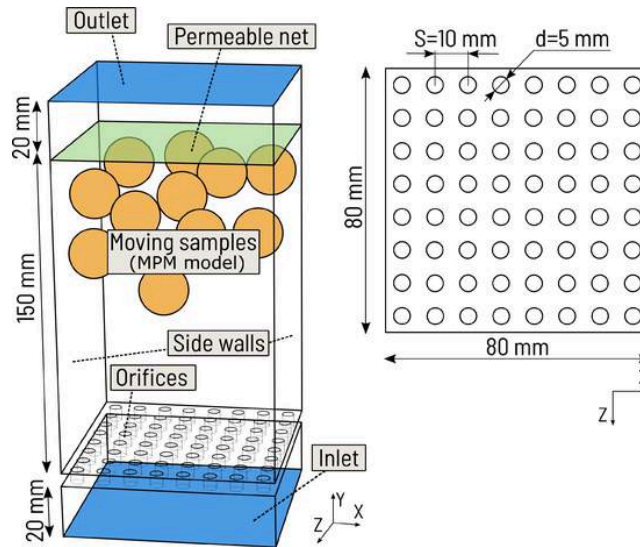
Fig. 1. Geometrical domain of the modelled HF tank with the characteristic dimensions and boundary conditions.

COP	Coefficient of Performance
DEM	Discrete Element Method
DPM	Discrete Phase Model
HF	Hydrofluidisation Freezing
IF	Immersion Freezing
LBM	Lattice Boltzmann Method
LES	Large Eddy Simulation
MPM	Macroscopic Particle Model
PIV	Particle Imaging Velocimetry
RMSE	Root Mean Squared Error
SST	Shear Stress Transport
TFM	Two-Fluid Model

Greek Symbols

ρ	Density, kg m^{-3}
μ	Dynamic viscosity, kg·m^{-1}·s^{-1}
δ_{ij}	Kronecker delta
σ_K	Turbulent Prandtl number for turbulence kinetic energy
σ_ω	Turbulent Prandtl number for specific dissipation rate
τ	Shear stress, kg·m^{-1}·s^{-2}
ω	Specific dissipation rate, s^{-1}

Subscripts

D	Drag
f	Fluid
i,j	Cartesian coordinates
m	Mass force component
n	Normal direction
o	Orifice
P	Particle, sphere
p	Pressure force component
T	Turbulent
t	Tangential direction
v	Viscous force component

w	Wall

1. Introduction

The most common methods used for food product preservation are chilling and freezing. According to the International Institute of Refrigeration report (IIR, 2020), approximately 46% of the total world food production should benefit from refrigeration, while less than half of that is refrigerated. It results in enormous food losses. Therefore, food freezing is a constantly growing branch of industry, and there is still a high interest in research regarding food product quality improvement and the development of new freezing methods.

A novel method of food freezing that guarantees a high quality of final products is the hydrofluidisation freezing (HF). It is a form of immersion freezing (IF) where turbulent fluid flow is present, which additionally enhances convective heat transfer. In this technique, food products are submerged in the tank with a liquid solution pumped through an array of orifices located at the bottom. Therefore, the freezing rate of foods is intensified by the agitating jets, and the food products behave as a fluidised bed. The method was proposed by Fikiin (1992), who presented an HF system for the chilling and freezing of fish. According to the author, HTCs reach 900 W·m^{-2}·K^{-1} for the freezing of a small fish. More recently, the method was developed and comprehensively described in (Fikiin and Fikiin, 1998) and in further works (Fikiin, 2003; 2008; Fikiin et al., 2005). The authors described the advantages of the HF method, i.e., reducing the processing time in comparison with IF, possible reduction of the operational costs, and better final quality of food products due to higher freezing rates. Fikiin and Fikiin (1998), Fikiin (2003, 2008) and Fikiin et al. (2005) reported HTCs of the order of 1 000-2 000 W·m^{-2}·K^{-1} when involving ice slurries as a refrigerating medium. As a consequence, the authors of these studies pointed out that HF permits to use single-stage refrigeration systems with higher coefficients of performance (COP) because the refrigerating medium temperature does not need to be as low as typical for air-blast freezing.
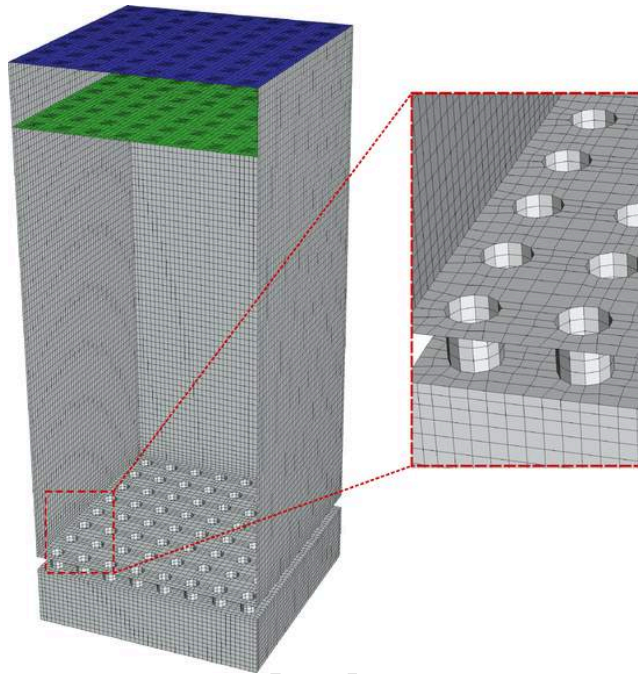
Fig. 2. Mesh of the HF tank used in the numerical model with a close-up of the inflow plate.

Table 1
Coefficients a_1, a_2 and a_3 for the drag coefficient formulation according to Morsi and Alexander (1972).

Range of Re	a_1	a_2	a_3
0 < Re < 0.1	0	24	0
0.1 < Re < 1	3.360	22.73	0.0903
1 < Re < 10	1.222	29.1667	-3.8889
10 < Re < 100	0.6167	46.50	-116.67
100 < Re < 1000	0.3644	98.33	-2 778
1000 < Re < 5000	0.357	148.62	-47 500

Table 2
Thermo-physical properties of water-based solutions used in this study.

Solution	Temp	Freezing temp	Density	Th conductivity	Specific heat	Dyn viscosity	Pr
(mass concentration)	·C	·C	kg·m−3	W·m−1·K−1	J·kg−1 ·K−1	kg·m−1·s −1	-
Glycerol (40%)	-15.0	-15.3	1 111.5	0.4197	3 294	0.017641	138
Ethanol (30%)	-15.0	-20.1	971.4	0.3880	4 100	0.017304	183
Ethanol-glucose (15%/25%)	-15.0	-20.0	1 087.3	0.4119	3 180	0.025376	196

The effect of the process parameters on HTC was studied experimentally by Verboven et al. (2003). The authors used aluminium spheres at a fixed position instead of free-moving food products for the experimental evaluation of HTC based on thermal measurements. They used a ternary solution of water (50%), ethanol (30%), and glucose (20%) as a freezing medium with a flow rate of up to 15 litres per minute. The authors obtained HTCs in the range of 154 to 1 548 W·m−2·K−1 depending on the sample diameter, flow rate, temperature of the solution and level of agitation. Peralta et al. (2009) performed a similar experimental study using sodium chloride aqueous solution (23%) as a refrigerating medium in the lab-scale HF unit. The authors analysed various geometrical parameters, namely, the spherical sample diameter (D) and position (H) of the sphere stagnation point above the single orifice with a known diameter (d). Then proposed a correlation for the Nusselt number in such a system with a fixed position of the frozen sample. The same system was investigated numerically in the next work of those authors (Peralta et al., 2010) by using computational fluid dynamics (CFD) to present the liquid jet turbulent flow and investigate HTC in such a simplified configuration. This CFD model was extended in (Peralta et al., 2012) with heat and mass transfer analyses within a real food product (potato).

A most recent experimental study related to the geometrical parameters in the HF method was performed by Palacz et al. (2019) on a test rig equipped with a transparent HF tank. The authors captured the velocity fields of the refrigerating medium by employing the particle image velocimetry (PIV) technique. It allowed for the experimental investigation of the velocity distribution around a spherical sample at a fixed position in a system with an aqueous ethanol solution as a refrigerating medium for freezing. The same HF system was investigated numerically in the paper by Stebel et al. (2020), where CFD analysis was performed for various geometrical arrangements. The authors selected the appropriate turbulence model for such a flow and validated their model using the gathered PIV results. In the next step, Palacz et al.

Table 3

Operating conditions used for the food sample flow verification and validation.

Case No	Solution	$\dot{m}$	S	d	Number of	Number of
	(mass concentration)	kg·s⁻¹	mm	mm	orifices	samples
Test Case 1	Glycerol (40%)	0.83	10	5	64	1

Table 5

Operating conditions used for the numerical campaign and the parametric study.

Case No	Solution	$\dot{m}$	S	d	Number of	Number of
	(mass concentration)	kg·s⁻¹	mm	mm	orifices	samples
Effect of the solution type and mass flow rate						
Case 1	Ethanol (30%)	0.1	10	5	64	12
Case 2	Ethanol (30%)	0.2	10	5	64	12
Case 3	Ethanol (30%)	0.5	10	5	64	12
Case 4	Ethanol (30%)	1.0	10	5	64	12
Case 5	Ethanol (30%)	2.0	10	5	64	12
Case 6	Glycerol (40%)	0.1	10	5	64	12
Case 7	Glycerol (40%)	0.2	10	5	64	12
Case 8	Glycerol (40%)	0.5	10	5	64	12
Case 9	Glycerol (40%)	1.0	10	5	64	12
Case 10	Glycerol (40%)	2.0	10	5	64	12
Case 11	Eth-glu (15%/25%)	0.1	10	5	64	12
Case 12	Eth-glu (15%/25%)	0.2	10	5	64	12
Case 13	Eth-glu (15%/25%)	0.5	10	5	64	12
Case 14	Eth-glu (15%/25%)	1.0	10	5	64	12
Case 15	Eth-glu (15%/25%)	2.0	10	5	64	12
Effect of the food load in HF tank						
Case 16	Glycerol (40%)	0.5	10	5	64	24
Case 17	Glycerol (40%)	2.0	10	5	64	24
Case 18	Glycerol (40%)	0.5	10	5	64	30
Case 19	Glycerol (40%)	2.0	10	5	64	30

(2021) performed an experimental study to evaluate HTC using a spherical steel sample and the freezing time of different real food samples. Within the range of the conditions analysed in this paper, the HTC obtained for the steel sample at the fixed position was nearly 3 000 W·m⁻²·K⁻¹. The same group of authors performed also a numerical study to evaluate HTC and simulate the freezing process under similar flow conditions with several spherical food samples (Stebel et al., 2021). According to their results, HTC can reach from approximately 2 500 to nearly 5 000 W·m⁻²·K⁻¹ when multiple jets are employed and achieve a very high velocity of nearly 8 m·s⁻¹ in the orifice. The most advanced numerical model of the HF process was presented by Oroná et al. (2017) to simulate the realistic flow of food samples in the HF system with sodium chloride as a refrigerating medium. Their model was developed as multiphase with liquid as continuous phase and solid food products as discrete phase. This work was extended by the sensitivity analysis of the same system (Oroná et al., 2018) to assess the parameters affecting freezing mostly in such a configuration.

In general, the flow of fluid through packed bed is a process widely used in the industry. Depending on the fluid used for the process, one can distinguish a gas or a liquid fluidisation. According to Di Felice (1995), the liquid fluidisation is of a minor interest of researchers because the gas fluidisation found more industrial applications. Nevertheless, liquid fluidisation can be used in food and biochemical processing, separation of minerals, adsorption, etc. (Di Felice, 1995; Khan et al., 2017).

There are several approaches used for in numerical studies focused on fluidisation modelling. A simple way to simulate a liquid-solid fluidised system is two-fluid model (TFM), where both phases are treated as the continuum in the Eulerian-Eulerian framework. According to Peng et al. (2020) and Xie et al. (2021), the shortcoming of that approach is that solid phase is not treated as individual discrete particles, therefore the collisions of solids cannot be introduced appropriately in

such a model. A more complex and completely different approach is the Lattice Boltzmann method (LBM) in which the hydrodynamics of the whole fluid system is based on a particle representation. It is a promising approach due to the ability to provide a detailed description of local fluid flow (Rong et al., 2014) but its drawback is the large computational expense (Peng et al., 2020).

The most common method employed for the numerical study of fluid flow in fluidisation systems is the discrete element method (DEM) used to support CFD simulations. In such an approach, the fluid component of the multiphase system is solved using a CFD solver as the Eulerian phase, while the individual solids are treated as particles in a Lagrangian frame of reference. In CFD-DEM simulations, the continuity of the fluid is conserved and the interactions between particles are well represented. Such an approach is an effective and common practice in numerical studies on granular food materials (Malekjani and Jafari, 2018) and is especially popular with transportation and drying analyses (Horabik and Molenda, 2016). However, it has a major disadvantage that becomes significant in particular applications. Namely, the CFD-DEM coupling is numerically problematic and not stable for cases where the particle size is larger than a computational mesh cell of the Eulerian phase related to the fluid flow (Chara and Kysela, 2018). This requirement is a considerable limitation for performing multiphase simulations with large particles, especially when the primary phase flow has to be accurately modelled. The model developed by Oroná et al. (2017) overcomes that limitation because a coarse mesh for the fluid phase was used in the HF system analysis. However, as a consequence, the local flow phenomena could not be considered in this model, which could affect the accuracy of the results.

A macroscopic particle model (MPM) proposed by Agrawal (2004) is an appropriate tool for large particle behaviour modelling in a continuous phase flow. In this method, each individual particle is tracked in the Lagrangian frame of reference, but it is assumed to span several computational cells of the fluid phase. The MPM model is not a commonly used tool thus far, but was adopted with a good result in different applications by its developers (Agrawal, 2004) (e.g., the separation of particles in the filter, fluidised bed simulation, interaction with rotating paddle), as well as in another study describing a detailed flow over a spherical object modelled using large eddy simulation (LES) and MPM (Chara and Kysela, 2018) or in a paper related to graphite pebble pneumatic transportation in a fuel system for gas-cooled reactors (Sun et al., 2020).

Apart from the physical representation of the flow of both phases in HF system, a correct estimation of the heat transfer between both phases and the determination of the HTC are important aspects as well. In single-phase CFD analyses, this aspect is well known and straightforward. Numerous studies have been devoted to estimate the HTC for the fluid flow over static spherical objects in a fixed position. In most cases where one wants to investigate the fundamental phenomena of the flow, a single sphere is used. For example, Dixon et al. (2011) compared the drag coefficient and Nusselt number distribution in the flow of air over a single sphere using k-ω shear stress transport (SST) turbulence model and the LES approach with the experiments. The authors also tested the popular correlations for the Nusselt number in a wide range of Reynolds number and obtained a satisfactory accuracy for the correlation by Whitaker (1972). More recently, Kao et al. (2014) numerically determined HTC in the flow of air through the array of 14 spheres and assessed the effect of the mutual position of the spheres on the heat transfer. The authors underlined that such simulations can be considered a good benchmark for analyses of full-size applications because they can be fairly well validated and provide a good degree of process understanding.

This study aims to develop a numerical model of the hydrofluidisation process to evaluate HTCs expected in a lab-scale HF food freezing unit. The mass flow of the refrigerating medium was in the range of 0.1 to 2.0 kg·s⁻¹. Several different fluids are compared in this study regard-
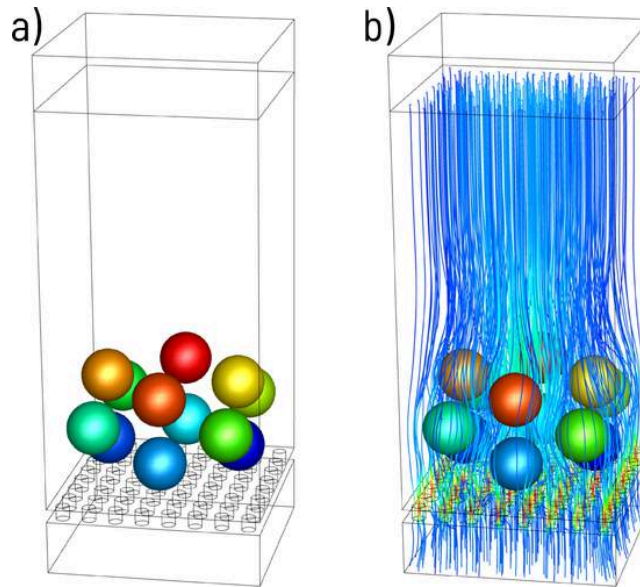
Fig. 3. Initial state of an example case presenting (a) the location of the injection of the particles and (b) the streamlines of the developed refrigerating medium velocity field.

Table 4

Operating conditions used for the HTC verification and validation with the reference data from (Stebel et al., 2021).

Case No	Solution (mass concentration)	$\dot{m}$ kg·s⁻¹	S mm	d mm	Number of orifices	H mm	Number of samples	Case No in (Ref)
Test Case 2	Ethanol (30%)	3.37	8	3	64	50	7	Case 43
Test Case 3	Ethanol (30%)	3.37	8	3	64	60	7	Case 44
Test Case 4	Ethanol (30%)	3.37	8	3	64	70	7	Case 45
Test Case 5	Ethanol (30%)	3.37	12	3	64	50	7	Case 52
Test Case 6	Ethanol (30%)	3.37	12	3	64	60	7	Case 53
Test Case 7	Ethanol (30%)	3.37	12	3	64	70	7	Case 54
Test Case 8	Ethanol (30%)	9.36	12	5	64	50	7	Case 67
Test Case 9	Ethanol (30%)	9.36	12	5	64	60	7	Case 68
Test Case 10	Ethanol (30%)	9.36	12	5	64	70	7	Case 69

ing their effect on the HF system dynamics and the HTC. These fluids are a binary aqueous solution of glycerol (40% mass basis), a binary aqueous solution of ethanol (30% mass basis), and a ternary aqueous solution of ethanol-glucose (15%/25% mass basis). The glycerol solution was selected due to the commonness of glycerol in the food industry and harmlessness for health. Ethanol solution was already used in the previous studies by the authors (Palacz et al., 2019; 2021; Stebel et al., 2020), while ternary solutions of ethanol and glucose were pro-

posed by Fikiin et al. (2001) as having potential for applications related to IF and HF freezing. The MPM model was used to simulate the behaviour of the spherical food sample group and the interaction between the samples and their movement forced by buoyancy forces and agitating fluid jets. The approach used in the presented study offers the most realistic representation of large particles movement in multiphase flow. To the best knowledge of the authors, it is the first attempt when the hydrofluidisation process was modelled using the approach offering such detailed representation of two-phase flow and interaction between the particles and the fluid. High-speed camera recordings allowed us to validate the food sample movement modelling by comparing the path of the food sample during floating in the HF tank. The work presented in this paper can be used to evaluate the freezing times for different food products, assess the HF method potential, and characterise the dynamics of the HF system.

2. Laboratory test rig

The laboratory test rig is described in detail in the experimental paper by Palacz et al. (2019). The original HF tank size was reduced to a column 150 mm high, 80 mm wide and deep. The number of orifices was 64. Each orifice was 5 mm in diameter (d). To prevent the samples from falling out of the tank, the column was equipped with a net attached near its top.

The experiments used for the model validation were based on recording a path of a single food sample movement in the HF unit. For that reason, a high-speed Vision Research Phantom v5.1 camera was used. During the experiments the solution mass flow rate was maintained at the level of 0.83 kg·s⁻¹. An aqueous solution of glycerol with a mass concentration of 30% was used in the test rig. To capture the vertical movement of the sample, the initial moment of each experiment was when the sample was located directly above the plate with orifices at the bottom of the HF tank in the middle of the orifice arrays. To ensure
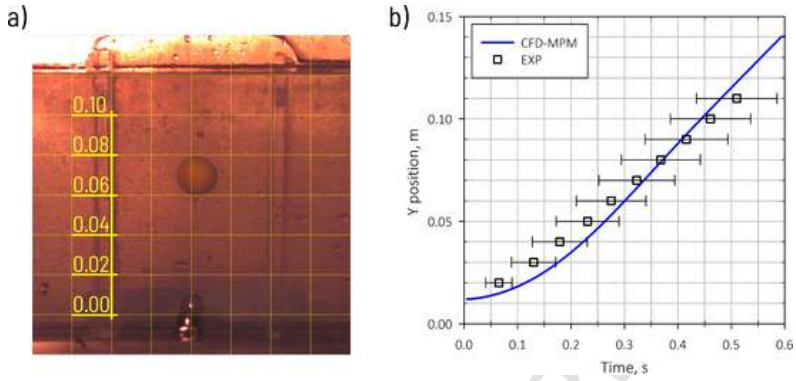
Fig. 4. (a) Single frame from one of the experimental runs and (b) the comparison between the experimental and numerical results.
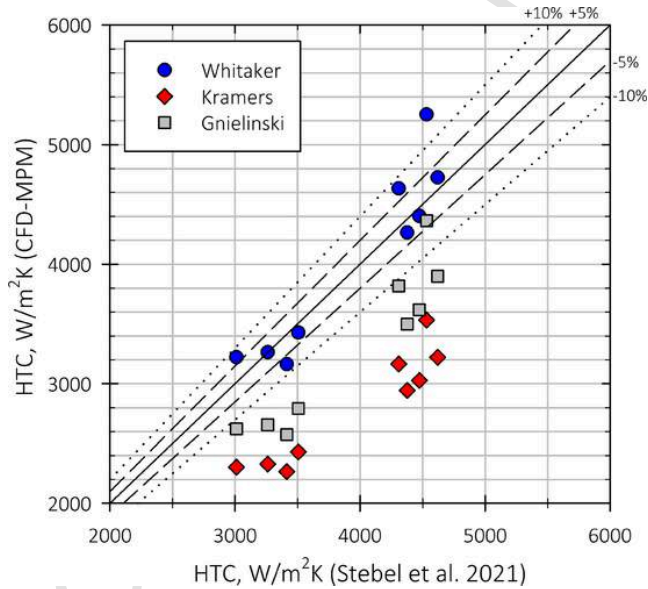
Fig. 5. Values of HTC for Test Cases 2-9 obtained using CFD-MPM model with three different Nu number correlations compared with direct CFD results from (Stebel et al., 2021).

such a fixed position and not disturb the fluid flow, the position of the sample was maintained using a string released at the initial moment to allow for the free movement of the sample. In this study, a spherical potato sample (*Solanum tuberosum L.*) having a diameter (*D*) of 20 mm was used. The sample was carefully cut out from the fresh potato using a melon baller.

3. Mathematical modelling

3.1. Geometrical domain

The geometrical domain of the model presented in this study included the column built in the HF tank and a small section of the fluid below the orifices to obtain a proper distribution of the velocity in all the orifices. Fig. 1 presents the whole geometrical domain with characteristic dimensions and boundary conditions described in detail in Section 3.5. As mentioned before, a net was used to prevent food samples from leaving the HF tank. It was represented in the numerical
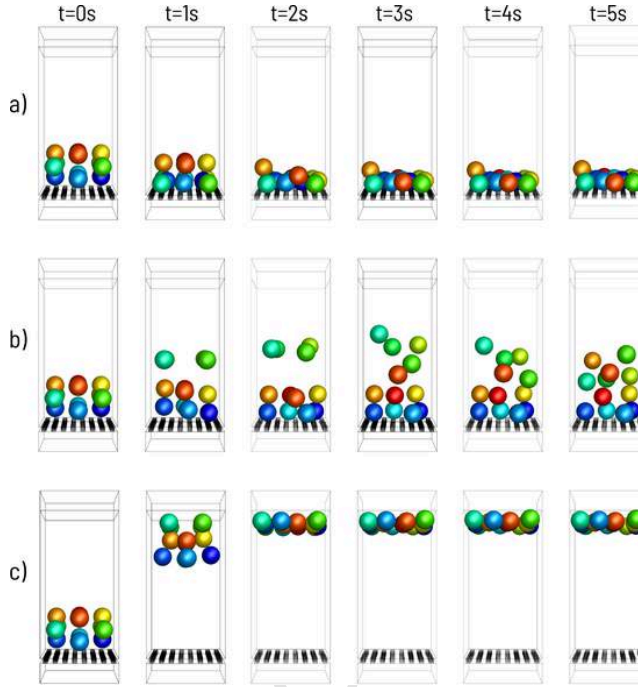
Fig. 6. The position of potato samples evaluated using MPM model during HF with ethanol solution for (a) Case 1, (b) Case 3, (c) Case 4 characterised by different mass flow rate of the refrigerating medium in the first 5 seconds of the process. The colour indicates the individual sample.

model by a surface (green colour) that was fully permeable for the fluid phase but not for the free-floating food samples. The fluid flowed into the domain by the bottom surface (inlet - blue colour) and flowed out the domain by the top surface (outlet - blue colour).

Spherical food samples can move within the zone limited by the orifice plate, side boundaries of the domain, and the permeable net. In the numerical model, food samples are simulated using the MPM model; therefore, their presence and movement within the domain are maintained by this numerical approach. In this study, scenarios with a group of 12 spheres are mostly analysed. The exception is the case used for the model validation when the movement of only a single sample was considered and the analysis of the HF freezer load, with 24 and 36 spheres. The diameter (D) of each sample was assumed to be 20 mm.

3.2. Numerical mesh

The numerical mesh was prepared using a blocking technique that allowed for the generation of a fully structured mesh composed of high-quality hexahedral cells. For each orifice, the O-grid structure was applied. Fig. 2 presents the numerical mesh in an isometric view with a close-up of the plate with orifices.

In contrast to the more popular DPM and DEM numerical approaches, the MPM model requires each spherical particle to span several cells; therefore, relatively fine mesh was considered in this study. This mesh has a total number of cells of 380 018 and a maximum edge size of 1.25 mm, which corresponds to the food sample covering 16 cells in its diameter.

3.3. Governing equations

3.3.1. Primary phase flow - CFD

The primary phase of the developed numerical model addresses the flow of the refrigerating medium. That flow is treated as adiabatic and incompressible and is solved in the unsteady state. There is no need to solve the energy balance equation in this case because the refrigerating medium is assumed to be isothermal, and the values of HTC are evaluated based on the Reynolds number, as described in Section 3.3.2. The continuum and momentum balances of that phase are given in Eqs. (1) and (2), respectively. As the flow in the HF unit is turbulent, a proper approach should be selected to consider such a flow in the numerical model. As confirmed in a previous study (Stebel et al., 2020), $k - \omega$ SST is appropriate for fluid flow modelling in the HF unit. This model is represented by a set of two equations for the turbulent kinetic energy (Eq. (3)) and the specific dissipation rate (Eq. (4)).

$$\frac{\partial \rho}{\partial t} + \frac{\partial}{\partial x_i} \left(\rho u_i \right) = 0 \tag{1}$$

$$
\begin{aligned}
\frac{\partial}{\partial t} \left(\rho u_i \right) + \frac{\partial}{\partial x_j} \left(\rho u_i u_j \right) = & -\frac{\partial p}{\partial x_i} + \frac{\partial}{\partial x_j} \left[\mu \left(\frac{\partial u_i}{\partial x_j} + \frac{\partial u_j}{\partial x_i} \right. \right. \\
& \left. \left. - \frac{2}{3} \delta_{ij} \frac{\partial u_k}{\partial x_k} \right) \right] \\
& + \frac{\partial}{\partial x_j} \left(-\overline{\rho u_i' u_j'} \right) \\
& + \rho g_j + S_{MPM}
\end{aligned}
\tag{2}
$$
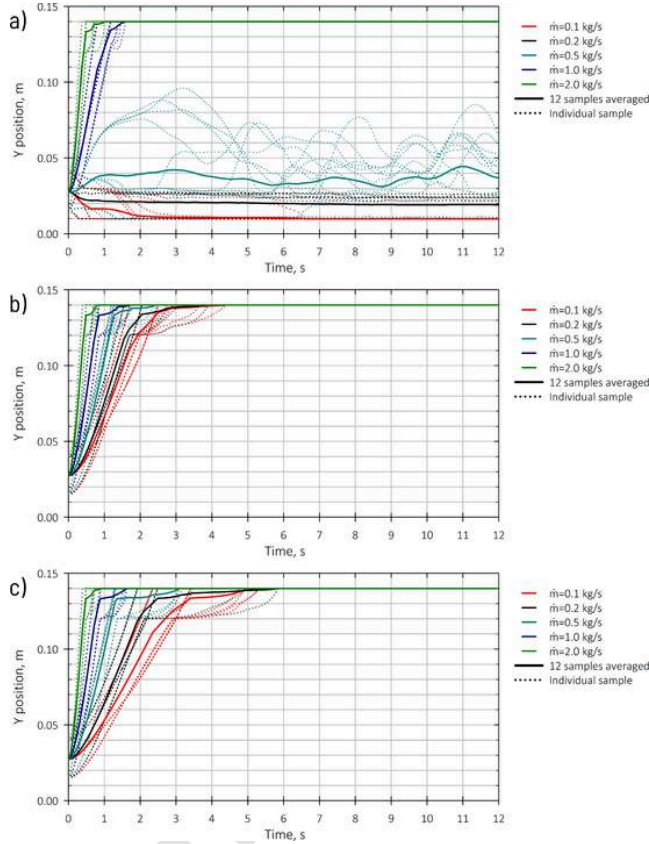
Fig. 7. Positions of individual food samples and the average position of the entire group of food products during the process for (a) Cases 1-5, (b) Cases 6-10 and (c) Cases 11-15 characterised by different solutions used for the process with the mass flow rate range of 0.1-2.0 kg·s−1.

$$\frac{\partial}{\partial x_i}\left(\rho K u_i\right) = \frac{\partial}{\partial x_j}\left[\left(\mu + \frac{\mu_T}{\sigma_K}\right)\frac{\partial K}{\partial x_j}\right] + G_K - Y_K \tag{3}$$

$$\frac{\partial}{\partial x_i}\left(\rho \omega u_i\right) = \frac{\partial}{\partial x_j}\left[\left(\mu + \frac{\mu_T}{\sigma_\omega}\right)\frac{\partial \omega}{\partial x_j}\right] + G_\omega - Y_\omega + D_\omega \tag{4}$$

where ρ is the density, t is the time, u_i is the average velocity vector component, u_i' is the fluctuating velocity component, p is the average pressure, μ is the dynamic viscosity, δ_{ij} is the Kronecker delta, g_j is the gravitational acceleration vector component, S_{MPM} is the source term representing the effect of the MPM model influence on the primary phase, K is turbulence kinetic energy, μ_T is the turbulent viscosity, σ_K is the turbulent Prandtl number for K, G_K is the generation of K due to mean velocity gradients Y_K is the dissipation of K due to turbulence, ω is the specific dissipation rate, σ_ω is the turbulent Prandtl number for ω, G_ω is the generation of ω, Y_ω is the dissipation of ω due to turbulence, and D_ω is the cross-diffusion term.

3.3.2. Particles flow - MPM

In the MPM model, during each time step, the sum (Eq. (5)) of the fluid forces that act on each sphere consists of the virtual mass component, which expresses the drag force and the pressure, and the viscous fluid components (ANSYS, 2016), represented by Eqs. (6) - (8).

$$F_{i\,MPM} = F_{m\,i} + F_{p\,i} + F_{v\,i} \tag{5}$$

$$F_{m,i} = \left(\sum_{vol\,cells} m_f u_{f,i} - \sum_{vol\,cells} m_f u_{P,i}\right)\frac{1}{\Delta t} \tag{6}$$

$$F_{p,i} = \sum_{surf\,cells} p\,D^2\,\frac{r_i}{|\mathbf{r}|} \tag{7}$$

$$F_{v,i} = \sum_{surf\,cells}\sum_j \tau_{ij}D^2\left(-\frac{r_j}{|\mathbf{r}|}\right) \tag{8}$$

where $F_{i\,MPM}$ is the total fluid force acting on a macroscopic particle, $F_{m,i}$ is a virtual component of fluid forces, $F_{p,i}$ is a pressure component of fluid force, $F_{v,i}$ is a viscous component of fluid force, m_f is the cell fluid mass, $u_{f,i}$ and $u_{P,i}$ are the fluid and particle velocities in i-th direction, respectively, Δt is the time step size, $\mathbf{r}$ is the radius vector
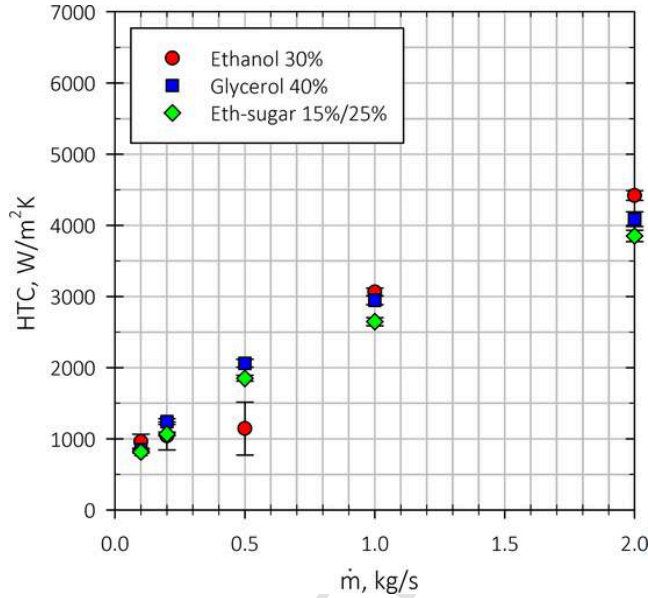
Fig. 8. Average values of HTC for Cases 1-15 characterised by various mass flow rate and the refrigerating medium type.

from the fluid cell centre to the particle centre, r_i and r_j are the Cartesian components of vector $\mathbf{r}$ and τ is the shear stress.

In the MPM model, collisions are assumed to occur quasi-instantaneously at a single point via the hard-sphere collision algorithm (ANSYS, 2016). The interaction between two macroscopic particles is expressed by the Newtonian conservation of momentum for the linear and angular velocity estimation. The impulse forces in the normal and tangential directions are expressed by Eqs. (9) and (10), respectively (ANSYS, 2016).

$$J_n = -\left(1+e_n\right)\frac{u_{12}\cdot\mathbf{n}}{1/m_1 + 1/m_2} \tag{9}$$

$$J_t = -\left(1+e_t\right)\frac{u_{12}\cdot\mathbf{t}}{1/m_1 + 1/m_2} \tag{10}$$

where J_n is the impulse force in the normal direction, J_t is the impulse force in the tangential direction assuming sticking collision, e_n and e_t are the normal and tangential coefficients of restitution, respectively, u_{12} is the relative velocity of the two particles, $\mathbf{n}$ is the unit vector in the normal direction and $\mathbf{t}$ is the unit vector in the tangential direction.

In the ANSYS Fluent software, the implemented MPM model directly computes the drag force acting on each sphere. In typical analyses related to discrete phase flow, the drag force, particle Reynolds number, drag coefficient, and the relative velocity between the fluid and particle phases are correlated. Eq. (11) represents the drag force determination in such a way, Eq. (12) determines the drag coefficient according to Morsi and Alexander (1972), which covers a wide range of Reynolds numbers. Eq. (13) describes the Reynolds number for the particle based on the particle diameter as the reference length and the relative velocity between the fluid phase and the macroscopic particle.

$$F_D = \frac{1}{2} A \rho u_{fp}^2 C_D \tag{11}$$

$$C_D = a_1 + \frac{a_2}{\mathrm{Re}_P} + \frac{a_3}{\mathrm{Re}_P^2} \tag{12}$$

$$\mathrm{Re}_P = \frac{\rho D u_{fp}}{\mu} \tag{13}$$

where F_D is the drag force, u_{fp} is the relative (slip) velocity between the fluid phase and the particle, C_D is the drag coefficient, a_1, a_2, and a_3 are the coefficients for the Morsi-Alexander formulation, and Re_P is the Reynolds number for the particle. Three coefficients in the formulation of C_D depend on the Reynolds number according to the values presented in Table 2.

In similar analyses related to the dispersed phase and modelled using the DPM approach, the heat transfer coefficient in the model proposed in this paper is determined according to an appropriate empirical correlation of the Nusselt number. The correlation proposed by Whitaker (1972) was selected (Eq. (14)). That formulation was defined for the sphere in cross-flow and is based only on the local values of the Re number and viscosity. In addition, Whitaker (1972) definition is suitable for a wide range of Pr numbers corresponding to the refrigerating fluid applied. Hence, that definition is easier for implementation in the case of the HF system with moving and interacting particles. The value of HTC can be determined in the last step given in Eq. (15).

$$\mathrm{Nu} = 2 + \left(0.4\mathrm{Re}_P^{0.5} + 0.06\mathrm{Re}_P^{0.67}\right)\mathrm{Pr}^{0.4}\left(\mu/\mu_w\right)^{0.25} \tag{14}$$

$$\mathrm{HTC} = \frac{\mathrm{Nu}\,k}{D} \tag{15}$$

where Nu is the Nusselt number, Pr is the Prandtl number, (μ/μ_w) is the ratio of the viscosity of the fluid at bulk temperature and the wall temperature (assumed in this study as 1 due to immediate reduction of

94
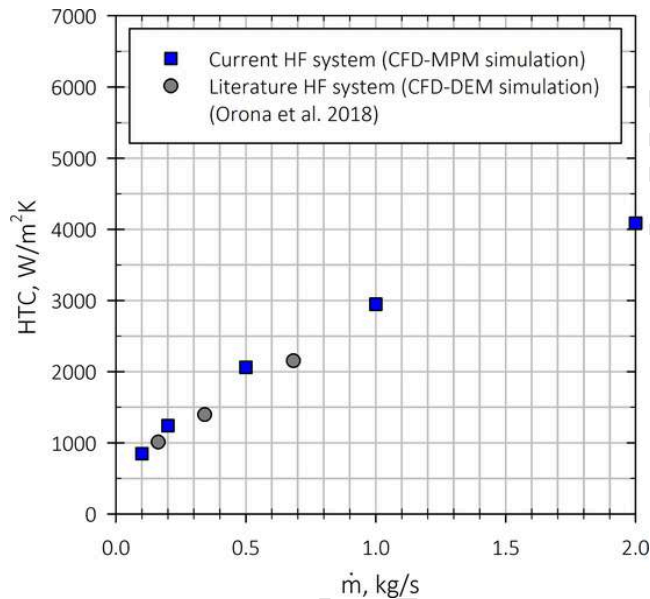
Fig. 9. Comparison of HTC values for Cases 1-5 characterised by various mass flow rates with results from other HF study where CFD-DEM approach was used to simulate a system with different geometry and refrigerating medium (Oroná et al., 2018).

the food sample surface temperature) and k is the thermal conductivity of the fluid.

3.4. Thermophysical properties

As mentioned before, three water-based solutions were considered refrigerating liquids in this study. Their properties are presented in Table. A temperature of -15∘C was assumed to be sufficient for rapid freezing and quick passing through the critical zone of water crystallisation, which covers the range from -1∘C to -8∘C (Fikiin, 2008). The properties of the glycerol and ethanol aqueous solutions were defined according to Melinder (2010), while the properties of the ethanol-glucose ternary solution were determined according to the expressions described in the study of Fikiin et al. (2001).

Apart from the refrigerating fluid properties, the properties related to the food product, i.e., potato, have to be assumed. The density of each sample was defined as 1 062 kg·m−3 according to the density measurements presented in (Stebel et al., 2020). Coefficients of restitution that affect the mechanism of collisions in the MPM model were defined based on the data presented in a similar study of spherical potato samples freezing in the HF system using the DPM-DEM approach (Oroná et al., 2017). Their values are 0.52 and 0.77 for particle-wall and particle-particle collisions, respectively.

3.5. Boundary and initial conditions

Several external and internal boundary conditions were defined at the characteristic surfaces of the geometrical domain of the model described previously in Fig. 1. They are related to the primary fluid phase and the macroscopic particles as follows:

- The inlet boundary condition located at the bottom surface of the domain was defined by the liquid mass flow rate ($\dot{m}$) value in the range from 0.1 to 2.0 kg·s−1, depending on the individual case, listed in Section 5.
- The outlet boundary condition located near the top edge of the tank was defined as the *outflow* boundary condition.
- The surface preventing the food samples from leaving the HF tank and marked with green colour in Fig. 1 was defined with a 0-D *porous jump* boundary condition. It allows the fluid to flow through with no resistance but prevents the particles from crossing it by applying the *reflect* condition.
- All walls present in the domain (side walls of the HF column, and inflow plate) were defined using *no-slip wall* boundary conditions with the *reflect* condition for the macroscopic particles.

In Section 4, the boundary conditions defining the operating conditions used for the experimental validation of the particle movement modelling are listed in Table 3. Furthermore, the conditions used for the parametric study are described in Table 5 in Section 5.

In addition, time-dependent simulations require defining the initial conditions, i.e., the state of the analysed unit in the initial moment of each analysis. In this study, the initial moment was defined with the particles injected in the HF tank at predefined positions near the tank bottom in three layers located 15 mm, 28 mm, and 40 mm above the orifices, as presented in Fig. 3(a). Four spheres were placed in the array in each row. In the case of simulations with a larger number of food samples, the other layers of food products were added within the HF tank in the initialisation moment. The velocity field was developed within the numerical domain in the initial stage using steady-state analysis with the particles in their injection positions, which is shown in Fig. 3(b).
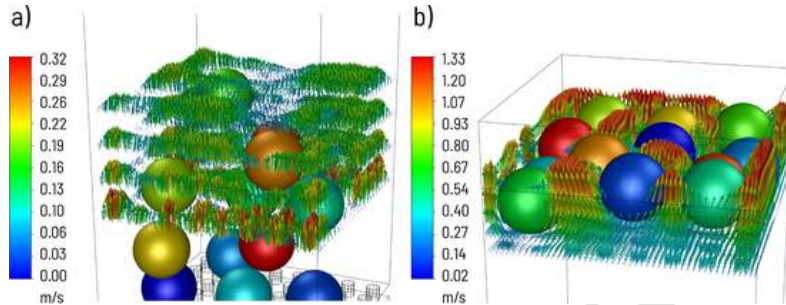
Fig. 10. Vectors presenting the local velocities around the food samples for (a) Case 3 and (b) Case 5 after achieving a quasi-steady state.

4. Numerical model verification and validation

To verify the numerical model, the flow of a single sphere was validated based on the experiments performed on the test rig as described in Section 4.1. The operating conditions used for this comparison are identified as Test Case 1 as given in Table 3. Additionally, to confirm that HTCs are correctly determined using the selected correlation of the Nusselt number, the results obtained in this paper using the CFD-MPM model were compared with the direct CFD results presented in the previous paper of the authors (Stebel et al., 2021) regarding the HF system with spherical food samples in a fixed position H above the orifices under more intensive fluid flow conditions. For these cases identified in Table 4 as Test Cases 2-10, the movement of the food samples in the MPM model was disabled, therefore the flow conditions could be exactly repeated.

4.1. Macroscopic particle flow validation

The experimental validation of the numerical model covers a comparison of the single food sample position above the orifices during the first second of the flow when the sample flowed upwards from its initial position near the orifices. A high-speed camera was used to record the samples movement and determine the time in which the sample reached a given position after it was released. Fig. 4(a) presents an example frame from the recording with the yellow grid used to determine the position of the sample. Fig 4(b) presents the comparison between the numerical results and the experiments after the averaging of 9 test runs, with the error bars indicating the standard deviation of the time needed to reach a given position. As seen, the position of a single sample during the flow in Test Case 1 is determined correctly using the developed model. Differences between the numerical results and the experiments are not significant and are lower than the standard deviation marked by the error bars.

The Root Mean Squared Error (RMSE) for all 9 trials is 0.0675 s, comparing the predicted and experimentally evaluated times required to reach a specific position. The highest discrepancy between the numerical and experimental results in terms of the specific position above the orifices is less than 10 mm, which refers to half the diameter of the food sample. Consequently, the experimental validation confirms that the CFD model based on the MPM approach can predict the physics of the flow in the HF system with satisfactory accuracy.

4.2. Verification of the heat transfer modelling approach

To confirm the validity of the heat transfer modelling, the HTC was compared in cases with a fixed position of food samples, as described previously. In the proposed CFD-MPM model, the Nusselt number correlation by Whitaker (1972) was selected to determine HTC, but two

different approaches by Kramers (1946) and Gnielinski (1981) were also considered which are appropriate for such a flow regime. Fig. 5 presents the HTCs for Test Cases 2-10 where all three correlations were used for the determination of the HTC and compared with the results of the previous study by the authors (Stebel et al., 2021) where the spherical samples were assumed static. These results were obtained for a similar configuration of the flow in the HF tank, but the HTC values were obtained directly using a local heat flux integration for a fixed grid between the fluid and solid domains in the experimentally validated model. Therefore, these results can be treated as reliable for such a comparison.

According to the results presented in Fig. 5, the proposed methodology for HTC determination using the CFD-MPM approach guarantees fairly high accuracy, i.e., in most cases, the error was less than ±5% with respect to the CFD simulations and an error of more than 10% was observed only for one case. These are very satisfying results. The correlations by Kramers (1946) and Gnielinski (1981) underestimated the HTC for all Cases 2-10. It proves that the Whitaker's correlation given in Eq. (14) was an appropriate assumption. In addition, that correlation was confirmed as the best in different works presented in the literature. In the study by Niazmand and Renksizbulut (2003) in which the flow over the rotating sphere was analysed, the authors confirmed that Whitaker's correlation is the best fit of the average HTC to the experimental data for stationary and rotating spheres. Kiani and Sun (2016) came to the same conclusions in their numerical study, where the cooling of 20 mm spheres made of potato and copper was analysed in an ethylene-glycol-water mixture.

5. Results

The results presented in this section are related to the parameters affecting the flow within the HF tank and the HTC possible to obtain. All the operating conditions are listed in Table 5.

5.1. Effect of the solution type and the flow rate

The movement of food products during the HF process strongly depends on the relation of the density of food products and the density of the liquid in which the samples are immersed. In the case of liquid fluidisation, the density of the liquid is often of the same order as the solids or even higher (Di Felice, 1995). In the case of glycerol and ethanol-glucose aqueous solutions, potatoes and many other food products are expected to flow upwards only due to buoyancy forces. Such a flow was present in the HF system study by Oroná et al. (2017), where a sodium chloride aqueous solution was used. Different behaviour is present in the case of the ethanol solution. In that case, the movement of foods depends on the mass flow rate of the refrigerating medium in the HF system and some characteristic fluidisation regimes can be distin-
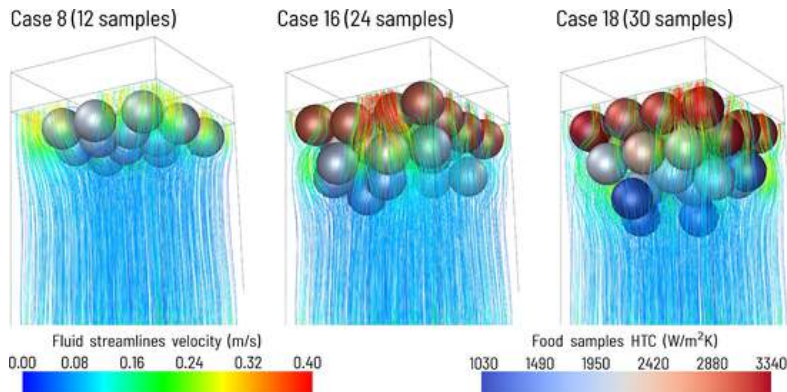
Fig. 11. Comparison of the local velocities and the values of HTC for three cases characterised by a different number of food samples.

guished. Fig. 6 presents the movement of samples in the HF process with the ethanol-based solution during the first 5 seconds of the process after the initialisation. In this figure, three cases are compared with different mass flow rates, i.e., Case 1 with an $\dot{m}$ of 0.1 kg·s−ı, Case 3 with an $\dot{m}$ of 0.5 kg·s−ı, and Case 4 with an $\dot{m}$ of 1.0 kg·s−ı.

As seen, a low flow of the refrigerating medium in Case 1 allowed the food samples to descend, and as an effect, they were at the HF tank bottom during freezing. In that case, the fluid velocity was not sufficient to cause the fluidisation effect. The fluid superficial velocity did not exceed the minimum fluidisation velocity and the food products remained in static flow regime in a fixed bed (Khawaja, 2015). In Case 3, the food samples tend to float within the HF tank freely. The fluid velocity exceeded the critical value of the minimum fluidisation velocity where the weight of the solid particles was supported by the buoyancy forces and the drag force (Di Felice and Di Renzo, 2020). A quasi-suspension of food products within the HF tank was present, enabling for the collisions between the samples, rotation of food samples, and mixing. The increase in the fluid mass flow rate in Case 4 induced the samples to freely flow upward.

To compare the movement of the group of food samples for Cases 1-15, where three different solutions were used for HF freezing with $\dot{m}$ in the range of 0.1-2.0 kg·s−ı, the positions of the food samples in the y-coordinate, i.e., along the HF tank height, are presented in Fig. 7 during the first seconds of the process. In this figure, solid thick lines represent the average position of all samples to characterise the position of the whole group, and dotted lines refer to the individual food samples. Fig. 7(a) shows the movement of food samples in the ethanol solution. As discussed before, in that case, the behaviour of food products strongly depends on the fluid mass flow rate. In cases with the $\dot{m}$ of 0.1-0.2 kg·s−ı, the food products descended to the HF tank bottom forming a fixed-bed. A particular situation was recorded for the case with an $\dot{m}$ of 0.5 kg·s−ı. A moderate flow of the fluid allowed the samples to float within the tank volume, and the collisions between them resulted in bouncing and mixing. Such movement is desired for HF freezing, as it may result in proper mixing of individual food samples and a uniform freezing rate. For higher $\dot{m}$ values, i.e., 1.0 and 2.0 kg·s−ı, the food products immediately flew upwards and, after 1-2 seconds, were stacked underneath the semi-permeable net, preventing samples from leaving the HF tank. In this case, the fluidisation regime can be identified with the lean phase fluidisation (called pneumatic transport in gas-solid fluidisation). The same behaviour was observed for cases where denser fluids were used for the HF process despite the mass flow rate value. Figs. 7(b) and (c) present the movement of food samples immersed in the glyc-

erol-based water solution and the ternary water-ethanol-sugar solution, respectively. For all cases characterised by various mass flow rates of the fluid, the same movement character was present, i.e., the buoyancy forces induced the samples to flow upwards. In the numerical study by Oroná et al. (2017) where an aqueous solution of sodium chloride and 13 potato samples were used in the HF system, similar behaviour was observed. Namely, the particles flew upwards the tank and the flow did not affect their position. In the following study of the authors (Oroná et al., 2018), similar results were presented with more samples in the HF tank. Under a flow rate defined by the fluid velocity in orifices of 0.30 m·s−ı, group of spherical samples were stacked at the top of the HF tank after approximately 2 seconds. After the flow rate increase by almost four times, that time was reduced to approximately 1 second. In case of results presented in Fig. 7(b) and (c) with refrigerating liquids denser than food, a similar tendency was observed. The $\dot{m}$ increase from 0.5 kg·s−ı to 2.0 kg·s−ı resulted in twice faster movement of samples. In both HF systems, the geometrical or flow parameters are different, but the tendency discussed here is comparable.

As seen, in the HF process with small vegetables, the formation of a fixed bed at the top of the HF tank occurs most often due to the use of dense liquids, i.e. water solutions of NaCl, glucose or glycerol. In these cases, to achieve a pure fluidised flow of food products, the *inverse fluidisation* process could be introduced, which is based on changing the flow direction by placing the inflow section on the top (Di Felice and Di Renzo, 2020). As the fluid flows downwards the tank, the drag force acts against the buoyancy. On the other hand, a completely new system of transportation of fresh and frozen food products through the HF tank would have to be introduced.

The most crucial outcome of this paper is the determination of HTC possible to obtain using the HF method for different solutions in a wide range of mass flow rates. Fig. 8 presents the average values of HTC assessed for Cases 1-15 based on the methodology described in Section 3.3.2. The data presented in this figure refer to the average HTC for all samples for each case, and the error bars describe the standard deviation of HTC evaluated for all 12 samples present in each case. Because in most cases, the position of food samples is established a few seconds after the initialisation, the HTC was evaluated in the quasi-steady state when the position of food samples was stabilised. The exception is Case 3, where the food samples were freely floating within the HF tank. In that case, the HTC was determined from ten probes (process time from 3 s to 12 s every 1 second) and averaged.

The HTC values depend strongly on the refrigerating medium mass flow rate. For cases characterised by a relatively low mass flow rate of
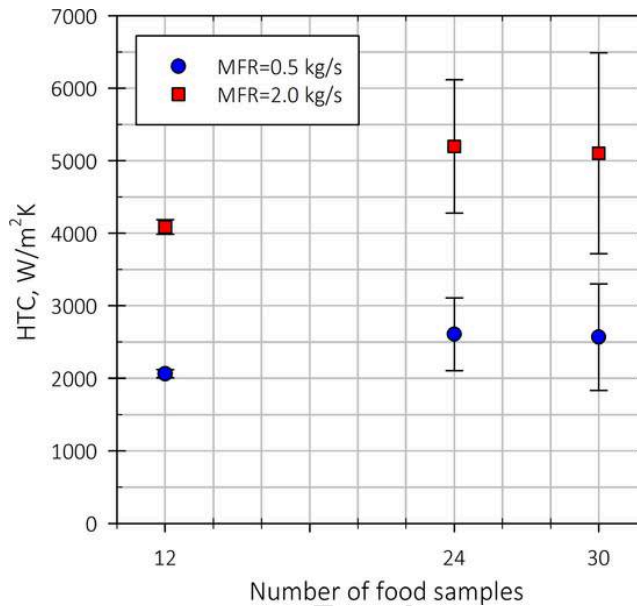
Fig. 12. Average values of HTC for Cases 8, 10, and 16-19 characterised by a various number of food samples and two different values of mass flow rate.

0.1-0.2 kg·s−₁, the HTC values are in the range of approximately 800-1 300 W·m−₂K−₁. In the case of a very high $\dot{m}$ of 1.0 or 2.0 kg·s−₁, the HTC is in the range of approximately 2 600-3 100 W·m−₂·K−₁ and 3 800-4 500 W·m−₂·K−₁, respectively. The highest HTC values were noted for the ethanol-based solution and the lowest HTC values were reached for the ternary solution of water, ethanol, and sugar. However, the type of solution used for freezing has a minor effect on HTC. The exception is Case 3, where the aqueous ethanol solution was used at the moderate mass flow rate. In that case, the food products float freely within the HTC tank. Such a flow results in lowered HTC because of a more dispersed arrangement of food samples.

The results related to HTC determination were compared with a similar numerical study by Oroná et al. (2018), where a different numerical approach was used for HF modelling and the unit was slightly different. In that study, CFD-DEM approach was used for simulations of food products movement. The organisation of the flow in the HF tank was similar (inflow from bottom, outlets near the top, no food transportation system), but it was cylindrical. In the geometrical configuration selected for the results comparison, 69 orifices having 3 mm in diameter were present. In the HF tank, 13 spherical potato samples having a diameter of 10 mm were used. In addition, the refrigerating medium was a sodium chloride aqueous solution having the Prandtl number of 9.22 and the density of 1 186.4 kg·m−₃ (Peralta et al., 2009). For that reason, the glycerol solution used in the current paper was selected for the comparison of the results, because its properties are closest to sodium chloride aqueous solution.

The comparison of results from both studies is shown in Fig. 9. In that figure, HTC is presented as a function of the mass flow rate, because, due to a slightly different geometry of both systems, that parameter is appropriate as an indicator of the refrigerating medium flow intensity. As seen, the results obtained from the CFD-MPM model developed in this study are in a good agreement with results presented by Oroná et al. (2018) where the authors used well-established CFD-DEM

approach. The HTC obtained using the model developed in the current paper is slightly higher than the results from the literature. Nevertheless, the tendency of HTC rise along with the mass flow rate increase is the same and the results are in general comparable. It is worth underlining that both HF lab-scale systems are similar, but there are some differences in geometry and a different liquid was used which is a possible reason for minor differences in results.

Fig. 10 presents the local velocities of the fluid in Case 3 compared to Case 5, where the foods were stacked near the semi-permeable net in the HF tank. It should be pointed out that the average bulk velocity in the empty HF tank due to the relation of the fluid mass flow rate and the tank cross-sectional area is 0.08 m·s−₁ and 0.32 m·s−₁ for Case 3 and Case 5, respectively. In Case 3, the presence of food samples disturbs the velocity distribution in the vertical direction; however, the velocity vectors are rather uniform. The velocities in the presented region are in the range of approximately 0.13-0.20 m·s−₁, which corresponds to the local acceleration of the fluid by up to 1.5-2.5. Higher values are observed in the lowest cross-section of the presented region due to the presence of the jets. In Case 5, the local velocities of the fluid in the presented region reach 1.00-1.33 m·s−₁, which corresponds to an acceleration rate of 3.1-4.1 due to the lower clearance of the HF tank cross-section and small gaps between spherical samples. In the LBM study by Rong et al. (2014), the authors analysed the local velocities in the packed bed of spheres. They highlighted that the flow is complex and not uniform in such a domain and they indicated that channel-like and jet-like flow streams can occur locally. In these regions, the local velocity was increased by up to a few times. The same patterns can be seen between particles in Fig. 10(b). Such a velocity distribution affects the drag forces acting on individual spheres (Rong et al., 2014) and consequently, variations in HTC can be observed for different spherical samples.

5.2. Effect of the food load in HF tank

From a practical point of view, the cross-section of the HF tank should be filled with the highest possible volume of foods as long as the process is still favourable in terms of the freezing process. For that reason, the HF method should also be tested for a larger load of food products. In Cases 16-19, the number of food samples was increased in the freezing process in the glycerol solution with two mass flow rate values. Consequently, the effect of the food load could be compared for three groups of 12, 24, and 30 food samples, which correspond to food volume to flow cross-section ratios of 0.008, 0.016 and 0.020 $m_3 \cdot m_{-2}$, respectively. Fig. 11 presents the arrangement of food samples after flow stabilisation for Cases 8, 16, and 18, characterised by a different number of food samples and the same $\dot{m}$ of 0.5 kg·s–₁. Two colour scales were used in this figure to compare the local velocity of the fluid flowing through the bed of the food samples and the HTC values obtained for all the samples. As seen in Cases 16 and 18, the food products form stacked groups. As discussed in Section 5.1, such an arrangement results in higher local velocities of the fluid and an increase in HTC. In Cases 16 and 18, the fluid was locally accelerated above the average HF tank velocity of approximately 0.08 m·s–₁ up to 0.40 m·s–₁. Consequently, a more intensive flow of the fluid leads to an HTC increase. In Case 8, with 12 food samples, the HTC is approximately at the same level for each food sample. For cases with 24 and 30 samples, HTC varies more. In particular, in regions with a more stacked arrangement of food samples, e.g., the top layer of food samples, the HTC values are significantly higher than in the case of the samples detached from the whole group. An example of the latter is the three food samples at the bottom in Case 18, where the values of HTC are the lowest.

Fig. 12 presents the average HTC obtained for food product groups of 12, 24, and 30 samples. As seen, for a larger food load in the HF tank, a slightly higher HTC can be reached. For an $\dot{m}$ of 0.5 kg·s–₁, HTC was increased from approximately 2000 W·m–₂·K–₁ to over 2500 W·m–₂·K–₁ when the number of food samples was 24 and 30. In the case of an $\dot{m}$ of 2.0 kg·s–₁, the HTC values were approximately twice as high for each food load size than for the lower flow rate. It is worth noting that for a larger food load, the average HTC value is slightly higher. Similar behaviour was observed in a numerical study by Oroná et al. (2018) where DPM-DEM approach was used to simulate the movement of a food product group. In a similar lab-scale HF system, authors compared the process with 13, 29 and 61 spherical samples within the HF tank and HTC increased by approximately 10% and 17% when the food load was increased to 29 and 61 samples, respectively. Error bars in Fig. 12 indicate the standard deviation of HTC for individual samples in each case. As discussed before, for a larger food load, higher HTC variations in HTC can be noticed if the whole group is considered. That is the result of various local conditions of the fluid flow in different areas within the HF tank. It suggests that the continuous system for food transportation would be beneficial not only in terms of the organisation of the whole process on an industrial scale but also to guarantee uniform conditions of the freezing process for all the food samples in the process. Such a system was proposed in the original proposition of the hydrofluidisation chilling and freezing for food products (Fikiin, 1992; Fikiin and Fikiin, 1998).

6. Conclusions

This paper presents a numerical study of the HF process modelled using the MPM approach, which is appropriate for the movement simulation of spherical particles of a relatively large size. The model was validated using single food product movement recordings using a high-speed camera. A parametric study was performed to analyse the selection of the solution type and the mass flow rate used for the HF process. Furthermore, the effect of the food load size in the HF tank was tested to assess the HTC possible to obtain.

In the case of two fluids, i.e., the solution of glycerol and the solution of ethanol and glucose, the fluid density was higher than that of the food sample. Consequently, the food samples flew upwards, and no other movement was present in such a situation during the HF process. In the case of the less dense ethanol solution, the food sample behaviour was strongly dependent on the fluid mass flow rate. For the ethanol solution $\dot{m}$ of 0.5 kg·s–₁, potato samples floated within the HF tank. Such a flow guarantees the expected hydrofluidisation effect; however, lower values of HTC can be reached than in the case of the food sample group stacked near the top of the HF tank.

The HTC values were strongly related to the fluid mass flow rate. For relatively low $\dot{m}$ values (0.1-0.5 kg·s–₁), HTC was in the range of approximately 1 000-2 000 W·m–₂·K–₁. A higher flow of the fluid with an $\dot{m}$ of 1.0-2.0 kg·s–₁ resulted in an HTC increase to approximately 3 000-4 500 W·m–₂·K–₁.

Consequently, the effect of the food product group size was investigated. The HF tank load was defined by the food product volume to the fluid cross-sectional area ratio. According to the results, the average HTC is not significantly affected by the food load size, but a higher discrepancy of HTC between individual food products was observed in the case of groups of 24 and 30 samples, characterised by food load ratios of 0.016 and 0.020 $m_3 \cdot m_{-2}$.

The results presented in this paper allow for the prediction of HF system behaviour and the assessment of the HTC values expected during the freezing of food products using the HF method. Moreover, it may allow for the selection of the appropriate aqueous solution used for the freezing of foods.

Declaration of Competing Interest

The authors declare that they have no known competing financial interests or personal relationships that could have appeared to influence the work reported in this paper.

Acknowledgements

References

Agrawal, M., 2004. Macroscopic particle model tracking big particles in cfd. AIChE Annual Meeting, Austin, USA, 2004.

ANSYS, 2016. Chapter 4. Fluent Macroscopic Particle Module. Canonsburg, PA. 193–226

Chara, Z., Kysela, B., 2018. Application of macroscopic particle model to simulate motion of large particles. AIP Conference Proceedings. AIP Publishing LLC, p. 30031. https://doi.org/10.1063/1.5043681.

Di Felice, R., 1995. Hydrodynamics of liquid fluidisation. Chemical Engineering Science 50 (8), 1213–1245. https://doi.org/10.1016/0009-2509(95)98838-6.

Di Felice, R., Di Renzo, A., 2020. Liquid Fluidization. John Wiley and Sons, Ltd, pp. 33–53.

Dixon, A.G., Ertan Taskin, M., Nijemeisland, M., Stitt, E.H., 2011. Systematic mesh development for 3d cfd simulation of fixed beds: Single sphere study. Computers & Chemical Engineering 35 (7), 1171–1185. https://doi.org/10.1016/j.compchemeng.2010.12.006.

Fikiin, A., 1992. New method and fluidized water system for intensive chilling and freezing of fish. Food Control 3 (3), 153–160. https://doi.org/10.1016/0956-7135(92)90100-O.

Fikiin, K., 2003. Novelties of Food Freezing Research in Europe and Beyond. Flair-Flow Europe Synthetic Brochure, INRA: Institut National de la Recherche Agronomique, Paris, France. https://doi.org/10.6084/m9.figshare.13371128.

Fikiin, K., 2008. Emerging and novel freezing processes chapter 5. Frozen Food Science and Technology. Wiley Blackwell, Oxford, pp. 101–123. https://doi.org/10.1002/9781444302325.ch5.

Fikiin, K., Fikiin, A., 1998. Individual quick freezing of foods by hydrofluidisation and pumpable ice slurries. Refrigeration Science and Technology, International Institute of Refrigeration 319–326. https://doi.org/10.13140/RG.2.1.3901.1283/1.

Fikiin, K., Tsvetkov, O., Laptev, Y., Fikiin, A., Kolodyaznaya, V., 2001. Thermophysical and engineering issues of the immersion freezing of fruits in ice slurries based on sugar-ethanol aqueous solutions. Proceedings of the Third IIR Workshop on Ice

Slurries, Lucerne (Switzerland) 147–154.

Fikiin, K., Wang, M., Kauffeld, M., Hansen, T., 2005. Direct contact chilling and freezing of foods in ice slurries chapter 9. Handbook on Ice Slurries Fundamentals and Engineering. International Institute of Refrigeration, pp. 251–271. https://doi.org/10.13140/RG.2.2.28391.68009.

Gnielinski, V., 1981. Equations for the calculation of heat and mass transfer during flow through stationary spherical packings at moderate and high peclet numbers. International Journal of Chemical Engineering 21 (3), 378–383.

Horabik, J., Molenda, M., 2016. Parameters and contact models for dem simulations of agricultural granular materials: A review. Biosystems Engineering 147, 206–225. https://doi.org/10.1016/j.biosystemseng.2016.02.017.

IIR, 2020. The Role of Refrigeration in Worldwide Nutrition–6th Informatory Note on Refrigeration and Food. International Institute of Refrigeration (IIR) Paris.

Kao, M., Tung, Y., Ferng, Y., Chieng, C., 2014. Investigating effects of sphere blockage ratio on the characteristics of flow and heat transfer in a sphere array. Energy Conversion and Management 81, 455–464. https://doi.org/10.1016/j.enconman.2014.02.057.

Khan, M.S., Evans, G.M., Peng, Z., Doroodchi, E., Moghtaderi, B., Joshi, J.B., Mitra, S., 2017. Expansion behaviour of a binary solid-liquid fluidised bed with different solid mass ratio. Advanced Powder Technology 28 (12), 3111–3129. https://doi.org/10.1016/j.apt.2017.09.009.

Khawaja, H., 2015. Review of the phenomenon of fluidization and its numerical modelling techniques. The International Journal of Multiphysics 9, 397–408. https://doi.org/10.1260/1750-9548.9.4.397.

Kiani, H., Sun, D.-W., 2016. Numerical modeling of particle to fluid heat transfer during ultrasound assisted immersion cooling. Chemical Engineering and Processing: Process Intensification 99, 25–32. https://doi.org/10.1016/j.cep.2015.11.001.

Kramers, H., 1946. Heat transfer from spheres to flowing media. Physica 12 (2), 61–80. https://doi.org/10.1016/S0031-8914(46)80024-7.

Malekjani, N., Jafari, S., 2018. Simulation of food drying processes by computational fluid dynamics (cfd); recent advances and approaches. Trends in Food Science & Technology 78, 206–223. https://doi.org/10.1016/j.tifs.2018.06.006.

Melinder, A., 2010. Properties of Secondary Working Fluids (Secondary Refrigerants or Coolants, Heat Transfer Fluids) for Indirect Systems. IIF-IIR.

Morsi, S., Alexander, A., 1972. An investigation of particle trajectories in two-phase flow systems. Journal of Fluid Mechanics 55 (2), 193–208. https://doi.org/10.1017/S0022112072001806.

Niazmand, H., Renksizbulut, M., 2003. Transient three-dimensional heat transfer from rotating spheres with surface blowing. Chemical Engineering Science 58 (15), 3535–3554. https://doi.org/10.1016/S0009-2509(03)00191-X.

Oroná, J., Zorrilla, S., Peralta, J., 2017. Computational fluid dynamics combined with discrete element method and discrete phase model for studying a food hydrofluidization system. Food and Bioproducts Processing 102, 278–288. https://doi.org/10.1016/j.fbp.2017.01.005.

Oroná, J., Zorrilla, S., Peralta, J., 2018. Sensitivity analysis using a model based on computational fluid dynamics, discrete element method and discrete phase model to study a food hydrofluidization system. Journal of Food Engineering 237, 183–193. https://doi.org/10.1016/j.jfoodeng.2018.05.019.

Palacz, M., Adamczyk, W., Piechnik, E., Stebel, M., Smolka, J., 2019. Experimental investigation of the fluid flow inside a hydrofluidisation freezing chamber. International Journal of Refrigeration 107, 52–62. https://doi.org/10.1016/j.ijrefrig.2019.08.009.

Palacz, M., Piechnik, E., Halski, M., Stebel, M., Adamczyk, W., Eikevik, T., Smolka, J., 2021. Experimental analysis of freezing process of stationary food samples inside a hydrofluidisation freezing chamber. International Journal of Refrigeration. https://doi.org/10.1016/j.ijrefrig.2021.06.034.

Peng, Z., Doroodchi, E., Moghtaderi, B., 2020. Heat transfer modelling in discrete element method (dem)-based simulations of thermal processes: Theory and model development. Progress in Energy and Combustion Science 79, 100847. https://doi.org/10.1016/j.pecs.2020.100847.

Peralta, J., Rubiolo, A., Zorrilla, S., 2009. Design and construction of a hydrofluidization system. study of the heat transfer on a stationary sphere. Journal of Food Engineering 90 (3), 358–364. https://doi.org/10.1016/j.jfoodeng.2008.07.004.

Peralta, J., Rubiolo, A., Zorrilla, S., 2010. Mathematical modeling of the heat transfer and flow field of liquid refrigerants in a hydrofluidization system with a stationary sphere. Journal of Food Engineering 99 (3), 303–313. https://doi.org/10.1016/j.jfoodeng.2010.03.003.

Peralta, J., Rubiolo, A., Zorrilla, S., 2012. Mathematical modeling of the heat and mass transfer in a stationary potato sphere impinged by a single round liquid jet in a hydrofluidization system. Journal of Food Engineering 109 (3), 501–512. https://doi.org/10.1016/j.jfoodeng.2011.10.032.

Rong, L., Dong, K., Yu, A., 2014. Lattice-boltzmann simulation of fluid flow through packed beds of spheres: Effect of particle size distribution. Chemical Engineering Science 116, 508–523. https://doi.org/10.1016/j.ces.2014.05.025.

Stebel, M., Smolka, J., Palacz, M., Adamczyk, W., Piechnik, E., 2020. Numerical investigation of the fluid flow distribution for the hydrofluidisation food freezing method. International Journal of Thermal Sciences 151, 106284. https://doi.org/10.1016/j.ijthermalsci.2020.106284.

Stebel, M., Smolka, J., Palacz, M., Piechnik, E., Halski, M., Knap, M., Felis, E., Eikevik, T., Tolstorebrov, I., Peralta, J., Zorrilla, S., 2021. Numerical modelling of the food freezing process in a quasi-hydrofluidisation system. Innovative Food Science and Emerging Technologies 74, 102834. https://doi.org/10.1016/j.ifset.2021.102834.

Sun, Q., Ye, P., Peng, W., Yu, S., Zhou, H., Wang, J., 2020. Wear of graphite pebbles modeled using a macroscopic particle model in a pneumatic transport lifting pipe. Powder Technology 361, 581–590. https://doi.org/10.1016/j.powtec.2019.11.075.

Verboven, P., Scheerlinck, N., Nicolai, B., 2003. Surface heat transfer coefficients to stationary spherical particles in an experimental unit for hydrofluidisation freezing of individual foods. International Journal of Refrigeration 26 (3), 328–336. https://doi.org/10.1016/S0140-7007(02)00110-X.

Whitaker, S., 1972. Forced convection heat transfer correlations for flow in pipes, past flat plates, single cylinders, single spheres, and for flow in packed beds and tube bundles. AIChE Journal 18, 361–371. https://doi.org/10.1002/aic.690180219.

Xie, Z., Wang, S., Shen, Y., 2021. Cfd-dem study of segregation and mixing characteristics under a bi-disperse solid-liquid fluidised bed. Advanced Powder Technology. https://doi.org/10.1016/j.apt.2021.09.012.

Paper IV: Numerical modelling of conjugate heat and mass transfer during hydrofluidisation freezing

Numerical modelling of conjugate heat and mass transfer during hydrofluidisation food freezing in different water solutions

Michal Stebel [a,*], Jacek Smolka [a], Michal Palacz [a], Trygve M. Eikevik [b], Ignat Tolstorebrov [b]

[a] *Institute of Thermal Technology, Silesian University of Technology, Konarskiego 22, 44-100 Gliwice, Poland*
[b] *Norges Teknisk-Naturvitenskapelige Universitet, Kolbjørn Hejes Vei 1D, Trondheim 7049, Norway*

A B S T R A C T

A novel method of hydrofluidisation food freezing is numerically investigated in this paper. This technique is based on freezing small food products in a liquid medium under highly turbulent flow conditions when the heat transfer coefficient is higher than 1 000 $W \cdot m^{-2} \cdot K^{-1}$, which depends on the operating and flow conditions. A numerical model was developed to characterise the freezing process in terms of the heat transfer and diffusion of liquid solution components into the food product. The study investigates the freezing process of spherical samples in binary solutions of ethanol (30%) and glycerol (40%) and ternary solution of ethanol and glucose (15%/25%). The developed model was employed to determine the concentration of the liquid solution in food samples and to quantify the effect of sample size, heat transfer coefficient, solution temperature and concentration on the process. The food sample size varied from 5 to 30 mm, and the heat transfer coefficients varied from 1 000 to 4 000 $W \cdot m^{-2} \cdot K^{-1}$. The results confirm that a freezing time of 15 min for 30 mm diameter samples or less than 1 min for 5 mm diameter samples can be achieved with the hydrofluidisation method. The solution uptake was influenced by the solution type, sample size and process parameters and varied from 8.9 to 35 g of solute per kg of product for ethanol-glucose and glycerol solutions, respectively. This paper quantifies the advantages and possible limitations of hydrofluidisation, which has not yet been entirely studied, especially in terms of the mass absorption of different solutes.

1. Introduction

Cooling and freezing are the most popular and well-established methods for the preservation of food products. However, a report by the International Institute of Refrigeration (IIR, 2020) states that over 175 M tonnes of food in well-developed countries and 300 M tonnes in developing countries were lost in 2013 due to a lack of refrigeration, and these amounts correspond to approximately 13% of global food production. Furthermore, during freezing followed by storage and thawing, the quality of food products deteriorates. Consequently, cold chain is an important issue in the food industry, and numerous new methods for food freezing have been developed for the efficient freezing of foods with the highest possible final quality (James, Purnell, & James, 2015).

The most common methods of freezing in a cold air environment have several disadvantages, e.g., water loss by moisture evaporation from frozen food surfaces and tissue degradation due to ice crystal growth. Numerous novel methods have been developed to address the latter issue, e.g., by employing microwaves (Xanthakis, Le-Bail, &

Ramaswamy, 2014) or ultrasounds (Xu, Zhang, Bhandari, Sun, & Gao, 2016) to assist the freezing process or by conducting the freezing process under low temperature and high pressure (Luscher, Schlüter, & Knorr, 2005). However, according to the survey conducted by Khouryieh (2021), despite the advantages related to the quality of foods, the main limitation of such sophisticated methods is a very high investment cost.

According to the review by James et al. (2015), food products with a small size can benefit from methods characterised by a very high heat transfer coefficient (HTC) and shorter processing time. During rapid freezing, ice crystals are smaller and more dispersed within the food product structure (Fikiin, 2008). The author of the aforementioned study pointed out the *critical zone of water crystallisation* as the temperature range from $-1°C$ to $-8°C$ where most of the water changes the phase during freezing. If that temperature range is passed through quickly during freezing, then the ice crystals will be finer and the food quality will not be as deteriorated. Because freezing in cold air has limitations related to HTC, methods based on liquid media may be beneficial due their better potential for enhancing convective conditions. In addition, freezing in a liquid environment minimises water loss

Nomenclature

A	Area, m^2
c_p	Specific heat capacity, J·kg^{-1}·K^{-1}
D	Sample diameter, m
$\mathscr{D}$	Mass diffusion coefficient, m^2·s^{-1}
$\mathscr{D}_{eff}$	Effective mass diffusion coefficient, m^2·s^{-1}
h	Specific enthalpy, J·kg^{-1}
HTC	Heat transfer coefficient, W·m^{-2}·K^{-1}
k	Thermal conductivity, W·m^{-1}·K^{-1}
l	Length, m
L_0	Latent heat of fusion of ice, (333 600 J·kg^{-1})
m	Mass flux, kg·s^{-1}·m^{-2}
MTC	Mass transfer coefficient, m·s^{-1}
q	Heat flux, W·m^{-2}
t	Time, s
T	Temperature, K
v	Volume fraction, m^3·m^{-3}
V	Volume, m^3
w	Partial density of a given component, kg·m^{-3}
x	Mass fraction, kg·kg^{-1}
Le	Dimensionless Lewis number
Pr	Dimensionless Prandtl number
Sc	Dimensionless Schmidt number

Greek symbols

ε	Porosity, m^3·m^{-3}
μ	Dynamic viscosity, kg·m^{-1}·s^{-1}
ν	Kinetic viscosity, m^2·s^{-1}
ρ	Density, kg·m^{-3}
τ	Tortuosity, m^1·m^{-1}

Abbreviations

CFD	Computational Fluid Dynamics
COP	Coefficient of Performance
ETH	Ethanol aqueous solution
FVM	Finite Volume Method
GLY	Glycerol aqueous solution
HF	Hydrofluidisation Freezing
IF	Immersion Freezing
PIV	Particle Imaging Velocimetry
SUG	Ethanol-glucose aqueous solution

Subscripts

ℓ	Liquid phase
F	food product surface
wat	Liquid water as a food component
ice	Ice as a food component
n	n-th component of the solution
wo	Total humidity as a food component
if	Initial freezing point
ref	Reference point
$refr$	Refrigerant
s	Solid food components
$t0$	Initial moment

during the process (Fikiin, 2008).

Immersion freezing (IF) is a simple method based on submerging food products in a liquid medium under free-convection conditions. Appropriate aqueous solutions used for that process can be based on NaCl (Zorrilla & Rubiolo, 2005a), CaCl$_2$ (Galetto, Verdini, Zorrilla, & Rubiolo, 2010), or ethanol-sugar mixtures (Fikiin, Tsvetkov, Laptev, Fikiin, & Kolodyaznaya, 2003). According to the review by Lucas and Raoult-Wack (1998), IF guarantees high food quality and HTC on the order of 200–300 W·m^{-2}·K^{-1}. The authors, however, highlighted the main disadvantage of that method, which is unwanted solute uptake. More recently, the same authors formulated a simple mathematical model to investigate the behaviour of the food surface (Lucas, Flick, & Raoult-Wack, 1999), followed by the coupled heat and mass transfer numerical model to assess the process of solute absorption in the IF process. Zorrilla and Rubiolo (2005a) developed a 3-D numerical model based on Whitaker's averaging volume method (Whitaker, 1977) to predict the mass uptake during cheese freezing in NaCl solution using the IF method. In their results, Zorrilla and Rubiolo (2005b) highlighted that a lower solute average concentration after the process can be achieved in the case of a higher HTC.

The method of hydrofluidisation freezing (HF) is a form of IF in which, the liquid flow is forced; hence, convection is more intensive. Small food products are frozen in the HF tank equipped with an array of orifices at its bottom. Then, the liquid is pumped into the tank through orifices, and the flow is turbulent and the heat transfer is enhanced. The method was proposed by Fikiin (1992) as an effective method for cooling and freezing of fish. The author highlighted the advantages of HF, e.g., higher freezing rate in comparison with IF, reduction of the processing time, high quality of foods, lower cost of operation, and the possibility to equip the HF system with efficient primary refrigerating units characterised by high coefficient of performance (COP). According to the author, HTCs reach 900 W·m^{-2}·K^{-1}. This method was developed further for the freezing of small fruits and vegetables, for which HF is the most beneficial. Fikiin and
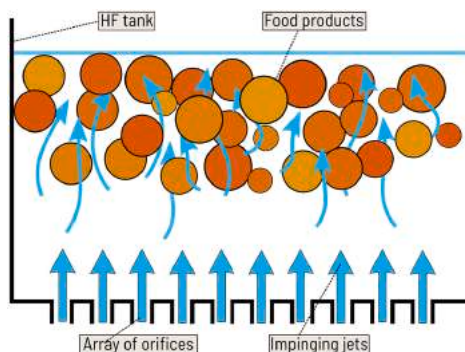
Fig. 1. General scheme of the HF method.

Fikiin (2001) presented the results of HF freezing using ice slurry as a refrigerating liquid, and the achieved HTC ranged from 1 000 to 2 000 W·m^{-2}·K^{-1}.

The effect of the process parameters on HTC in the HF method was studied experimentally by Verboven, Scheerlinck, and Nicolai (2003). The authors used aluminium spheres at fixed positions instead of free-moving food products for the experimental evaluation of HTC based on thermal measurements in the system with aqueous ternary solution of ethanol and glucose (30%/20% mass basis) used as a refrigerating liquid. Peralta, Rubiolo, and Zorrilla (2009) performed a similar experimental study using NaCl aqueous solution (23%) as a refrigerating medium in a lab-scale HF unit. The same system was investigated

numerically in their subsequent work (Peralta, Rubiolo, & Zorrilla, 2010) by using computational fluid dynamics (CFD) to present the liquid jet turbulent flow and investigate HTC in such a simplified configuration. This CFD model was further extended (Peralta, Rubiolo, & Zorrilla, 2012) with heat and mass transfer analysis within a real food product, i. e., potato. The most realistic numerical work of the same group of authors covers the modelling of free-moving spherical samples in the HF system by employing discrete phase modelling (Oroná, Zorrilla, & Peralta, 2017), which was followed by a sensitivity study (Oroná, Zorrilla, & Peralta, 2018) performed using the same model. The authors identified the parameters affecting the transport phenomena in a liquid medium, heat transfer and mass transfer in a potato sample. According to their results, heat transfer was affected by the flow rate and the temperature of the refrigerating medium, while the mass transfer was mainly affected by the temperature within the range of analysed conditions.

The most recent studies related to experimental and numerical investigation of the HF system were performed using an ethanol-based solution as a refrigerating liquid. Palacz, Adamczyk, Piechnik, Stebel, and Smolka (2019) performed an experimental study focused on fluid flow in a simplified HF system with a stationary spherical sample. The authors employed the particle image velocimetry (PIV) method to capture and analyse the fluid flow field of impinging jets in the HF unit. This study was followed by a numerical investigation of the same system (Stebel, Smolka, Palacz, Adamczyk, & Piechnik, 2020), in which the authors developed and validated the numerical model of jet and fluid flow in an HF system. The most appropriate turbulence model was selected for the further development of their CFD model. Recently, Palacz et al. (2021) analysed the freezing process of real food samples experimentally. The authors confirmed that the HTC exceeds 2 000 W·m^{-2}·K^{-1} in the HF system and that the freezing time may be shortened by half with respect to the IF method. Hence, food freezing using the novel HF method may be considered a promising alternative for other well-known methods, but more studies should be performed to fully characterise that technique.

This study aims to numerically investigate the heat and mass transfer processes within food products during freezing with the HF method. A numerical model based on the finite volume method (FVM) has been developed to perform a conjugate analysis of the freezing process with simultaneous solute uptake. This model is based on Fourier's and Fick's laws, and all properties are easily determined. Consequently, the implementation of the proposed model is straightforward and versatile. The food product analysed in this paper was a spherical-shaped potato sample with a diameter from 5 to 30 mm. Cases related to the convective conditions characteristic for HF as well as IF method were defined to assess whether the HF method is more beneficial not only due to the higher freezing rate, but also in terms of the unwanted solute uptake. Consequently, the HTC was assumed to be 300 W·m^{-2}·K^{-1} for IF and in the range of 1 000 to 4 000 W·m^{-2}·K^{-1} for the HF method. Previous studies by the authors proved that such an HTC range can be achieved in the HF process. The highest HTC value may be considered the best possible condition that can be reached. Moreover, three different solutions were compared in this analysis, i.e., an aqueous ethanol solution (30% mass basis), an aqueous glycerol solution (40% mass basis), and a binary aqueous solution of ethanol and glucose (15%/25% mass basis) having the same temperature of −15°C. In addition, the effect of the refrigerating liquid temperature on the freezing time and solution uptake was assessed for various sizes of food samples for the ethanol solution (30%) at temperatures of −10°C, −15°C, and − 20°C. The outcome of that comparison quantifies the benefit of temperature lowering for different sizes of products in terms of both freezing rate and solute uptake. Lowering of that temperature is limited by the solute concentration. The lower the temperature shall be, the highest concentration must be provided. However, an increase of that concentration can be not beneficial for the final concentration of the unwanted solute in the product. Therefore, an analysis was performed to compare the solute uptake for cases with various glycerol concentrations in the range from 20% to 50% at the lowest possible temperature.

The outcome of this study is the assessment of the HF method potential considering its numerous advantages but also the major drawback, which is the unwanted solution uptake. The most important parameters of the process were compared to find the best practices to conduct HF process effectively with simultaneously maintaining a low solute uptake. It is essential because the solute accumulation is a major food quality indicator in HF method.

2. Methodology

2.1. Geometrical domain and numerical mesh

The geometrical domain considered in this study includes only the food product interior with a spherical shape as shown in Fig. 2(a). Such samples were used in previous studies by the authors (Palacz et al., 2019; Palacz et al., 2021; Stebel et al., 2020) and in other papers related to the HF method, e.g., (Peralta et al., 2012). The spherical shape is an appropriate representation of a vast number of food products, e.g., berries or peas. The diameter (*D*) of the food sample was in the range from 5 mm to 30 mm, depending on the case. Due to the symmetrical shape of the sample and uniform boundary conditions over the food sample surface, a 2-D axisymmetric domain could be used in the developed model. In this study, potato samples were analysed, because they are a globally available foodstuff and can represent a vast set of fruits and vegetables in terms of water content.

The numerical mesh was prepared using ICEM CFD software. It was fully structured and composed of 6 592 quadrilateral elements, as presented in Fig. 2(b). To accurately determine the solute uptake that occurs near the food product surface, the mesh was refined in the radial dimension near the surface. Consequently, the first cell thickness was approximately 1 800 thinner than the sphere diameter, and the mesh had 180 elements along the sphere axis. Simultaneously, the average
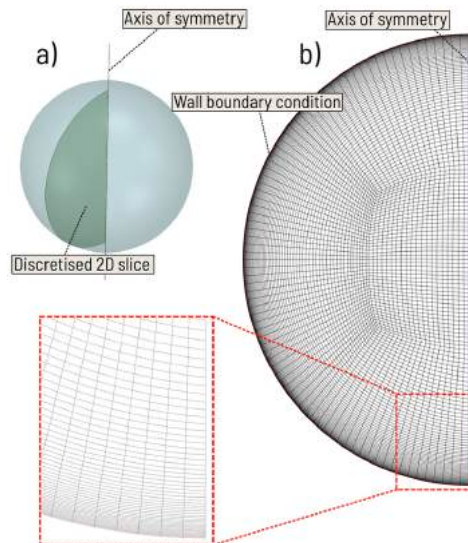
Fig. 2. a) 2-D axisymmetric numerical domain of the spherical food product and (b) discretised mesh.

orthogonal quality of cells was 0.98 (0.69 in the worst case), while the mean skewness was 0.09 (0.54 in the worst case). Therefore, the numerical mesh can be considered high-quality. To verify if the resolution of the numerical mesh is appropriately refined, a mesh independence study was performed as presented further in Section 3 using four meshes with different resolution.

2.2. Governing equations

In the developed numerical model, two phenomena are considered, i. e., mass transfer of liquid water and solutes and the heat transfer, which are assumed to follow Fick's and Fourier's laws, respectively. Because the solute uptake occurs locally and the time scale of mass diffusion mechanism is lower than that of the heat diffusion, heat transfer was assumed as not dependent on the solute uptake.

The numerical model presented in this paper follows the principles of the approach proposed by Whitaker (1977) for the drying process. This approach was adopted by Zorrilla and Rubiolo (2005a) for IF followed by Peralta et al. (2012) for HF. In general, three phases may be distinguished within the food product structure: solid skeleton, solid ice, and the liquid fraction. In the model presented in this paper, the heat transfer does not need to consider these phases separately, while the mass diffusion deals with only the liquid phase. Such an approach can be considered a convenient simplification of the analysed problem. The liquid phase consists of the unfrozen water and solutes absorbed from the liquid solution used for the HF process. Consequently, these components are considered in the mass transfer analysis.

2.2.1. Mass diffusion

Because HF is conducted in a liquid environment, water loss is not a problematic aspect in terms of food quality. However, the liquid water transport equation was formulated in the numerical model because it is a major fraction of the liquid phase in food products. The mass conservation for liquid water is described in Eq. (1). This equation follows Fick's law for diffusion. The first term on the left-hand side is time-dependent and accounts for the rate of change of the mass fraction of water. It can be recognised as the accumulative term in the transport equation. The second term deals with the mass diffusion within the numerical domain. The equation also includes the additional source term on the right-hand side, which characterises liquid water crystallisation if the local temperature is below the initial freezing temperature. The definition of this temperature-dependent term is strictly related to the properties formulation. Therefore, it is described in detail in Section 2.3.2. The diffusion of solutes was determined using a similar equation (Eq. (2)). Each solute (ethanol, glucose, glycerol) is described by an individual equation. Therefore, in the case of ternary solution of water, glucose, and ethanol, two identical equations are solved for the solutes diffusion.

$$\frac{\partial(\rho_\ell x_{wat})}{\partial t} - \nabla\left(\rho_\ell \mathscr{D}_{eff} x_{wat}\right) = \frac{\partial x_{ice}(T)}{\partial t} \tag{1}$$

$$\frac{\partial(\rho_\ell x_n)}{\partial t} - \nabla\left(\rho_\ell \mathscr{D}_{eff} x_n\right) = 0 \tag{2}$$

where ρ_ℓ is the density of liquid phase assumed as the water density, x_{wat} is the mass fraction of liquid water, t is the time, $\mathscr{D}_{eff}$ is the effective mass diffusion coefficient, $x_{ice}(T)$ is the ice mass fraction, which is temperature-dependent and x_n is the mass fraction of n-th solution component.

2.2.2. Heat transfer

Energy conservation is described in Eq. (3). As mentioned before, it is based on Fourier's law for heat conduction. In this numerical model, the latent heat is included in the apparent heat capacity formulation. Therefore, no additional source term is needed to characterise the thermal effect of liquid water crystallisation during freezing. For the

model stability, the energy balance is solved using the enthalpy-based formulation. Such a methodology is well established and popular in numerical solutions for heat transfer in different numerical methods (Pham, 2006).

$$\frac{\partial \rho h}{\partial t} - \nabla\left(\frac{k}{c_p} h\right) = 0 \tag{3}$$

where ρ is the density of the food product, h is the specific enthalpy of food product, k is the thermal conductivity, and c_p is the apparent heat capacity.

All the equations Eq. (1–3) were solved numerically using ANSYS Fluent software which is based on the control volume basis to discretise and solve the governing equations. This numerical solver was based on the implicit formulation for solving the solution. Second-order schemes were used for spatial and time discretisation of all the equations in order to guarantee the appropriate accuracy of the solution.

2.3. Thermophysical properties

2.3.1. Refrigerating liquids

In this study, three water-based solutions were considered refrigerating liquids in the HF system, i.e., a binary aqueous solution of glycerol (20%–50% mass basis), a binary aqueous solution of ethanol (30% mass basis) and a ternary aqueous solution of ethanol-glucose (15%/25% mass basis). Although the numerical model does not solve the flow of these fluids, the formulation of their properties is necessary to characterise the mass absorption at boundaries, as described in detail in Section 2.4. The values of the necessary properties are listed in Table 1.

2.3.2. Food product

In this study, the properties of the food sample were estimated based on the composition of the potato. The water content of the fresh sample was evaluated experimentally, while the mass fractions of the remaining components were adjusted based on the literature data (ASHRAE, 2006). Table 2 presents the initial composition of the fresh food sample.

During the freezing process, liquid water crystallises and ice is formed. The initial freezing temperature of the potato was determined by the tangential method based on experimental measurements of potato temperature during HF (Palacz et al., 2021). This method is based on determining the point of crossing two curves. One curve is a linear extrapolation of the slope characteristic for the prefreezing stage of the process when the temperature is decreasing. The second curve is the extension of nearly isothermal freezing plateau that can be observed in the temperature course while the food freezing process is progressing. The initial freezing temperature corresponds to the point where these two linear curves cross. It was assumed to be −1.65°C based on the averaging of over 30 individual cases investigated in the previous work of the authors related to the heat transfer and phase change phenomena in HF process (Stebel et al., 2021). Below that temperature, the liquid water successively crystallises into ice along with the temperature decrease. The empirical relationship proposed by Tchigeov (1979) given in Eq. (4) was used to determine the ice content during the HF process as a function of the food product temperature when it decreases below the initial freezing point. Because the total water content does not change significantly during the HF process, this property was assumed to be independent of the mass diffusion process. The increase in the ice content during the freezing process allowed to characterise the deficit of liquid water in the mass balance equation for liquid water (Eq. (1)).

$$x_{ice} = \frac{1.105 x_{wo}}{1 + \frac{0.7138}{\ln(T_{if} - T + 1)}} \tag{4}$$

where x_{ice} is the mass fraction of ice, x_{wo} is the total mass fraction of moisture in the fresh food product, T_{if} is the initial freezing temperature in °C and T is the food product temperature in °C.

Table 1

Values of thermophysical properties for water-based solutions according to (Melinder, 2010) for the glycerol and ethanol solutions and (Fikiin et al., 2003) for the ethanol-glucose ternary solution.

Solution and concentration	Temperature °C	Freezing Temperature °C	Density kg·m^{-3}	Thermal conductivity W·m^{-1}·K^{-1}	Specific heat J·kg^{-1}·K^{-1}	Dynamic viscosity kg·m^{-1}·s^{-1}	Prandtl number
Glycerol (GLY) 40%	−15.0	−15.3	1 111.5	0.4197	3 294	0.01764	138
Ethanol (ETH) 30%	−15.0	−20.1	971.4	0.3880	4 100	0.01730	183
Ethanol-glucose (SUG) 15%/25%	−15.0	−20.0	1 087.3	0.4120	3 180	0.02538	196
Ethanol (ETH) 30%	−10.0	−20.1	969.4	0.3911	4 124	0.01226	129
Ethanol (ETH) 30%	−20.0	−20.1	973.1	0.3950	4 072	0.02521	267
Glycerol (GLY) 20%	−5.0	−5.6	1 052.1	0.4893	3 811	0.004198	33
Glycerol (GLY) 30%	−9.5	−9.8	1 080.8	0.4530	3 572	0.007831	62
Glycerol (GLY) 50%	−23.0	−23.2	1 144.7	0.3881	2 983	0.05894	453

Table 2

Mass fractions of the food product components for the potato sample.

Initial Moisture	Protein	Fat	Carbohydrate	Fibre	Ash
80.05%	1.97%	0.09%	15.53%	1.52%	0.84%

In this study, the density of the food sample was determined using Eq. (5) based on the composition of potato and the density of individual components described according to common temperature-dependent relationships available in the literature (Choi & Okos, 1986). An important parameter related to the density and composition of a food product is the porosity, i.e., the volumetric fraction of the liquid phase. This parameter is given in Eq. (6) which assumed that the liquid phase (water with dissolved solutes) density is close to the water density.

$$\rho = \frac{1}{\sum(x_i/\rho_i)} \tag{5}$$

$$\varepsilon = \frac{x_\ell}{\rho_\ell} \frac{1}{\sum(x_i/\rho_i)} \tag{6}$$

where x_i and ρ_i are the mass fraction and the density of i-th food product component, ε is the porosity, x_ℓ is the mass fraction of the liquid phase (water and solutes) and ρ_ℓ is the density of the liquid phase.

To characterise the mass diffusion within the real food sample, the effective diffusion coefficient for each component was determined as given in Eq. (7). It represents the ability of a given component to diffuse through the liquid phase in the food product structure. Therefore, it was defined as the diffusion coefficient of the n-th component in water, including the volumetric fraction of the liquid phase and the tortuosity. The latter accounts for the increase in the path for the transport of molecules through the porous medium matrix. The value of this parameter found in the literature was 2.0 or 9.6 in similar papers dealing with mass transfer during potato freezing (Lucas et al., 1999; Peralta et al., 2012). Therefore, to analyse *the worst case scenario*, a tortuosity value of 2.0 was assumed in this study.

$$\mathscr{D}_{eff,n} = \varepsilon \frac{\mathscr{D}_n}{\tau} \tag{7}$$

where $\mathscr{D}_{eff,n}$ is the effective mass diffusivity of n-th component in potato, $\mathscr{D}_n$ is the mass diffusivity of n-th component at infinite dilution in water and τ is the tortuosity.

Data related to the mass diffusion coefficients of different substances in water are available in the literature. Unfortunately, the values are most commonly given for constant and relatively high temperatures. To determine the relationship describing the temperature-dependent mass diffusivity of the n-th component in water, the Einstein-Stokes relation was used (Cussler, 1984). It allows to determine the mass diffusivity at any temperature if the mass diffusivity at a reference temperature and the solvent (water) kinetic viscosity are known, as shown in Eq. (8). In this way, the temperature-dependent mass diffusivities of glucose,

ethanol, and glycerol were determined, as shown in Fig. 3. Only one value of the mass diffusivity at a known temperature was necessary as a reference value to determine that relationship, but different data from the literature were collected in that figure to verify the accuracy of the temperature-dependent mass diffusivity function. The exception was water because the temperature-dependent self-diffusion coefficient was available in the literature for water (Holz, Heil, & Sacco, 2000), as given in Eq. (9)

$$\mathscr{D}_n(T) = \mathscr{D}_n(T_{ref}) \frac{T_{ref}}{T} \frac{\nu_{wat}(T)}{\nu_{wat}(T_{ref})} \tag{8}$$

$$\mathscr{D}_{wat} = 1.635 \cdot 10^{-8}((T/215.05) - 1)^{2.063} \tag{9}$$

where $\mathscr{D}_n(T)$ is the mass diffusion coefficient of component n in water at temperature T given in K, $\mathscr{D}_n(T_{ref})$ is the known mass diffusion coefficient of component n in water at the reference temperature T_{ref} given in K, $\nu_{wat}(T)$ is the kinematic viscosity of water at temperature T, $\nu_{wat}(T_{ref})$ is the kinetic viscosity of water at the reference temperature and $\mathscr{D}_{wat}$ is the self-diffusion coefficient of water.

For the correct determination of the temperature within the food product as well as the phase change phenomena modelling, the apparent heat capacity was applied in the numerical model according to the formulation proposed by Chen (1985), which allows for the determination of the food temperature change along with the sensible and latent heat release during freezing. This formulation is given in Eqs. (10) and (11) for temperatures above and below the characteristic initial freezing temperature, respectively. Consequently, the specific enthalpy of the food product is represented by Chen's formula given in Eq. (12) for temperatures above the initial freezing temperature and in Eq. (13) below that point.

$$c_p = 4.19 - 2.30x_s - 0.628x_s^3 \tag{10}$$

$$c_p = 1.55 + 1.26x_s - \frac{(x_{wo} - x_b)L_0 T_{if}}{T^2} \tag{11}$$

$$h = h_{if} + (T - T_{if})(4.19 - 2.30x_s - 0.628x_s^3) \tag{12}$$

$$h = (T - T_{ref})\left[1.55 + 1.26x_s - \frac{(x_{wo} - x_b)L_0 T_{if}}{T_{ref}T}\right] \tag{13}$$

where x_s is the mass fraction of solid components, x_b is the mass fraction of bounded water, L_0 is the latent heat of fusion of water (333.6 kJ·kg^{-1}), T is the food product temperature in °C, h_{if} is the food product specific enthalpy at the initial freezing point evaluated using Eq. (13) and T_{ref} is the reference temperature for that formulation (−40°C).

The thermal conductivity of potato was defined based on Levy's formulation (Levy, 1981), which is a multistage approach appropriate for nonporous frozen food products (Carson, Wang, North, & Cleland, 2016). According to that formulation, thermal conductivity must be evaluated first for all food product components, excluding ice,
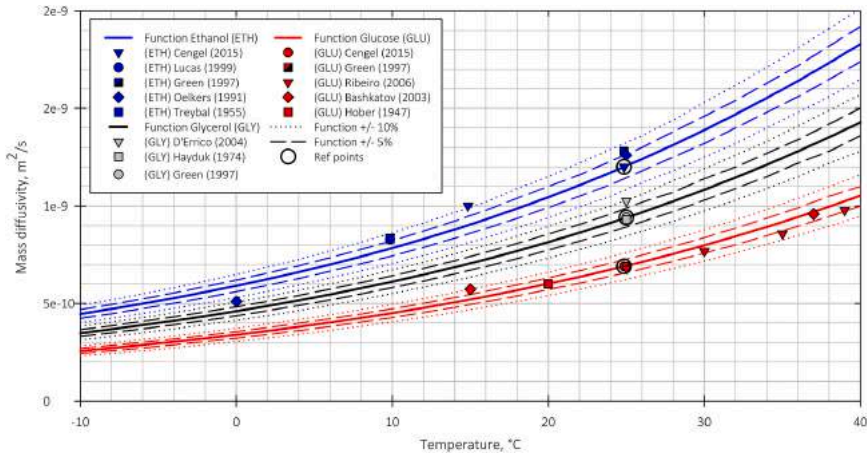
Fig. 3. Temperature-dependent functions describing the mass diffusivity of glycerol, ethanol and glucose in water according to the Einstein-Stokes relationship. The reference data are as follows: (Cengel, 2015) (ETH, SUG); (Green, 1997) (GLY); and verification data: (Bashkatov et al., 2003; D'Errico, Ortona, Capuano, & Vitagliano, 2004; Hayduk & Laudie, 1974; Hober, Hitchcock, Bateman, Goddard, & Fenn, 1946; Lucas et al., 1999; Oelkers, 1991; Ribeiro et al., 2006; Treybal, 1955). (For interpretation of the references to colour in this figure legend, the reader is referred to the web version of this article.)

preferably using the parallel model (Wang, Carson, Willix, North, & Cleland, 2009), which is given in Eq. (14). In the second step, the frozen food product thermal conductivity is evaluated using Eq. (15) considering the food sample mixture of ice and unfrozen components.

$$k_I = \sum k_i v_i \tag{14}$$

$$k_{Levy} = k_{ice} \frac{2k_{ice} + k_I - 2(k_{ice} - k_I)F}{2k_{ice} + k_I + (k_{ice} - k_I)F} \tag{15}$$

with

$$F = \frac{2/G - 1 + 2(1 - v_{ice}) - \sqrt{[2/G - 1 + 2(1 - v_{ice})]^2 - 8(1 - v_{ice})/G}}{2}$$

and

$$G = \frac{(k_{ice} - k_I)^2}{(k_{ice} + k_I)^2 + k_{ice}k_I/2}$$

where k_I is the thermal conductivity of single-stage components, i.e., liquid water, protein, fat, carbohydrate, fibre, and ash, k_i is the thermal conductivity of the *i*-th single-stage component, v_i is the volumetric fraction of the *i*-th single-stage component, k_{Levy} is the thermal conductivity of food product according to Levy's model, k_{ice} is the thermal conductivity of ice, v_{ice} is the volumetric fraction of ice, and F and G are the functions related to mathematical formulation of Levy's model.

2.4. Boundary and initial conditions

Conjugate heat and mass transfer analysis of the food product frozen in a liquid medium requires defining convective boundary conditions. In the IF and HF methods, HTCs have been assessed in numerous studies. Therefore, the values of 300 W·m^{-2} K^{-1} for IF and the range from 1 000 to 4 000 W·m^{-2} K^{-1} for HF were assumed in this study. To evaluate the mass transfer coefficients (MTCs) in the mass transfer analysis, the Chilton-Colburn analogy (Cengel, 2015) was used to determine the

MTCs based on HTCs. This relationship is based on the characteristic Prandtl, Schmidt, and Lewis numbers, which can be expressed using Eqs. (16)–(18), respectively. The MTC is evaluated according to the relationship given in Eq. (19). The thermophysical properties in these formulas have to be determined for the refrigerating medium at its bulk temperature, while the mass diffusivity in the Schmidt number formulation deals with the diffusivity of ethanol, glycerol or glucose in water. As an effect, the MTC values defined using Chilton-Colburn analogy are dependent on the refrigerating medium properties and the HTC. Table 3 presents these values within the range of conditions used in this study, which covers (1) three solutes under different HTCs at a constant temperature of −15°C, (2) ethanol solution (30%) at a constant HTC of 2 000 W·m^{-2} K^{-1} and two different temperatures of −10°C and − 20°C, and (3) glycerol solution at three different temperatures from −5°C to −23°C and various solute concentrations (20%–50%) adjusted to the temperature.

$$Pr = \frac{c_p \mu}{k} \tag{16}$$

Table 3
Values of MTC obtained using Chilton-Colburn analogy for the range of conditions considered in this study for three solutions.

HTC W·m^{-2} K^{-1}	Temperature of solution (°C)	ETH 30%	GLY 40%	SUG 15%/25%	
		Ethanol	Glycerol	Ethanol	Glucose
		MTC ·10^{-5} (m·s^{-1})			
300	−15.0	0.190	0.157	0.191	0.132
1 000	−15.0	0.632	0.523	0.637	0.440
2 000	−15.0	1.265	1.046	1.273	0.881
3 000	−15.0	1.897	1.569	1.910	1.321
4 000	−15.0	2.529	2.092	2.547	1.761
2 000	−10.0	1.164			
2 000	−20.0	1.376			
2 000	−5.0 (GLY 20%)		1.144		
2 000	−9.5 (GLY 30%)		1.122		
2 000	−23.0 (GLY 50%)		1.017		

$$\text{Sc} = \frac{\mu}{\rho \mathscr{D}} \tag{17}$$

$$\text{Le} = \frac{\text{Sc}}{Pr} \tag{18}$$

$$MTC = \frac{HTC}{\rho c_p \text{Le}^{2/3}} \tag{19}$$

where Pr is the Prandlt number, Sc is the Schmidt number, Le is the Lewis number, μ is the dynamic viscosity, MTC is the mass transfer coefficient, and HTC is the heat transfer coefficient.

In the numerical model, these boundary conditions are implemented according to Eq. (20) for the mass transfer and Eq. (21) for the heat transfer.

$$m = MTC \cdot \left(\rho_R x_{n\,refr} - \rho_W x_{nW} \right) \tag{20}$$

$$q = HTC \cdot \left(T_{refr} - T_W \right) \tag{21}$$

where m and q are the mass and heat fluxes defined at the boundary, ρ_{refr} is the density of refrigerating medium, $x_{n\,refr}$ is the mass fraction of component n in the refrigerating medium, ρ_W is the local density of food product at its surface, x_{nW} is the local mass fraction of component n in the food product at the surface, T_{refr} is the refrigerating medium temperature, T_W is the temperature of food product locally at the surface.

The initial conditions for each case considered in this paper were the same and they were related to fresh food products prior to the HF process. Therefore, the initial temperature was established as 20°C and uniform within the food product and no solute was present in its structure.

3. Numerical model verification

Before the accuracy of the numerical results was examined, first, the numerical mesh developed for the model was tested in terms of its impact on results. As mentioned before, four meshes were generated having 2 944, 6 088, 6 592, and 7 600 quadrilateral elements. Because this study focuses on heat and mass transfer analysis, the mesh sensitivity study covers the comparison of the local temperature within the food sample and the average concentration of a solute within the food sample volume. Fig. 4(a) compares this local temperature for four

meshes, while Fig. 4(b) compares the solution uptake for a selected case with glycerol solution, the food sample diameter of 20 mm, and HTC of 3 000 W·m^{-2}·K^{-1}.

The comparison of the local temperature in the food sample centre proved that all four meshes provide accurate results in terms of heat transfer prediction. All the temperature curves were identical. The modelling of the solution uptake was slightly more demanding in terms of the numerical mesh resolution. The mesh composed of 6 592 elements was considered appropriate for the model. Two coarse meshes having 2 944 and 6 088 elements overestimated the concentration of solute within the food product with respect to the final mesh. The most refined mesh having 7 600 elements provided the same accuracy that the final one having 6 592 elements. It proved that the further mesh refinement does not affect the results and the results obtained using the final mesh are not dependent on its resolution.

The verification of the numerical model was twofold. First, the solute concentration profiles were compared with the transient analytical solution for simplified cases with constant properties to determine whether the mass diffusion was properly modelled under different isothermal conditions. Then, the results obtained using the developed numerical model were compared with the freezing simulation results available in the literature related to HF (Peralta et al., 2012).

Numerical model verification using an analytical solution under simplified conditions aimed to determine whether the mathematical formulation and numerical implementation of the mass transport equation were correct. A similar comparison was performed in the numerical study of Lucas et al. (1999), which was related to mass transfer in the IF method. The standard heat and mass transfer literature (Cengel, 2015)] provides the mathematical solution for transient mass diffusion analysis with the convective-type boundary condition. This solution is presented in Eq. (22). Several minor simplifications were applied to make this analysis possible; the analytical solution was solved as a 1-D problem in Cartesian coordinates because only the outer layer of the food product with a thickness of 0.5 mm was considered, the porosity had a fixed value, and the numerical analysis was performed as isothermal to maintain constant values of the mass diffusion coefficient. Because the bulk density of the food product and the fluid are different, the analytical solution is related to the partial density w_n that can be easily transferred into the mass concentration.
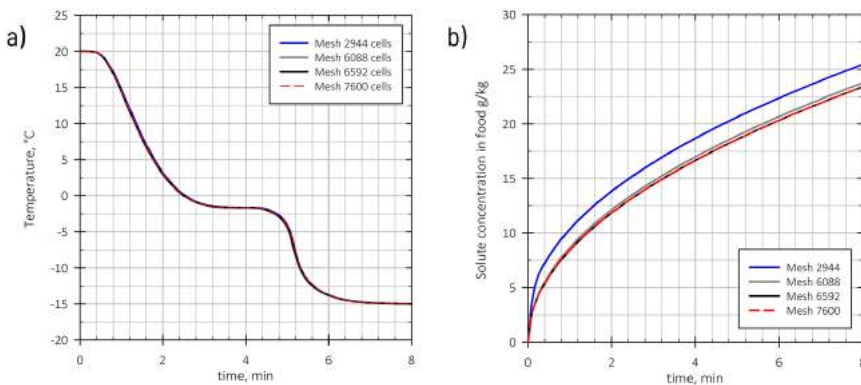
Fig. 4. Comparison of the: (a) local temperature of the potato sample centre and (b) the average concentration of the solute within the food product for four different numerical meshes for a selected case.

$$\frac{w_n(l,t) - w_{n,0}}{w_{n,R} - w_{n,0}} = erfc\left(\frac{l}{2\sqrt{\mathscr{D}_{eff,n}t}}\right) - exp\left(\frac{MTCl}{\mathscr{D}_{eff,n}} + \frac{MTC^2 t}{\mathscr{D}_{eff,n}}\right)\left[erfc\left(\frac{l}{2\sqrt{\mathscr{D}_{eff,n}t}}\right.\right.$$
$$\left.\left. + \frac{MTC\sqrt{\mathscr{D}_{eff,n}t}}{\mathscr{D}_{eff,n}}\right)\right]$$

(22)

with

$$w_n(l,t) = x_n \rho_\ell$$

and

$$w_{n,refr} = x_{n\,refr}\rho_{refr}$$

where $w_n(l,t)$ is the partial density of component n at the given location l and time t, $w_{n,\,t0}$ is the partial density of n at the initial state, $w_{n,\,R}$ is the partial density of n in the refrigerant, and erfc is the complementary error function, which is available in every common software for mathematical operations (e.g. MATLAB (MATLAB, 2020)).

Two different conditions were analysed with a fixed porosity value of 0.8 under a constant temperature of 0°C: Test Case #1 with the glycerol aqueous solution (40%) and Test Case #2 with ethanol solution having a lower concentration (30%). The assumptions for these analyses are given in Table 4.

The results of the model verification analysis are presented in Fig. 5 using the profiles of the solute mass concentrations in food near the food product outer surface in the radial direction simplified in 1-D after 30 s, 60 s and 120 s.

Fig. 5(a) and 5(b) present the profiles of the mass concentrations of glycerol and ethanol, respectively. As seen, no differences are observed between the numerical and analytical results. Different boundary conditions related to the solute mass concentration and MTCs as well as the solution type that affected the mass diffusivity did not affect the solution accuracy. The verification procedure confirms that the mathematical formulation of the model is correct under different conditions related to the solute type, properties and boundary conditions.

The process of conjugated food freezing and solute uptake during HF was numerically studied by Peralta et al. (2012) and validated taking into consideration the average concentration of the solute in food products measured after a given time. The referenced study is focused on HF in a NaCl-based solution with different simulation parameters (e.g., tortuosity) assumed by its authors. Nevertheless, for the verification of the numerical model presented in this study, a comparison with the literature results may be done after assuming all the needed values, i.e., tortuosity, solute mass diffusivity, boundary conditions, and initial conditions, in accordance with Peralta et al. (2012). Fig. 6(a) and 6(b) present the numerical results of potato sample freezing obtained using the model developed in this study with NaCl uptake results taken from Peralta et al. (2012) for the same potato samples under NaCl-based aqueous solution temperatures of −10°C and − 15°C, respectively. To model the mass diffusion of a new solute, the tortuosity value was set as 9.6 (that value was assumed by the authors), and the mass diffusivity was calculated using Eq. (8) assuming the NaCl diffusivity at a temperature of −15°C as a reference value. These values were taken from the literature (Peralta et al., 2012).

The consistency between the model developed in this study and the

literature results is fairly acceptable. The shape and tendency of the solute concentration curves do not differ significantly. In the first case shown in Fig. 6(a), the solute concentration in a food sample according to Peralta et al. (2012) was approximately 11.7 g·kg^{-1} while the model presented in this study determined that value as 11.1 g·kg^{-1} after 10 min of the process. It corresponds to a 5.1% relative difference with respect to the referred literature value. In the second case, compared in Fig. 6 (b), the solute concentrations in food were 7.2 g·kg^{-1} and 7.7 g·kg^{-1} after the same period of time according to Peralta et al. (2012) and the model presented in this paper, respectively. The relative difference of these results is 7.1% with respect to the literature data. Such a variation is fairly acceptable taking into consideration all the differences in both models. It is worth noting that the properties were defined in a different way, and the mathematical model presented in this study is less complex than that developed by Peralta et al. (2012). To sum up, that comparison allowed to state that the numerical model developed in this study is able to predict the mass transfer with acceptable accuracy, especially when considering the difficulties related to a proper definition of food product properties.

4. Results

The developed numerical model of conjugate heat and mass transfer was used to investigate several parameters of the HF process: the size of the sample, the intensity of the convection represented by HTC, and the solution type, temperature and concentration. All the cases used in this study are listed in Table 5.

The range of the numerical parametric study was defined to analyse three aspects as follows:

- Cases 1–30 were defined to analyse the effect of different HTCs in the freezing process of samples having different sizes. To compare the effect of the solution type within the operating conditions defined in this group of cases, the results were gathered for all the solutions used in this study. Therefore, every case in this group was simulated three times.
- Cases 31–36 were defined for quantification of how much the reduction of the refrigerating medium temperature affects freezing process indicators such as the process time and solution uptake. Only the ethanol solution (30%) was used in this analysis because its freezing temperature is below −20°C. In this analysis, Cases 13, 15, and 18 were also considered to analyse three temperatures: -10°C, −20°C and −15°C (reference value).
- Cases 37–45 allow to assess whether lowering the solution temperature is beneficial when the solute concentration is simultaneously increased to maintain the liquid state of the solution. In this analysis, a glycerol solution was used at a mass concentration range of 20–50% in which the freezing temperature of the solution is between approximately −5°C to −23°C. In this analysis, Cases 13, 15, and 18 were also used.

4.1. Characteristics of the freezing process with solute uptake

In this paper, two aspects were investigated: the time related to the freezing process and the solute uptake during that process. During the cooling and freezing of a spherical sample, the highest temperature point is located in the geometrical centre. Therefore, the centre temperature was the value considered for determination of the freezing process time. In this study, the total freezing process time was assumed as the time when the centre temperature was less than 0.5 K above the refrigerating medium temperature. In addition, the period of time was determined and compared where the centre temperature was in the range of the critical zone of water crystallisation, i.e., between −1°C and − 8°C. For the mass transfer analysis, the volume average concentration of the solute with respect to the fresh food sample mass was

Table 4
Assumptions for the model verification cases.

Parameter	Test Case #1	Test Case #2
Solution	Glycerol (40%)	Ethanol (30%)
Solute diffusivity, m^2·s^{-1}	$3.393 \cdot 10^{-10}$	$4.603 \cdot 10^{-10}$
HTC, W·m^{-2}·K^{-1}	2 000	2 000
MTC, m·s^{-1}	$1.395 \cdot 10^{-5}$	$1.694 \cdot 10^{-5}$
Solution density, kg·m^{-3}	1 106.86	965.05
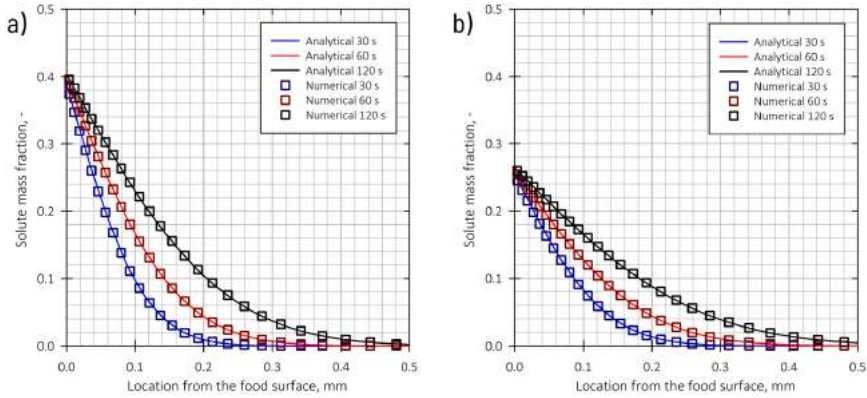
Fig. 5. Comparison of the solute mass concentration profiles after 30 s, 60 s and 120 s along the 1-D direction from the food sample surface towards the centre for the (a) glycerol solution and (b) ethanol solution.
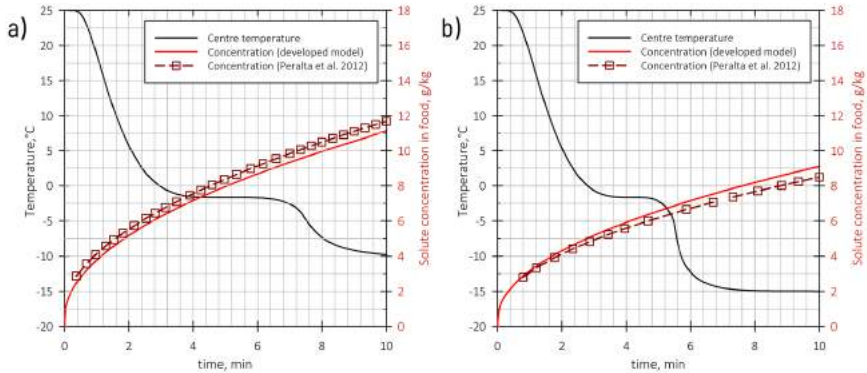
Fig. 6. Verification results related to potato samples freezing using HF in NaCl solution (23% concentration): (a) at $-10°C$ and (b) at $-15°C$, obtained using the model developed in this study compared with the literature results related to numerical study of HF process (Peralta et al., 2012).

considered.

During the HF process, heat and mass transfer mechanisms affect the solution uptake as well as the temperature change and water crystallisation within the food product. Fig. 7 compares the distribution of the glycerol concentration, ice fraction, and temperature within the food sample in characteristic points during HF in Case 16. These points are related to: (1) the beginning of HF process, (2) entering the critical zone of water crystallisation when the centre temperature reached $-1°C$, (3) plateau of the freezing curve, when the freezing process in the sample centre was nearly isothermal and the majority of the heat transfer was related to the latent heat dissipation, (4) leaving the critical zone of water crystallisation and (5) end of the freezing process where the middle temperature was 0.5 K above the refrigerating medium temperature.

The results presented in Fig. 7 allow to describe the progress of the food freezing process in liquid medium. During the first stage of the process, the outer layer of the food product freezes rapidly. As a result, the ice formed in this region inhibits the solute uptake, which was confirmed in the chart by the curve describing the solute concentration.

The solute uptake was the most intensive in the first seconds of the process. Its progress was decreased along with the progress of the freezing. As seen in the fields of solute concentration, only the region near the surface of the food product absorbs the solute. The concentration is near the solution concentration, i.e., 30%, at the surface. Along with the process, the ice front propagates towards the centre of the food product. The final ice content within the food product was approximately 70%, which is associated with the temperature of $-15°C$ according to Tchiegov's relationship described in Eq. (4). It is worth mentioning that the temperature change is the slowest in the centre of food product. It remained nearly constant for almost 2 min of the process and lasted within the critical zone of water crystallisation for approximately 2.5 min. Because of that, the temperature should be analysed in that most sensitive localisation during the HF process.

4.2. Effect of the HTC and sample size

As mentioned before, the HF method is most beneficial for the freezing of small food products. Fig. 8 presents the freezing process time

Table 5
Operating conditions used in the numerical campaign.

Case No	Solution type and concentration	Sample size (D) mm	HTC W·m⁻² K⁻¹	Temperature of freezing solution (°C)
Different solutions, various D and HTC				
Case 1	ETH (30%)/GLY (40%)/SUG (15%/25%)	5	300 (IF)	−15.0
Case 2	ETH (30%)/GLY (40%)/SUG (15%/25%)	10	300 (IF)	−15.0
Case 3	ETH (30%)/GLY (40%)/SUG (15%/25%)	15	300 (IF)	−15.0
Case 4	ETH (30%)/GLY (40%)/SUG (15%/25%)	20	300 (IF)	−15.0
Case 5	ETH (30%)/GLY (40%)/SUG (15%/25%)	25	300 (IF)	−15.0
Case 6	ETH (30%)/GLY (40%)/SUG (15%/25%)	30	300 (IF)	−15.0
Case 7	ETH (30%)/GLY (40%)/SUG (15%/25%)	5	1 000	−15.0
Case 8	ETH (30%)/GLY (40%)/SUG (15%/25%)	10	1 000	−15.0
Case 9	ETH (30%)/GLY (40%)/SUG (15%/25%)	15	1 000	−15.0
Case 10	ETH (30%)/GLY (40%)/SUG (15%/25%)	20	1 000	−15.0
Case 11	ETH (30%)/GLY (40%)/SUG (15%/25%)	25	1 000	−15.0
Case 12	ETH (30%)/GLY (40%)/SUG (15%/25%)	30	1 000	−15.0
Case 13	ETH (30%)/GLY (40%)/SUG (15%/25%)	5	2 000	−15.0
Case 14	ETH (30%)/GLY (40%)/SUG (15%/25%)	10	2 000	−15.0
Case 15	ETH (30%)/GLY (40%)/SUG (15%/25%)	15	2 000	−15.0
Case 16	ETH (30%)/GLY (40%)/SUG (15%/25%)	20	2 000	−15.0
Case 17	ETH (30%)/GLY (40%)/SUG (15%/25%)	25	2 000	−15.0
Case 18	ETH (30%)/GLY (40%)/SUG (15%/25%)	30	2 000	−15.0
Case 19	ETH (30%)/GLY (40%)/SUG (15%/25%)	5	3 000	−15.0
Case 20	ETH (30%)/GLY (40%)/SUG (15%/25%)	10	3 000	−15.0
Case 21	ETH (30%)/GLY (40%)/SUG (15%/25%)	15	3 000	−15.0
Case 22	ETH (30%)/GLY (40%)/SUG (15%/25%)	20	3 000	−15.0
Case 23	ETH (30%)/GLY (40%)/SUG (15%/25%)	25	3 000	−15.0
Case 24	ETH (30%)/GLY (40%)/SUG (15%/25%)	30	3 000	−15.0

Table 5 (*continued*)

Case No	Solution type and concentration	Sample size (D) mm	HTC W·m⁻² K⁻¹	Temperature of freezing solution (°C)
Case 25	ETH (30%)/GLY (40%)/SUG (15%/25%)	5	4 000	−15.0
Case 26	ETH (30%)/GLY (40%)/SUG (15%/25%)	10	4 000	−15.0
Case 27	ETH (30%)/GLY (40%)/SUG (15%/25%)	15	4 000	−15.0
Case 28	ETH (30%)/GLY (40%)/SUG (15%/25%)	20	4 000	−15.0
Case 29	ETH (30%)/GLY (40%)/SUG (15%/25%)	25	4 000	−15.0
Case 30	ETH (30%)/GLY (40%)/SUG (15%/25%)	30	4 000	−15.0
Various D and different solution temperature under the constant solute concentration				
Case 31	ETH (30%)	5	2 000	−10.0
Case 32	ETH (30%)	15	2 000	−10.0
Case 33	ETH (30%)	30	2 000	−10.0
Case 34	ETH (30%)	5	2 000	−20.0
Case 35	ETH (30%)	15	2 000	−20.0
Case 36	ETH (30%)	30	2 000	−20.0
Various D and different solution temperature under the lowest possible solute concentration				
Case 37	GLY (20%)	5	2 000	−5.0
Case 38	GLY (30%)	5	2 000	−9.5
Case 39	GLY (50%)	5	2 000	−23.0
Case 40	GLY (20%)	15	2 000	−5.0
Case 41	GLY (30%)	15	2 000	−9.5
Case 42	GLY (50%)	15	2 000	−23.0
Case 43	GLY (20%)	30	2 000	−5.0
Case 44	GLY (30%)	30	2 000	−9.5
Case 45	GLY (50%)	30	2 000	−23.0

for food samples having a diameter from 5 mm to 30 mm under different HTC conditions. After the HTC increased from 300 W·m⁻² K⁻¹ to 1 000 W·m⁻² K⁻¹, i.e., changing the IF to HF of moderate intensity, the freezing time was reduced by approximately 30% to 65%, depending on the food sample size. The highest freezing time reduction was achieved for the smallest food samples having a diameter of 5 mm. In this case, changing the freezing method allowed to reduce the freezing time from over 4 min to approximately 1.5 min, which refers to approximately 65% of the freezing time reduction. The internal thermal resistance that is low for small food products allowed for such a significant reduction. In the case of food product with a diameter of 20 mm, the freezing time was reduced from approximately 13.5 min to 8 min, which leads to approximately 40% freezing time reduction. In the case of the 30 mm sample, the freezing time for IF was 23 min, while in the case of HF with an HTC value of 1 000 W·m⁻² K⁻¹, the food sample was frozen after 16
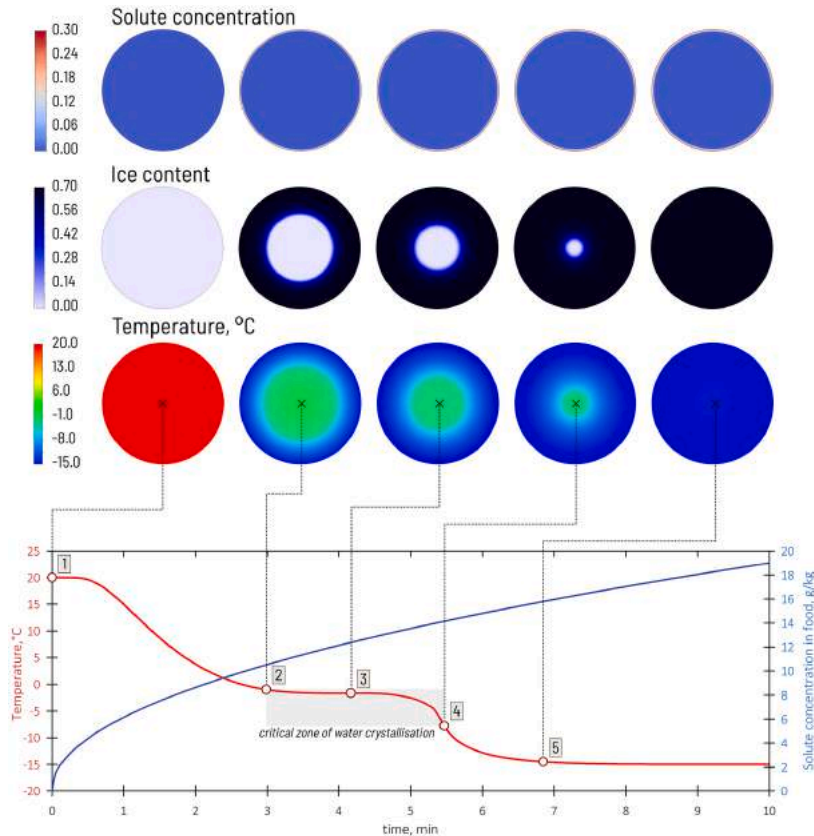
Fig. 7. The spatial distribution of the solution (glycerol) concentration, ice content, and the temperature within the potato sample in characteristic points of the freezing process for Case 16.

min; thus, the freezing time was reduced by 30%. Further HF intensification resulted in an even higher reduction in the freezing time, i.e., by approximately 35% to 80% in the case of an HTC of 2 000 W·m^{-2} K^{-1} with respect to the IF conditions. In the case of HTCs of 3 000 W·m^{-2} K^{-1} or 4 000 W·m^{-2} K^{-1}, a freezing time reduction occurred, but it was not as significant as in case of lower HTCs. These results confirmed that in the case of small food products with a diameter from 5 mm to 15 mm, HF guarantees a freezing time from less than 1 min to approximately 4 min for HTC conditions of 2 000 W·m^{-2} K^{-1}. Similar numbers were presented in the study of Fikiin and Fikiin (2001) who described the freezing times for small fruits and vegetables (berries and peas).

Similar trends are related to the time of residence in the critical zone of water crystallisation, compared with the same cases in Fig. 9. In the case of the IF method, these periods of time were in the range from almost 1.5 min for the smallest potato samples to over 9 min for 30 mm samples. The increase in the HTC to 2 000 W·m^{-2} K^{-1} reduced these times to 0.3 min in the case of the smallest foods to slightly over 5 min for the largest samples. These numbers correspond to a reduction of 40%–80% for the largest and smallest samples, respectively. Such a reduction can result in a significant improvement in food quality in

terms of ice crystal growth. A further increase in HTC resulted in a minor reduction in the time of residence within the critical zone of water crystallisation. This finding suggests that there is no need to ensure very intensive conditions of turbulent flow of refrigerating medium in the HF system in terms of the freezing time reduction and that the HTC range of 1 000–2 000 W·m^{-2} K^{-1} is sufficient to effectively conduct the HF process in terms of rapid freezing process.

Apart from the results related to the freezing time and the time of residence within the critical zone of water crystallisation, solute uptake during the process was compared for the same cases. Fig. 10(a), (b), and (c) compare the average solute concentration in the potato sample after the freezing process for Cases 1–30 during freezing in aqueous solutions of ethanol (30%), glycerol (40%) and ethanol-glucose (15%/25%), respectively. The end of the freezing process in these results was defined based on the freezing process times presented previously in Fig. 8. According to the results presenting the solute concentration, the highest solute concentration was present in the smallest food samples. Such behaviour is a result of the external sample area to sample volume ratio, which is higher when spherical food sample diameter is lower. For spherical food samples, doubling the diameter values results in a twice
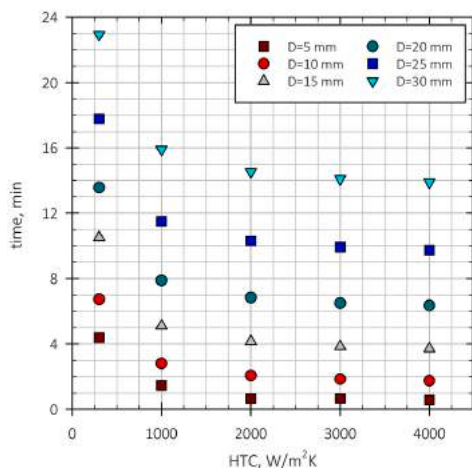
Fig. 8. Total process time in Cases 1–30 characterised by different HTCs and the sample diameter from 5 mm to 30 mm.
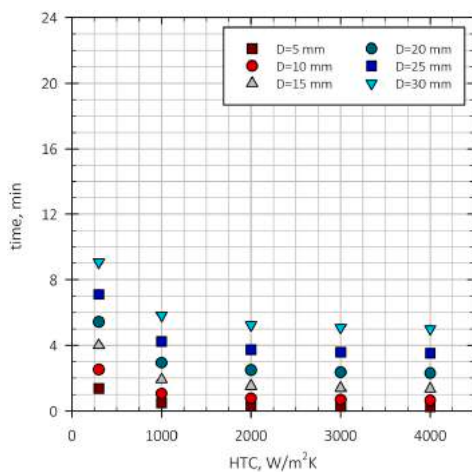
Fig. 9. Total time of the potato central temperature being within the range of the critical zone of water crystallisation in Cases 1–30 characterised by different HTCs and sample diameters from 5 mm to 30 mm.

Fig. 10. Comparison of the average concentration of each solute in g per 1 kg of food after HF freezing in (a) ethanol solution (30%), (b) glycerol solution (40%) and (c) ethanol-glucose (15%/25%) solution in Cases 1–30, which were characterised by different HTCs and the sample diameter.

lower A/V ratio, which reduces the ability to absorb the solute at the interface between the food product and the liquid medium.

For example, in Case 13, which is characterised by an HTC of 2 000 W·m^{-2} K^{-1} and a sample diameter of 5 mm, the glycerol concentration in food was approximately 29.1 g·kg^{-1}. Under the same conditions, the glycerol concentrations for larger samples of 10 mm, 20 mm, and 30 mm after freezing were 23.1 g·kg^{-1}, 21.5 g·kg^{-1}, and 21.1 g·kg^{-1}, respectively. As seen, the differences are not significant for larger samples.

It is worth emphasising that an increase in the HTC results in a

reduction in solute uptake. There are two reasons for such a behaviour. First, a higher HTC guarantees a shorter freezing time leading to a shorter contact with the liquid medium, and second, a more intensive freezing rate accelerates food surface freezing, which inhibits solute uptake, as discussed in Section 4.1. An increase in the HTC from 300 W·m^{-2} K^{-1} to 2 000 W·m^{-2} K^{-1} resulted in a reduction in the glycerol uptake from 8% for 30 mm samples to almost 40% for 5 mm samples.

This finding suggests that the HF method significantly reduces the unwanted solute uptake in comparison with the IF method. For smaller food samples, the improvement is more significant.

Comparison of three solutions with different concentrations for the same cases allowed to conclude that the final concentration in the food product is proportional to the solution composition. For example, in Case 16 characterised by HTC of 2 000 W·m^{-2} K^{-1} and the sample diameter of 20 mm, the solute concentration in food was 21.5 g·kg^{-1} in the case of using the glycerol solution (40%), while in the case of using the binary ethanol solution (30%), the solute concentration in food was 15.8 g·kg^{-1}. The same relationship was observed in all the analysed cases.

The selection of the appropriate solution is a key factor for the utilisation of HF for food freezing. In the case of the glycerol solution (40%), the average concentration of pure glycerol was approximately 30.2 g·kg^{-1} in a 5 mm potato sample, taking into consideration the mean value from cases characterised by the HTC in a range of 1 000–3 000 W·m^{-2} K^{-1}. In the case of the 20 mm and 30 mm samples, the mean concentrations were 21.7 g·kg^{-1} and 21.2 g·kg^{-1}, respectively. In the case of the ethanol solution (30%), for the same cases, the solute concentrations were 22.3 g·kg^{-1}, 15.9 g·kg^{-1} and 15.5 g·kg^{-1} for the samples with diameters of 5 mm, 20 mm, and 30 mm, respectively. The advantage of using the ternary solution of ethanol and glucose (15%/25%) is the possibility of reducing the ethanol concentration in food products after HF. If this solution was used in the same cases, the ethanol concentration in food samples was 12.8 g·kg^{-1}, 9.1 g·kg^{-1}, and 8.9 g·kg^{-1}, respectively. For this solution, additional glucose absorption will be present. However, glucose gain in some cases can be a desired side effect, e.g., for the production of desserts (Fikiin, 2008).

The results discussed above suggest that the final concentration of any solute after the HF is strongly dependent on the food product size. The ratio A/V, which is the relationship between the external food product surface and its volume, allows to assess the final solute concentration in foods of various sizes and shapes. The area of the interface between the liquid phase and the food product strongly affects the total mass flux, and the food product volume affects the average concentration. Fig. 11 presents the relationship between the A/V ratio of the food sample and the solute concentration in food after the HF process for different HTC values. Only the results for the ethanol solution are presented because the relationship is the same for other solutions. As seen, the general relationship is linear within the investigated range of conditions; therefore, the final concentration can be easily predicted if the A/V ratio and the HTC are known. It is worth mentioning that a higher HTC corresponds to a lower slope of the linear regression curve. Hence, in case of HF characterised by a high HTC, the solute concentration is not as sensitive to the change in A/V as the IF method achieving lower HTCs.
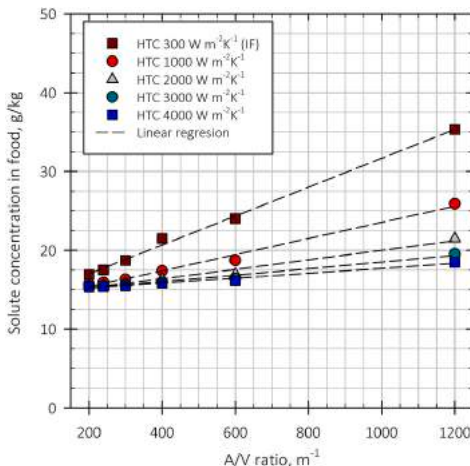
4.3. Effect of refrigerating medium temperature change under a constant concentration of solution

In the food freezing process in a liquid medium, the reduction of the medium temperature significantly improves the freezing conditions. This fact was confirmed in numerous papers related to the freezing methods referenced in Section 1, e.g., in numerical studies by Zorrilla and Rubiolo (2005b) and Oroná et al. (2018) focused on IF and HF, respectively. Nevertheless, quantifying this effect in this study is worthwhile and comparing the results with the analysis of the other parameters investigated in the HF method provides important insights.

Fig. 12 presents the results related to the total freezing process time and the time of food centre temperature residence in the critical zone of water crystallisation for Cases 13, 15, 18, and 31–36. These cases are represented by the same HTC of 2 000 W·m^{-2} K^{-1}, which was recognised as sufficient to assure a significant reduction of the freezing time and unwanted solute uptake. Spheres with diameters of 5 mm, 15 mm, and 30 mm are compared in this figure. Another variable in this comparison is the refrigerating medium temperature, which was $-10°C$, $-15°C$ and $-20°C$. Because the ethanol aqueous solution with a mass concentration of 30% has a freezing temperature below $-20°C$, this solution was selected as appropriate for the analysis of the refrigerating liquid effect in a solution without changes in composition.

As expected, a reduction of the refrigerating medium temperature allowed to reduce the HF process time. Within the investigated range of conditions, lowering the refrigerating medium temperature from $-10°C$

Fig. 11. Average concentration of the solute in g per 1 kg of food after HF freezing in ethanol solution (30%) for various size spherical samples having A/V ratios between 200 m^{-1} (diameter 30 mm) and 1 200 m^{-1} (diameter 5 mm) under different HTCs.
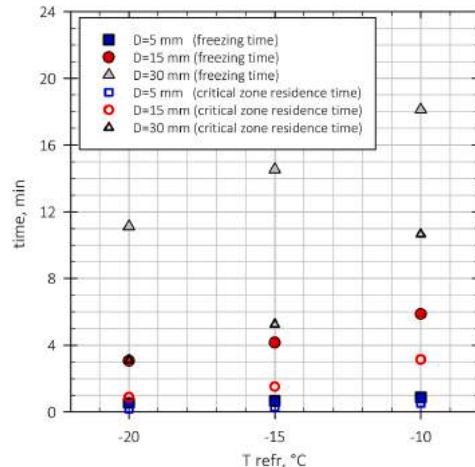
Fig. 12. Total process time and total time of the potato centre temperature being within the range of the critical zone of water crystallisation in Cases 13, 15, 18 and 31–36 characterised by potato sample diameters of 5 mm, 15 mm and 30 mm during the HF process in a refrigerating liquid at $-10°C$, $-15°C$ and $-20°C$.

by 5 K resulted in a freezing time reduction of approximately 25%. A greater temperature reduction from −10°C to −20°C allowed to reduce the freezing time from 22 min to approximately 11 min for the sample with a diameter of 30 mm. These results prove that the temperature reduction results in a considerable reduction in the freezing time. The lower the temperatures are, the better the freezing time reduction because the temperature gradients are higher.

Reductions in the residence time within the critical zone of water crystallisation are even more significant if the medium temperature is reduced. When the temperature was lowered from −10°C to −15°C, the characteristic period was reduced by approximately 50%, e.g., from 3 min to 1.5 min for the 15 mm sample. In the case of a solution temperature change from −10°C to −20°C, the time at which the food centre temperature occurs within that zone was lowered to less than 1 min for the same sample, which corresponds to a 70% reduction with respect to the medium temperature higher by 10 K.

Furthermore, as a consequence of the reduced time of food contact with the liquid solution, the average concentrations of solutes were lowered along with the temperature reduction. Fig. 13 presents the results related to the average solute concentration in food samples after the freezing process for the same set of cases. As seen, after reducing the solution temperature from −10°C to −15°C, the solute concentration in the frozen foods was decreased from 26.0 g·kg⁻¹ to 21.5 g·kg⁻¹ for the 5 mm sample, which corresponds to an approximately 20% reduction. In the case of larger potato samples with diameters of 15 mm and 30 mm, the reduction was approximately 25%. A change in the solution temperature from −10°C to −20°C resulted in a reduction of the solute concentration in potato by 26% and approximately 37% for the 5 mm sample and larger samples, respectively. To sum up, a reduction in the freezing solution temperature allows to minimise the unwanted uptake of solutes during HF. However, the changes are associated with a reduction of the total freezing time rather than with the absorption conditions because in all cases, the freezing of the outer surface of food samples is rapid.

Additionally, the effect of A/V was investigated for different temperatures of the refrigerating medium. Fig. 14 presents the relationship
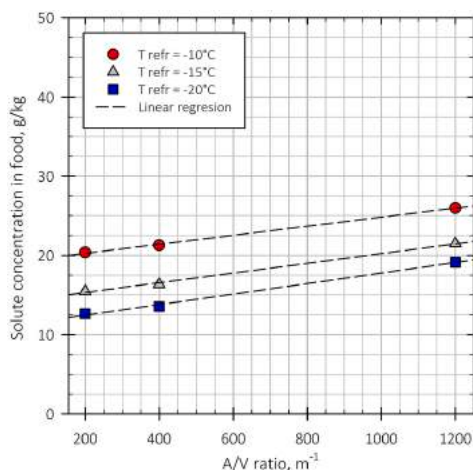
Fig. 14. Average concentration of the solute in g per 1 kg of food after HF freezing in ethanol solution (30%) for various size spherical samples having A/V ratios between 200 m⁻¹ (diameter 30 mm) and 1 200 m⁻¹ (diameter 5 mm) under different refrigerating medium temperatures.

between the specific food sample A/V ratio and the solute concentration after freezing at different temperatures. As seen, linear behaviour is still seen, but the slope of each curve is the same. Reduction of the refrigerating medium temperature resulted in a lower solute concentration but did not affect the dependency on the A/V ratio.

4.4. Effect of the refrigerating medium temperature change by keeping the lowest concentration of a liquid solution

The results related to the solute uptake presented above reveal that the freezing solution temperature and convective conditions affect the amount of unwanted solution gain during HF. Moreover, the analysis of different solutions having various concentrations proved that the concentration of solute in the selected solution is a key factor determining the final concentration of a given solute in the food sample after HF. Therefore, an analysis was performed under conditions in which the solute concentration was adjusted as low as possible in a wide range of temperatures to ensure the liquid state of the refrigerating medium. Thus, the glycerol solution was selected for comparison in a temperature range from −5°C to −23°C, which corresponds to solute concentrations from 20% to 50%. Fig. 15 presents the average concentration of glycerol in potato samples having 5 mm, 15 mm and 30 mm in diameter after HF freezing under different solution temperatures and concentrations. These conditions are represented by Cases 13, 15, 18 and 37–45.

As seen, for samples with diameters of 15 mm and 30 mm, lowering the solution temperature to −23°C resulted in a reduction in the glycerol concentration in food products to 18.6–20.0 g·kg⁻¹, even though the solution was more concentrated with glycerol. For cases characterised by higher temperatures and lower concentrations of glycerol in the solution, the concentration of glycerol was in the range of 20.8–21.8 g·kg⁻¹. Such differences in results were not significant. The opposite relationship was seen for the smallest sample of 5 mm. In this case, the increase in the solute concentration in solution significantly affected the final concentration of glycerol in the food product. It increased up to 32.2 g·kg⁻¹ for the lowest temperature of −23°C and a solution concentration of 50%. Such behaviour is related to a very high external area

Fig. 13. Comparison of the average concentration of each solute in g per 1 kg of food after HF freezing in ethanol solution (30%) in Cases 13, 15, 18 and 31–36 characterised by potato sample diameters of 5 mm, 15 mm, and 30 mm during the HF process in refrigerating liquid at 10°C, 15°C and 20°C.
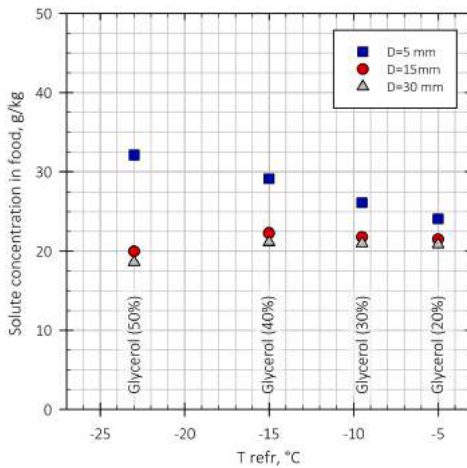
Fig. 15. Comparison of the average concentration of each solute in g per 1 kg of food after HF freezing in glycerol solution having various mass concentration and temperature in Cases 13, 15, 18 and 37–45 characterised by potato sample diameters of 5 mm, 15 mm, and 30 mm.

to volume ratio of a sample with a diameter of 5 mm (A/V=1 200 m^{-1}). In summary, lowering the refrigerating medium temperature in most cases is undoubtedly beneficial in terms of lowering the final concentration of the solute in food products, even if the solution needs to be more concentrated with a given solute to achieve a lower temperature of a liquid. An exception may occur for small food products with a diameter of approximately 5 mm. In that case, the solute concentration in the food product was increased.

5. Conclusions

This paper presents a numerical study of the food freezing process using a novel HF method. A numerical model was developed based on Fourier's and Fick's laws to characterise the heat transfer and mass diffusion within the food product. Potato sample was selected as an example food product with a spherical shape, and the samples had diameters between 5 mm and 30 mm. The HTC values characteristic for HF were assumed to be in the range from 1 000 W·m^{-2} K^{-1} to 4 000 W·m^{-2} K^{-1} based on previous HF process analyses conducted by the authors. Additionally, that method was compared with IF in the same environment but with a lower HTC of 300 W·m^{-2} K^{-1}.

According to the obtained results, higher values of HTC positively affected the freezing process in terms of freezing time, residence within the critical zone of water crystallisation and solute uptake. In the case of an HTC of 2 000 W·m^{-2} K^{-1}, the freezing times with respect to IF were reduced by 35% for the sample with a diameter of 30 mm and by 80% for the smallest sample with a diameter of 5 mm. The reduction in the residence time within the critical zone of water crystallisation was in a similar range. Moreover, the solution uptake was reduced after changing the freezing method from IF to HF. In the case of an HTC of 2 000 W·m^{-2} K^{-1}, the reduction of the average concentration of glycerol was 8% to 40% compared with the IF method for samples with diameters of 30 mm and 5 mm.

It is worth emphasising that a further increase in the HTC resulted in an insignificant reduction in the processing time or lowered the solute concentration in food samples. Yet, the value of 2 000 W·m^{-2} K^{-1} was

sufficient to assure the most favourable conditions for the HF process for small food freezing with reasonable effort. The intensification of the flow conditions in the HF system could result in an unnecessary increase in the power required for refrigerating liquid pumping.

In addition, three different solutions were compared in this study: two binary aqueous solutions of glycerol (40% mass concentration) and ethanol (30% mass concentration) and a ternary solution of ethanol-glucose (15%/25% mass concentration). In all the considered cases, the concentration of each of these solutes in the food product was strongly related to the solute concentration in the liquid solution. No effect of the mass diffusivity of these substances was noticed, i.e., for cases differing by only the solution type, the final concentration of a given solute in food product was related to its concentration in solution rather than the diffusivity of the solute. For the assumed conditions, the final concentration of solutes in food was the highest for the 5 mm food samples due to the high ratio of the outer surface of the sample to the volume. In the case of glycerol solution (40% mass concentration), the concentration was 30.2 g·kg^{-1}. For larger samples with diameters of 20 mm and 30 mm, the glycerol concentrations in potato samples were 21.7 g·kg^{-1} and 21.2 g·kg^{-1}, respectively. In the case of the ethanol (30%) solution, the solute concentrations in samples of different sizes were 22.3 g·kg^{-1}, 15.9 g·kg^{-1}, and 15.5 g·kg^{-1} for diameters of 5 mm, 20 mm and 30 mm, respectively. It is worth mentioning that in the case of the ternary solution where the ethanol concentration was only 15%, the ethanol concentration in the food samples was significantly lower, i.e., 12.8 g·kg^{-1}, 9.1 g·kg^{-1}, and 8.9 g·kg^{-1} for the same samples. It should be pointed out that in the developed numerical model, the tortuosity value was assumed to be 2.0 considering the worst case scenario. In addition, no peel was present in the potato samples. Therefore, in the case of different fruits or vegetables, e.g., cherries or peas, the concentration of solutes in the frozen foods may be even lower.

The effect of the parameter A/V was investigated, and it represents the food product external surface area to its volume ratio. In general, the solute concentration after HF is higher for food samples with a higher A/V ratio. However, in the case of a high HTC, an increase in the concentration of solute in the food sample after freezing in not as affected by an increase in the A/V relative to that at lower HTC values. This finding suggests that the HF method is beneficial over the IF method in terms of solute uptake for small or nonspherical foods characterised by high A/V. Moreover, relationship between the A/V and the concentration can characterise the uptake of solution for foods with different shapes.

In addition, the effect of the solution temperature was investigated. In general, the temperature of the solution should be maintained as low as possible because the reduction of the solution temperature significantly affects the freezing process. Lowering the refrigerating medium temperature from $-10°C$ to $-15°C$ resulted in a freezing time reduction of 25%. However, a decrease in the solution temperature requires to increase the concentration. In the case of the smallest food samples of 5 mm, using a more concentrated glycerol solution (50%) at a temperature of $-23°C$ resulted in a higher concentration of the solute in frozen food products by approximately 10% with respect to the reference conditions, which were characterised by a glycerol solution with a mass concentration of 40% and a temperature of $-15°C$. Thus, the selection of the solution and its concentration should be performed carefully, especially in the case of the smallest food products characterised by a large external area/volume ratio. On the other hand, for larger samples, the reduction of the temperature was beneficial, even in the case of a more concentrated solution. After the temperature reduction from $-15°C$ to $-23°C$ which required to change the glycerol concentration in the solution from 40% to 50%, the final glycerol concentration was reduced by 11% or 12% in the food samples with diameters of 15 mm or 30 mm, respectively. In general, in all the investigated cases, the solute concentration in food products under HF process conditions was significantly lower than that after the IF process characterised by a lower HTC.

This study compared the most significant parameters of the HF method appropriate for freezing small food products. This promising

method was characterised as beneficial in terms of the freezing rate and reducing the freezing time. Although unwanted solution uptake occurs during freezing using that method, the average concentration of solutes in food samples can be significantly reduced with respect to the well-established IF method.

Declaration of Competing Interest

The authors declare that they have no known competing financial interests or personal relationships that could have appeared to influence the work reported in this paper.

Acknowledgements

References

ASHRAE. (2006). *ASHRAE handbook: Refrigeration : SI Edition*. American Society of Heating, Refrigerating and Air-Conditioning Engineers.

Bashkatov, A. N., Genina, E. A., Sinichkin, Y. P., Kochubey, Y. I., Lakodina, N. A., & Tuchin, V. V. (2003). Glucose and mannitol diffusion in human dura mater. *Biophysical Journal, 85*(5), 3310–3318.

Carson, J. K., Wang, J., North, M. F., & Cleland, D. J. (2016). Effective thermal conductivity prediction of foods using composition and temperature data. *Journal of Food Engineering, 175*, 65–73.

Cengel, Y. A. (2015). *Heat transfer: A practical approach*. McGraw-Hill.

Chen, C. S. (1985). Thermodynamic analysis of the freezing and thawing of foods: Enthalpy and apparent specific heat. *Journal of Food Science, 50*(4), 1158–1162.

Choi, Y., & Okos, M. R. (1986). Effects of temperature and composition on the thermal properties of food. *Food Engineering and Process Applications*, 93–101.

Cussler, E. L. (1984). Diffusion in concentrated solutions. In *Diffusion: Mass transfer in fluid systems* (pp. 55–84). New York: Cambridge University Press.

D'Errico, G., Ortona, O., Capuano, F., & Vitagliano, V. (2004). Diffusion coefficients for the binary system glycerol+water at 25 c. a velocity correlation study. *Journal of Chemical & Engineering Data, 49*(6), 1665–1670.

Fikiin, A. G. (1992). New method and fluidized water system for intensive chilling and freezing of fish. *Food Control, 3*(3), 153–160. https://doi.org/10.1016/0956-7135(92)90100-O

Fikiin, K., Tsvetkov, O., Laptev, Y., Fikiin, A., & Kolodyaznaya, V. (2003). Thermophysical and engineering issues of the immersion freezing of fruits in ice slurries based on sugar-ethanol aqueous solution. *Ecolibrium, Aug*, 10–15.

Fikiin, K. A. (2008). *Emerging and novel freezing processes* (pp. 101–123). Oxford, UK: Blackwell Publishing Ltd.. https://doi.org/10.1002/9781444302325.ch5. ISBN 9781444302325.

Fikiin, K. A., & Fikiin, A. G. (2001). Individual quick freezing of foods by hydrofluidisation and pumpable ice slurries. *55*, 15–18, 11.

Galetto, C. D., Verdini, R. A., Zorrilla, S. E., & Rubiolo, A. C. (2010). Freezing of strawberries by immersion in cacl2 solutions. *Food Chemistry, 123*(2), 243–248. https://doi.org/10.1016/j.foodchem.2010.04.018. ISSN 0308-8146.

Green, D. W. (1997). *Perry's chemical engineers' handbook*.

Hayduk, W., & Laudie, H. (1974). Prediction of diffusion coefficients for nonelectrolytes in dilute aqueous solutions. *AICHE Journal, 20*(3), 611–615.

Hober, R., Hitchcock, D. I., Bateman, J. B., Goddard, D. R., & Fenn, W. O. (1946). Physical chemistry of cells and tissues. *The Journal of Physical Chemistry, 50*(4), 386–387.

Holz, M., Heil, S. R., & Sacco, A. (2000). Temperature-dependent self-diffusion coefficients of water and six selected molecular liquids for calibration in accurate 1h nmr pfg measurements. *Physical Chemistry Chemical Physics, 2*(20), 4740–4742.

IIR. (2020). *The role of refrigeration in worldwide nutrition - 6th informatory note on refrigeration and food*.

James, C., Purnell, G., & James, S. J. (2015). A review of novel and innovative food freezing technologies. *Food and Bioprocess Technology, 8*(8), 1616–1634.

Khouryieh, H. A. (2021). Novel and emerging technologies used by the u.s. food processing industry. *Innovative Food Science and Emerging Technologies, 67*, 102559. https://doi.org/10.1016/j.ifset.2020.102559

Levy, F. L. (1981). A modified maxwell-eucken equation for calculating the thermal conductivity of two-component solutions or mixtures. *International Journal of Refrigeration, 4*(4), 223–225.

Lucas, T., Flick, D., & Raoult-Wack, A. L. (1999). Mass and thermal behaviour of the food surface during immersion freezing. *Journal of Food Engineering, 41*(1), 23–32. https://doi.org/10.1016/S0260-8774(99)00068-0

Lucas, T., & Raoult-Wack, A. L. (1998). Immersion chilling and freezing in aqueous refrigerating media: review and future trends. *International Journal of Refrigeration, 21*(6), 419–429. https://doi.org/10.1016/S0140-7007(98)00014-0

Luscher, C., Schlüter, O., & Knorr, D. (2005). High pressure–low temperature processing of foods: impact on cell membranes, texture, color and visual appearance of potato tissue. *Innovative Food Science and Emerging Technologies, 6*(1), 59–71. https://doi.org/10.1016/j.ifset.2002.05.001

MATLAB. (2020). *version 9.9.0.1467703 (R2020b)*. Natick, Massachusetts: The MathWorks Inc.

Melinder, A. (2010). *Properties of secondary working fluids (secondary refrigerants or coolants, heat transfer fluids) for indirect systems*. IIF-IIR.

Oelkers, E. H. (1991). Calculation of diffusion coefficients for aqueous organic species at temperatures from 0 to 350 c. *Geochimica et Cosmochimica Acta, 55*(12), 3515–3529.

Oroná, J. D., Zorrilla, S. E., & Peralta, J. M. (2017). Computational fluid dynamics combined with discrete element method and discrete phase model for studying a food hydrofluidization system. *Food and Bioproducts Processing, 102*, 278–288. https://doi.org/10.1016/j.fbp.2017.01.005

Oroná, J. D., Zorrilla, S. E., & Peralta, J. M. (2018). Sensitivity analysis using a model based on computational fluid dynamics, discrete element method and discrete phase model to study a food hydrofluidization system. *Journal of Food Engineering, 237*, 183–193. https://doi.org/10.1016/j.jfoodeng.2018.05.019

Palacz, M., Adamczyk, W., Piechnik, E., Stebel, M., & Smolka, J. (2019). Experimental investigation of the fluid flow inside a hydrofluidisation freezing chamber. *International Journal of Refrigeration, 107*, 52–62. https://doi.org/10.1016/j.ijrefrig.2019.08.009

Palacz, M., Piechnik, E., Halski, M., Stebel, M., Adamczyk, W., Eikevik, T. M., & Smolka, J. (2021). Experimental analysis of freezing process of stationary food samples inside a hydrofluidisation freezing chamber. *International Journal of Refrigeration*. https://doi.org/10.1016/j.ijrefrig.2021.06.034

Peralta, J. M., Rubiolo, A. C., & Zorrilla, S. E. (2009). Design and construction of a hydrofluidization system. study of the heat transfer on a stationary sphere. *Journal of Food Engineering, 90*(3), 358–364. https://doi.org/10.1016/j.jfoodeng.2008.07.004

Peralta, J. M., Rubiolo, A. C., & Zorrilla, S. E. (2010). Mathematical modeling of the heat transfer and flow field of liquid refrigerants in a hydrofluidization system with a stationary sphere. *Journal of Food Engineering, 99*(3), 303–313. https://doi.org/10.1016/j.jfoodeng.2010.03.003

Peralta, J. M., Rubiolo, A. C., & Zorrilla, S. E. (2012). Mathematical modeling of the heat and mass transfer in a stationary potato sphere impinged by a single round liquid jet in a hydrofluidization system. *Journal of Food Engineering, 109*(3), 501–512. https://doi.org/10.1016/j.jfoodeng.2011.10.032

Pham, Q. T. (2006). Modelling heat and mass transfer in frozen foods: a review. *International Journal of Refrigeration, 29*(6), 876–888. https://doi.org/10.1016/j.ijrefrig.2006.01.013

Ribeiro, A., Ortona, O., Simoes, S. M., Santos, C. I., Prazeres, P. M., Valente, A. J., Lobo, V. M., & Burrows, H. D. (2006). Binary mutual diffusion coefficients of aqueous solutions of sucrose, lactose, glucose, and fructose in the temperature range from (298.15 to 328.15) k. *Journal of Chemical & Engineering Data, 51*(5), 1836–1840.

Stebel, M., Smolka, J., Palacz, M., Adamczyk, W., & Piechnik, E. (2020). Numerical investigation of the fluid flow distribution for the hydrofluidisation food freezing method. *International Journal of Thermal Sciences, 151*, Article 106284. https://doi.org/10.1016/j.ijthermalsci.2020.106284

Stebel, M., Smolka, J., Palacz, M., Piechnik, E., Halski, M., Knap, M., Felis, E., Eikevik, T. M., Tolstorebrov, I., Peralta, J. M., & Zorrilla, S. E. (2021). Numerical modelling of the food freezing process in a quasi-hydrofluidisation system. *Innovative Food Science and Emerging Technologies, 74*, Article 102834. https://doi.org/10.1016/j.ifset.2021.102834

Tchigeov, G. (1979). *Thermophysical processes in food refrigeration technology*. Moscow, Russia: Food Industry.

Treybal, R. E. (1955). *Mass transfer operations*. McGraw-Hill.

Verboven, P., Scheerlinck, N., & Nicolai, B. M. (2003). Surface heat transfer coefficients to stationary spherical particles in an experimental unit for hydrofluidisation freezing of individual foods. *International Journal of Refrigeration, 26*(3), 328–336. https://doi.org/10.1016/S0140-7007(02)00110-X

Wang, J. F., Carson, J. K., Willix, J., North, M. F., & Cleland, D. J. (2009). Application of a co-continuous composite model of effective thermal conductivity to ice–air systems. *International Journal of Refrigeration, 32*(3), 556–561.

Whitaker, S. (1977). *Simultaneous heat, mass, and momentum transfer in porous media: A theory of drying. volume 13 of Advances in Heat Transfer* (pp. 119–203). Elsevier. https://doi.org/10.1016/S0065-2717(08)70223-5

Xanthakis, E., Le-Bail, A., & Ramaswamy, H. (2014). Development of an innovative microwave assisted food freezing process. *Innovative Food Science and Emerging Technologies, 26*, 176–181. https://doi.org/10.1016/j.ifset.2014.04.003

Xu, B., Zhang, M., Bhandari, B., Sun, J., & Gao, Z. (2016). Infusion of co2 in a solid food: A novel method to enhance the low-frequency ultrasound effect on immersion freezing process. *Innovative Food Science and Emerging Technologies, 35*, 194–203. https://doi.org/10.1016/j.ifset.2016.04.011

Zorrilla, S. E., & Rubiolo, A. C. (2005a). Mathematical modeling for immersion chilling and freezing of foods: Part i: Model development. *Journal of Food Engineering, 66*(3), 329–338. https://doi.org/10.1016/j.jfoodeng.2004.03.026

Zorrilla, S. E., & Rubiolo, A. C. (2005b). Mathematical modeling for immersion chilling and freezing of foods: Part ii: Model solution. *Journal of Food Engineering, 66*(3), 339–351. https://doi.org/10.1016/j.jfoodeng.2004.03.027